ENGINEERING PHOSPHOFRUCTOKINASE AND CITRATE SYNTHASE TO MODULATE *ESCHERICHIA COLI* METABOLISM AND BIOCHEMICAL PRODUCTION

by

HEMSHIKHA RAJPUROHIT

(Under the Direction of Mark Andrew Eiteman)

ABSTRACT

A biorefinery using sugars derived from lignocellulose is a sustainable route for chemical synthesis. To compete with traditional chemical processes, microbes and bioprocesses must be engineered for improved yield and productivity. Glucose is typically consumed by microbes through glycolytic, pentose phosphate and Entner-Doudroff pathways. Enzymes are responsible for catalyzing the many reactions, and traditionally, overexpression or deletion of genes coding these enzymes has been used to direct carbon to desired pathways.

Another approach is to modify key enzymes in metabolism to redirect flow to target pathways. Modulating activity offers a means to fine tune biochemical fluxes to match the microbial needs for growth while optimizing product formation. In this work, two enzymes were studied: Phosphofructokinase 1, which phosphorylates fructose-6-phosphate into fructose-1,6-bisphosphate, and citrate synthase, which converts acetyl-CoA and oxaloacetate into citrate at the start of the tricarboxylic acid cycle.

In a first research study, glycolytic flux was altered by constructing 22 phosphofructokinase (PfkA) variants which each contained single amino acid substitutions at residues associated with mobile loops and adjacent to active site residues. These variants displayed

a wide range of growth phenotypes under batch or nitrogen-limited steady-state conditions. Strains containing more severe substitutions showed decreased glucose uptake, decreased acetate formation, decreased intracellular concentrations of glycolytic intermediates, and decreased expression of the *pta* gene, despite identical growth rates.

In a second study, five citrate synthase (GltA) variants were examined for the formation of an acetyl-CoA-derived product, 3-hydroxybutyrate. GltA variants showed five-fold greater yield of 3-hydroxybutyrate compared to the strain with the wild-type enzyme in a glucose defined medium under batch conditions. A repeated batch process using the GltA[A267T] variant led to 16 g/L 3-hydroxybutyrate with a yield of 0.16 g/g.

In a third study, modifications in both GltA and PfkA were compared for the production of mevalonate, an acetyl-CoA-derived product. Several combined GltA and PfkA variants increased the yield of mevalonate by 50% over the yield obtained by the wild-type strain.

These results demonstrate the benefit of modifying central metabolism at key biochemical junctures to direct glucose into desirable biochemical products.

INDEX WORDS: *Escherichia coli*, protein engineering, site directed mutagenesis, variants, acetyl-CoA, NADPH, PfkA, GltA, Glucose, Pyruvate, Acetate, Batch process, Chemostat

ENGINEERING PHOSPHOFRUCTOKINASE AND CITRATE SYNTHASE TO MODULATE *ESCHERICHIA COLI* METABOLISM AND BIOCHEMICAL PRODUCTION

by

HEMSHIKHA RAJPUROHIT

B.E., Panjab University, Chandigarh, India, 2012

M.Tech., Anna University, Chennai, India, 2014

A Dissertation Submitted to the Graduate Faculty of The University of Georgia in Partial Fulfillment of the Requirements for the Degree

DOCTOR OF PHILOSOPHY

ATHENS, GEORGIA

2023

ENGINEERING PHOSPHOFRUCTOKINASE AND CITRATE SYNTHASE TO MODULATE *ESCHERICHIA COLI* METABOLISM AND BIOCHEMICAL PRODUCTION

by

HEMSHIKHA RAJPUROHIT

Major Professor:	Mark A. Eiteman
Committee:	James R. Kastner
	Melissa K. Hallow
	William S. Kisaalita
	William N. Lanzilotta

Electronic Version Approved:

Ron Walcott

Vice Provost for Graduate Education and Dean of the Graduate School
The University of Georgia
December 2023

ACKNOWLEDGMENTS

I am extremely grateful to my advisor Dr. Mark A. Eiteman who guided me with his invaluable patience and expertise throughout my Ph.D. This endeavor would not be possible without my committee members: Dr. James R. Kastner, Dr. Melissa K. Hallow, Dr. William S. Kisaalita, and Dr. William N. Lanzilotta who provided me with precious time and extremely vital feedback and assessment. Also, I thank funding agencies NSF and USDA for financial support as well as graduate school for supporting my summer research work.

My lab members Rachel Brown, Hayden Lippelman, Jacoby Shipmon, Brisbane Tovilla, and Jeff Dodelin helped me with adjustments in this new country and provided me with their moral support. Particularly, I appreciate my mentors Sarah Lee, Chris Moxley, and Ajay Arya who taught me technical aspects of this work: without them I could not have succeeded. My undergraduate students Reese Lofgren, Fred Lee, and Kieli Miles taught me skills to be a better mentor.

I am also grateful to my friends and cohort at UGA. Most importantly, Dr. Sarada Sripada (శారద శ్రీపాద) and Rashmi Pandey (रश्मी पांडे) played a major role during my stay here. Without their unconditional moral and technical support, it would have been a difficult journey away from home.

मैं अपनी मां शारदा राजपुरोहित के प्रति अपने आभार को शब्दों में व्यक्त नहीं कर सक्ती , जिन्होंने मुझ पर विश्वास किया और मुझे उच्च शिक्षा प्राप्त करने के लिए प्रोत्साहित किया। मेरे भाई-बहन जीतशिखा राजपुरोहित, मूमल राजपुरोहित और यशवर्धन राजपुरोहित को हमेशा मेरे साथ रहने के लिए बहुत धन्यवाद। अंत में, मुझे बिना शर्त कृतज्ञता सिखाने के लिए मेरी और स्काई को मैं धन्यवाद देना चाहूंगी।

TABLE OF CONTENTS

Page

LIST OF TABLES

LIST OF FIGURES

CHAPTER 1

INTRODUCTION AND LITERATURE REVIEW

Central carbon metabolism in heterotrophic bacteria involves how an input carbon source is used by cells to make precursor molecules which are withdrawn to make new cells and biochemical products (e.g., acetyl-CoA and oxaloacetate). Most carbon sources are metabolized through glycolysis (Embden-Meyerhof-Parnas Pathway, or EMP), the Entner-Doudoroff Pathway (EDP), the Pentose Phosphate Pathway (PPP), tricarboxylic acid (TCA) cycle, and other pathways which are active under specific conditions (Holms, 1986; Sauer and Eikmanns, 2005; Wu et al., 2023). Carbon catabolizing routes in these central pathways contain about 30 metabolites which are either phosphorylated (e.g., glucose-6-phosphate or glucose-6P, ribose-5P) or are carboxylic acids (e.g., pyruvic acid, citric acid) (Holms, 1986). In *Escherichia coli*, among these metabolites, 12 precursors (e.g., glucose-6P, pyruvate, acetyl-CoA) serve as a branchpoint exit for biomass forming pathways including amino acids, RNA/DNA nucleotides, lipids, cell membrane (Noor et al., 2010). *E. coli* cells growing at their maximum growth rate (0.94 h^{-1}) divert about 78% of glucose-6P towards the EMP (6.84 mmol/g biomass) and about 22% to the PPP (Holms, 1986). Metabolites located at important junctions respond to changes in carbon input or the environment (Holms, 1986), and are targets for metabolic engineering (Bailey, 1991).

1.1 MODIFYING THE CARBON FLUX WITH NUTRIENT-LIMITED GROWTH

A continuous process called a chemostat allows steady-state to be achieved under a specific nutrient limitation. Such a process allows precise analysis of the metabolic fluxes which exist in wild-type cells, and in response to pathway perturbations (i.e., due to gene knockouts). Cells respond to changes in growth rate as determined by dilution rate by adjusting the partitioning between glycolysis and the PPP using different nutrient limitation.

1.1.1 Glucose limitation

When glucose is limited, changing growth rate from 0.066 h^{-1} to 0.375 h^{-1} relative PPP flux changes from 41% to 67% (Kayser et al., 2005). This redistribution was attributed to Cra-dependent repression of key glycolysis genes including *pfkA* (phosphofructokinase isozyme 1) with increased growth rate (Hardiman et al., 2007). Decreasing growth rate leads to repression of the *gnd* gene coding 6-phosphogluconate dehydrogenase, the second enzyme of the PPP (Lemuth et al., 2008). Whereas, limiting TCA cycle or respiratory chain at high dilution rates in glucose-limited chemostats leads to flexible PPP and shift from cell-carbon limitation to energy carbon limitation (Kayser et al., 2005).

1.1.2 Nitrogen limitation

Nitrogen-limited growth generally results in a greater glycolytic flux compared to carbon-limited growth. Higher catabolic fluxes through glycolysis at the expense of PPP flux were observed under nitrogen limitation in *E. coli* MG1655 chemostat cultures (Sauer et al., 1999). Proteomics study revealed that key enzymes of TCA cycle including citrate synthase (GltA), isocitrate lyase (AceA), succinyl-CoA synthase (SucD), malic enzyme (MaeAB), and PEP carboxykinase (PckA) showed 40% lower expression under ammonium limitation compared to glucose-limited cultures (Hua et al., 2004, Folsom and Carlson, 2015). Unlike TCA cycle genes, greater levels of

key glycolysis enzymes (Pgi, TpiA (triose phosphate isomerase), and GpmA (glycerate phosphoglycerate mutase)) and PPP enzymes (TktA, TktB (transketolase) and TalA, TalB (transaldolase)) are observed in ammonium-limited cultures compared to glucose-limited cultures at all growth rates (Hua et al., 2004, Folsom and Carlson, 2015). Also, ammonium-limited cultures consume glucose at a higher rate than glucose-limited cultures at all dilution rates (0.1-0.4 h^{-1}), and cells show lower biomass yields (g cells per g glucose) under nitrogen limitation (Folsom and Carlson, 2015). For example, at 0.1 h^{-1}, the specific glucose uptake rate was 8.4 mmol carbon g^{-1} h^{-1} under glucose-limited conditions, but 17.4 mmol carbon g^{-1} h^{-1} in ammonium-limited chemostat cultures (Hua et al., 2003).

1.1.3 Phosphate limitation

Phosphate plays an important role in cellular energy management and growth. Growth under phosphate limitation (P-limitation) allows excess carbon and nitrogen for the production of industrial commodities. Phosphate influences energy, central carbon metabolism, and stress regulatory circuits (Schuhmacher et al., 2014). P-limitation also leads to uncoupling of anabolic and catabolic reaction, causing low biomass yield compared to N- and C- limitation (Dauner et al., 2001). Under P-limitation, organisms maintain high respiratory rates and high ADP availability which increases phosphate uptake from environment. Since many metabolites are phosphorylated, cells tend to regulate phosphate levels through dephosphorylation reactions. The oxidation of one mole of glucose to pyruvate generates 2 moles of ATP via the EMP pathway, but only 1.67 moles ATP via the PPP pathway, thus the latter pathway requires less phosphate for carbon metabolism. Expression of genes such as *pfkA* and *gltA* is downregulated by 5× in the later stages of P-limited batch *E. coli* cultures (van Bogelen et al., 1996). This decrease in *pfkA*

and *gltA* expression demonstrates that flux towards glycolysis and TCA cycle decreases at lower growth rates in P-limited cultures (van Bogelen et al., 1996).

1.1.4 Comparison of glucose, nitrogen, and phosphate limitation to affect metabolic nodes

Variation in the limiting nutrient and growth rate can affect the carbon flux towards the pathways involved in central carbon metabolism. Under glucose limitation, high growth rates cause a diversion of carbon flux towards PPP due to repression of glycolytic enzymes and TCA cycle while lower growth rates repress PPP genes (Kayser et al., 2005, Hardiman et al., 2007, Lemuth et al., 2008). Nitrogen limitation increases glycolytic flux and represses TCA cycle with no significant increase in carbon flux towards PPP at all growth rates (Hua et al., 2003). In contrast to glucose limitation, P-limited cultures showed greater flux towards PPP at lower growth rates but increasing growth rates exhibited no significant increase in PPP flux compared to other limitations (Dauner et al., 2001).

1.2 ENZYMES: FUNCTION, KINETICS, ENGINEERING

In general, there are two genetic/enzymatic strategies to alter the flux distribution between these central metabolic pathways: either increasing or reducing the expression or activity of key enzymes at a branchpoint. Overexpressing genes from either pathway can redirect carbon flux to that pathway. In *E. coli* and many other bacteria, glucose is transported and phosphorylated mainly by the phosphoenol:pyruvate:sugar phosphotransferase (PTS) system to glucose-6P that is catabolized (Erni, 1989). In absence of PTS system, *E. coli* uses glucokinase to phosphorylate glucose and other glucose-containing disaccharides (Meyer et al., 1997). Glucose-6P is later distributed between three pathways the glycolysis, PPP, and EDP (Holms, 1986). In this section, enzymes involved in metabolic nodes of glycolysis and PPP will be discussed.

1.2.1 Pentose phosphate enzymes

Because entry into the oxidative PPP generates 2 mol NADPH/mol glucose-6P and pentose sugar phosphates with a loss of carbon dioxide, the flux distribution between the EMP and the PPP impacts availability of PPP products to perform reduced biosynthetic reactions and anabolism of essential metabolites including amino acids and nucleotides (Wood, 1986; Romeo and Snoep, 2005). Besides native metabolism, overexpression of enzymes in PPP has been used to increase the production of NADPH-dependent biochemicals including 3-hydroxybutyrate (Perez-Zabaleta et al., 2016), riboflavin (Lin et al., 2014), lycopene (Alper et al., 2005), mevalonate (Li et al., 2021). This section describes the enzymes of interest in pentose phosphate pathway.

1.2.1.1 Glucose-6-phosphate dehydrogenase and 6-Phosphogluconate dehydrogenase

Glucose-6P dehydrogenase [D-glucose-6-phosphate: nicotinamide adenine dinucleotide phosphate (NADP) oxidoreductase, EC 1.1.1.49, encoded by *zwf*] catalyzes the first step for entry in PPP and oxidizes glucose-6P to generate 6-phosphogluconate, a mole of NADPH and a mole of CO_2 (Scott and Cohen, 1953). Sequentially, 6-phosphogluconate is oxidized by 6-phosphogluconate dehydrogenase (6PGDH, EC:1.1.1.44, encoded by *gnd* gene) in the central carbon metabolism (Berg et al., 2002, 5th edition). The sequential reaction catalyzed by these enzymes is below:

$$\text{Glucose-6P} + 2\ NADP^+ + 2\ H_2O \rightarrow \text{ribose-5P} + 2\ NADPH + 2\ H^+ + CO_2$$

These two enzymes are source of NADPH in PPP therefore, overexpression of *zwf* or *gnd* increases the intracellular NADPH/$NADP^+$ ratio by 3-6× compared to wild-type *E. coli* (Lim et al., 2002). Overexpression of *zwf* does not significantly change glucose uptake rate or specific growth rate in *E. coli* under batch conditions with glucose as the sole carbon source (Nicolas et

al., 2007). Overexpression of *zwf, gnd* (expressing 6-phosphogluconate dehydrogenase), *ppnK* (expressing NAD kinase), *pntAB,* or *sthA* improved the NADPH-dependent formation of the antibiotic bacitracin in *Bacillus licheniformis*. The strain overexpressing *zwf* exhibited the greatest increase of bacitracin (12%) compared to the wild type (Zhu et al., 2019). In a Δ*zwf* strain, malic enzyme contributes about 6% of the NADPH needed for biosynthesis, whereas overexpression of *zwf* eliminates the malic enzyme contribution to NADPH generation, similar to the negligible contribution in a wild-type strain (Nicolas et al., 2007). Overexpressing *zwf* or suppressing *pfkA* through CRISPRi improved mevalonate production through EP-bifido pathway in recombinant *E. coli*. The EP-bifido pathway is combination of the EMP, the PPP, and a bifido shunt to reduce carbon dioxide loss and produce more acetyl-CoA from glucose (Li et al., 2021).

Overexpression of *zwf* and 3-hydroxybutyrate producing genes from *Halomonas boliviensis* in recombinant *E. coli* improved 3-hydroxybutyric acid (3-HB) production from 0.5 g/L to 1 g/L. Further, N-limited fed-batch cultures overexpressing *zwf* produced 12.7 g/L 3-HB in 30 h. N-limitation was used to control the growth rate and restrict the TCA cycle by the accumulation of NADH, which inhibits citrate synthase and leads to acetyl-CoA accumulation. Acetyl CoA is a primary metabolite towards 3-HB production thus increased acetyl-CoA pools can improve 3-HB (Perez-Zabaleta et al., 2016).

Overexpression of *zwf* in a γ-poly glutamic acid (γ-PGA)-producing *Bacillus lichenformis* strain generated 9.13 g/L γ-PGA, 35% higher than control strain. Overexpression of *zwf* also displayed lower growth and glucose uptake rates while limiting production of byproducts acetoin and 2,3 butanediol (Cai et al., 2017). *E. coli* containing riboflavin-producing genes and overexpressing *zwf, gnd* (from *Corynebacterium glutamicum*), *pgl*, and *acs* (encoding acetyl

CoA synthase) and deleting *pgi* and ED pathway genes generated 582.2 mg/L, twice as great as the control strain (Lin et al., 2014).

1.2.2 Glycolytic enzymes

Flux distribution and cell physiology are affected by knocking out key genes at the beginning of either the EMP or PPP. This section discusses key enzymes in upper glycolysis.

1.2.2.1 Phosphoglucose isomerase

Phosphoglucose isomerase (EC 5.3.1.9, encoded by *pgi*) catalyzes the reversible isomerization of glucose-6P to fructose-6P and both hexose phosphates exists in mixtures called as "Embden ester" at an equilibrium (Mann and Lutwak-Mann, 1944). K_M values for substrates glucose-6P and fructose-6P are 1.02 mM and 0.08 mM, respectively, while phosphoenolpyruvate serves as an inhibitor (K_i 0.26 mM) (Ogawa et al., 2007). Because Pgi catalyzes a reversible reaction, maximum velocities are the same in both directions (Kahana et al., 1960).

Pgi is the first step of glycolysis, and Pgi mutants have been studied for their effect on cell growth on different substrates (Fraenkel and Levisohn, 1967; Kabir and Shimizu, 2003) and cell physiology (Hua et al., 2003). For a Δ*pgi* strain, excess NADPH generated through PPP (2 mol/mol glucose) causes 13% of glucose through the EDP, a pathway which generates only 1 mol NADPH/mol glucose (Hua et al., 2003). Decreasing the expression of the *pgi* gene compared to the wild-type activates the glyoxylate shunt, suggesting that *E. coli* with lower *pgi* expression uses the glyoxylate shunt instead of PEP carboxylase for the anaplerotic generation of oxaloacetate (Usui et al., 2012). However, carbon flux into the glyoxylate shunt reduces significantly to 20% in a Δ*pgi* strain compared to cells merely with a low expression of *pgi* (40%) (Usui et al., 2012). Cells also respond to a *pgi* knockout by reducing flux through NADPH-generating enzymes such as isocitrate dehydrogenase (Usui et al., 2012). Not quite as

severe as a Δ*pfkA* deletion, a Δ*pgi* knockout impairs growth by 70-80% because of the limited capacity of the PPP and the excess NADPH (Canonaco et al., 2001; Long et al., 2018). Evolution studies using *E. coli* Δ*pgi* conducted for 50 days in continuous cultures led to mutations in transhydrogenases, stress response enzymes, and the *crr* gene coding the cytosolic subunit of enzyme II in the PTS glucose transport system (Long et al., 2018). Also, a Δ*pgi* strain evolves to increase flux into the EDP and then towards non-oxidative PPP. Mutations occur in transhydrogenase and isocitrate lyase which alter their specificity from NADPH to NADH generation (McCloskey et al., 2018). These results demonstrate the evolutionary pressure for a Δ*pgi* strain to improve its growth and NADPH oxidation (Long et al., 2018). Introduction of NADPH utilizing pathway like poly(hydroxybutyrate) does improve the cell growth by 18% in a Δ*pgi* strain (Kabir and Shimizu, 2003).

Although a *pgi* deletion decreases growth of *E. coli* on glucose, a Δ*pgi* strain grows well on alternative carbon sources and mixtures of carbon sources with glucose (Ahn et al., 2011). Deletions in *mgsA* (coding methylglyoxal synthase), *pgi*, and *ptsG* (coding Enzyme IICB of the PEP-dependent sugar phosphotransferase system) enable *E. coli* to consume multiple sugars simultaneously but glucose at a lower rate (Yao et al., 2011). Catabolite repression relaxes in these gene knockout strains because the transcript levels of *crp* (encoding cAMP-activated global transcriptional regulator CRP) increases and inactivates *ptsG* (Yao et al., 2011). A Δ*pgi* strain grows 2× faster on a fructose-glucose medium than on a glucose-only medium (Ahn et al., 2011).

1.2.2.2 Phosphofructokinase

6-Phosphofructokinase (EC 2.7.1.11, Pfk, encoded by *pfkA* and *pfkB*) catalyzes the irreversible phosphorylation of fructose-6P to fructose-1$6P_2$ (Blangy et al., 1968). Pfk exists as two isoenzymes: an allosteric PfkA that accounts for 90% of the activity and non-allosteric PfkB

(Robinson and Fraenkel, 1978; Kotlarz and Buc, 1977; Babul, 1978). PfkA is allosterically inhibited by phosphoenolpyruvate (PEP), shows cooperativity with fructose-6P and hyberbolic kinetics with ATP (Blangy et al., 1968). Monophosphonucleosides (AMP), fructose-6P, diphosphonucleosides (ADP, GDP) are the activators of PfkA (Atkinson and Walton, 1965).

Deletion of *pfkA* or *pfkB* coding phosphofructokinase genes directs carbon flux towards the PPP (Siedler et al., 2011, Wang et al., 2013). A Δ*pfkA* strain still shows 20-30% of residual phosphofructose kinase activity due to the isoenzyme coded by the *pfkB* gene (Siedler et al., 2011, Siedler et al., 2012). As a consequence of a *pfkA* deletion and the resulting limited availability of phosphoenolpyruvate (PEP), glucose uptake rate slows by 64-75% (Siedler et al., 2012). Also, deletion of *pfkA* directs 62% of carbon towards PPP compared to 11% in the wild-type strain (Hollinshead et al., 2016). The double mutant Δ*pfkA* Δ*pfkB* fails to grow on glucose because neither the EDP nor the PPP can exclusively support cell growth (Fischer and Sauer, 2003; Lovingshimer et al., 2006; Wang et al., 2013).

Growth of Δ*pfkA* strains on glucose as the sole carbon source results in partial cyclization of carbon through the PPP because negative net flux was observed from glucose-6P to fructose-6P catalyzed by a reversible enzyme Pgi (Siedler et al., 2012). That is, fructose-6P generated from PPP partially is converted to glucose-6P. Also, flux towards triose-3P increases to divert a limited carbon from PPP towards lower glycolysis in absence of phosphofructokinase A (Siedler et al., 2012).

Despite catabolite repression which typically inhibits microbes such as *E. coli* from consuming multiple sugars simultaneously such as xylose in the presence of glucose (Magasanik, 1961, Desai and Rao, 2010), a Δ*pfkA* strain metabolizes glucose and xylose simultaneously and also exhibits 2× the growth rate in this mixture compared to a glucose-only medium. Thus,

deleting the *pfkA* gene mitigates catabolite repression in *E. coli* (Hollinshead et al., 2016). The EMP enzymes phosphofructokinase and pyruvate kinase regulate gluconeogenesis under glucose excess, and a wild-type *E. coli* does not consume non-sugar metabolite such as acetate (Hollinshead et al., 2016). However, a Δ*pfkA* strain can co-metabolize acetate and glucose to compensate for the low EMP flux, leading to gluconeogenesis for utilization of non-sugar substrates by *E. coli* (Hollinshead et al., 2016). Unlike xylose, the presence of acetate in a glucose defined medium does not increase the growth rate of a Δ*pfkA* strain (Hollinshead et al., 2016). Deletion of *pfkA* in a 1,3-diaminopropane (1,3-DAP)-producing *E. coli* strain (overexpressing *ppc* and *aspC*) improved the titers of 1,3-DAP from 0.2 g/L to 1.4 g/L. Fed-batch fermentation using this strain produced 13 g/L 1,3-DAP (Chae et al., 2015).

The reduction of β-keto ester methyl acetoacetate to the chiral hydroxy ester (R)-methyl 3-hydroxybutyrate (MHB) is catalyzed via a biotransformation by an R-specific alcohol dehydrogenase (Siedler et al., 2011). Deletion of *pfkA* increased the yield to 4.78 mol MHB/mol glucose (Siedler et al., 2012). The reduction of 2-chloroacrylate to 2-chloropropionic acid is mediated by NADPH-dependent 2-haloacrylate reductase from the soil bacterium *Burkholderia* in a one-step bioconversion process (Wang et al., 2013). *E. coli* with a *pfkA* knockout and overexpressing NADPH-dependent GAP dehydrogenase improved 2-chloropropionic acid yield from 0.1 to 0.6 mol/mol glucose (Wang et al., 2013).

In contrast to a Δ*pfkA* strain, a Δ*pfkB* strain grows well on glucose as the sole carbon source (Wang et al., 2013). In some bacteria such as *Corynebacterium glutamicum* growing on glucose the deletion of *pfkB1* increases glycolytic flux by 10% compared to wild-type *C. glutamicum* (Hasegawa et al., 2016). Interestingly, addition of fructose increases glucose consumption rate by 2× in *C. glutamicum* Δ*pfkB* (Hasegawa et al., 2016).

1.2.3 TCA cycle

1.2.3.1 Isocitrate dehydrogenase

Isocitrate dehydrogenase (IDH) [D_s-*threo*-isocitrate $NAD(P)^+$ oxidoreductase (decarboxylating), EC 1.1.1.42] is an $NADP^+$-dependent dehydrogenase, a key enzyme at the branch point of TCA cycle and glyoxylate shunt (Lee et al., 1995). IDH catalyzes the decarboxylation reaction to generate NADPH:

$$\text{isocitrate} + NADP^+ \rightarrow \alpha\text{-ketoglutarate} + NADPH + CO_2$$

IDH is a major NADPH contributor in wild-type *E. coli* cultivated under aerobic batch (2.3 mmol g^{-1} h^{-1}) (Sauer et al., 2004), C-limited (1.2 mmol g^{-1} h^{-1}) and N-limited (approx. 2.3 mmol g^{-1} h^{-1}) (Hua et al., 2003) cultures. Carbon flux towards IDH reaction decreases by 78% in a Δ*zwf* strain cultivated under N-limited conditions but remains similar under glucose limitation compared to wild-type (Hua et al., 2003). However, a Δ*pgi* strain showed a 70% decrease in carbon flux in IDH reaction compared to wild-type in glucose-limited cultures (D of 0.1h^{-1}) (Hua et al., 2003). Overexpression of IDH increased the production of NADPH-requiring GDP-D-fucose concentration to 5.8 mg/L, 31% higher than the wild-type *E. coli* strain (Lee et al., 2011).

1.2.3.2 Malic enzyme

$NADP^+$-dependent malic enzyme (EC 1.1.1.40, encoded by *maeB* gene) catalyzes the oxidative decarboxylation of malate to pyruvate and CO_2 in the presence of Mg^{2+} metal (Bologna et al., 2007). Malic enzyme facilitates the conversion of C3 to C4 metabolites, thus overexpression of *maeB* increased the production of C4 metabolites 2× in *E. coli* under anaerobic conditions (Kwon et al., 2007). Levels of C4 metabolites such as succinic acid can be increased with overexpressing *maeB* (Shin et al., 2007).

1.2.4 Acetyl-CoA forming enzymes/degradation pathways

1.2.4.1 Acetyl-CoA synthase

Acetyl-CoA synthase (ACS, EC 6.2.1.1, encoded by *acs*) catalyzes an ATP-dependent irreversible conversion of acetate to acetyl-CoA via intermediate acetyl phosphate (Berg 1956). In *E. coli*, cells secrete acetate while growing aerobically in presence of excess glucose (Eiteman and Altman, 2006). Acetate is assimilated through ACS induction due to various metabolic factors including high cyclic AMP levels, stationary phase, transcription factors IclR and FadR (regulate glyoxylate shunt), absence of catabolite repression, oxygen regulator FNR, and decrease in acetyl-CoA pools (Kumari et al., 2000). ACS has a K_M of 0.2 mM for acetate (Brown et al., 1977). Cells growing at higher growth rate are unable to assimilate acetate due to repression of ACS activity by catabolite repression in presence of glucose leading to overflow metabolism (Eiteman and Altman, 2006; Valgepea et al., 2010).

A reductive acetyl-CoA pathway known as the Wood-Ljungdahl pathway is used by anaerobes such as sulfate reducers, methanogens, and acetogens to convert CO or CO_2 to biomass. The conversion is catalyzed by a bifunctional nickel-iron-sulfur enzyme called carbon monoxide dehydrogenase/acetyl-CoA synthase (CODH/ACS) where CODH reduces CO_2 to CO and the latter facilitates condensation of CO, a methyl group, and CoA for acetyl-CoA formation (Seravalli et al., 2002).

ACS is responsible for acetate assimilation which leads to a greater interest in modifying ACS enzyme or *acs* allele to control acetate consumption via genetic and protein engineering. Deletion of *acs* gene leads to poor growth of *E. coli* cells on acetate as a sole carbon source and eliminates conversion of acetate to acetyl-CoA for biomass and energy generation (Kumari et al., 2000). Ovrexpression of ACS has been studied to increase acetyl-CoA pools (Zhang et al., 2019;

Wegner et al., 2021), decrease acetate accumulation (Lin et al., 2006), or increase acetate consumption (Ding et al., 2015; Novak et al., 2018; Song et al., 2018). Protein engineering using site-directed mutagenesis of ACS broadens the substrate range of the enzyme (Sofeo et al., 2019). High concentration of acetyl-CoA inhibits ACS therefore replacing *E. coli* ACS with a feedback insensitive acetyl-CoA synthase from *Salmonella faecalis* improves availability of acetyl-CoA for acetyl-CoA-derived products (Wegner et al., 2021).

1.2.4.2 Pyruvate dehydrogenase complex

Pyruvate dehydrogenase complex includes 24 units of pyruvate dehydrogenase (E1, EC 1.2.4.1, encoded by *aceE*), 24 units of dihydrolipoamide acetyltransferase (E2, EC 2.3.1.12, encoded by *aceF*), and 12 units lipoamide dehydrogenase (E3, EC 1.6.4.3, encoded by *lpdA*) in *E. coli* (Arjunan et al., 2002). The complex catalyzes oxidative decarboxylation of 3-carbon pyruvate to acetyl CoA catalyzing the following overall reaction (Koike et al., 1960, Arjunan et al., 2002):

$$\text{Pyruvate} + \text{CoA} + \text{NAD}^+ \rightarrow \text{acetyl-CoA} + \text{NADH} + \text{CO}_2$$

The PDH complex is expressed under a single operon and regulated by PdhR transcription factor (Quail et al., 1994), substrate (pyruvate, CoA), the cofactor thiamine diphosphate (Hennig et al., 1997), NAD/NADH (Hansen and Henning, 1966), Mg^{2+} (Arjunan et al., 2002), and products (Schwartz and Reed, 1970). High NADH/NAD ratio inhibits the lipoamide dehydrogenase component of the complex especially when switching from aerobic to anaerobic conditions (Hansen and Henning, 1966; Shen and Atkinson, 1970). While not as strong an inhibitor as NADH, acetyl-CoA/CoA ratio above 0.8 inhibits the complex by 57% (Hansen and Henning, 1966). Elevated glycolytic intermediates like fructose-16P_2 also enhances the rate of conversion of pyruvate to acetyl-CoA (Shen and Atkinson, 1970). Accumulation of acetyl-CoA inhibits the

first component pyruvate dehydrogenase of PDH complex (Shen and Atkinson, 1970; Schwartz and Reed, 1970). Binding of pyruvate to the active loop (residues 401-413) in E1 component (AceE) initiates communication between E1-E2 subunits of the PDH complex (Kale et al., 2007). The rate limiting enzyme AceE has a k_{CAT} of 38 s^{-1} and K_M of 0.26 mM for pyruvate (Kale et al., 2007).

To control the flux at pyruvate node, the AceE enzyme is generally targeted to modulate PDH complex (Zhu et al., 2008, Moxley and Eiteman, 2021, Ziegler et al., 2021). Pyruvate accumulation improves by limiting/eliminating conversion of pyruvate to acetyl-CoA (Zhu et al., 2008; Moxley and Eiteman, 2021). Deletion of *aceE* gene completely eliminates the activity and leads to acetate/acetyl-CoA auxotrophy (Tomar et al., 2003; Zelić et al., 2003; Maleki et al., 2018). Modulating the enzyme activity through RNA silencing (Nakashima et al., 2014), protein engineering (Moxley and Eiteman, 2021), and CRISPR interference (Ziegler et al., 2021) increases the pyruvate yield without growth requirement on acetate.

The E3 component (Lpd) of PDH complex is inhibited by high concentrations of NADH (Shen and Atkinson, 1970), therefore replacing NADH sensitive AceE with a thermophilic bypass PDH enzyme system consisting pyruvate decarboxylase (from *Acetobacter pastuerianus*) and CoA-acylating aldehyde dehydrogenase (from *Thermus thermophilus*) lead to 65 % acetyl-CoA molar yield in a biotransformation reaction (Krutsakorn et al., 2013). Modifying active residues of Lpd component using site directed mutagenesis lowers the NADH sensitivity of the PDH complex (Sun et al., 2012; Wang et al., 2018) and restores the cell growth under anaerobic conditions (Sun et al., 2012).

1.2.4.3 PTA-ACKA

Conversion of acetyl-CoA to acetate is performed through a sequence of two reactions: phosphorylation of acetyl-CoA to acetyl-phosphate by phosphate acetyltransferase (PTA, EC 2.3.1.8, encoded by *pta*) (Shimizu et al., 1969) and dephosphorylation of acetyl-P to acetate by acetate kinase (ACKA, EC 2.7.2.1) (Fox and Roseman, 1986). These cascade reactions are reversible where net production/utilization of acetate is thermodynamically controlled by the extracellular concentration of acetate (Enjalbert et al., 2017). PTA has a K_M of 0.045 mM and k_{CAT} of 29.6 s^{-1} for acetyl-CoA as a substrate while acetyl-CoA-forming reaction has a k_{CAT} of 227 s^{-1} and K_M of 0.9 mM for acetyl-P (Campos-Bermudez et al., 2010). ACKA has approximately 40× affinity for acetyl-P (K_M of 0.16 mM) than acetate (K_M of 7 mM) (Fox and Roseman, 1986) and 2× greater catalytic activity towards acetate formation (Tang et al., 2014).

Deletion of *ackA*, *pta*, or *ackA-pta* in *E. coli* cells slightly decreases growth rate and reduces acetate formation under aerobic conditions, while these deletions reduce growth rate by 34-62% and increase lactate formation under anaerobic conditions compared to the wild-type (Schütze et al., 2020). Gene deletions of Pta-AckA pathway have been attempted to improve acetyl-CoA derived products (Centeno-Leija et al., 2014; Parimi et al., 2017; Wu et al., 2020; Atsumi et al., 2008) or study microbial physiology (Dittrich et al., 2005; Schütze et al., 2020).

1.2.4.4 Pyruvate oxidase

Pyruvate oxidase (POXB, EC 1.2.5.1, encoded by *poxB*) catalyzes the oxidative decarboxylation of pyruvate to acetyl-P and CO_2 in the presence of cofactors thiamine pyrophosphate (TPP) and flavin adenine dinucleotide (Cunningham and Hager, 1971). Binding of POXB to the phospholipid bilayer activates the enzyme and increases its affinity towards pyruvate and TPP (Chang and Cronan, 1984). Reduction of enzyme-bound flavin on the

peripheral membrane leads to binding of C terminus and transferring 2 electrons to ubiquinone 8, a mobile carrier of electron transport chain (Neumann et al., 2008). Absence of PDH complex or presence of fatty acids activates PoxB for acetyl-CoA production for biomass and metabolites formation (Fleischer et al., 1961), therefore PDH mutants require acetate supplementation for growth (Parimi et al., 2017). Activation of POXB to consume pyruvate causes the energy deficiency of 16 kcal per mole of pyruvate to yield acetyl-CoA because of ATP consumption from acetate to acetyl-CoA reaction by PTA (Cunningham and Hager, 1971). Presence of high pyruvate levels also activates POXB through POXB binding to membrane and increasing k_{CAT} by 30-fold and decreasing K_M for pyruvate by 8-fold (Neumann et al., 2008).

A *poxB* deletion has been used to decrease the acetate production from pyruvate to manipulate pyruvate node to induce physiological changes (Dittrich et al., 2005; Valgepea et al., 2010) and increase yields of pyruvate-derived products (Moxley et al., 2023, Parimi et al., 2017, Wu et al., 2020).

1.2.4.5 Acetyl-CoA transferase

Acetyl-CoA transferase (EC 2.3.1.16, encoded by *atoB*) catalyzes reversible reaction of acetyl-CoA to acetoacetyl-CoA (Feigenbaum and Schulz, 1975). The enzyme shows specificity to acetoacetyl-CoA and induced in presence of acetate (Duncombe and Frerman, 1976). The tetrameric enzyme AtoB has a K_M of 0.017 mM and k_{CAT} of 220 s^{-1} for acetoacetyl-CoA substrate reaction while for substrate acetyl-CoA, a K_M of 0.138 mM and k_{CAT} of 6.5 s^{-1} which shows greater specificity of enzyme towards acetoacetyl-CoA degradation (Ithayaraja et al., 2016).

Overexpression of *atoB* has been used to increase acetyl-CoA based products including mevalonate (Satowa et al., 2020), propane (Menon et al., 2015), and butanol (Kim et al., 2015).

1.2.4.6 Acetyl-CoA carboxylase

Acetyl-CoA carboxylase complex in *E. coli* is composed of three catalytic subunits acetyl-CoA carboxytransferase α unit (AccA), carboxytransferase β unit (AccD), and biotin carboxylase (AccC) plus a carrier protein (AccB) (Bilder et al., 2006). Enzyme acetyl-CoA carboxytransferase (EC 2.1.3.15) comprising both units (AccA-AccD) decarboxylates acetyl-CoA to malonyl-CoA, second reaction of Acetyl-CoA carboxylase complex in the fatty acid synthesis cycle (Bilder et al., 2006) as well as last step of aerobic β-oxidation (Campbell et al., 2003). Enzyme is inhibited by acylated derivatives of acyl-carrier protein (ACP) having chain lengths of C6-C20 atoms (Davis and Cronan, 2001). Also, overexpression of thioesterases leads to cleavage of acyl-ACPs to fatty acids and can relieve the inhibition of fatty acid synthesis (Jiang and Cronan, 1994). For this enzyme, K_M apparent for acetyl-CoA is 0.018 mM (Soriano et al., 2006) and malonyl-CoA is 0.04 mM while k_{CAT} is 211 min^{-1} (Meades et al., 2010).

Overexpression of ACC increases the malonyl-CoA levels involved in fatty acid biosynthesis (Davis et al., 2000) and malonyl-CoA derived product such as 3-hydroxypropionic acid (Wang et al., 2022).

1.2.4.7 Citrate synthase

Citrate synthase (EC 2.3.3.1, encoded by *gltA*) catalyzes the aldol-Claisen condensation of acetyl-CoA and oxaloacetate for citrate formation (Weigand and Remington, 1986). Citrate synthase diverts more than 60% of acetyl-CoA towards TCA cycle (Zhao et al., 2004) and is a key metabolic node in central metabolism into the TCA cycle for biomass, organic acids and precursor synthesis (Weitzman 1966; Danson and Weitzman, 1973). In Gram-type negative bacteria like *E. coli* citrate synthase exists as a type II hexameric form that is allosterically regulated by NADH under aerobic conditions (Duckworth and Tong, 1976; Weitzman and

Dunmore, 1969). Loss of ability to form hexamers diminishes allosteric inhibition by NADH (Stokell et al., 2003), and causes the Type II citrate synthase to exist in dimeric form similar to type I citrate synthase found in Gram-type positive microbes (Eikmanns et al., 1994; Jin and Sonenshein, 1996) and eukaryotes (Sievers et al., 1997; Eikmanns et al., 1994; Grossebüter and Görisch, 1985; Weigand and Remington, 1986). Type II citrate synthase is comprised of 430 amino acids and has molecular weight of about 48 kDa, 280 kDa in hexameric form (Tong and Duckworth, 1975; Anderson and Duckworth, 1988; Sievers et al., 1997). The metabolite α-ketoglutarate competitively inhibits the enzyme (Anderson and Duckworth, 1988) which was previously considered to be allosteric inhibition (Weitzman and Dunmore, 1969). Type II citrate synthase has a k_{CAT} of 81 s^{-1} and K_M of 0.026 mM for oxaloacetate and 0.120 mM for acetyl-CoA (Pereira et al., 1994).

Genetic engineering of *gltA* leads to improvement of acetyl-CoA based products such as citramalate (Wu and Eiteman, 2016), lysine (van Ooyen et al., 2012), and mevalonate (Satowa et al., 2020). Overexpression of *gltA* improved the vanillin production in a Δ*icd E. coli* strain by two-fold in the complex medium (Lee et al., 2008). Enzyme engineering of citrate synthase modified its activity and affected production acetyl-CoA-derived products like acetate (Tovilla-Coutiño et al., 2020), citramalate (Wu et al., 2020), and propanediol (Lee et al., 2019).

1.3 ACTIVE SITE RESIDUES OF CITRATE SYNTHASE AND PFKA

1.3.1 Active Site Residues of Citrate synthase

Due to its location at metabolic node and allosteric properties, structure function properties, the allosteric and physiological characteristics of Type II citrate synthase have been investigated thoroughly (Handford et al., 1987; Donald et al., 1991; Pereira et al., 1994; Stokell et al., 2003; Maurus et al., 2003). Residues H264, D362, and F383 are involved in acetyl-CoA

binding while oxaloacetate binds to residues H229, H305, R314L, R387, and R407 of the enzyme (Pereira et al., 1994). Substitutions H264A, D362A, and F383A displayed a 97-99% decrease in k_{CAT} compared to the wild-type, while F383A also increased K_M for acetyl-CoA by 17× (Pereira et al., 1994). H229Q substitution decreased k_{CAT} by 88% and increased K_M by 17× for oxaloacetate (Anderson and Duckworth, 1988), while H305A and R314L led to more than 99% decrease in catalytic activity (Anderson and Duckworth 1989). Crystalline structure of the enzyme revealed that the polypeptide chain (residues 267-297) adjacent to the H264 residue is extremely mobile and undergoes conformational refolding upon binding of acetyl-CoA to the enzyme, and it plays a critical role in substrate binding in Type II citrate synthase (Nguyen et al., 2001). NADH binds to six equivalent sites close to the dimer-dimer point of contact of citrate synthase enzyme where each hexamer has three identical sites in both direction (Maurus et al., 2003). NADH inhibition increased in substitutions R167L by 77% and T111A by 87% whereas NADH binding increased by nearly 2× in R109L mutant (Stokell et al., 2003). Hexamer formation is essential for NADH allosteric inhibition, and this inhibition is curtailed by substitutions in residues R163L and K167A (Stokell et al., 2003).

1.3.2 Active Site Residues of Phosphofructokinase A

The PfkA tetrameric enzyme shows cooperative kinetics with fructose-6P, hyperbolic kinetics with ATP, allosteric activation by ADP and GDP, and inhibition by phosphoenolpyruvate (PEP) (Berger et al., 1992).

At the active site, the aspartate group serves an essential role for phosphoryl group transfer from ATP to the enzyme. D127 acts as a base in the reaction mechanism of phosphoryl transfer and facilitates the nucleophilic attack of the 1-hydroxyl group of fructose-6P by the γ-phosphoryl group of the ATP. Moreover, D127 also reduces the affinity of the enzyme towards

product fructose-16P_2 due to repulsion between negatively charged carboxyl group and the newly formed 1-phosphate (Shirakihara and Evans 1988). The PfkA variant D127S showed a very low turnover number of 0.0052 s^{-1} (1/18000 of wild-type) in forward reaction with fructose-6P, and a lower K_M of 8 mM (1/45 of wild-type) for fructose-16P_2 in reverse reaction (Hellinga and Evans 1987). Similarly, D127E lowered k_{CAT} by 99% and D127Y lowered k_{CAT} by 99.8% (Berger et al., 1992), while D127A lowered k_{CAT} by 99.99% (1/44000 of wild-type) (Zheng and Kemp, 1994 a), showing the importance of D127 in PfkA catalysis. The spatially adjacent arginine residue R171 has a comparatively minor effect on phosphorylation. R171S lowered k_{CAT} by a factor of 1/3.4 (Hellinga and Evans, 1987), while the R171H substitution decreased k_{CAT} by 48% and increased K_M (fructose-6P) by about 3.4× (Zheng and Kemp, 1994a). Another aspartate residue (D129) interacts with two water molecules stabilizing the Mg^{2+} ion for which proper orientation is important for phosphate transfer (Shirakihara and Evans, 1988). The D129S substitution lowered k_{CAT} by 99.8% (Berger and Evans, 1992; Zheng and Kemp, 1994a). Besides D127 and D129, D103 is also ionizable and interacts with the ATP-Mg^{2+} complex (Laine et al., 1992). D103 and D129 both are important to position Mg^{2+} and stabilize the transition state. The D103A substitution in *E. coli* PfkA had no effect on K_M but lowered the k_{CAT} by 96% (Berger and Evans, 1992).

R72 of the *E. coli* ATP-dependent PfkA stabilizes the transition state by interacting with the 6-phosphate of fructose-6P (Zheng and Kemp, 1992). R72H decreased k_{CAT} by nearly 99.8% at pH 8.5 relative to the wild-type enzyme (Zheng and Kemp, 1994a). Several other arginine residues, R162, R243, and R252, are positioned near and interact with the 6-phosphate of fructose-6P (Shirakihara and Evans, 1987). The R162S substitution increased K_M by 53×, while the R243S substitution increased K_M by 162× with little change in k_{CAT} (Berger and Evans,

1990). In another study, the substitution R252Q decreased k_{CAT} 95% and increased K_M by 1600× (Zheng and Kemp, 1994b). The R252 and R243 residues in the fructose-6P binding site for the *E. coli* enzyme are equivalent to R315 and R326, respectively, in the pyrophosphate-dependent enzyme from *P. freundenreichii* (Xu et al., 1994). Two highly conserved residues near the active site of *E. coli* PfkA are I126 and N128 which do not participate directly with substrate binding (Zheng and Kemp, 1994b). The I126 and D12 residues are believed to stabilize R252 and orient the guanidinium group with fructose-6P (Zheng and Kemp, 1992). The absence of I126 can induce the R252 side chain to "flop around" into the binding cleft and affect the reaction. The I126A substitution increased the K_M by nearly 600× and decreased k_{CAT} by 61.5% (Zheng and Kemp, 1992). Similarly, the I126S substitution increased the K_M by nearly 300× and decreased k_{CAT} by 72% (Zheng and Kemp, 1994b).

1.4 GENETIC ENGINEERING STRATEGIES TO INCREASE ACETYL-COA POOLS OR DERIVED PRODUCTS

Acetyl-CoA is a precursor for various biochemicals including acetone (May et al., 2013) and 1-butanol (Atsumi et al., 2008). Strategies to improve bacterial acetyl-CoA formation from glucose have been reviewed extensively (Zhu et al., 2022).

One method to increase the acetyl-CoA pool is the use of phosphoketolase (PKT) from *Bifidobacteria* species to bypass pyruvate dehydrogenase and accumulate acetyl-CoA, avoiding carbon loss due to CO_2. This pathway is known as the bifido-shunt pathway (Chinen et al., 2007) or non-oxidative glycolysis (NOG) and requires the elimination of competing genes responsible for byproducts and the EMP pathway (Bogorad et al., 2013). This pathway removes PEP dependent PTS system, bypasses lower EMP and diverts the carbon towards PPP and relies on PKT to generate acetyl-P from sugar phosphates like fructose-6P and xylulose-5P followed

by converting acetyl-P to acetyl-CoA using PTA (Chinen et al., 2007). Because NOG generates 2 moles of ATP from xylose and no reducing equivalents, it is not found in nature, as the pathway cannot be used for biomass synthesis and for products that require reducing equivalents (Bogorad et al., 2013). Even though non-oxidative PPP generates one mole of CO_2, it also provides 2 moles of NADPH, therefore the combination of PKT and PPP compensates for reducing equivalents for biomass and products without decreasing theoretical yield of acetyl-CoA on carbon significantly compared to just EMP (Henard et al., 2015). Another approach is to engineer a NOG strain through rational gene deletions followed by adaptive evolution to encourage biomass formation and pyruvate generation via malate using an active TCA cycle under aerobic conditions and 100% acetyl-CoA yield under anaerobic conditions using glucose as a carbon source (Lin et al., 2018).

A combination of Δ*ptsG::glk,* Δ*galR::zglf*, Δ*poxB::acs,* Δ*ldhA*, and Δ*pta* produced 62% of N-acetyl-glucosamine/glucose, a product of acetyl-CoA and glutamate in a biotransformation reaction (Zhang et al., 2019). Deletion of *pta-ackA* increased poly(3-hydroxybutyrate) yield on glucose by 48% and reduced acetate formation (Centeno-Leija et al., 2014). Overexpressing NADPH-dependent glyceraldehyde 3-phosphate to improve NADPH availability in a Δ*pta-ackA E. coli* strain increased poly(3-hydroxybutyrate) yield on glucose by 63% (Centeno-Leija et al., 2014). Blocking lactate and acetate formation leads to 3× greater pyruvate levels than wild-type in *E. coli* overexpressing isoprenoid pathway (Kim et al., 2016) and 10-20× pyruvate in 1-butanol producing strain (Atsumi et al., 2008). Preventing formation of byproducts lactate (deleting *ldhA* and *dld*), ethanol (deleting *adhE*), acetate (deleting *poxB* and *pta-ackA*), acetoacetate (deleting *atoDA*), and phosphoenolpyruvate (deleting *pps*) in *E. coli* strain overexpressing exogenous mevalonate pathway genes and isoprene synthase improved isoprene

production by 2× (1.8 g/L) from glycerol supplemented complex medium in shake flask cultures (Kim et al., 2016).

In *E. coli* BL21 (DE3), deletion of genes responsible for global transcriptional regulators IclR and ArcA decreases acetate by 70% but does not affect the cellular physiology including glucose uptake rate. The strain can also co-utilize glucose and acetate (Waegeman et al., 2012). For production of acetyl-CoA-derived products, often BL21 (DE3) is used due to its reduced catabolite repression and ability to reduce acetate formation (Liu et al., 2017; Perez-Zabaleta et al., 2019). Deletion of the *arcA* gene coding for global transcriptional factor ArcA, decreased acetate formation and improved acetyl-CoA-derived products phloroglucinol and 3-hydroxypropionic acid (Liu et al., 2016). Eliminating activity of another transcriptional factor in a Δ*iclR* strain, decreases acetate by 50% and improves production of phloroglucinol and 3-hydroxypropionic by 2× (Liu et al., 2017) but deleting both ArcA and IclR does not further improve the production of acetyl-CoA-derived compounds (Liu et al., 2017).

Acetyl-CoA intracellular concentration was reported to be 20% greater in a Δ*gltA* strain (Wu and Eiteman, 2016). In another work, increased acetyl-CoA pool was observed in strain having various deletions: Δ*gltA* (2×), Δ*ppc* (1.25×), and Δ*gltA* Δ*ppc* (1.5×) (Satowa et al., 2020).

1.5 PROTEIN ENGINEERING: GLYCOLYTIC ENZYMES

Engineering enzyme to impact the kinetic parameters can be accomplished by rational modification of the critical catalytic residues, adaptive evolution, or random mutagenesis (Moxley et al., 2021; Yang et al., 2023). These strategies can alter many facets of enzyme kinetics such as increase enzyme activity, modulate residues responsible for feedback inhibition, decrease substrate binding. For example, mutating the residues responsible for NADH binding in the E3 component of the PDH complex leads to an enzyme which is less sensitive to NADH

inhibition compared to the wild-type, and alters cell physiology (Wang et al., 2018). Saturation mutagenesis is a random mutagenesis technique to replace each single codon with all possible combinations. This approach often achieves desired catalytic characteristics but requires screening of multiple colonies (Yang et al., 2023). Enzyme engineering also allows a change in substrate affinity, allowing new 'non-native' substrates to undergo conversion. Such a strategy has been applied to increase the breath of substrate utilization by aldolase (Güclü et al., 2016) and acetyl-CoA synthetase (Sofeo et al., 2019), and also to change the affinity of acetoacetyl-CoA dehydrogenase from NADPH to NADH (Olavarria et al., 2022). Enzyme engineering has also been examined for its effects on product distribution: increased pyruvate by modification of pyruvate dehydrogenase (Moxley and Eiteman, 2021), increased acetate (Tovilla et al., 2020) or citramalate (Wu et al., 2020) by modification of citrate synthase.

1.6 MOTIVATION OF THIS WORK

Deletion of critical glycolytic enzymes to divert the carbon flow often leads to a significant growth defect in microbes using glucose as the sole carbon source (Sauer et al., 1999; Siedler et al., 2011) and in some cases, cells become auxotrophic (Gilvarg and Davis, 1956; Zelić et al., 2003). To overcome auxotophy and enable cell growth, medium is often supplied with either a specific substrate (e.g., acetate for pyruvate dehydrogenase complex mutant) (Zelić et al., 2003) or complex medium components (e.g., yeast extract, peptone) (Li et al., 2019; Taylor et al., 2023). Addition of undefined components like yeast extract and peptone increases the cost of scale-up as well as challenges the reproducibility of the process if obtained from different suppliers (Cardoso et al., 2020). Since most of the metabolic engineering work is performed at small scale (e.g., microtiter plates, shake flasks), the production cost of using complex medium components is often neglected in pursuit of developing novel synthetic biology

tools to improve yield and titer of product of interest. Development of a robust engineered strain with a deeper understanding of its physiology and metabolism at an early stage is imperative to translate technology for large scale biochemical production (Neubauer et al., 2013; Chubukov et al., 2016).

Genetic engineering is performed to optimize the carbon flow between biomass and product formation (Dittrich et al., 2005) to create a balance between yield and productivity. For example, since citrate synthase diverts more than 60% of carbon towards biomass formation through TCA cycle (Zhao et al., 2004), products that require acetyl-CoA invariably compete with the native pathway for the limited precursor (Wu et al., 2020). Therefore, deletion of citrate synthase eliminates the carbon flow towards TCA cycle and diverts acetyl-CoA towards product formation which significantly improved yield of acetyl-CoA derived products such as citramalate (Wu and Eiteman, 2016) and mevalonate (Satowa et al., 2020). Another strategy is protein engineering, where the activity of native enzymes that compete for precursors is reduced, creating a metabolic valve which also eliminates the auxotrophy and growth defect (Wu et al., 2020). For example, a Δ*pfkA* strain with a 70% lower growth rate than wild-type has been used for the production of biochemicals like lycopene (Wang et al., 2013) and 1,3 diaminopropane (Chae et al., 2015) at the cost of either productivity or medium components. Dynamic regulation using strategies such as CRISPRi (Li et al., 2021), induce gene degradation (Brockman and Prather, 2015) and quorum sensing (Gupta et al., 2017) have been used to trigger the *pfkA* gene inhibition/downregulation after certain time or biomass formation. However, most of these works were conducted at shake flask scale (Brockman and Prather, 2015; Li et al., 2021), and involve multiple plasmids and synthetic pathways to control the glycolytic flux via PfkA enzyme. To achieve an optimum control at metabolic node of central carbon metabolism, the key

hypothesis of this work is that rational protein engineering of enzymes will offer a simple strategy to alter the carbon flux between two competing pathways. Specifically, making targeted substitutions at PfkA and GltA will alter the metabolism of *E. coli* and increase the formation of products derived from acetyl-CoA, offering an alternative to outright deletion which either decreases production rate or requires complex medium components.

1.7 DISSERTATION OUTLINE

This dissertation work is divided into four sections. Chapter 2 is a literature review which details current understanding of the effects of nutrient limitation on cell physiology, maintenance, and product formation. Operational strategies such as batch, chemostat and fed-batch are critically investigated and reviewed (Rajpurohit and Eiteman, 2022).

Chapter 3 is a proof-of-concept work that targets the PfkA enzyme node of glycolysis with an intent to decrease carbon flow through phosphofructokinase enzyme. Because Pgi catalyzes a reversible reaction, the second step of glycolysis was selected for mutagenesis. The specific amino acid substitutions were conceptualized using a structure-guided approach to generate 22 variant strains. An initial shake flask screening using glucose as the sole carbon source revealed that 14 PfkA variants displayed similar growth as a Δ*pfkA* strain while other variants had intermediate growth rates between wild-type and the Δ*pfkA* strain. A nitrogen-limited chemostat process, known to increase glycolytic flux and acetate formation, was selected as a process to assess the metabolism of five strains: three PfkA variants having a range of growth rates, the wild-type strain, and a Δ*pfkA* strain. Under a nitrogen-limited process operating at 0.1 h^{-1}, *pfkA* alleles with greater maximum specific growth rate (μ_{max}) showed physiological properties such as glucose consumption rate and acetate formation rate similar to the wild-type. Also, intracellular metabolites including fructose-16P_2, glyceraldehyde 3-phosphate, acetyl-CoA,

and dihydroxyacetone are directly proportional to the μ_{max} of the PfkA variant strain. Mutation severity also affected transcript levels of *pfkA, zwf* and *pta* genes. This study highlights the function of PfkA variants to yield varying levels of glycolytic flux under carbon excess conditions at the same growth rate which otherwise is achieved during glucose-limited process by varying the dilution rate.

Chapter 4 considers the application of citrate synthase (GltA) variants to improve generation of the acetyl-CoA-derived product 3-hydroxybutyrate. The mutated alleles of *gltA* were chromosomally integrated into the *E. coli* W Δ*poxB* Δ*ldhA* Δ*pta-ackA* genotype to construct 5 GltA variant strains. GltA variants displayed significantly greater 3-HB yield than the wild-type in shake flask screening. Pyruvate accumulation was a metabolic bottleneck in these variants. Therefore, overexpression of thioesterases (*yciA* or *tesB*) or pantothenase kinase (encoded by *CoaA*) was examined during 3-HB formation, but these approaches did not significantly improve 3-HB yield. Indeed, *yciA* overexpression not only diminished both pyruvate and 3-HB production, but substantially increased acetate formation. Among the GltA variants, 3 strains with varying 3-HB yield on glucose were investigated at 1.25 L nutrient excess batch conditions. Accumulated pyruvate was assimilated to 3-HB and biomass in absence of glucose.

Chapter 5 explores the possibility of combining citrate synthase and phosphofructokinase variants for the production of mevalonate, biochemical that uses acetyl-CoA and NADPH. Based on previous chapters, four phosphofructokinase A variants were tested for mevalonate production using wild-type and a knockout strain as a control. With increase in severity of mutation in PfkA, mevalonate production decreased indicating that glycolytic product is also

limited by acetyl-CoA. Later, citrate synthase variant alleles were integrated in PfkA variants and showed improved mevalonate yield on glucose compared to the wild-type enzymes.

Chapter 6 summarizes the previous chapters, drawing conclusions on application of variants at metabolic nodes in central carbon metabolism.

1.8 REFERENCES

Ahn J, Chung BKS, Lee DY, Park M, Karimi IA, Jung JK, Lee H. 2011. NADPH-dependent *pgi*-gene knockout *Escherichia coli* metabolism producing shikimate on different carbon sources. FEMS Microb Lett 324:10-16.

Alper H, Miyakou K, Stephanopolous G. 2005. Construction of lycopene-overproducing *E. coli* strains by combining systematic and combinatorial gene knockout targets. Nat Biotechnol 23:612-616.

Anderson DH, Duckworth HW. 1988. *In vitro* mutagenesis of *Escherichia coli* citrate synthase to clarify the locations of ligand binding sites. J Biol Chem 263(5):2163-2169.

Anderson DH, Duckworth HW. 1989. Mutation of amino acids thought to polarize the oxaloacetate carbonyl in citrate synthase severely reduces but does not abolish activity of the enzyme. Biochem Cell Biol 67(2-3):98-102.

Arjunan P, Nemeria N, Brunskill A, Chandrasekhar K, Sax M, Yan Y, Jordan F, Guest JR, Furey W. 2002. Structure of the pyruvate dehydrogenase multienzyme complex E1 component from *Escherichia coli* at 1.85 Å resolution. Biochem 41(16):5213-21.

Atkinson DE, Walton GM.1965. Kinetics of regulatory enzymes. *Escherichia Coli* phosphofructokinase. J Biol Chem 240:757-63.

Atsumi S, Cann AF, Connor MR, Shen CR, Smith KM, Brynildsen MP, Chou KJ, Hanai T, Liao JC. 2008. Metabolic engineering of *Escherichia coli* for 1-butanol production. Metab Eng 10(6): 305–311.

Babul J. 1978. Phosphofructokinases from *Escherichia coli*. J Biol Chem 253:4350-4355.

Bailey JE. 1991. Toward a science of metabolic engineering. Science 252(5013):1668-1675.

Berg P. 1956. Acyl adenylates; an enzymatic mechanism of acetate activation. J Biol Chem 222(2):991-1013.

Berg JM, Tymoczko JL, Stryer L. 2002. 20.3 The pentose phosphate pathway generates NADPH and synthesizes five-carbon sugars. *Biochemistry*. 5th edition. New York: W H Freeman.

Berger SA, Evans PR. 1992. Site-directed mutagenesis identifies catalytic residue in the active site of *Escherichia coli* phosphofructokinase. Biochem 31:9237-9242.

Bilder P, Lightle S, Bainbridge G, Ohren J, Finzel B, Sun F, Holley S, Al-Kassim L, Spessard C, Melnick M, Newcomer M, Waldrop GL.2006. The structure of the carboxyltransferase component of acetyl-coA carboxylase reveals a zinc-binding motif unique to the bacterial enzyme. Biochemistry 45(6):1712-22.

Blangy D, Buc H, Monod J. 1968. Kinetics of the allosteric interactions of phosphofructokinase from *Escherichia coli*. J Mol Biol 31(1):13-35.

Bogorad IW, Lin TS, Liao JC. 2013. Synthetic non-oxidative glycolysis enables complete carbon conservation. Nature 502(7473):693-697.

Bologna FP, Andreo CS, Drincovich MF. 2007. *Escherichia coli* malic enzymes: two isoforms with substantial differences in kinetic properties, metabolic regulation, and structure. J Bacteriol 189(16):5937-46.

Brockman IM, Prather KLJ. 2015. Dynamic knockdown of *E. coli* central metabolism for redirecting fluxes of primary metabolites. Metabol Eng 28:104-113.

Brown TD, Jones-Mortimer MC, Kornberg HL. 1977. The enzymic interconversion of acetate and acetyl-coenzyme A in *Escherichia coli*. J Gen Microbiol 102(2):327-36.

Cai D, He P, Lu X, Zhu C, Zhu J, Zhan Y, Wang Q, Wen Z, Chen S. 2017. A novel approach to improve poly-γ-glutamic acid production by NADPH regeneration in *Bacillus licheniformis* WX-02. Sci Rep 7:43404.

Campbell JW, Morgan-Kiss RM, Cronan JE Jr. 2003. A new *Escherichia coli* metabolic competency: growth on fatty acids by a novel anaerobic beta-oxidation pathway. Mol Microbiol 47(3):793-805.

Cardoso VM, Campani G, Santos MP, Silva GG, Pires MC, Gonçalves VM, de C Giordano R, Sargo CR, Horta ACL, Zangirolami TC. 2020. Cost analysis based on bioreactor cultivation conditions: Production of a soluble recombinant protein using *Escherichia coli* BL21(DE3). Biotechnol Rep (Amst) 26:e00441.

Centeno-Leija S, Huerta-Beristain G, Giles-Gómez M, Bolivar F, Gosset G, Martinez A. 2014. Improving poly-3-hydroxybutyrate production in *Escherichia coli* by combining the increase in the NADPH pool and acetyl-CoA availability. Antonie van Leeuwenhoek 105(4):687-696.

Chae TU, Kim WJ, Choi S, Park SJ, Lee SY. 2015. Metabolic engineering of *Escherichia coli* for the production of 1,3-diaminopropane, a three carbon diamine. Sci Rep 5:13040.

Chang YY, Cronan JE. 1984. An *Escherichia coli* mutant deficient in pyruvate oxidase activity due to altered phospholipid activation of the enzyme. Proc Natl Acad Sci U S A 81(14):4348-52.

Chinen A, Kozlov YI, Hara Y, Izui H, Yasueda H. 2007 Innovative metabolic pathway design for efficient L-glutamate production by suppressing CO_2 emission. J Biosci Bioeng 103(3):262-269.

Chubukov V, Mukhopadhyay A, Petzold CJ, Keasling JD, Martín HG. 2016. Synthetic and systems biology for microbial production of commodity chemicals. NPJ Syst Biol Appl 2:16009.

Cunningham CC, Hager LP. 1971. Crystalline pyruvate oxidase from *Escherichia coli*. 3. Phospholipid as an allosteric effector for the enzyme. J Biol Chem 246(6):1583-1589.

Danson MJ, Weitzman D.J. 1973. Functional groups in the activity and regulation of *Escherichia coli*. Biochem J 135:513-524.

Dauner M, Storni T, Sauer U. 2001. *Bacillus subtilis* metabolism and energetics in carbon-limited and excess-carbon chemostat cultures. J Bacteriol 183:7308-7317.

Davis MS, Cronan JE Jr. 2001. Inhibition of *Escherichia coli* acetyl coenzyme A carboxylase by acyl-acyl carrier protein. J Bacteriol 183(4):1499-503.

Davis MS, Solbiati J, Cronan JE Jr. 2000. Overproduction of acetyl-CoA carboxylase activity increases the rate of fatty acid biosynthesis in *Escherichia coli*. J Biol Chem 275(37):28593-8.

Desai TA, Rao CV. 2010. Regulation of arabinose and xylose metabolism in *Escherichia coli*. Appl Environ Microbiol 76:1524-1532.

Ding J, Holzwarth G, Penner MH, Patton-Vogt J, Bakalinsky AT. 2015. Overexpression of acetyl-CoA synthetase in *Saccharomyces cerevisiae* increases acetic acid tolerance. FEMS Microbiol Lett 362(3):1-7.

Dittrich CR, Bennett GN, San KY. 2005. Characterization of the acetate-producing pathways in *Escherichia coli*. Biotechnol Prog 21(4):1062-7.

Donald LJ, Crane BR, Anderson DH, Duckworth HW. 1991. The role of cysteine 206 in allosteric inhibition of *Escherichia coli* citrate synthase. J Biol Chem 266:20709-20713.

Duckworth HW, Tong EK. 1976. The binding of reduced nicotinamide adenine dinucleotide to citrate synthase of *Escherichia coli* K12. Biochem 15(1):108-114.

Eikmanns BJ, Thum-Schmitz N, Eggeling L, Lüdtke K-U, Sahm H. 1994. Nucleotide sequence, expression and transcriptional analysis of the *Corynebacterium glutamicum gltA* gene encoding citrate synthase. Microbiol 140:1817-1828.

Eiteman MA, Altman E. 2006. Overcoming acetate in *Escherichia coli* recombinant protein fermentations. Trends Biotechnol 24(11):530-6.

Enjalbert B, Millard P, Dinclaux M, Portais JC, Létisse F. 2017. Acetate fluxes in Escherichia coli are determined by the thermodynamic control of the Pta-AckA pathway. Sci Rep 7:42135.

Erni B. 1989. Glucose transport in *Escherichia coli*. FEMS Microbiol Rev 63:13-24.

Farmer WR, Liao JC. 1997. Reduction of aerobic acetate production by *Escherichia coli*. Appl Environ Microbiol 63(8):3205-10.

Feigenbaum J, Schulz H. 1975. Thiolases of *Escherichia coli*: purification and chain length specificities. J Bacteriol 122(2):407-11.

Fischer E, Sauer U. 2003. Metabolic flux profiling of *Escherichia coli* mutants in central carbon metabolism using GC-MS. Eur J Biochemistry 270:880-891.

Fleischer S, Klouwen H, Brierley G. 1961. Studies of the electron transfer system. 38. Lipid composition of purified enzyme preparations derived from beef heart mitochondria. J Biol Chem 236:2936-2941.

Folsom JP, Carlson RP. 2015. Physiological, biomass elemental composition and proteomic analyses of *Escherichia coli* ammonium-limited chemostat growth, and comparison with iron- and glucose-limited chemostat growth. Microbiology 161:1659-1670.

Fox DK, Roseman S. 1986. Isolation and characterization of homogeneous acetate kinase from *Salmonella typhimurium* and *Escherichia coli*. J Biol Chem 261(29):13487-13497.

Gilvarg C, Davis BD. 1956. The role of the tricarboxylic acid cycle in acetate oxidation in *Escherichia coli*. J Biol Chem 222:307-319.

Grossebüter W, Görisch H. 1985. Partial purification and properties of citrate synthases from the thermoacidophilic archaebacteria *Thermoplasma acidophilum* and *Sulfolobus acidocaldarius*. Systematic Appl Microbiol 6(2):119-124.

Güclü D, Szekrenyi A, Garrabou X, Kickstein M, Junker S, Clapés P, Fessner WD. 2016. Minimalist protein engineering of an aldolase provokes unprecedented substrate promiscuity. ACS Catal 6(3):1848-1852.

Gupta A, Reizman IM, Reisch CR, Prather KL. 2017. Dynamic regulation of metabolic flux in engineered bacteria using a pathway-independent quorum-sensing circuit. Nat Biotechnol 35(3):273-279.

Handford PA, Ner SS, Bloxhanm DP, Wilton DC. 1987. Site-directed mutagenesis of citrate synthase; the role of the active-site aspartate in the binding of acetyl-CoA but not oxaloacetate. Biochimica et Biophysica Acta 953:232-240.

Hansen HG, Henning U. 1996. Regulation of pyruvate dehydrogenase activity in *Escherichia coli* K12. Biochim Biophys Acta 122(2):355-8.

Hardiman T, Lemuth K, Keller MA, Reuss M, Siemann-Herzberg M. 2007. Topology of the global regulatory network of carbon limitation in *Escherichia coli*. J Biotechnol 132:359-374.

Hasegawa S, Tanaka Y, Suda M, Jojima T, Inui M. 2017. Enhanced glucose consumption and organic acid production by engineered *Corynebacterium glutamicum* based on analysis of a *pfkB*1 deletion mutant. Appl Environ Microbiol 83:e02638-16.

Hellinga HW, Evans PR. 1987. Mutations in the active site of *Escherichia coli* phosphofructokinase. Nature 327:437-439.

Henard CA, Freed EF, Guarnieri MT. 2015. Phosphoketolase pathway engineering for carbon-efficient biocatalysis. Curr Opin Biotechnol 36:183-8.

Hennig J, Kern G, Neef H, Spinka M, Bisswanger H, Hübner G. 1997. Molecular mechanism of regulation of the pyruvate dehydrogenase complex from *E. coli*. Biochem 36(50):15772-9.

Hollinshead WD, Rodriguez S, Martin HG, Wang G, Baidoo EEK, Sale KL, Keasling JD, Mukhopadhyay A, Tang YJ. 2016. Examining *Escherichia coli* glycolytic pathways, catabolite repression, and metabolite channeling using *Δpfk* mutants. Biotechnol Biofuels 9:212.

Holms WH. 1986. The central metabolic pathways of *Escherichia coli*: relationship between flux and control at a branch point, efficiency of conversion to biomass and excretion of acetate. Curr Top Cell Regul 28:69-105.

Hua Q, Yang C, Baba T, Mori H, Shimizu K. 2003. Responses of the central metabolism in *Escherichia coli* to phosphoglucose isomerase and glucose-6-phosphate dehydrogenase knockouts. J Bacteriology 185:7053-7067.

Hua Q, Yang C, Oshima T, Mori H, Shimizu K. 2004. Analysis of gene expression in *Escherichia coli* in response to changes of growth-limiting nutrient in chemostat cultures. Appl Environ Microbiol 70:2354-2366.

Ithayaraja M, Janardan N, Wierenga RK, Savithri HS, Murthy MR. 2016. Crystal structure of a thiolase from *Escherichia coli* at 1.8 Å resolution. Acta Crystallogr F Struct Biol Commun 72(Pt 7):534-44.

Jin S, Sonenshein AL. 1996. Characterization of the major citrate synthase of *Bacillus subtilis*. J Bacteriol 178(12):3658-3660.

Kabir MM, Shimizu K. 2003. Fermentation characteristics and protein expression patterns in a recombinant *Escherichia coli* mutant lacking phosphoglucose isomerase for poly(3-hydroxybutyrate) production. Appl Microbiol Biotechnol 62(2-3):244-55.

Kahana SE, Lowry OH, Schulz DW, Passonneau JV, Crawford EJ. 1960. The kinetics of phosphoglucoisomerase. J Biol Chem 235:2178-84.

Kale S, Arjunan P, Furey W, Jordan F. 2007. A dynamic loop at the active center of the *Escherichia coli* pyruvate dehydrogenase complex E1 component modulates substrate utilization and chemical communication with the E2 component. J Biol Chem 282(38):28106-16.

Kayser A, Weber J, Hecht V, Rinas U. 2005. Metabolic flux analysis of *Escherichia coli* in glucose-limited continuous culture. I. Growth-rate-dependent metabolic efficiency at steady state. Microbiol 151:693-706.

Kim JH, Wang C, Jang HJ, Cha MS, Park JE, Jo SY, Choi ES, Kim SW. 2016. Isoprene production by *Escherichia coli* through the exogenous mevalonate pathway with reduced formation of fermentation byproducts. Microb Cell Fact 15(1):214.

Kim S, Clomburg JM, Gonzalez R. 2015. Synthesis of medium-chain length (C6-C10) fuels and chemicals via β-oxidation reversal in *Escherichia coli*. J Ind Microbiol Biotechnol 42(3):465-75.

Koike M, Reed LJ, Carroll WR. 1960. alpha-Keto acid dehydrogenation complexes. I. Purification and properties of pyruvate and alpha-ketoglutarate dehydrogenation complexes of *Escherichia coli*. J Biol Chem 235:1924-30.

Kotlarz D, Buc H. 1977. Two *Escherichia coli* fructose-6-phosphate kinases. Preparative purification, oligomeric structure and immunological studies. Biochimica et Biophysica Acta 484:35-48.

Krutsakorn B, Imagawa T, Honda K, Okano K, Ohtake H. 2013. Construction of an *in vitro* bypassed pyruvate decarboxylation pathway using thermostable enzyme modules and its application to N-acetylglutamate production. Microb Cell Fact 12:91.

Kumari S, Beatty CM, Browning DF, Busby SJ, Simel EJ, Hovel-Miner G, Wolfe AJ. 2000. Regulation of acetyl coenzyme A synthetase in *Escherichia coli*. J Bacteriol 182(15):4173-4179.

Kwon YD, Kwon OH, Lee HS, Kim P. 2007. The effect of NADP-dependent malic enzyme expression and anaerobic C4 metabolism in *Escherichia coli* compared with other anaplerotic enzymes. J Applied Microbiol 103:2340-2345.

Laine R, Deville-Bonne D, Auzat I, Garel J-R. 1992. Interaction between the carboxyl groups of Asp127 and Asp129 in the active site of *Escherichia coli* phosphofructokinase. Eur J Biochem 207:1109-1114.

Lee ME, Dyer DH, Klein OD, Bolduc JM, Stoddard BL, Koshland DE Jr. 1995. Mutational analysis of the catalytic residues lysine 230 and tyrosine 160 in the NADP(+)-dependent isocitrate dehydrogenase from *Escherichia coli*. Biochem 34(1):378-84.

Lee WH, Chin YW, Han NS, Kim MD, Seo JH. 2011. Enhanced production of GDP-L-fucose by overexpression of NADPH regenerator in recombinant *Escherichia coli*. Appl Microbiol Biotechnol 91(4):967-76.

Lee JH, Jung H-M, Jung M-Y, Oh M-K. 2019. Effects of *gltA* and *arcA* mutations on biomass and 1,3-propanediol production in *Klebsiella pneumoniae*. Biotechnol Bioprocess Eng 24:95-102.

Lemuth K, Hardiman T, Winter S, Pfeiffer D, Keller MA, Lange S, Reuss M, Schmid RD, Siemann-Herzberg M. 2008. Global transcription and metabolic flux analysis of *Escherichia coli* in glucose-limited fed-batch cultivations. App Environ Microbiol 74(22):7002-7015.

Li Y, Xian H, Xu Y, Zhu Y, Sun Z, Wang Q, Qi Q. 2021. Fine tuning the glycolytic flux ratio of EP-bifido pathway for mevalonate production by enhancing glucose-6-phosphate dehydrogenase (Zwf) and CRISPRi suppressing 6-phosphofructo kinase (PfkA) in *Escherichia coli*. Microb Cell Fact 20:32.

Lim S-J, Jung Y-M, Shin H-D, Lee Y-H. 2002. Amplification of the NADPH-related genes *zwf* and *gnd* for the oddball biosynthesis of PHB in an *E. coli* transformant harboring a cloned *phbCAN* operon. J Biosci Bioeng 93(6):543-549.

Lin H, Castro NM, Bennett GN, San KY. 2006. Acetyl-CoA synthetase overexpression in *Escherichia coli* demonstrates more efficient acetate assimilation and lower acetate accumulation: a potential tool in metabolic engineering. Appl Microbiol Biotechnol 71(6):870-4.

Lin PP, Jaeger AJ, Wu TY, Xu SC, Lee AS, Gao F, Chen PW, Liao JC. 2018. Construction and evolution of an *Escherichia coli* strain relying on nonoxidative glycolysis for sugar catabolism. Proc Natl Acad Sci U S A 115(14):3538-3546.

Lin Z, Xu Z, Li Y, Wang Z, Chen T, Zhao X. 2014. Metabolic engineering of *Escherichia coli* for the production of riboflavin. Microbial Cell Fact 13:104.

Liu M, Yao L, Xian M, Ding Y, Liu H, Zhao G. 2016. Deletion of *arcA* increased the production of acetyl-CoA-derived chemicals in recombinant *Escherichia coli*. Biotechnol Lett 38:97-101.

Liu L, Duan X, Wu J. 2016. L-tryptophan production in *Escherichia coli* improved by weakening the Pta-AckA pathway. PloS One 11(6):e0158200.

Liu M, Ding Y, Chen H, Zhao Z, Liu H, Xian M, Zhao G. 2017. Improving the production of acetyl-CoA-derived chemicals in *Escherichia coli* BL21(DE3) through *iclR* and *arcA* deletion. BMC Microbiol 17:10.

Long CP, Gonzalez JE, Feist AM, Palsson BO, Antoniewicz MR. 2017. Dissecting the genetic and metabolic mechanisms of adaptation to the knockout of a major metabolic enzyme in *Escherichia coli*. Proc Nat Acad Sci 115:222-227.

Lovingshimer MR, Siegele D, Reinhart GD. 2006. Construction of an inducible, *pfkA* and *pfkB* deficient strain of *Escherichia coli* for the expression and purification of phosphofructokinase from bacterial sources. Protein Expr Purif 46:475-482.

Magasanik B. 1961. Catabolite Repression. Cold Spring Harb Symp Quant Biol 26: 249-256.

Maleki N, Safari M, Eiteman MA. 2018. Conversion of glucose-xylose mixtures to pyruvate using a consortium of metabolically engineered *Escherichia coli*. Eng Life Sci 18:40-47.

Mann T, Lutwak-Mann C. 1944. Non-oxidative enzymes. Annual Review of Biochem, 13:25-50.

Maurus R, Nguyen NT, Stokell DJ, Ayed A, Hultin PG, Duckworth HW, Brayer GD. 2003. Insights into the evolution of allosteric properties. The NADH binding site of hexameric type II citrate synthases. Biochem 42:5555-5565.

May A, Fischer RJ, Maria Thum S, Schaffer S, Verseck S, Dürre P, Bahl H. 2013. A modified pathway for the production of acetone in *Escherichia coli*. Metab Eng15:218-25.

McCloskey D, Xu S, Sandberg TE, Brunk E, Hefner Y, Szubin R, Feist AM, Palsson BO. 2018. Multiple optimal phenotypes overcome redox and glycolytic intermediate metabolite imbalances in *Escherichia coli pgi* knockout evolutions. Appl Environ Microbiol 84(19):e00823-18.

Meades G Jr, Benson BK, Grove A, Waldrop GL. 2010. A tale of two functions: enzymatic activity and translational repression by carboxyltransferase. Nucleic Acids Res 38(4):1217-27.

Menon N, Pásztor A, Menon BR, Kallio P, Fisher K, Akhtar MK, Leys D, Jones PR, Scrutton NS. 2015. A microbial platform for renewable propane synthesis based on a fermentative butanol pathway. Biotechnol Biofuels 10;8:61.

Meyer D, Schneider-Fresenius C, Horlacher R, Peist R, Boos W. 1997. Molecular characterization of glucokinase from *Escherichia coli*. J Bacteriol 179(4):1298-1306.

Moxley WC, Eiteman MA. 2021. Pyruvate production by *Escherichia coli* by use of pyruvate dehydrogenase variants. Appl Environ Microbiol 87(13):e0048721.

Moxley WC, Brown RE, Eiteman MA. 2023. *Escherichia coli aceE* variants coding pyruvate dehydrogenase improve the generation of pyruvate-derived acetoin. Eng Life Sci 23(3):e2200054.

Nakashima N, Ohno S, Yoshikawa K, Shimizu H, Tamura T. 2014. A vector library for silencing central carbon metabolism genes with antisense RNAs in *Escherichia coli*. Appl Environ Microbiol 80(2):564-73.

Neubauer P, Cruz N, Glauche F, Junne S, Knepper A, Raven M. 2013. Consistent development of bioprocesses from microliter cultures to the industrial scale. Eng Life Sci 13:224-238.

Neumann P, Weidner A, Pech A, Stubbs MT, Tittmann K. 2008. Structural basis for membrane binding and catalytic activation of the peripheral membrane enzyme pyruvate oxidase from *Escherichia coli*. Proc Natl Acad Sci U S A 105(45):17390-17395.

Nguyen NT, Maurus R, Stokell DJ, Ayed A, Duckworth HW, Brayer GD. 2001. Comparative analysis of folding and substrate binding sites between regulated hexameric type II citrate synthases and unregulated dimeric type I enzymes. Biochem 40:13177-13187.

Nicolas C, Kiefer P, Letisse F, Krömer J, Massou S, Soucaille P, Wittmann C, Lindley ND, Portais JC. 2007. Response of the central metabolism of *Escherichia coli* to modified expression of the gene encoding the glucose-6-phosphate dehydrogenase. FEBS Lett 581:3771-6.

Noor E, Eden E, Milo R, Alon U. 2010. Central carbon metabolism as a minimal biochemical walk between precursors for biomass and energy. Mol Cell 39(5):809-820.

Novak K, Flöckner L, Erian AM, Freitag P, Herwig C, Pflügl S. 2018. Characterizing the effect of expression of an acetyl-CoA synthetase insensitive to acetylation on co-utilization of glucose and acetate in batch and continuous cultures of *E. coli* W. Microb Cell Fact 17(1):109.

Ogawa T, Mori H, Tomita M, Yoshino M. 2007. Inhibitory effect of phosphoenolpyruvate on glycolytic enzymes in *Escherichia coli*. Res Microbiol 158(2):159-63.

Olavarria K, Pijman YO, Cabrera R, van Loosdrecht MCM, Wahl SA. 2022. Engineering an acetoacetyl-CoA reductase from *Cupriavidus necator* toward NADH preference under physiological conditions. Sci Rep12(1):3757.

Parimi NS, Durie IA, Wu X, Niyas AMM, Eiteman MA. 2017. Eliminating acetate formation improves citramalate production by metabolically engineered *Escherichia coli*. Microb Cell Fact 16(1):114.

Pereira DS, Donald LJ, Hosfield DJ, Duckworth HW. 1994. Active site mutants of *Escherichia coli* citrate synthase. J Biol Chem 269:412-417.

Perez-Zabaleta M, Sjöberg G, Guevara-Martínez M, Jarmander J, Gustavsson M, Quillaguamán J, Larsson G. 2016. Increasing the production of (R)-3-hydroxybutyrate in recombinant *Escherichia coli* by improved cofactor supply. Microb Cell Fact 15:91.

Perez-Zabaleta M, Guevara-Martínez M, Gustavsson M, Quillaguamán J, Larsson G, van Maris AJA. 2019. Comparison of engineered *Escherichia coli* AF1000 and BL21 strains for (R)-3-hydroxybutyrate production in fed-batch cultivation. Appl Microbiol Biotechnol 103(14):5627-5639.

Quail MA, Haydon DJ, Guest JR. 1994 The pdhR-aceEF-lpd operon of *Escherichia coli* expresses the pyruvate dehydrogenase complex. Mol Microbiol 12(1):95-104.

Rajpurohit H, Eiteman MA. 2022. Nutrient-limited operational strategies for the microbial production of biochemicals. Microorganisms 10(11):2226.

Reynolds TS, Courtney CM, Erickson KE, Wolfe LM, Chatterjee A, Nagpal P, Gill RT. 2017. ROS mediated selection for increased NADPH availability in *Escherichia coli*. Biotechnol Bioeng 114:2685-2689.

Robinson JP, Fraenkel DG. 1978. Allosteric and non-allosteric *E. coli* phosphofructokinases: effects on growth. Biochem Biophys Res Comm 81:858-863.

Romeo T, Snoep JL. 2005. Glycolysis and flux control. EcoSal Plus 1(2):10.1128/ecosalplus.3.5.1.

Satowa D, Fujiwara R, Uchio S, Nakano M, Otomo C, Hirata Y, Matsumoto T, Noda S, Tanaka T, Kondo A. 2020. Metabolic engineering of *E. coli* for improving mevalonate production to promote NADPH regeneration and enhance acetyl-CoA supply. Biotechnol Bioeng 117:2153-2164.

Sauer U, Lasko DR, Fiau J., Hochuli M, Glaser R, Szyperski T, Wüthrich K, Bailey JE. 1999. Metabolic flux ratio analysis of genetic and environmental modulations of *Escherichia coli* central carbon metabolism. J Bacteriol 181:6679-6688.

Sauer U, Canonaco F, Heri S, Perrenoud A, Fischer E. 2004. The soluble and membrane-bound transhydrogenases UdhA and PntAB have divergent functions in NADPH metabolism of *Escherichia coli.* J Biol Chem 279:6613-6619.

Sauer U, Eikmanns BJ. 2005. The PEP-pyruvate-oxaloacetate node as the switch point for carbon flux distribution in bacteria. FEMS Microbiol Rev 29:765-794.

Schuhmacher T, Löffler M, Hurler T, Takors R. 2014. Phosphate limited fed-batch processes: impact on carbon usage and energy metabolism in *Escherichia coli*. J Biotechnol 190:96-104.

Schütze A, Benndorf D, Püttker S, Kohrs F, Bettenbrock K. 2020. The impact of *ackA*, *pta*, and *ackA-pta* mutations on growth, gene expression and protein acetylation in *Escherichia coli* K-12. Front Microbiol 11:233.

Schwartz ER, Reed LJ. 1970. Regulation of the activity of the pyruvate dehydrogenase complex of *Escherichia coli*. Biochem 9(6):1434-9.

Scott DB, Cohen SS. 1953. The oxidative pathway of carbohydrate metabolism in *Escherichia coli*. 1. The isolation and properties of glucose 6-phosphate dehydrogenase and 6-phosphogluconate dehydrogenase. Biochem J 55(1):23-33.

Seravalli J, Kumar M, Ragsdale SW. 2002. Rapid kinetic studies of acetyl-CoA synthesis: evidence supporting the catalytic intermediacy of a paramagnetic NiFeC species in the autotrophic Wood-Ljungdahl pathway. Biochem 41(6):1807-19.

Shen LC, Atkinson DE. 1970. Regulation of pyruvate dehydrogenase from *Escherichia coli*. Interactions of adenylate energy charge and other regulatory parameters. J Biol Chem 245(22):5974-8.

Shimizu M, Suzuki T, Kameda KY, Abiko Y. 1969. Phosphotransacetylase of *Escherichia coli* B, purification and properties. Biochim Biophys Acta 191(3):550-558.

Shin JA, Kwon YD, Kwon OH, Lee HS, Kim P. 2007. 5-Aminolevulinic acid biosynthesis in *Escherichia coli* coexpressing NADP-dependent malic enzyme and 5-aminolevulinate synthase. J Microbiol Biotechnol 17:1579-1584.

Shirakihara Y, Evans PR. 1988. Crystal structure of the complex of phosphofructokinase from *Escherichia* coli with its reaction products. J Mol Biol 204:973-994.

Siedler S, Bringer S, Blank LM, Bott M. 2012. Engineering yield and rate of reductive biotransformation in *Escherichia coli* by partial cyclization of the pentose phosphate pathway and PTS-independent glucose transport. Appl Microbiol Biotechnol 93:1459-1467.

Siedler S, Bringer S, Bott M. 2011. Increased NADPH availability in *Escherichia coli*: improvement of the product per glucose ratio in reductive whole-cell biotransformation. Appl Microbiol Biotechnol 92:929-937.

Sievers M, Stöckli M, Teuber M. 1997. Purification and properties of citrate synthase from *Acetobacter europaeus*. FEMS Microbiol Lett 146(1):53-58.

Sofeo N, Hart JH, Butler B, Oliver DJ, Yandeau-Nelson MD, Nikolau BJ. 2019. Altering the substrate specificity of acetyl-coA synthetase by rational mutagenesis of the carboxylate binding pocket. ACS Synth Biol 8(6):1325-1336.

Song HS, Seo HM, Jeon JM, Moon YM, Hong JW, Hong YG, Bhatia SK, Ahn J, Lee H, Kim W, Park YC, Choi KY, Kim YG, Yang YH. 2018. Enhanced isobutanol production from acetate by combinatorial overexpression of acetyl-CoA synthetase and anaplerotic enzymes in engineered *Escherichia coli*. Biotechnol Bioeng 115(8):1971-1978.

Soriano A, Radice AD, Herbitter AH, Langsdorf EF, Stafford JM, Chan S, Wang S, Liu YH, Black TA. 2006. *Escherichia coli* acetyl-coenzyme A carboxylase: characterization and development of a high-throughput assay. Anal Biochem 349(2):268-76.

Stokell, D. J., Donald, L. J., Maurus, R., Nguyen, N. T., Sadler, G., Choudhary, K., Hultin, P. G., Brayer, G. D., Duckworth, H. W. (2003). Probing the roles of key residues in the unique regulatory NADH binding site of type II citrate synthase of *Escherichia coli*. J Biol Chem 278: 35435-35443.

Sun Z, Do PM, Rhee MS, Govindasamy L, Wang Q, Ingram LO, Shanmugam KT. 2012. Amino acid substitutions at glutamate-354 in dihydrolipoamide dehydrogenase of *Escherichia coli* lower the sensitivity of pyruvate dehydrogenase to NADH. Microb (Reading) 2158:1350-1358.

Tang MA, Motoshima H, Watanabe K. Cold adaptation: structural and functional characterizations of psychrophilic and mesophilic acetate kinase. Protein J. 2014;33(4):313-322.

Taylor JE, Palur DSK, Zhang A, Gonzales JN, Arredondo A, Coulther TA, Lechner AB, Rodriguez EP, Fiehn O, Didzbalis J, Siegel JB, Atsumi S. 2023. Awakening the natural capability of psicose production in *Escherichia coli*. NPJ Sci Food *7*(1):54.

Tomar A, Eiteman MA, Altman E. The effect of acetate pathway mutations on the production of pyruvate in *Escherichia coli*. Appl Microbiol Biotechnol. 2003 Jul;62(1):76-82.

Tovilla-Coutiño DB, Momany C, Eiteman MA. 2020. Engineered citrate synthase alters acetate accumulation in *Escherichia coli*. Metabolic Eng 61:171-180.

Usui, Y., Hirasawa, T., Furusawa, C., Shirai, T., Yamamoto, N., Mori, H., Shimizu, H (2012). Investigating the effects of perturbations to *pgi* and *eno* gene expression on central carbon metabolism in *Escherichia coli* using ^{13}C metabolic flux analysis. *Microb Cell Fact* 11, 87

Valgepea K, Adamberg K, Nahku R, Lahtvee PJ, Arike L, Vilu R. Systems biology approach reveals that overflow metabolism of acetate in *Escherichia coli* is triggered by carbon catabolite repression of acetyl-CoA synthetase. BMC Syst Biol. 2010 Dec 1;4:166.

van Bogelen R, Olso ER, Wanner BL, Neidhardt FC. 1996. Global analysis of proteins synthesized during protein restriction in *Escherichia coli*. J Bacteriol 178(15):4344-4366.

Waegeman H, Maertens J, Beauprez J, De Mey M, Soetaert W. 2012. Effect of *iclR* and *arcA* deletions on physiology and metabolic fluxes in *Escherichia coli* BL21 (DE3). Biotechnol Lett 34(2):329-337.

Wang X, Wang A, Zhu L, Hua D, Qin J. 2018. Altering the sensitivity of *Escherichia coli* pyruvate dehydrogenase complex to NADH inhibition by structure-guided design. Enzyme Microb Technol 119:52-57.

Wang Y, Zhou S, Li R, Liu Q, Shao X, Zhu L, Kang MK, Wei G, Kim SW, Wang C. Reassessing acetyl-CoA supply and NADPH availability for mevalonate biosynthesis from glycerol in *Escherichia coli*. Biotechnol Bioeng. 2022 Oct;119(10):2868-2877.

Wang Y, San K-Y, Bennett GN. 2013. Improvement of NADPH bioavailability in *Escherichia coli* through the use of phosphofructokinase deficient strains. Appl Microbiol Biotechnol 97:6883-6893.

Wegner SA, Chen JM, Ip SS, Zhang Y, Dugar D, Avalos JL. 2021. Engineering acetyl-CoA supply and ERG9 repression to enhance mevalonate production in *Saccharomyces cerevisiae*. J Ind Microbiol Biotechnol 48(9-10):kuab050.

Weigand G, Remington SJ. (1986). Citrate synthase: structure, control, and mechanism. Ann Rev Biophys Biophys Chem 15:97-117.

Weitzman PDJ. 1966. Regulation of citrate synthase activity in *Escherichia coli*. Biochmi Biophys Acta 128:211-213.

Weitzman PDJ, Dunmore P. 1969. Regulation of citrate synthase activity by α-ketoglutarate. Metabolic and taxonomic significance. FEBS Lett 3(4):265-267.

Wood T. 1986. Physiological functions of the pentose phosphate pathway. Cell Biochem Funct 4:241-247.

Wu X, Eiteman MA. 2016. Production of citramalate by metabolically engineered *Escherichia coli*. Biotechnol Bioeng 113(12):2670-2675.

Wu X, Tovilla-Coutiño DB, Eiteman MA. 2020. Engineered citrate synthase improves citramalic acid generation in *Escherichia coli*. Biotechnol Bioeng 117:2781-2790.

Wu Z, Liang X, Li M, Ma M, Zheng Q, Li D, An T, Wang G. 2023. Advances in the optimization of central carbon metabolism in metabolic engineering. Microb Cell Fact 22:76.

Xu J, Green PC, Kemp RG. 1994. Identification of basic residues involved in substrate binding and catalysis by pyrophosphate-dependent phosphofructokinase from *Propionibaterium freudenreichii*. J Biol Chem 269:15553-15557.

Yang Y, Li, Y, Zhao H, Liu D, Zhang J, Cheng J, Yang Q, Chu H, Lu X, Luo M, Sheng X, Zhang YPJ, Jiang H, Ma Y. 2023. Construction of an artificial phosphoketolase pathway that efficiently catabolizes multiple carbon sources to acetyl-CoA. PLoS Biol 21(9):e3002285.

Yao R, Hirose Y, Sarkar D, Nakahigashi K, Ye Q, Shimizu K. 2011. Catabolic regulation analysis of *Escherichia coli* and its *crp, mlc, mgsA, pgi* and *ptsG* mutants. Microb Cell Fact 10:67.

Zelić B, Gerharz T, Bott M, Vasić-Rački Đ, Wandrey C, Takors R. 2003. Fed-Batch process for pyruvate production by recombinant *Escherichia coli* YYC202 strain. Eng Life Sci 3:299-305.

Zhang S, Yang W, Chen H, Liu B, Lin B, Tao Y. 2019. Metabolic engineering for efficient supply of acetyl-CoA from different carbon sources in *Escherichia coli.* Microb Cell Fact 18(1):130.

Zhao J, Baba T, Mori H, Shimizu K. 2004. Effect of *zwf* gene knockout on the metabolism of *Escherichia coli* grown on glucose or acetate. Metabol Eng 6:164-174.

Zheng,R-L, Kemp, RG. 1992. The mechanism of ATP inhibition of wild type and mutant phosphofructo-1-kinase from *Escherichia coli*. J Biol Chem 267:23640-23645.

Zheng R-L, Kemp RG. 1994a. Identification of interactions that stabilize the transition state in *Escherichia coli* phosphofructo-1-kinase. J Biol Chem 269:18475-1847.

Zheng R-L, Kemp RG. 1994b. Site-directed mutagenesis of highly conserved residues near the active site of phosphofructo-1-kinase. Biochem Biophys Res Comm 199:577-581.

Zhu L, Zhang J, Yang J, Jiang Y, Yang S. 2022. Strategies for optimizing acetyl-CoA formation from glucose in bacteria. Trends Biotechnol 40(2):149-165.

Zhu S, Cai D, Liu Z, Zhang B, Li J, Chen S, Ma X. 2019. Enhancement of bacitracin production by NADPH generation via overexpressing glucose-6-phosphate dehydrogenase Zwf in *Bacillus licheniformis.* Appl Biochem Biotechnol 187:1502-1514.

Zhu Y, Eiteman MA, Altman R, Altman E. 2008. High glycolytic flux improves pyruvate production by a metabolically engineered *Escherichia coli* strain. Appl Environ Microbiol 74:6649-6655.

Ziegler M, Hägele L, Gäbele T, Takors R. 2021. CRISPRi enables fast growth followed by stable aerobic pyruvate formation in *Escherichia coli* without auxotrophy. Eng Life Sci 22(2):70-84.

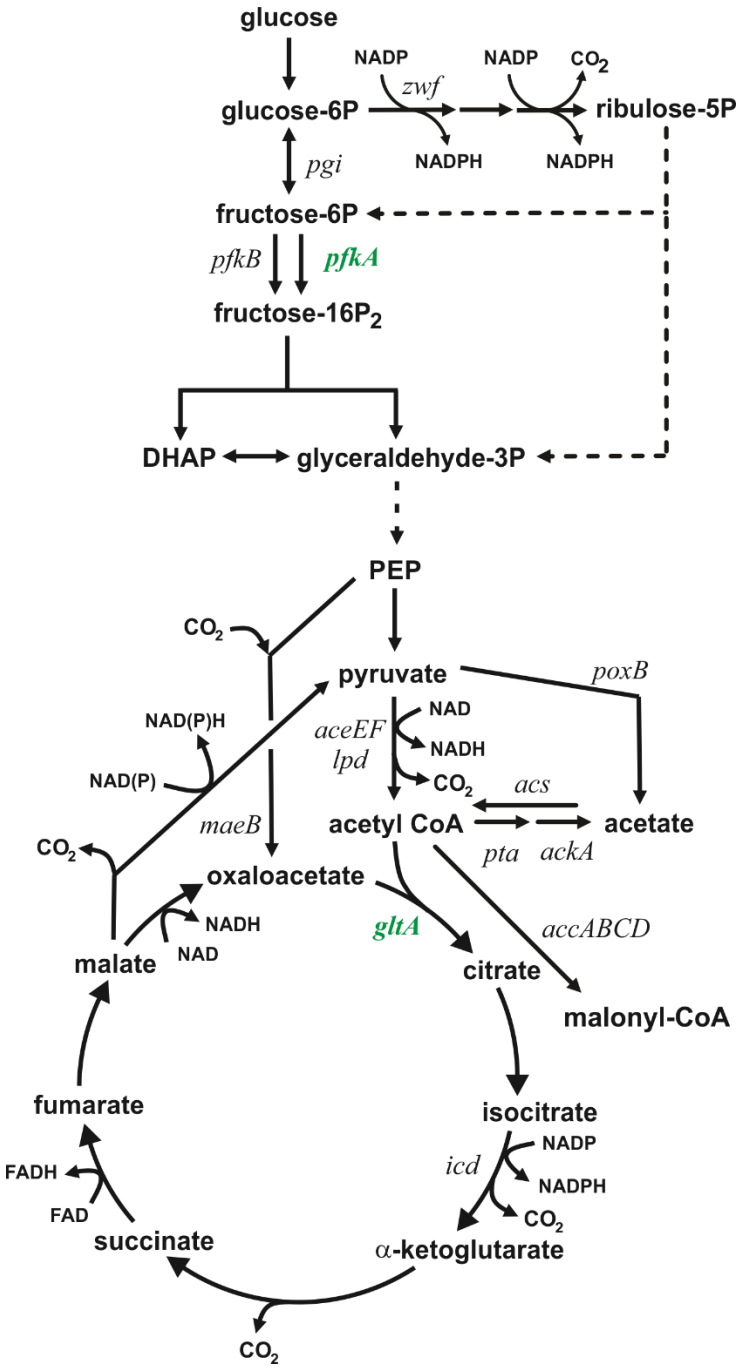

Figure 1.1- Central carbon metabolism of *E. coli* cells growing on glucose. All the genes (black, italics). encoding enzymes are highlighted. Key metabolic nodes of citrate synthase coded by *gltA (*green) and phosphofructokinase A coded by *pfkA* (green) were targeted in this work.

CHAPTER 2

NUTRIENT-LIMITED OPERATIONAL STRATEGIES FOR THE MICROBIAL PRODUCTION OF BIOCHEMICALS

[1]Rajpurohit, H. and Eiteman, M.A. (2022) *Microorganisms* 10(11): 2226.

2.1 ABSTRACT

Limiting an essential nutrient has a profound impact on microbial growth. The notion of growth under limited conditions was first described using simple Monod kinetics proposed in the 1940s. Different operational modes (chemostat, fed-batch processes) were soon developed to address questions related to microbial physiology and cell maintenance and to enhance product formation. With more recent developments of metabolic engineering and systems biology, as well as high-throughput approaches, the focus of current engineers and applied microbiologists has shifted from these fundamental biochemical processes. This review draws attention again to nutrient-limited processes. Indeed, the sophisticated gene editing tools not available to pioneers offer the prospect of metabolic engineering strategies which leverage nutrient limited processes. Thus, nutrient-limited processes continue to be very relevant to generate microbially derived biochemicals.

Keywords: chemostat; *Escherichia coli*; fed-batch; metabolic engineering; nutrient-limitation; *Saccharomyces cerevisiae*

2.2 INTRODUCTION

Biochemical processes use enzymes or microorganisms as catalysts to convert a substrate to a product, and are analogous to chemical processes in terms of basic design parameters including stoichiometry, energy relationships, kinetics, and equilibria (Gaden, 1960). Design and implementation of microbial bioprocesses additionally requires an understanding of metabolic activity and its effect on growth and product formation as well as factors which influence organisms and these cellular reactions.

Operationally, microbial bioprocesses are often classified by the strategies used for substrate addition and product removal (Figure 2.1). In a *batch* process, the carbon-substrate/energy source as well as other nutrients are at the onset charged into the reactor, and

product is harvested at the conclusion of the process, typically when the carbon source is depleted. Although material can be introduced into the reactor for oxygenation, pH control, foaming and other minor reasons, a batch process is considered a closed system. Other operations in contrast are implemented as distinctly open systems. A *chemostat* occurs when the flowrates of a nutrient-containing feed and an effluent of products and residual nutrients are equal (Maxon, 1955). The dilution rate (D) normalizes that feed rate F by the constant volume of the system V ($D = F/V$). In addition, any of several semi-continuous *fed-batch* processes involve the feeding of nutrients often without product withdrawal (Yoshida et al., 1973; Pirt, 1974). Variations on these basic operational modes include a *turbidostat* (Fox, 1955; Maxon, 1960), wherein the feed rate is controlled to maintain a constant cell density, and an *accelerostat* (Paalme et al., 1995), wherein the dilution rate is changed progressively and slowly to maintain prolonged pseudo-steady-state conditions over a range of growth rates. A two-reactor cascade in which biomass formation and product formation are spatially distinct is another novel continuous operational mode which increases volumetric productivity of intracellular products (Schmideder and Weuster-Botz, 2017). Several of the methods for continuous cultivation have been critically compared for their utility in high-resolution characterization of metabolism (Adamberg et al., 2015).

Microbial bioprocesses are further categorized by whether or not the growth of the microorganisms is *limited* by the availability of nutrients. The term descriptively suggests a process in which cellular growth and metabolism are less than maximal as a result of the limited availability of one or more nutrients during the course of the process. Whereas many authors use *limitation* in the context of cessation of growth (e.g., Merchant and Helmann, 2012), we use the term to refer to the state where cells are indeed metabolizing nutrients and even steadily growing,

albeit at a lower than maximal rate because of the *limited* availability of one or more nutrients, a condition which can be sustained simply by feeding that limiting nutrient at a controlled rate. A batch process is not a nutrient-limited process (at least until the very end of the process), whereas a chemostat must be a nutrient-limited process. A fed-batch process might or might not be nutrient-limited, depending on the nature of the feeding. Fed-batch operations may also be distinguished by whether or not feedback control is used in establishing the feed (Yamanè and Shimizu 1984), a classification which focuses on externally applied control rather than on the resulting physiological behavior of the cells. The type of nutrient limitation has a profound effect on the performance of cells in a bioreactor.

In order to establish whether or not cell growth is nutrient-limited, one must consider that a relationship exists between the concentration of any nutrient and the specific growth rate. Among the many models available, the relationship is often satisfactorily described by the hyperbolic Monod Equation (Monod, 1942, 1949):

$$\mu = \mu_{max}\left(\frac{S}{K_S+S}\right) \qquad 1$$

where μ_{max} is the maximum specific growth rate (h^{-1}) which occurs in the absence of inhibitors and when nutrients are plentiful under those culture conditions, K_S is the saturation constant (e.g., g/L), and S is the nutrient concentration (g/L). Although a great simplification of true microbial growth dynamics, this Monod Equation does capture the idea that a single nutrient can limit the specific growth rate, and shows that the growth rate approaches the maximum specific growth rate when $S >> K_S$. The saturation "constant" is not actually a constant, but itself depends on culture conditions (e.g., temperature, pH), the nutrients themselves (e.g., glucose versus glycerol; ammonium versus nitrate) and even the degree of adaptation of the cells (Senn et al., 1994). The value of K_S reflects the overall metabolic affinity for a substrate and can be affected by altering

the enzyme kinetics of a single reaction in cellular metabolism (Rutgers et al., 1987). Considering the example of *Escherichia coli* with glucose as the carbon source, values for K_S have been reported as low as 50 μg/L (Shehata and Marr, 1971; Senn et al., 1994) to greater than 8 mg/L (Jannasch, 1968; Dykhuizen, 1978; Ishida et al., 1982). Regardless of the precise numeric value of K_S, these results demonstrate that the saturation constant can be three orders of magnitude lower than a typical initial substrate concentration, so that the specific growth rate is essentially independent of *S* for the duration of a batch process. Since the growth rate is usually less than maximal only at very low nutrient concentrations, using a sensor feedback control strategy directly to maintain the concentration of a carbon/energy source or another nutrient at limiting conditions is generally impractical. Despite the difficulty in determining a value for the saturation constant (Owens and Legan, 1987), the Monod Equation is useful. For example, the equation can also be used to estimate the expected concentration of the limiting nutrient (i.e., when the process is operated in that way). Specifically, by rearranging the Monod Equation, the concentration of the growth limiting nutrient (S_{lim}) needed to sustain a given growth rate ($\mu < \mu_{max}$) is:

$$S_{lim} = \frac{\mu K_S}{\mu_{max} - \mu} \qquad 2$$

Due to their simplicity, batch processes are often used to study many microbial phenomena such as growth, carbohydrate utilization, and product formation. However, the flexibility and degrees of control in a batch process are limited. Because the microbes in a batch process invariably encounter nutrients in excess relative to K_S, the microbes grow for essentially the entire process at their maximum rate after an initial acclimatization, or lag period, until one or more nutrients suddenly becomes depleted. Thus, one has no operational ability to influence the nutrient-dependent physiological state of the culture. Nutrient-limited processes are

underappreciated, particularly in the context of modern molecular tools, and a goal of this review is to highlight current knowledge on these processes.

2.3 CHEMOSTAT PROCESSES

Originally developed to study bacterial cultures for a long duration (Novick and Szilard, 1950), the chemostat maintains the cell growth rate lower than the maximum specific growth rate (μ_{max}). The chemostat is an indispensable tool to investigate how growth rate affects cellular processes and how cells or consortia of cells evolve in response to nutrient limitation as a selective pressure (Ziv et al., 2013), though it is particularly difficult to operate for microbes which grow on walls or aggregate such as filamentous fungi (Lameiras et al., 2015). One can dictate which nutrient limits cell growth (e.g., C, N, P, etc.) merely by adjusting the medium composition (Egli, 2015). Mean residence time in the chemostat is equal to the inverse of the dilution rate *1/D* (Herbert et al., 1956). If the selected dilution rate is lower than the maximum specific growth rate (μ_{max}) at the given environmental conditions, then a steady-state is normally achieved: the growth rate the microbes experience (μ) becomes equal to *D*, and the limiting nutrient attains a low, constant concentration (e.g., Equation 2). If the dilution rate approaches or exceeds the maximum specific growth rate, then the cells cannot grow as quickly as the medium is withdrawn, leading to net loss of cells and culture washout. Because chemostat processes maintain a high biomass concentration compared to batch processes, a chemostat achieves a fairly high product and biomass volumetric productivity or space time yield. Unfortunately, a continuous operation has an increased prospect of contamination or genetic drift during a prolonged biological process because of competition for the limiting nutrients (Powell, 1958; Rosenzweig et al., 1994; Weikert et al., 1997). Indeed, given the likelihood for mutations, a chemostat does not strictly reach a physiological “steady-state” (Bull 2010). In fact, at a long

time-scale, the chemostat is an invaluable tool to evolve strains with greater substrate affinity (Wick et al., 2002, Jansen et al., 2005; Gresham and Hong, 2015; Brickwedde et al., 2017), with relieved auxotrophy (van Maris et al., 2004) or with a gain of substrate utilization (Arensdorf et al., 2002). Different limiting nutrients (e.g., N-limited versus Fe-limited) change the profile of mutations that occur, and the rate of mutations (Maharjan and Ferenci, 2017). Nutrient limited conditions also encourage phenotypic heterogeneity (Schreiber et al., 2016).

Care must be made in medium design for nutrient limited processes because cells use a portion of the carbon/energy source for maintenance and also often to accumulate storage products. Therefore, the proportion of nutrients needed for a growth limitation itself depends on the growth rate, and dual-nutrient limited regions are possible (Cooney and Wang, 1976; Egli, 1991, Egli and Zinn, 2003, Zinn et al., 2004). Indeed, one fixed medium composition can lead to C-limited growth at a low dilution rate, dual C/N-limited growth at an intermediate dilution rate, and N-limited growth at a high dilution rate (Egli, 1991). Nevertheless, operation of a chemostat is useful to identify optimal conditions for fed-batch operations for biochemical generation (e.g., Lis et al., 2019), and therefore the chemostat is an indispensable tool for bioprocess development. Chemostat processes have been previously reviewed in the context of recombinant protein production (Peebo and Neubauer, 2018), in which case C-limited growth is typically employed to avoid overflow metabolism, a situation in which extra carbon is diverted to an undesirable by-product such as acetate (Eiteman and Altman, 2006).

2.4 FED-BATCH PROCESSES

Fed-batch is a semi-continuous process in which one or more nutrients is supplied to the growing microbial culture with or without periodic withdrawal (Yamanè and Shimizu 1984). A fed-batch process can be implemented so that nutrients are intermittently added to the reactor and

are always in excess from the perspective of the cells (i.e., relative to K_S), resulting in a process physiologically similar to a batch process. Such a culture allows prolonged growth at μ_{max} and can be considered a non-limited-nutrient fed-batch or a *repeated fed-batch*, although the latter term is often applied to a fill-and-draw process in which a portion of culture is periodically withdrawn and fresh nutrients supplied (Trilli et al., 1977). This type of fed-batch process is particularly beneficial in cases for which a high concentration of a particular nutrient inhibits microbial growth, since that nutrient can be maintained below its inhibitory concentration while achieving a near maximal growth rate (Yano et al., 1991b; Hu et al., 2010). Alternatively, a *nutrient-starved fed-batch* is a common process which involves growing a culture first with ample nutrients, and then in a subsequent cycle supplying the culture with a feed in which at least one essential nutrient is absent. In such a nutrient-starved process, often the carbon/energy source is supplied to satisfy the cultures' maintenance requirement, while the *absence* of another nutrient (e.g., N) prevents growth (Jørgensen et al., 2002). In this case, cells cannot continue growing without the missing essential nutrient(s), but they often remain able to metabolize the supplied carbon source and accumulate storage products or transform that carbon source into a desired product (Shang et al., 2003; Shen et al., 2016; Kim et al., 2019; Nayak et al., 2019).

A fed-batch process can also be implemented as a *nutrient-limited fed-batch*, which like a chemostat necessitates that a nutrient feed is introduced at a rate lower than the growing culture can maximally metabolize. In contrast to a nutrient-starved process, though, the culture is growing continuously, and the rate of introducing the limiting nutrient controls the metabolic and growth rates (Pirt 1979). Because no effluent typically exists, cells and products remain in the culture, enabling fed-batch processes to achieve high cell density and product concentration. A quasi-steady state is achieved in nutrient-limited fed-batch cultures (Pirt 1979).

Nutrient-limited fed-batch processes can be operated in several ways. For example, the growth limiting nutrient can be introduced into the culture at a constant rate or at an exponential rate (Yamanè and Shimizu 1984). When a growth limiting nutrient is fed at a fixed rate (F_c) the growth rate of the culture decreases with time (Dunn and Mor 1975; Yamanè and Shimizu 1984). In an exponential fed-batch process the nutrients are fed at an exponentially increasing rate to match the needs of the growing culture, to maintain a constant growth rate μ_c less than μ_{max}. The time-varying feed rate of a process limited by the carbon-energy source during an exponential fed-batch process is:

$$F = (V_i X_i / S_f)\left(m_s + \frac{\mu_c}{Y_{X/S}}\right) e^{\mu_c t} \qquad 3$$

where volumetric feed rate (F) is related to initial cell concentration (X_i), initial volume (V_i), substrate concentration in feed (S_f), biomass yield coefficient ($Y_{X/S}$), cell maintenance coefficient (m_s) and the desired constant specific growth rate (μ_c) (Korz et al. 1995). An exponential fed-batch operational mode has been used to obtain high cell density, avoid oxygen limitation, minimize metabolic heat generation, and minimize by-product formation (Korz et al. 1995, Lee 1996, Riesenberg et al. 1991). Like the saturation constant, the maintenance coefficient should not be considered a constant value, as it includes multiple cellular phenomena that may change over the course of a process (Neijssel and Tempest, 1976; van Bodegom, 2007). This simple parameter is merely an attempt to encapsulate quantitatively the portion of substrate consumption not used for growth or for product formation.

2.5 NUTRIENT LIMITATION COMPARED TO NUTRIENT STARVATION

From the cells' perspective, nutrient *limitation* is quite different from nutrient *starvation* (Förberg and Häggström, 1987), the latter which is often called a "resting cell" process. Nutrient limitation permits continued, possibly steady-state growth, whereas starvation in one or more

essential nutrient induces dynamic stress responses and ultimately prevents further growth (Werner-Washburne et al., 1996; Gasch and Werner-Washburne, 2002; Peterson et al., 2005). Many researchers examine the effect of nutrient scarcity by *restricting* an essential nutrient in the medium to cause that nutrient to be depleted first, or by transferring washed and concentrated cells from a complete to a depleted medium (e.g., Brauer et al., 2006). Similarly, batch processes are typically composed of a medium from which carbon is depleted first, leading many to refer to such a batch process as "carbon-limited". The term "starved" would be preferred to describe a batch process: only after a period of maximal growth do the cells transition quickly to non-growth due to first deficiency then absence of that one (or more) nutrient. The distinction is more important when a nutrient other than the carbon source is the first to be depleted, because the remaining excess carbon/energy source often continues to be consumed and converted into an intracellular or extracellular product despite, or often because of, the lack of growth.

Because of these physiological differences, care should be taken when comparing results from nutrient *starvation* with nutrient *limitation*, wherein growth is maintained by the slow addition of one or more limiting nutrients. The literature is replete with studies describing "nutrient limitation", when in fact the initial medium was merely adjusted so that the cells experience a short batch process until a specified nutrient is depleted, that is, the cells transition from a higher growth rate to being *starved* for that nutrient. Typically, these studies examine the culture for the metabolism of a remaining excess carbon source while the culture transitions from nutrient scarcity to nutrient exhaustion. *Nutrient limitation* implies a process in which the cells *continue to grow*.

To understand physiological response of an organism to nutrient limitation, it is very important to have controlled conditions (pH, temperature, and oxygen) and a well-defined

medium since common complex components such as yeast extract and peptone complicate the identification of the limiting nutrient and interpretation of the cellular response (Herbert 1956, Minihane and Brown 1986). For example, enzymes in a pathway to a particular required metabolite (e.g., a vitamin) may require iron, and if the complex medium contains a small quantity of that metabolite then the effect of iron limitation could differ in that complex medium compared to a medium with a single carbon/energy source. Comparing vastly different media compositions, using complex medium components such as protein hydrolysate, or using microbial consortia can make identification of the limiting nutrient(s) virtually impossible (e.g., Vazques-Lima et al., 2014; Varrone et al., 2018; Zhang et al., 2021), and make results difficult to interpret.

One important measurement associated with nutrient limitation and cell growth in general is the biomass yield (Y, Table 2.1), which expresses the quantity of cells on a dry basis generated per quantity of nutrient consumed (e.g., units of g cells/g nutrient). For nutrients not used as an energy source or in a product, the biomass yield is the reciprocal of fractional composition of that nutrient (e.g., g nutrient/g cell). The steady-state biomass yield of a nutrient is greatest when that nutrient is limiting. For example, the *E. coli* biomass yield on nitrogen ($Y_{X/N}$, dry basis) is 8.8-9.8 g cells/g N during an N-limited chemostat, but 7.8-7.9 g cells/g N during glucose-limited growth and 7.2-7.5 g cells/g N during Fe-limited growth (Folsom and Carlson, 2015). In other words, *E. coli* is composed of 10.1-11.4% N when N is limiting, but 12.5-13.5% N when N is in excess and the cells are limited by something else: a loss of about 20 mg of N in one gram of cells when growth is limited by N. Similarly, *E. coli* biomass yield on iron ($Y_{X/Fe}$) is about 100,000-150,000 g/g (i.e., 8 μg Fe per g of cells) during an Fe-limited chemostat (Folsom et al., 2014), but is 5,000-7,000 g/g (200 μg Fe per g of cells) in Fe-excess batch cultivation (Abdul-

Tehrani et al., 1999). These bacterial cells are thus composed of roughly 20-25 times more Fe when excess Fe is in the medium compared to when this element is limiting (largely irrespective of growth rate). These observations demonstrate how the physiological steady-state differs with conditions, and how cells would likely undergo an extraordinary dynamic response in a Fe-starvation process. Cells initially experiencing low but excess Fe would transition through a wide range of states (from 200 μg Fe to 8 μg Fe per g of cells) before becoming truly depleted in Fe and unable to grow further. Such a dynamic response has been noted with high resolution in nitrogen-limited anaerobic processes using *Saccharomyces cerevisiae*, where a 7% increase in biomass occurs shortly after N depletion, largely as a consequence of trehalose and glycogen accumulation (Schulze et al., 1996). Such a growth dynamic cannot be explained exclusively by the Monod equation, and requires the use of at least two independent growth rates, one representing growth in the presence of N, and a second corresponding to carbohydrate-accumulating growth after N depletion (Henriques and Balsa-Canto, 2021). The unsurprising lesson is that cells have great flexibility to adjust their composition in response to the environment (Egli, 1991), and usually minimize their composition of a limiting nutrient at the expense of energy efficiency, typically by upregulating pathways using less of that nutrient, or otherwise avoiding unnecessary use of the limiting nutrient. As cells optimize their metabolic network, biomass yields also vary with growth rate and temperature (Chrzanowski and Grover, 2008).

The method of measurement affects the calculation of the yield coefficient. One method is called a “pulse shift technique” (Mateles and Battat, 1974; Kuhn et al., 1979). This technique involves achieving a steady-state, and then injecting a pulse of a suspected growth limiting nutrient into the reactor. If the injected nutrient is indeed growth limiting, then the culture will

no longer be limited by that nutrient, and the biomass will increase until the injected nutrient is depleted. Typically, an elemental analysis is not performed on the medium, the technique does not account for potentially multiple, simultaneous nutrient limitations, and it does not consider the cellular flexibility that an injected nutrient might be incorporated into cells without an observed biomass change. Thus, values calculated using this technique are generally low compared to values using other measurements. The dry mass of the cells is measured by drying a selected volume of washed cells at defined conditions of temperature and duration, and thus this measurement also introduces variability into the yield calculation.

Most biochemical products of interest are composed of carbon, oxygen and hydrogen. A common approach to maximize microbial formation of such products is by a two-step culture system in which a first phase achieves high cell density potentially without nutrient limitation, followed by a second phase in which cells are either limited (allowing some growth) or starved (allowing no growth) by the absence of one or more nutrients other than C (e.g., Jung et al., 2001; Dragone et al., 2011; Richter et al., 2013). After achieving a high biomass concentration such nutrient starvation/limitation generally maximizes carbon conversion to the product at the expense of additional biomass. For example, intracellular storage products such as poly(hydroxybutyrate) accumulate under N-, P-, S-, or Mg-limitation (Kim et al., 1994ab, Ahn et al., 2000). In an analogous fashion, photosynthetic microbes (Fogg, 1983; Braakman et al., 2017; Szul et al., 2019) and plants (Ryan et al., 2001) exude carbon under non-carbon nutrient limitation. Thus, we now consider some physiological effects of microbes growing under conditions of the limitation or starvation of nutrients other than carbon.

2.6 PHYSIOLOGICAL EFFECTS OF NON-CARBON NUTRIENT LIMITATION

Nitrogen

Nitrogen occurs throughout cells, in proteins, nucleotides and many metabolites. Nitrogen as ammonium is assimilated in *E. coli* and most bacteria and yeast into glutamine and glutamate (Reitzer, 2003), which are the primary intracellular nitrogen donors. In bacteria 88% of the cellular nitrogen is derived from glutamate, while 12% is derived from glutamine (Hu et al., 1999). Glutamate is the most abundant metabolite in *E. coli*, accounting for about 40% of the total metabolite concentration (Bennett et al., 2009). In many bacteria such as *E. coli*, two ammonium-assimilating pathways are available, a NADPH-dependent glutamate dehydrogenase and a high affinity glutamate synthase (glutamine oxoglutarate aminotransferase, GOGAT)/glutamine synthase. Glutamate dehydrogenases generally have high values of K_M for ammonium, so that during N-limited growth, glutamine synthase expression is elevated to maintain sufficient glutamate (Reitzer, 1996). Dynamic N starvation in *E. coli* and *S. cerevisiae* growing on glucose depletes glutamine and to a lesser extent glutamate while α-ketoglutarate increases markedly and can even be excreted (Brauner et al., 2006, Boer et al., 2010). Accumulation of α-ketoglutarate occurs in cyanobacteria also, a signal which upregulates nitrogen assimilation via the global regulator NtcA and other regulators (Muro-Pastor, 2005; Espinosa et al., 2014). In yeast the concentration of tryptophan, which relies on glutamine for its synthesis, decreases, while phenylalanine and tyrosine, which rely on glutamate for nitrogen, do not change, resulting in an accumulation of phenylpyruvate and phenylethanol, a quorum-sensing signal (Chen and Fink, 2006). Accumulated α-ketoglutarate in *E. coli* noncompetitively and cooperatively inhibits EI of the PTS (Doucette et al., 2011), citrate synthase (Pereira et al.,

1994) and PEP synthase (Chulavatnatol and Atkinson, 1973). Furthermore, sudden nitrogen availability in N-starved wild-type *E. coli* induces a decrease in α-ketoglutarate and rapid increase in glucose uptake rate, while in a PTS-deficient strain with elevated galactose permease, glucose uptake is insensitive to N availability (Doucette et al., 2011). In general, *S. cerevisiae* N-limitation leads to depletion of intracellular amino acids, particularly at low dilution rates (Boer et al., 2010). Because intracellular glutamine and arginine concentration correlates strongly with dilution rate, these compounds likely control growth in N-limited *S. cerevisiae* (Boer et al., 2010). *Synechocystis* accumulate α-ketoglutarate (Muro-Pastor et al., 2001) under N-starvation and also glycogen, which is associated with the induction of the *glgX* gene (de Marsac et al., 1980, Osanai et al., 2006, Yoo et al., 2007). *E. coli* has a high protein turnover under N-limited conditions compared to C-limited or P-limited conditions (Gupta et al., 2022).

Under steady-state conditions, cells tend to have greater uptake of the carbon/energy source when grown under carbon-excess conditions compared to carbon-limited conditions. For example, under N-limited conditions at 0.2 h^{-1}, *E. coli* shows a 2.3-fold greater specific glucose-consumption compared to under glucose-limited conditions (Sauer et al., 1999), while *S. cerevisiae* shows 2-3 greater specific glucose consumption compared to glucose-limited conditions at all growth rates (Kumar et al., 2021). This extra carbon at the same growth rate is diverted to energy consuming reactions, and *E. coli* also generates substantially more acetate under N-limited conditions compared to C-limited conditions: 0.19 g/g during N-limited growth at 0.10 h^{-1}, but no acetate during C-limited growth (Hua et al., 2003). In *E. coli* several genes associated with TCA cycle enzymes (isocitrate lyase, fumarase, succinate dehydrogenase) are downregulated under N-limitation compared to glucose-limitation, while genes of the Embden-Meyerhof-Parnas and pentose phosphate pathways are induced (Hua et al., 2004). N-limited

conditions generally increase the flux through glycolysis relative to the pentose phosphate pathway (Sauer et al., 1999). Some cells grown under carbon excess conditions induce ATP-dissipating futile cycles. For example, under N-limited conditions *Bacillus subtilis* increases flux through the oxaloacetate-PEP-pyruvate cycle (PEP carboxykinase, pyruvate kinase, pyruvate carboxylase) leading to the net loss of one ATP per cycle (Dauner et al., 2001). N-limited *S. cerevisiae* cultures showed much lower intracellular concentrations of NAD and NADH compared to C-limited cultures (Kumar and Bruheim, 2021). Increasing dilution rate of *S. cerevisiae* increased the CO_2 generation under N-limited conditions. In general, CO_2 emission increases with growth rate irrespective of nutrient limitation (Hua et al., 2004; Dauner et al., 2001, though CO2 evolution is greater under N-limitation compared to other nutrient limitation.

N-limitation, or more generally C-excess conditions, favor the formation of many biochemical products. For example, citric acid generation by *Aspergillus niger* is typically carried out under N-limited or dual N-/P-limited conditions (Kristiansen and Charley, 1981, Dawson et al., 1988), which are preferred operational modes because of nitrogen catabolite repression (Dawson et al., 1989). *Candida oleophila* also generates 0.7 g/g citrate under N-limited conditions at a dilution rate of 0.0185 h^{-1} (Anastassiadis and Rehm, 2006), while *Penicillium simplicissium* excreted both malate and citrate under N-limited conditions (Gallmetzer and Burgstaller, 2001), and *Yarrowia lipolytica* generated nearly 90 g/L citrate at the lowest dilution rate (<0.01 h^{-1}) though the greatest yield of 0.67 g/g was at a greater dilution rate (Rywińska et al., 2011). Citrate formation by *Penicillium ochrochloron* under N-limited (and P-limited) conditions is correlated with much lower nucleotide concentrations (Vrabl et al., 2017). Similarly, N-limitation yielded the largest quantity of lipids in an oleaginous *Candida* (Gill et al., 1977), *Cryptococcus curvatus* (Gong et al., 2015) and *Y. lipolytica* (Kerkhoven et al., 2016). in

In *Schizochytrium sp.* ammonium starvation resulted in the greatest squalene content (223 mg/g of total lipids) compared to phosphate starvation (30 mg/g) or excess nutrients (143.23 mg/g) (Sun et al., 2014). N-limited chemostats at 0.1 h^{-1} resulted in 59% of the catabolic flux directed to 1,3-propanediol, whereas under P-limited conditions 43% of the flux was directed to this product (Zheng et al., 2010). In N-limited fed-batch cultures, over 60 g/L 1,3-propanediol was obtained with a productivity of 1.7 g/L·h. Nitrogen starvation increased itaconate production ten-fold compared to batch conditions in a *Corynebacterium glutamicum* strain expressing cis-aconitate decarboxylase from *Aspergillus terreus* (Otten et al., 2015). Very low growth rate of recombinant *S. cerevisiae* under N-limited conditions generated over 0.61 mol/mol succinate for 500 hours (Liu et al., 2020). A two-reactor N-limited chemostat system, allowing very low dilution rates, yielded about 200 g/L erythritol using *Y. lipolytica* with a yield of 0.66 g/g glycerol (Rakicka et al., 2016; Rakicka et al., 2017).

Storage products such as polyhydroxyalkanoates are well-known to accumulate under N starvation (the processes are typically referred to as N-limitation). One approach is to grow *Alcaligenes eutrophus* (*Cupriavidus necator*) to a high cell density, and then stop providing N while maintaining a high glucose concentration (Kim et al. 1994ab, Kim et al., 2005). Such N-starvation led to about 120 g/L poly(hydroxybutyrate) or poly(3-hydroxybutyrate-co-3-hydroxyvalerate), depending on co-substrates provided. A similar approach using *Alcaligenes latus* leads to 112 g/L poly(hydroxybutyrate) with a productivity of about 5 g/L·h from sucrose (Wang and Lee, 1997). The cyanobacteria *Synechocystis* also accumulate poly(hydroxybutyrate) during N-starvation (Asada et al., 1999; Singh and Mallick, 2017), an observation attributed to the induction of the *phaC* gene coding PHA synthase during N-starvation (von Wobeser, 2010).

Compared to C-, S- or P-limited conditions, *S. cerevisiae* generates the greatest ethanol yield (0.35 g/g) at 0.1 h^{-1} under N-limited steady-state conditions (Boer et al., 2003). N-starvation during the production of actinorhodin by *Streptomyces lividans* also led to the formation of α-ketoglutarate (Bruhiem et al., 2002). N-starvation (referred to as limitation) led to the accumulation of cellobiose lipids in two ustilaginomycetous yeasts (Morita et al., 2013).

Although *Clostridium acetobutylicum* under C-limited conditions at neutral pH leads to acetate and butyrate formation (Bahl et al., 1982), N-limited conditions at a pH below 5.2 results in acetone and butanol solvent formation, but at a decreased rate (Andersch et al., 1982). No solvent formation is observed under N-limited conditions at pH 5.7 (Gottschal and Morris, 1981). Quite surprisingly, N-limited conditions results in the accumulation of pyruvate and amino acids such as valine in *C. thermocellum* is attributed to a shift resulting from the equilibrium of pyruvate-ferredoxin oxidoreductase and an increased malic enzyme flux (Holwerda et al., 2020).

N-limited conditions are widely used and easily implemented. N-limitation increases glycolytic flux, and therefore this operational mode is desirable for production of glycolytic metabolites or products directly derived from them (Zhu et al., 2008, Wang and Lee, 1997, Perez-Zabaleta et al., 2019).

Phosphorus

Phosphorus occurs in cells as phosphorylated organic compounds such as general sugar-phosphates, phospholipids, phosphorylated proteins, RNA, DNA and ATP. The response to a P deficiency is typically mediated by a two-component signal transduction system. The sensor kinase component, PhoR, phosphorylates a response regulator that amplifies its own response, increases expression of proteins which scavenge phosphate such as a high affinity phosphate

transporter (Devine, 2018). Thus, P-limitation has multiple physiological consequences. For example, P-limitation causes a shift in the structure of the cell wall of Gram-positive microbes such as *B. subtilis* from P-containing teichoic acid to teichuronic acid which lacks phosphorus (Ellwood and Tempest, 1967; Ellwood and Tempest, 1969). As a result, P-limited *B. subtilis* contain less than half as much cellular phosphate as bacteria grown in excess P, and phages which bind to teichoic acid bind less effectively under P-limited conditions (Anderson et al., 1978, Lang et al., 1982). In this case, phosphorylated PhoPR represses *tagAB* operon to restrict teichoic acid synthesis and activates the *tua* operon to stimulate teichuronic acid synthesis (Devine 2018). P-limitation triggers the synthesis of phosphate-mobilizing hydrolases such as alkaline phosphatases and ribonucleases (Wouters and Buysman, 1977). In *S. cerevisiae* genes responsible for uptake of inorganic phosphates and inositol phosphates are upregulated under steady-state P-limitation at 0.1 h^{-1}, and surprisingly, polyphosphates accumulate in this yeast's vacuoles (Boer et al., 2003). Cells appear to use ribosomes for protein synthesis at higher efficiency under phosphate limitation (Li et al., 2018), and the RNA content is 6-8-fold greater than expected to be necessary for maintenance of the growth rate, though this RNA is immediately usable when P-limitation is relieved (Alton and Koch, 1974).

Isotopic labeling and MFA analysis have been used to compared P-, N- and C-limited steady-state growth of *B. subtilis* at 0.1 h^{-1} and 0.4 h^{-1} (Dauner et al., 2001), showing that the TCA cycle is severely restricted under P-limitation (only 14% of the flux compared to C-limited conditions, and 12% of flux of N-limited conditions). The rate of glucose uptake is over 30% greater under P-limited conditions compared to C-limited conditions at both growth rates, and the formation of acetate, diacetyl and acetoin is much greater, with those by-products accounting for over one-third of the carbon utilization. A high conversion of malate to pyruvate via malic

enzyme and 'reverse' flux from oxaloacetate to malate occur at high steady-state growth rate (0.4 h^{-1}). Moreover, compared to C-, or N-limited condition, P-limited conditions lead to the greatest partitioning of flux into the pentose phosphate pathway (59% of glucose-6P entered this pathway at 0.1 h^{-1} and 44% at 0.4 h^{-1}). High transhydrogenase fluxes are needed to balance the excess reducing equivalents NADPH and NADH (Dauner et al., 2001). Cells under P-limited conditions also have a greater protein content compared to cells experiencing N-limited or C-limited conditions. Greater CO_2 production has been widely observed in cells grown under P-limited conditions compared to C-limited conditions, which is attributed to the realignment of metabolic fluxes between the pentose phosphate pathway and TCA cycle (Hommes et al., 1991; Dauner et al., 2001; Boer et al., 2003; Johannson and Lidén, 2006; Zhu et al., 2008). P-limited *S. cerevisiae* cultures showed much lower intracellular concentrations of CoA than other nutrient limited conditions (Kumar and Bruheim, 2021).

Specific glucose uptake rate is about 2× greater and acetate formation 20× greater in *E. coli* under P-limited conditions compared to C-limited conditions at 0.2 h^{-1} (Marzan and Shimizu, 2011). P-limited chemostat cultures of *Klebsiella aerogenes* using glucose as the sole carbon source (0.17 h^{-1}) secrete polysaccharides, 2-ketogluconate, and gluconate instead of pyruvate (Neijssel and Tempest 1975).

In P-limited *B. subtilis* cultures growing at comparatively high steady-state growth rates (0.4 h^{-1}) the futile cycle pyruvate-oxaloacetate-malate (pyruvate carboxylase, malate dehydrogenase, malic enzyme) is induced leading to the net loss of one ATP per cycle (Dauner et al., 2001). In comparison, in glucose-limited *E. coli* cultures malic enzyme flux apparently does not occur (Sauer et al., 1999). Interestingly, malate to pyruvate conversion increases with growth rate in *Bacillus megaterium*. However, this reaction does not take place in glucose- and

N-limited *B. subtilis* chemostat cultures and is replaced with conversion of oxaloacetate to PEP (Dauner et al., 2001).

In general, the concentrations of nitrogenous bases and nucleosides are elevated under P-limitation compared to N-limitation, and the concentration of these metabolites increase with increasing dilution rate (Boer et al., 2010). Because ATP concentration correlates with dilution rate during P-limited growth, ATP availability is thought to control the growth rate under P-limitation (Boer et al., 2010). The adenylate energy charge of cells is low, and the ADP concentration relatively elevated, under P-limitation (Chapman and Atkinson, 1977).

The formation of several biochemical products has been examined under P-limited conditions. P-limited conditions leads to a 3-fold greater vancomycin production by *Amycolatopsis orientalis* compared to glucose-limited conditions (McIntyre et al., 1995), and also increased formation of streptomycin by *Streptomyces griseus* (Fazeli et al., 1995) and oxytetracycline by *Streptomyes rimosus* (Rhodes, 1984). P-starvation (referred to as limitation) causes the greatest actinorhodin formation in *Streptomyces lividans* (Bruheim et al., 2002), and was more effective than N-starvation in generating rhamnolipids by *Pseudomonas aeruginosa* (Clarke et al., 2010). P-limited conditions leads to the greatest fatty acid formation in *E. coli* compared to C- or N-limited conditions in batch or chemostat culture (Youngquist et al., 2013), which was increased further by knockouts in genes associated with flagella (Youngquist et al., 2017). P-limited cultures generate the greatest yield of glucose from xylose in a strain unable to metabolize glucose and blocked in carbon entry into the oxidative pentose phosphate pathway (Δ*zwf*), likely because the final step of this conversion includes the dephosphorylation of glucose-6P (Niyas and Eiteman, 2017).

P-limited recombinant *E. coli* cultures showed consistent specific production rate of phenylalanine throughout the fermentation (Förberg and Häggström 1987). A hyperproducing *E. coli* mutant showed 8.7 g/L phenylalanine with a 0.44 g/L·h productivity in a P-limited chemostat (0.05 h^{-1}) (Choi and Tribe 1982). Compared to S-, Mg-, or K-limitation, P-limitation is the most efficient limiting nutrient for phenylalanine generation in recombinant *E. coli* continuous cultures at 0.1 h^{-1} (Park and Rogers, 1986). Decreased dilution rate (0.03 h^{-1}) leads to 16.4 g/L phenylalanine with a productivity of 0.49 g/L·h (Park and Rogers, 1986). Compared to C- or N-limitation, P-limitation resulted in the greatest 3-hydroxypropionate production in engineered strain of *S. cerevisiae* (Lis et al., 2019). Because nitrogen is a component of ε-poly-L-lysine, P-limited cultures are used to generate maximal formation using *Streptomyces albulus* under steady-state conditions, and using glucose and glycerol as dual carbon sources attained over 20 mg/g·h specific productivity compared to less than 8 mg/g·h for either single carbon source alone, a result correlated with much greater activity in aspartate kinase and several other associated enzymes (Zhang et al., 2018). P-limited conditions increase carbon flux into the isoprenoid pathway in *S. cerevisiae* associated with the upregulation of *PDC6* (Wadhwa et al., 2018).

Shikimic acid yield was 2.4× greater in *E. coli* grown under P-limited steady-state conditions compared to C-limited conditions, with much fewer by-products under P-limited growth (Johansson and Lidén, 2006; Johansson et al., 2005). Stipitatic acid was produced to a greater extent by *Penicillium stipitatum* under P-limited conditions compared with N-limited or C-limited conditions, a result which was attributed to the inhibitory effect of phosphate on the polyketide synthesis pathway (Linton et al., 1984). Xylitol can be generated from xylose under

oxygen-sufficient, P-limited conditions using the yeast *Debaryomyces hansenii* (Tavares et al., 1999).

In *C. necator* phosphate deficiency discourages the decarboxylation of propionyl-CoA to acetyl-CoA, and consequently leads to a higher fraction of hydroxyvalerate- compared to hydroxybutyrate-containing polyhydroxyalkanoates (Grousseau et al., 2014). P-limitation to sustain growth increases productivity (Grousseau et al., 2014). P-starvation has been proposed for high polyhydroxybutyrate formation because of the lower toxicity of *C. necator* to NH_4OH compared to NaOH (Ryu et al., 1997).

Several clostridia have been studied for solvent production under P-limited conditions. Under P-limited conditions at the low growth rate of 0.03 h^{-1}, *C. acetobutylicum* generates predominantly acetate and butyrate at a pH of 6.0 (more than 90% of products, mole basis), but butanol and acetone at pH 4.3 (87% of total) (Andersch et al., 1983). This result correlates with changes in observed activities of the enzymes associated pathways, in particular decreased activity in acetate and butyrate-forming enzymes at low pH. Under P-limited conditions at all pH values examined, *Clostridium pasteurianum* accumulates exclusively acetate and butyrate from glucose but ethanol, butanol and 1,3-propanediol from glycerol (Dabrock et al., 1992). With *Clostridium butyricum* the greatest H_2 production is found under P-limited conditions (Heyndrickx et al., 1990). An extended P-limited process of a *C. acetobutylicm* engineered for butanol production continuously generated 10 g/L butanol at a stable 14 g/L·h productivity and 0.15 g/g yield (Nguyen et al., 2018). A strain with deletions in the butyrate pathway generated 32-fold greater butanol and the unusual products 2-hydroxy-valerate and 2-keto-valerate under P-limited conditions (Yoo et al., 2017).

E. coli have a P yield coefficient of 36 g/g (Reiling et al., 1985), while an *E. coli* arginine auxotroph show a yield coefficient ($Y_{X/P}$) of 34 g/g (Table 2.1) (Yee and Blanch, 1992). The P yield coefficient of *Pseudomonas* C is 28 g/g (Mateles and Battat, 1974).

Because many carbohydrate metabolites and ATP are phosphorylated, P-limitation likely causes cells to conserve glycolytic metabolites, phosphate ion and ATP. P-starvation indeed quickly lowers cell adenylate energy charge (Schuhmacher et al., 2014). We expect P-limited conditions would be uniquely impactful for biochemicals utilizing ATP or having a dephosphorylation near the final step of the production pathway.

Sulfur

Sulfur is present in the amino acids methionine and cysteine, and important metabolites such as S-adenosylmethionine, Coenzyme A (CoA) and lipoic acid. In most media S is supplied as the sulfate ion, and thus S-limitation is often studied specifically as sulfate-limitation.

Unsurprisingly, S-limited growth leads to increased transcription of proteins encoding for the uptake of sulfur, such as in *S. cerevisiae* (Boer et al, 2003), *E. coli* (Gyaneshwar et al., 2005). Under S-limitation or S-starvation, several organisms preferentially express proteins having a low sulfur content (Cuhel et al., 1981; Mazel and Marlière, 1989; Boer et al., 2003; Merchant and Helmann, 2012). For example, under S-limitation *S. cerevisiae* upregulates by as great as 50-fold the PDC6 transcript expressing a protein with only 6 sulfur-containing amino acids compared to isozymes PDC1 and PDC5 having 17-18 sulfur-containing amino acids (Boer et al., 2003), while *K. aerogenes* maintains lower protein content in the cell wall under S-limitation compared to other nutrient-limited conditions, and this remaining protein contains a low sulfur content (Robinson and Tempest, 1973). The ABC transporter sulfate-binding proteins of *Salmonella typhimurium* and *E. coli* responsible for sulfate uptake in a low S environment

themselves contain no sulfur (Pardee, 1966). When *Pseudomonas putida* encounters S-depletion, it replaces proteins having high S content with proteins having lower amounts of cysteine and methionine (Beil et al., 1996). *K. aerogenes* also excretes proteins lacking S when grown under S-limited conditions on glucose (Neijssel and Tempest 1975). This phenomenon has been observed in many microbes, including cyanobacteria (Mazel & Marlière, 1989). In transitioning between S-limitation and S-enrichment cells must synthesize new RNA, whereas under C-limitation the cells use previously synthesized translation machinery, including inactive ribosomes (Koch and Deppe, 1971; Li et al., 2018). In *E. coli* S-starvation resulted in a 2.8-fold greater glucose uptake rate than N-starvation, and 40% greater glucose uptake rate than P-starvation, but about 70% less than the glucose uptake rate observed during Mg-starvation (Chubukov and Sauer, 2014). In *B. subtilis* S-starvation resulted in identical glucose uptake rates as observed during N-, P-starved conditions (Chubukov and Sauer, 2014). S-limitation in *E. coli* led to secretion of pyruvate (yield of 0.33 g/g), succinate (0.11 g/g) and acetate (0.10 g/g) despite the aerobic conditions (Chubukov and Sauer, 2014). S-limited chemostat cultures of *K. aerogenes* also secreted more pyruvate than N-, P- or C-limited growth on glucose (Neijssel and Tempest 1975), while S-limited chemostat cultures of *K. aerogenes* (formerly *Aerobacter aerogenes*) at high growth rate (0.42 h^{-1}) showed pyruvate and 2-oxoglutarate accumulation (Stouthamer and Bettenhaussen 1975). These observations may be explained by comparing a typical protein (~ 3% S content by mass) to the sulfur-containing cofactors CoA-SH (4.2% S), lipoic acid (31.1% S), and thiamine pyrophosphate (7.5% S). Each one of these cofactors is a component of the subsequent pyruvate/2-oxoglutarate dehydrogenase step, and the limitation of these cofactors would seem to limit metabolic conversion of pyruvate under S-limited conditions (Stouthamer and Bettenhaussen 1975). Further evidence identifies lipoic acid as the predominant

limiting factor (Zinebi et al., 1994). Interestingly, in contrast to growth on glucose which generated pyruvate and acetate, acetate was the only significant product when *K. aerogenes* was grown on glycerol, mannitol or lactate under S-limited conditions (Neijssel and Tempest, 1975).

S-limitation appears to favor plasmid stability compared to C-, N- or P-limitation, particularly at high growth rate (Chew et al., 1988). This observation was attributed to the fact that among these four nutrients only S is not a constituent of nucleic acids. S-starvation resulted in the greatest mevalonate yield from glucose (0.6 mol/mol) compared to Mg-, P- or N-starvation (Masuda et al., 2017; Li et al., 2016). S-starvation (referred to as $MgSO_4$ limitation) increased limonene formation by *E. coli* (Willrodt et al., 2016). Similarly, lipid formation elevated when the oleaginous yeast *Rhodosporidium toruloides* became starved for S (Wu et al., 2011). The fluxes through the TCA cycle and toward acetate formation were suppressed by S-starvation, and the pentose phosphate pathway appears to be the principal route for NADPH generation (Masuda et al., 2017).

The majority of ribosomal RNA synthesized during S-limitation is believed not to become functional for protein synthesis even after enrichment suggesting that S-limited cultures have limited reserved biosynthetic capability (Koch and Deppe 1971). Hydrogen photoproduction can be prolonged in the green alga *Chlamydomonas reinhardtii* by sulfate starvation (Melis et al., 2000; Kosourov et al., 2007). Sulfate starvation inactivates photosystem II, resulting in the cells consuming available O_2, experiencing anaerobic conditions, and inducing hydrogenases which generates H_2 and sustains the electron transport process (Zhang et al., 2002a, Volgusheva et al., 2013). Cell viability of microalgae *Chlorella* is more sensitive to nitrogen and phosphate starvation compared to sulfur for production of starch on a large-scale (Brànyikovà et al., 2011). S-starvation leads to the largest carbohydrate content (46.8%) in

microalgae *Choleralla sorokiniana* compared to control (2.6%) and is preferred over N- or P-limitation for starch production from algae (Wang et al., 2022).

Beil et al. 1996 report a sulfur yield $Y_{X/S}$ of 243 g/g for *P. putida* after 80 minutes of S starvation (Table 2.1). In studies using chemostats with different limiting nutrients the S yield coefficient of *E. coli* cells under sulfur limitation ($Y_{X/S}$) was 278 g/g at a dilution rate of 0.45 h^{-1} (Reiling et al., 1985), and 163 g/g with an arginine auxotroph at 0.4 h^{-1} (Yee and Blanch, 1992).

Magnesium

Magnesium is an integral component of ribosomes (Tissières & Watson, 1958), and stabilizes the outer membrane in Gram-negative prokaryotes through the creation of ionic bridges (Nikaido, 2003). The element as Mg^{2+} is also involved in DNA stability and repair (Hartwig, 2001), and it plays an important role as an enzyme cofactor. Many complex medium formulations supplemented with carbon source (such as "Lysogen Broth" medium) becomes starved for Mg, and can lead to protein acetylation at lysine residues (Christensen et al., 2017). There have been a few reports on cellular Mg composition (Table 2.1), and the yield coefficient is highly dependent on cell growth rate. For example, under Mg-limited conditions *K. aerogenes* showed a yield coefficient of 347-832 g/g ($Y_{X/Mg}$), with the lowest yields occurring at the highest dilution rates (Tempest et al., 1965), while *E. coli* showed a $Y_{X/Mg}$ of 278 g/g at a dilution rate of 0.4 h^{-1}, although cell lysis was reported (Yee and Blanch et al., 1992). Similarly, for *B. subtilis* under Mg-limited conditions, the yield coefficient was 714 g/g at a dilution rate of 0.1 h^{-1}, and 390 g/g at a dilution rate of 0.6 h^{-1} (Tempest et al., 1967). *S. cerevisiae* also showed a much greater Mg requirement at higher growth rates in chemostat (Walker and Maynard, 1996).

Mg starvation causes *E. coli* cells to restructure the outer membrane and redistribute Mg (Warsi et al., 2018; Fiil and Branton, 1969). Although the yield coefficient decreased with

increasing dilution rate, Mg-limited *K. aerogenes* cultures do not synthesize intracellular polysaccharides, which is attributed to an impaired ability to synthesize these materials when Mg is limiting (Tempest et al., 1965). Mg-limitation results in larger and filamentous *E. coli* cells (Brock, 1962; Dean and Rogers, 1967). Within 400 steady-state Mg-limited generations, mutations arise in genes involved in the cell-membrane in *E. coli* (Warsi et al., 2018). Under Mg-limited conditions both yeast (Smit et al., 1992) and bacteria (Warsi et al., 2018) reduce the surface hydrophobicity of the lipopolysaccharide (LPS) component of the outer membrane, likely by increasing the proportion of polar sugar residues in the LPS, such that lower amounts of Mg are needed for stabilization of the LPS. Consequently, *S. cerevisiae* shows reduced ability to flocculate under Mg-limitation (Smit et al., 1992). When Gram-negative and Gram-positive bacteria were grown together under Mg-limited conditions, Gram-negative bacteria invariably overtook the culture, suggesting that Gram-negative bacteria have a more efficient Mg uptake process, or in other words a lower value for the saturation constant, K_S (Meers and Tempest, 1968). Interestingly, *B. subtilis* exhibits very low incidence of sporulation under P- or Mg-limited conditions compared to carbon- or N-limited conditions (Dawes and Mandelstam, 1970). During hyperosmotic stress in *B. subtilis*, cell responds by exporting Mg^{2+} ions to import the K^+ ion. However, the decrease in free intracellular Mg^{2+} influences energy intensive processes including translation that requires magnesium as a cofactor (Wendel et al., 2022).

There is some research on the effect of Mg-starvation on product formation, and this work is usually conducted in batch studies using a medium in which Mg is depleted prior to the depletion of other nutrients (i.e., starvation). No research was found on the effect of Mg-limitation on product formation. In peptide based medium, Mg-starvation leads to accumulation of acetyl-CoA which is converted to acetyl-phosphate to regenerate CoA for the cellular

metabolism (Christensen et al., 2017). Mg-starvation has been shown to improve butanol formation by *C. acetobutylicum* (Mukherjee et al., 2019), particularly in the presence of excess zinc. Similarly, a lowered Mg concentration in the second phase of a two-phase fed-batch process increased final butanol titer by 25% using *C. acetobutylicum* (Ahlawat et al., 2019), a result attributed to ATP demand. In xanthan-producing *Xanthomonas campestris*, restriction of Mg in the medium decreases polysaccharide formation (Roseiro et al., 1993), a result attributed to low activity of phosphomannose isomerase. Resuspending a centrifuged culture into a medium lacking Mg, compared to other nutrients, led to the greatest glucose uptake rate and production rates of 3-hydroxypropionate and the flavonoid naringenin (Tokuyama et al., 2019), thought to be due to a high intracellular PEP concentration and lowered flux through Mg-requiring pyruvate kinase. Mg depletion during growth also elevated tyrosine and mevalonate formation (Li et al., 2016), though compared to S-starvation, Mg-starvation showed lower mevalonate, which was attributed to elevated acetate formation and low NADPH formation because of reduced flux through the pentose phosphate pathway (Masuda et al., 2017). In comparing *E. coli* cultures from which noncarbon nutrients were depleted before glucose, Mg-starvation showed the greatest glucose consumption rate (Chubukov and Sauer, 2014). This very high glucose consumption rate was accompanied by substantial pyruvate formation (0.74 g/g yield) and an increased PEP pool, effects which were attributed to inactivation of pyruvate dehydrogenase when Mg was depleted (Chubukov and Sauer, 2014). These results could not be explained solely by energy demand, unless the lack of Mg inhibits ATP synthase or increases membrane fluidity. Given that Mg limitation affects membrane structure, it is intriguing to speculate how Mg-limitation impacts not only oxidative phosphorylation, but also the cell's ability to transport certain products.

Given the central role that magnesium plays in the cell membrane and in enzymatic conversions involving ATP, the lack of significant research on Mg-limited process for the accumulation of biochemicals is surprising. We envision metabolic circuits involving magnesium which leverage the unique role this ion plays in metabolism.

Iron

Iron is a common element which exists in two cationic oxidation states, and the element often plays a central role in cellular redox processes, and is also critical in strategies pathogens use to infect their hosts (Almeida et al., 2009; Sheldon and Heinrichs, 2015). Under aerobic conditions and neutral pH, the ferric ion (Fe^{3+}) is the principal natural form of iron, a species with low aqueous solubility and the potential to promote the formation of reactive oxygen species. Fe-responsive regulation is often mediated by the Fe-dependent transcriptional factor called Fur. Under conditions of Fe-starvation or Fe-limitation and to ameliorate low Fe biological availability, Fur-based repression is typically relieved, resulting in the expression of numerous genes involved in secreting Fe-chelators, siderophores, and high-affinity siderophore outer-membrane receptors (Philpott and Protchenko, 2008; Andrews et al., 2003; Schrettl et al., 2009; Folsom et al., 2014). Fur also regulates the small RNAs which repress genes under Fe-limited conditions (Massé and Gottesman, 2002). Fur regulated aerobic ribonucleotide reductases encoded by *nrdE* and *nrdF* are manganese-dependent and become active under Fe-starvation (Martin et al., 2011; Chandrangsu et al., 2017). Many bacteria also possess a Fe^{2+} transport system, Feo, which is induced and important for survival under anaerobic conditions in which Fe^{2+} is stable (Hantke, 1987; Stojilijkovic et al., 1993).

Consistent with the theme of cells conserving limited resources, Fe-limitation causes cells to reduce their reliance on pathways which contain significant Fe, such as the tricarboxylic acid

cycle (aconitase, fumarate hydratase, succinate dehydrogenase) and the proton-pumping components of the electron transport chain (Parente et al., 2011; Folsom et al., 2014; McHugh et al., 2003). This realignment of metabolism has physiological consequences. For example, under Fe-limiting aerobic conditions, *E. coli* generates acetate at a yield of 0.25 g/g at a dilution rate of 0.4 h^{-1}, but accumulates predominantly lactate (yield of 0.60 g/g) at 0.1 h^{-1} (Folsom et al., 2014). Elevated lactate under the most severe steady-state Fe-limitation provides cells a means to oxidize NADH when the Fe-requiring Nuo complex is curtailed, while an increased glucose uptake rate serves to meet ATP demand (Folsom et al., 2014). Lactate formation is also observed for *Staphylococcus aureus* exposed to Fe-starvation (Friedman et al., 2006). The reduction in activity of TCA cycle enzymes and accumulation of NADH encourages the formation of ethyl acetate by *Kluyveromyces marxianus* (Löser et al., 2013) and *Candida utilis* (Armstrong and Yamazaki, 1984). Because of the restricted capacity of the electron transport chain subject to Fe-limited conditions, cells essentially behave like they are encountering anaerobic conditions. For example, *E. coli* accumulates acetate and formate under Fe-limited steady-state conditions, attains a 60% greater glycolytic flux, and reduces by a factor of 5 the fraction of glucose entering the TCA cycle (Baez et al., 2022). More generally, Fe-limitation impacts oxygenation and redox state because numerous electron-carrying enzymes contain Fe-S clusters, and many Fe-containing enzymes or pathways are constrained under Fe-limitation. For example, the nitrogenase enzyme system contains significant Fe (Georgiadis et al., 1992), and Fe-limitation thus severely reduces nitrogen fixation by *Azotobacter vinelandii* (Fekete et al., 1983). Notably, lactic acid bacteria, which lack cytochrome and show generally high tolerance to peroxide, do not require iron for growth at all (MacLoad and Snell, 1947, Archibald, 1983).

Iron strongly affects anaerobes, which have many Fe-containing enzymes. Under Fe-limited conditions *C. acetobutylicum* favors from glucose the formation of butanol over acetone at low pH, but the formation of lactate at a pH greater than 5.5 (Bahl et al., 1986), presumably because of the Fe-containing enzymes associated with the conversion of pyruvate to acetyl-CoA (pyruvate:ferredoxin oxidoreductase) and acetoacetate to acetone (acetoacetate decarboxylase). Also, Fe-limitation leads to a significant reduction in hydrogenase activity (Junelles et al., 1988). Similarly, for *C. pasteurianum* Fe-limited conditions favor lactate generation from glucose but 1,3-propanediol from glycerol (Dabrock et al., 1992). The transition between butanol (Fe-excess) and 1,3-propanediol (Fe-limited) from glycerol is attributed to the coupling of H_2-formation to the ferredoxin-dependent butyryl-CoA dehydrogenase (Groeger et al., 2017). Fe-limitation causes *C. pasteurianum* to substitute ferredoxin with flavodoxin (Schönheit et al., 1979), and flavodoxin is often used as an indicator for the lack of Fe availability (La Roche et al., 1996).

One of the more prevalent transition metals found in many cells (as noted above, $Y_{X/Fe}$ of 5,000-7,000 g/g under Fe-excess conditions, Abdul-Tehrani et al., 1999), Fe exemplifies a cofactor found in several specific enzymes that impact metabolic fluxes. Mateles and Battat (1974) measured a yield coefficient of 1,690 g/g under Fe-limited conditions. *E. coli* growing at a dilution rate of 0.45 h^{-1} under Fe-limited conditions showed a yield coefficient of 7,700 g/g (Reiling et al., 1985).

2.7 CONCLUSIONS

Over the last couple decades, research has focused on using metabolic engineering strategies to generate products. These strategies emphasize redirecting fluxes through modification of the metabolic network of reactions, including optimizing native pathways, expressing genes to code for introduced pathways, and statically or dynamically controlling

metabolism to redirect carbon to the desired product. Operational strategies have played a secondary role, and are usually limited to repeated batch processes to attain a high titer or introducing microaerobic conditions for biochemically reduced products. However, limiting a specific nutrient can have profound effects on microbial physiology and metabolic pathways. We propose that the growth under nutrient limitation can *leverage* the native or introduced pathways, which should encourage re-examination of operational strategies. For example, fluxes through competing pathways can be modulated by a nutrient required as a cofactor for one of the designed pathways. Thus, synthetic pathways and circuits can be constructed which by design are regulated by a single nutrient limitation. These include 1) substituting native pathways with enzymes requiring metal ions as cofactors, and which could serve as a control valve to partition flux under the limitation of that metal ion, and 2) designing pathways or metabolic processes which are induced by nutrient limitation.

2.8 REFERENCES

Abdul-Tehrani, H.; Hudson, A.J.; Chang, Y.-S.; Timms, A.R.; Hawkins, C.; Harrison, P.M.; Guest, J.R.; Andrews, S.C. Ferritin mutants of *Escherichia coli* are iron deficient and growth impaired, and *fur* mutants are iron deficient. *J. Bacteriol.* 1999, *181*, 1415-1428. https://doi.org/10.1128/JB.181.5.1415-1428.1999

Adamberg, K.; Valgepea, K.; Vilu, R. Advanced continuous cultivation methods for systems microbiology. *Microbiology* 2015, *161*, 1707-1719. https://doi.org/10.1099/mic.0.000146

Ahlawat, S.; Kaushal, M.; Palabhanvi, B.; Goswami, G.; Das, D. Flux balance analysis of nutritional modulation assisted changes in two-stage fed-batch fermentation by *Clostridium acetobutylicum*. *Bioresour Technol Reports*, 2019, *7*, 100264. https://doi.org/10.1016/j.biteb.2019.100264

Ahn, W.S.; Park, S.J.; Lee, S.Y. Production of poly(3-hydroxybutyrate) by fed-batch culture of recombinant *Escherichia coli* with a highly concentrated whey solution. *Appl. Environ. Microbiol*. 2000, *66*, 3624-3627. https://doi.org/10.1128/AEM.66.8.3624-3627.2000

Almeida, R.S.; Wilson, D.; Hube, B. *Candida albicans* iron acquisition within the host. *FEMS Yeast Res.* 2009, *9*, 1000-1012. https://doi.org/10.1111/j.1567-1364.2009.00570.x

Alton, T.H.; Koch, A.L. Unused protein synthetic capacity of *Escherichia coli* grown in phosphate-limited chemostats. *J. Mol. Biol.* 1974, *86*, 1-9. https://doi.org/10.1016/S0022-2836(74)80002-1

Anastassiadis, S.; Rehm, H.-J. Citric acid production from glucose by yeast *Candida oleophila* ATCC 20177 under batch, continuous and repeated batch cultivation. *Electron. J. Biotechnol.* 2006, *9*, 1. https://doi.org/10.2225/vol9-issue1-fulltext-5

Andersch, W.; Bahl, H.; Gottschalk, G. Acetone-butanol production by *Clostridium acetobutylicum* in an ammonium-limited chemostat at low pH values. *Biotechnol. Lett.* 1982, *4*, 29-32. https://doi.org/10.1007/BF00139278

Andersch, W.; Bahl, H.; Gottschalk, G. Level of enzymes involved in acetate, butyrate, acetone and butanol formation by *Clostridium acetobutylicum*. *Eur. J. Appl. Microbiol. Biotechnol.* 1983, *18*, 327-332. https://doi.org/10.1007/BF00504740

Anderson, A.J.; Green, R.S.; Archibald, A.R. Wall composition and phage-binding properties of *Bacillus subtilis* W23 grown in chemostat culture in media containing varied concentrations of phosphate. *FEMS Microbiol. Lett.* 1978, *4*, 129-132.

Andrews, S.C.; Robinson, A.K.; Rodríguez-Quiñones, F. Bacterial iron homeostasis. *FEMS Microbiol. Rev.* 2003, *27*, 215-237. https://doi.org/10.1016/S0168-6445(03)00055-X

Archibald, F. *Lactobacillus plantarum*, an organism not requiring iron. *FEMS Microbiol. Lett.* 1983, *19*, 29-32.

Arensdorf, J.J.; Loomis, A.K.; DiGarazia, P.M.; Monticello, D.J.; Piendos, P.T. Chemostat approach for the directed evolution of biodesulfurization gain-of-function mutants. *Appl. Environ. Microbiol.* 2002, *68*, 691-698. https://doi.org/10.1128/AEM.68.2.691-698.2002

Armstrong, D.W.; Yamazaki, H. Effect of iron and EDTA on ethyl acetate accumulation in *Candida utilis*. *Biotechnol. Lett.* 1984, *6*, 819-824. https://doi.org/10.1007/BF00134726

Asada, Y.; Miyake, M.; Miyake, J.; Kurane, R.; Tokiwa, Y. Photosynthetic accumulation of poly-(hydroxybutyrate) by cyanobacteria—the metabolism and potential for CO_2

recycling. *Intl. J. Biol. Macromol.* 1999, *25*, 37-42. https://doi.org/10.1016/S0141-8130(99)00013-6

Baez, A.; Sharma, A.K.; Bryukhanov, A.; Anderson, E.D.; Rudack, L.; Olivares-Hernandez, R.; Quan, D.; Shiloach, J. Iron availability enhances the cellular energetics of aerobic *Escherichia coli* cultures while upregulating anaerobic respiratory chains. *New Biotechnol.* 2022, *71*, 11-20. https://doi.org/10.1016/j.nbt.2022.06.004

Bahl, H.; Andersch, W.; Gottschalk, G. Continuous production of acetone and butanol by *Clostridium acetobutylicum* in a two-stage phosphate limited chemostat. *Eur. J. Appl. Microbiol. Biotechnol.* 1982, 15, 201-205. https://doi.org/10.1007/BF00499955

Bahl, H.; Gottwald, M.; Kuhn, A.; Rale, V.; Andersch, W.; Gottschalk, G. Nutritional factors affecting the ratio of solvents produced by *Clostridium acetobutylicum*. *Appl. Environ. Microbiol.* 1986, *52*, 169-172. https://doi.org/10.1128/aem.52.1.169-172.1986

Bauer, S.; Ziv, E. Dense growth of aerobic bacteria in a bench-scale fermentor. *Biotechnol. Bioeng.* 1976, *28*, 81-94. https://doi.org/10.1002/bit.260180107

Beil, S.; Kertesz, M.A.; Leisinger, T.; Cook, A. M. The assimilation of sulfur from multiple sources and its correlation with expression of the sulfate-starvation-induced stimulon in *Pseudomonas putida* S-313. *Microbiology*, 1996, *142*, 1989-1995. https://doi.org/10.1099/13500872-142-8-1989

Bennett, B.D.; Kimball, E.H.; Gao, M.; Osterhout, R.; van Dien, S.J.; Rabinowitz, J.D. Absolute metabolite concentrations and implied enzyme active site occupancy in *Escherichia coli*. *Nat. Chem. Biol*. 2009, *5*, 593-599. https://doi.org/10.1038/nchembio.186

Boer, V.M.; Crutchfield, C.A.; Bradley, P.H.; Botstein, D.; Rabinowitz, J.D. Growth-limiting intracellular metabolites in yeast growing under diverse nutrient limitations. *Mol. Biol. Cell.* 2010, *21*, 198-211. https://doi.org/10.1091/mbc.e09-07-0597

Boer, V.M.; de Winde, J.H.; Pronk, J.T.; Piper, M.D. The genome-wide transcriptional responses of *Saccharomyces cerevisiae* on glucose in aerobic chemostat cultures limited for carbon, nitrogen, phosphorous, or sulfur. *J. Biol. Chem.* 2003, *278*, 3265-3274. https://doi.org/10.1074/jbc.M209759200

Braakman, R.; Follows, M.; Chisholm, S.W. Metabolic evolution and the self-organization of ecosystems. *Proc. Natl. Acad. Sci. USA* 2017, *114*, e3091-e3100. https://doi.org/10.1073/pnas.16195731

Brányiková, I.; Maršálková, B.; Doucha, J.; Brányik, T.; Bišová, K.; Zachleder, V.; Vítová, M. Microalgae—novel highly efficient starch producers. *Biotechnol. Bioeng.* 2011, *108*, 766-776. https://doi.org/10.1002/bit.23016

Brauner, M.J.; Yuan, J.; Bennett, B.D.; Lu, W.; Kimball, E.; Botstein, D., Rabinowitz, J.D. Conservation of the metabolomic response to starvation across two divergent microbes. *Proc. Natl. Acad. Sci. USA* 2006, *103*, 19302-19307. https://doi.org/10.1073/pnas.0609508103

Brickwedde, A.; van den Broek, M.; Geertman, J.-M.A.; Magalhães, F.; Kuijpers, N.G.A.; Gibson, B.; Pronk, J.T.; Daran, J.-M.G. Evolutional engineering in chemostat cultures for improved maltotriose fermentation kinetics in *Saccharomyces pastorianus* lager brewing yeast. *Front. Microbiol.* 2017, *8*, 1690. https://doi.org/10.3389/fmicb.2017.01690

Brock, T.D. Effects of magnesium ion deficiency on *Escherichia coli* and possible relation to the mode of action of novobiocin. *J. Bacteriol.* 1962, *84*, 679-682. https://doi.org/10.1128/jb.84.4.679-682.1962

Bruheim, P.; Sletta, H.; Bibb, M.J.; White, J.; Levine, D.W. High-yield actinorhodin production in fed-batch culture by a *Streptomyces lividans* strain overexpressing the pathway-specific activator gene *act*II-ORF4. *J. Ind. Microbiol. Biotechnol.* 2002, *28*, 103-111. https://doi.org/10.1038/sj/jim/7000219

Bull, A.T. The renaissance of continuous culture in the post-genomics age. *J. Ind. Microbiol. Biotechnol.* 2010, *37*, 993-1021. https://doi.org/10.1007/s10295-010-0816-4

Chandrangsu, P.; Rensing, C.; Helmann, J.D. Metal homeostasis and resistance in bacteria. *Nat. Rev. Microbiol*. 2017, *15*, 338-350. https://doi.org/10.1038/nrmicro.2017.15

Chapman, A.G.; Atkinson, D.E. Adenine nucleotide concentrations and turnover rates. Their correlation with biological activity in bacteria and yeast. *Adv. Microbiol. Physiol.* 1977, *15*, 253-306. https://doi.org/10.1016/S0065-2911(08)60318-5

Chen, H.; Fink, G. R. Feedback control of morphogenesis in fungi by aromatic alcohols. *Genes Devel.* 2006, *20*, 1150-1161. https://doi.org/10.1101/gad.1411806

Chew, L.C.K., Tacon, W.C.A., Cole, J.A. Effect of growth conditions on the rate of loss of the plasmid pAT153 from continuous cultures of *Escherichia coli* HB101. *FEMS Microbiol*. 1988, *56*, 101-104. https://doi.org/10.1111/j.1574-6968.1988.tb03157.x

Choi, Y.J.; Tribe, D.E. Continuous production of phenylalanine using an *Escherichia coli* regulatory mutant. *Biotechnol. Lett.* 1982, *4*, 223–228. https://doi.org/10.1007/BF00132390

Christensen, D.G.; Orr, J.G.; Rao, V.G.; Wolfe, A.L. Increasing growth yield and decreasing acetylation in *Escherichia coli* by optimizing the carbon to magnesium ratio in peptide-based medium. *Appl. Environ. Microbiol.* 2017, *83*, e03034-16. https://doi.org/10.1128/AEM.03034-16

Chrzanowski, T.H.; Grover, J.P. Element content of *Pseudomonas fluorescens* varies with growth rate and temperature: A replicated chemostat study addressing ecological stoichiometry. *Limnol. Oceanogr.* 2008, *53*, 1242-1251. https://doi.org/10.4319/lo.2008.53.4.1242

Chubukov, V.; Sauer, U. Environmental dependence of stationary-phase metabolism in *Bacillus subtilis* and *Escherichia coli*. *Appl. Environ. Microbiol.* 2014, *80*, 2901-2909. https://doi.org/10.1128/AEM.00061-14

Chulavatnatol, M.; Atkinson, D.E. Phosphoenolpyruvate synthetase from *Escherichia coli*: Effects of adenylate energy charge and modifier concentrations. *J. Biol. Chem.* 1973, *248*, 2712-2715. https://doi.org/10.1016/S0021-9258(19)44064-7

Clarke, K.G.; Ballot, F.; Reid, S.J. Enhance rhamnolipid production by *Pseudomonas aeruginosa* under phosphate limitation. *World J. Microbiol. Biotechnol.* 2010, *26*, 2179-2184. https://doi.org/10.1007/s11274-010-0402-y

Cooney, C.L.; Wang, D.I. Transient response of *Enterobacter aerogenes* under a dual nutrient limitation in a chemostat. *Biotechnol. Bioeng*. 1978, *18*, 189-198. https://doi.org/10.1002/bit.260180205

Cuhel, R.L.; Taylor, C.D.; Jannasch, H.W. Assimilatory sulfur metabolism in marine microorganisms: sulfur metabolism, growth, and protein synthesis of *Pseudomonas*

halodurans and *Alteromonas luteo-violaceus* during sulfate limitation. *Arch. Microbiol.* 1981, *130*, 1-7. https://doi.org/10.1007/BF00527063

Dabrock, B.; Bahl, H.; Gottschalk, G. Parameters affecting solvent production by *Clostridium pasteurianum*. *Appl. Environ. Microbiol.* 1992, *58*, 1233-1239. https://doi.org/10.1128/aem.58.4.1233-1239.1992

Dauner, M.; Storni, T.; Sauer, U. *Bacillus subtilis* metabolism and energetics in carbon-limited and excess-carbon chemostat culture. *J. Bacteriol*. 2001, *183*, 7308-7317. https://doi.org/10.1128/JB.183.24.7308-7317.2001

Dawes, I.W.; Mandelstam, J. Sporulation of *Bacillus subtilis* in continuous culture. *J. Bacteriol.* 1970, *103*, 529-535. https://doi.org/10.1128/jb.103.3.529-535.1970

Dawson, M.W.; Maddox, I.S.; Brooks, J.D. Evidence for nitrogen catabolite repression during citric acid production by *Aspergillus niger* under phosphate-limited growth conditions. *Biotechnol. Bioeng.* 1989, *33*, 1500-1504. https://doi.org/10.1002/bit.260331119

Dawson, M.W.; Maddox, I.S.; Goab, I. F.; Brooks, J.D. Application of fed-batch culture to citric acid production by *Aspergillus niger*: The effects of dilution rate and dissolved oxygen. *Biotechnol. Bioeng.* 1988, *32*, 220-226. https://doi.org/10.1002/bit.260320212

De Marsac, N. T.; Castets, A.-M.; Cohen-Bazire, G. Wavelength modulation of phycoerythrin synthesis in *Synechocystis* sp. 6701. *J. Bacteriol.* 1980, *142*, 310-314. https://doi.org/10.1128/jb.142.1.310-314.1980

Dean, A.C.R.; Rogers, P.L. The cell size and macromolecular composition of *Aerobacter aerogenes* in various systems of continuous culture. *Biochim. Biophys. Acta* 1962, *148*, 267-279. https://doi.org/10.1016/0304-4165(67)90302-9

Devine, K.M. Activation of the PhoPR-mediated response to phosphate limitation is regulated by wall teichoic acid metabolism in *Bacillus subtilis*. *Front. Microbiol*. 2018, *9*, 2678. https://doi.org/10.3389/fmicb.2018.02678

Doucette, C.D.; Schwab, D.J.; Wingreen, N.S.; Rabinowitz, J.D. □-ketoglutarate coordinates carbon and nitrogen utilization via enzyme I inhibition. *Nat. Chem. Biol.* 2011, *7*, 894-901. https://doi.org/10.1038/nchembio.685

Dragone, G.; Fernandes, B.D.; Abreu, A.P.; Vicente, A.A.; Teixeira, J.A. Nutrient limitation as a strategy for increasing starch accumulation in microalgae. *Appl. Energy* 2011, *88*, 3331-3335. https://doi.org/10.1016/j.apenergy.2011.03.012

Dunn, I.J.; Mor, J.-R. Variable-volume continuous cultivation. *Biotechnol. Bioeng*. 1975, *17*, 1805-1822. https://doi.org/10.1002/bit.260171210

Dykhuizen, D. Selection for tryptophan auxotrophs of *Escherichia coli* in glucose-limited chemostats as a test of the energy conservation hypothesis of evolution. *Evolution* 1978, *32*, 125-150. https://doi.org/10.2307/2407415

Egli, T. Microbial growth and physiology: a call for better craftsmanship. *Front. Microbiol.* 2015, *6*, 287. https://doi.org/10.3389/fmicb.2015.00287

Egli, T. On multiple-nutrient-limited growth of microorganisms, with special reference to dual limitation by carbon and nitrogen substrates. *Ant. van Leeuwen*. 1991, *60*, 225-234. https://doi.org/10.1007/BF00430367

Egli, T.; Zinn, M. The concept of multiple-nutrient-limited growth of microorganisms and its application in biotechnological processes. *Biotechnol. Adv.* 2003, *22*, 35-43. https://doi.org/10.1016/j.biotechadv.2003.08.006

Eiteman, M.A.; Altman, E. Overcoming acetate in *Escherichia coli* recombinant protein fermentations. *Trends Biotechnol.* 2006, *24*, 530-536. https://doi.org/10.1016/j.tibtech.2006.09.001

Ellwood, D.C.; Tempest, D.W. Control of teichoic acid and teichuronic acid biosynthesis in chemostat cultures of *Bacillus subtilis* var. *niger*. *Biochem. J.* 1969, *111*, 1-5. https://doi.org/10.1042/bj1110001

Ellwood, D.C.; Tempest, D.W. Teichoic acid or teichuronic acid in the walls of *Bacillus subtilis* var. *niger*, grown in a chemostat. *Biochem. J.* 1967, *104*, 69P https://doi.org/10.1042/bj1040035P

Espinosa, J.; Rodriguez-Mateos, F.; Salinas, P.; Lanza, V.F.; Dixon, R.; de la Cruz, F.; Contreras, A. PipX, the coactivator of NtcA, is a global regulator in cyanobacteria. *Proc. Natl. Acad. Sci. USA* 2014, *111*, e2423-e2430. https://doi.org/10.1073/pnas.1404097111

Fazeli, M.R.; Cove, J.H.; Baumberg, S. Physiological factors affecting streptomycin production by *Streptomyces griseum* ATCC 12475 in batch and continuous culture. *FEMS Microbiol. Lett.* 1995, *126*, 55-62. https://doi.org/10.1111/j.1574-6968.1995.tb07390.x

Fekete, F.A.; Spence, J.T.; Emery, T. Siderophores produced by nitrogen-fixing *Azotobacter vinelandii* OP in iron-limited continuous culture. *Appl. Environ. Microbiol.* 1983, *46*, 1297-1300. https://doi.org/10.1128/aem.46.6.1297-1300.1983

Fiil, A.; Branton, D. Changes in the plasma membrane of *Escherichia coli* during magnesium starvation. *J. Bacteriol.* 1969, *98*, 1320-1327. https://doi.org/10.1128/jb.98.3.1320-1327.1969

Fogg, G.E. The ecological significance of extracellular products of phytoplankton photosynthesis. *Bot. Marina* 1983, *26*, 3-14. https://doi.org/10.1515/botm.1983.26.1.3

Folsom, J.P.; Carlson, R.P. Physiological, biomass elemental composition and proteomic analyses of *Escherichia coli* ammonium-limited chemostat growth, and comparison with iron- and glucose-limited chemostat. *Microbiol*, 2015, *151*, 1659-1570. https://doi.org/10.1099/mic.0.000118

Folsom, J.P.; Parker, A.E.; Carlson, R.P. Physiological and proteomic analysis of *Escherichia coli* iron-limited chemostat growth. *J. Bacteriol*. 2014, *196*, 2748-2761. https://doi.org/10.1128/JB.01606-14

Förberg, C.; Häggström, L. Effects of cultural conditions on the production of phenylalanine from a plasmid-harboring *E. coli* strain. *Appl. Microbiol. Biotechnol*. 1987, *26*, 136-140. https://doi.org/10.1007/BF00253897

Fox, M.S. A device for growing bacterial populations under steady state conditions. *J. Gen. Physiol*. 1955, *39*, 261-266. https://doi.org/10.1085/jgp.39.2.261

Friedman, D.B.; Stauff, D.L.; Pishchany, G.; Whitwell, C.W.; Torres, V.J.; Skaar, E.P. *Staphylococcus aureus* redirects central metabolism to increase iron availability. *PloS Path.* 2006, *2*, 777-789. https://doi.org/10.1371/journal.ppat.0020087

Gaden, Jr., E.L. Bioengineering and fermentation. *Appl. Microbiol.* 1960, *8*, 123–131. https://doi.org/10.1128/am.8.2.123-131.1960

Gallmetzer, M., Burgstaller, W. Citrate efflux in glucose-limited and glucose-sufficient chemostat culture of *Penicillium simplicissium*, *Ant van Leeuwen*, 2001, *79*, 81-87. https://doi.org/10.1023/A:1010295924549

Gasch, A.P.; Werner-Washburne, M. The genomics of yeast responses to environmental stress and starvation. *Funct. Integr. Genomics*, 2002, *2*, 181-192. https://doi.org/10.1007/s10142-002-0058-2

Georgiadis, M.M.; Komiya, H.; Chakrabarti, P.; Woo, D.; Kornuc, J.J.; Rees, D.C. Crystallographic structure of the nitrogenase iron protein from *Azotobacter vinelandii*. *Science* 1992, *257*, 1653-1659. https://doi.org/10.1126/science.1529353

Gill, C.O.; Hall, M.J.; Ratledge, C. Lipid accumulation in an oleaginous yeast (*Candida* 107) growing on glucose in single-stage continuous culture. *Appl. Environ. Microbiol.* 1977, *33*, 231-239. https://doi.org/10.1128/aem.33.2.231-239.1977

Gong, Z.; Shen, H.; Zhou, W.; Wang, Y.; Yang, X.; Zhao, Z.K. Efficient conversion of acetate into lipids by the oleaginous yeast *Cryptococcus curvatus*. *Biotechnol Biofuels* 2015, *8*, 189. https://doi.org/10.1186/s13068-015-0371-3

Gottschal, J.C.; Morris, J.G. Non-production of acetone and butanol by *Clostridium acetobutylicum* during glucose- and ammonium-limitation in continuous culture. *Biotechnol. Lett.* 1981, *3*, 525-530. https://doi.org/10.1007/BF00147566

Gresham, D.; Hong, J. The functional basis of adaptive evolution in chemostats. *FEMS Microbiol. Rev.* 2015, *39*, 2-16. https://doi.org/10.1111/1574-6976.12082

Groeger, C.; Wang, W.; Sabra, W.; Utesch, T.; Zeng, A.-P. Metabolic and proteomic analyses of product selectivity and redox regulation in *Clostridium pasteurianum* grown on glycerol under varied iron availability. *Microb. Cell Fact.* 2017, *16*, 64. https://doi.org/10.1186/s12934-017-0678-9

Grousseau, E.; Blanchet, E.; Déléris, S.; Albuquerque, M.G.E.; Paul, E.; Uribelarrea, J.-L. (2014). Phosphorus limitation strategy to increase propionic acid flux towards 3-hydroxyvaleric acid monomers in *Cupriavidus necator*. *Biores. Technol*. 2014, *153*, 206-215. https://doi.org/10.1016/j.biortech.2013.11.072

Gupta, M., Johnson, A., Cruz, E., Costa, E., Guest, R., Li, S. H.-J., Hart, E. M., Nguyen, T., Stadlmeier, M., Bratton, B.P., Silhavy, T.J., Wingren, N.S., Gitai, Z., Wühr, M. Global protein-turnover quantification in *Escherichia coli* reveals cytoplasmic recycling under nitrogen-limitation. *bioRxiv* 2022. https://doi.org/10.1101/2022.08.01.502339

Gyaneshwar, P.; Paliy, O.; McAuliffe, J.; Popham, D.L.; Jordan, M.I.; Kustu, S. Sulfur and nitrogen limitation in *Escherichia coli* K-12: specific homeostatic response. *J. Bacteriol.* 2005, *187*, 1074-1090 https://doi.org/10.1128/JB.187.3.1074-1090.2005

Hantke, K. Ferrous iron transport mutants in *Escherichia coli* K12. *FEMS Microbiol. Lett.* 1987, *4*, 53-57. https://doi.org/10.1111/j.1574-6968.1987.tb02241.x

Hartwig, A. Role of magnesium in genomic stability. *Mutation Res* 2001, *475*, 113-121.

Henriques, D., Balsa-Canto, E. The Monod model is insufficient to explain biomass growth in nitrogen-limited yeast fermentation. *Appl. Environ. Microbiol.* 2021, *87*, e01084-21. https://doi.org/10.1128/AEM.01084-21

Herbert, D.; Elsworth, R.; Telling, R. C. The continuous culture of bacteria; a theoretical experimental study. *J. Gen. Microbiol*. 1956, *14*, 601-622. https://doi.org/10.1099/00221287-14-3-601

Heyndrickx, M.; De Vos, P.; De Ley, J. H_2 production from chemostat fermentation of glucose by *Clostridium butyricum* and *Clostridium pasteurianum* in ammonium- and phosphate limitation. *Biotechnol. Lett.* 1990, *12*, 731-736. https://doi.org/10.1007/BF01024730

Holwerda, E.K.; Zhou, J.; Hon, S.; Stevenson, D.M.; Amador-Noguez, D.; Lynd, L.R.; van Dijken, J.P. Metabolic fluxes of nitrogen and pyrophosphate in chemostat cultures of *Clostridium thermocellum* and *Thermoanaerobacterium saccharolyticum*. *Appl. Environ. Microbiol.* 2020, *86*, e01795-20. https://doi.org/10.1128/AEM.01795-20

Hommes, R.W.J.; Simons, J.A.; Snoep, J.L.; Postma, P.W.; Tempest, D.W.; Neijssel, O.M. Quantitative aspects of glucose metabolism by *Escherichia coli* B/r, grown in the presence of pyrroloquinoline quinone. *Ant. van Leeuwen.* 1991, *60*, 373-382. https://doi.org/10.1007/BF00430375

Hu, P.; Leighton, T.; Ishkhanova, G.; Kustu, S. Sensing of nitrogen limitation by *Bacillus subtilis*: comparison to enteric bacteria, *J. Bacteriol.* 1999, *181*, 5042-5050. https://doi.org/10.1128/JB.181.16.5042-5050.1999

Hu, Z.-C.; Zheng, Y.-G.; Shen, Y.-C. Dissolved-oxygen-stat fed-batch fermentation of 1,3-dihydroxyacetone from glycerol by *Gluconobacter oxydans* ZJB09112. *Biotechnol. Bioprocess Eng.*, 2010, *15*, 651-656. https://doi.org/10.1007/s12257-009-3068-2

Hua, Q.; Yang, C.; Baba, T.; Mori, H.; Shimizu, K. Responses of the central metabolism in *Escherichia coli* to phosphoglucose isomerase and glucose-6-phosphate dehydrogenase knockouts. *J. Bacteriol.* 2003, *185*, 7053-7067. https://doi.org/10.1128/JB.185.24.7053-7067.2003

Hua, Q.; Yang, C.; Oshima, T.; Mori, H.; Shimizu, K. Analysis of gene expression in *Escherichia coli* in response to changes of growth-liming nutrient in chemostat cultures. *Appl. Environ. Microbiol*. 2004, *70*, 2354-2366. https://doi.org/10.1128/AEM.70.4.2354-2366.2004

Ishida, Y.; Imai, I.; Miyagaki, T.; Kadota, H. Growth and kinetics of a facultatively oligotrophic bacterium at low nutrient concentrations. *Microb. Ecol.* 1982, *8*, 23-32. https://doi.org/10.1007/BF02011458

Jannasch, H.W. Competitive elimination of *Enterobacteriaceae* from seawater. *Appl. Microbiol.* 1968, *16*, 1616-1618. https://doi.org/10.1128/am.16.10.1616-1618.1968

Jansen, M.L.A.; Diderich, J.A.; Mashego, M.; Hassane, A.; de Winde, J.H.; Pascale, D.-L.; Pronk, J.T. Prolonged selection in aerobic, glucose-limited chemostat cultures of *Saccharomyces cerevisiae* causes a partial loss of glycolytic capacity. *Microbiology* 2005, *151*, 1657-1669. https://doi.org/10.1099/mic.0.27577-0

Johansson, L., Lidén, G. Transcriptome analysis of a shikimic acid producing strain of *Escherichia coli* W3110 grown under carbon- and phosphate-limited conditions. *J. Biotechnol.* 2006, *126*, 528-545. https://doi.org/10.1016/j.jbiotec.2006.05.007

Johansson, L.; Lindskog, A.; Silfversparre, G.; Cimander, C.; Nielsen, K.F.; Lidén, G. Shikimic acid production by a modified strain of *E. coli* (W3110.shik1) under phosphate-limited and carbon-limited conditions. *Biotechnol. Bioeng.* 2005, *92*, 541-552. https://doi.org/10.1002/bit.20546

Jørgensen, H.; Olsson, L.; Rønnow, B.; Palmqvist, E. A. Fed-batch cultivation of baker's yeast followed by nitrogen or carbon starvation: effects on fermentative capacity and content of trehalose and glycogen. *Appl. Microbiol. Biotechnol.* 2002, *59*, 310-317. https://doi.org/10.1007/s00253-002-1017-5

Junelles, A. M.; Janati-Idrissi, R.; Petitdemange, H.; Gay, R. Iron effect on acetone–butanol fermentation. *Curr. Microbiol.* 1988, *17*, 299–303. https://doi.org/10.1007/BF01571332

Jung, K.; Hazenberg, H.: Prieto, M.; Witholt, B. Two-stage continuous process development for the production of medium-chain-length poly(3-hydroxyalkanoates). *Biotechnol. Bioeng.* 2001, *72*, 19-24. https://doi.org/10.1002/1097-0290(20010105)72:1<19::AID-BIT3>3.0.CO;2-B

Kerkhoven, E. J.; Pomraning, K.R.; Baker, S.E.; Nielsen, J. Regulation of amino-acid metabolism controls flux to lipid accumulation in *Yarrowia lipolytica. NPJ Syst. Biol. Appl.* 2016, *2*, 16005. https://doi.org/10.1038/npjsba.2016.5

Kim, B.S.; Lee, S.C.; Lee, S.Y.; Chang, H.N.; Chang, Y.K.; Woo, S.I. Production of poly(3-hydroxybutyric-*co*-3-hydroxyvaleric acid) by fed-batch culture of *Alcaligenes eutrophus* with substrate control using on-line glucose analyzer. *Enzyme Microb. Technol*. 1994, *16*, 556-561. https://doi.org/10.1016/0141-0229(94)90118-X

Kim, B.S.; Lee, S.C.; Lee, S.Y.; Chang, H.N.; Chang, Y.K.; Woo, S.I. Production of poly(3-hydroxybutyric acid) by fed-batch culture of *Alcaligenes eutrophus* with glucose concentration control. *Biotechnol. Bioeng*. 1994, *43*, 892-898. https://doi.org/10.1002/bit.260430908

Kim, H.M.; Chae, T.U.; Choi, S.Y.; Kim, W.J.; Lee, S.Y. Engineering of an oleaginous bacterium for the production of fatty acids and fuels. *Nat. Chem. Biol.* 2019, *15*, 721-729. https://doi.org/10.1038/s41589-019-0295-5

Kim, J.S.; Lee, B.H.; Kim, B.S. Production of poly(3-hydroxybutyrate *co*-4-hydroxybutyrate) by *Ralstonia eutropha*. *Biochem. Eng. J*. 2005, *23*, 169-174. https://doi.org/10.1016/j.bej.2005.01.016

Koch, A.L.; Deppe, C.S. *In vivo* assay of protein synthesizing capacity of *Escherichia coli* from slowly growing chemostat cultures. *J. Mol. Biol*. 1971, *55*, 549-562. https://doi.org/10.1016/0022-2836(71)90336-6

Korz, D.J.; Rinas, U.; Helmuth, K.; Sanders, E.A.; Deckwer, W.-D. Simple fed-batch technique for high cell density cultivation of *Escherichia coli*. *J. Biotechnol*. 1995, *39*, 59-65. https://doi.org/10.1016/0168-1656(94)00143-Z

Kosourov, S.; Patrusheva, E.; Ghirardi, M.L.; Seibert, M.; Tsygankov, A. A comparison of hydrogen photoproduction by sulfur-deprived *Chlamydomonas reinhardtii* under different growth conditions. *J. Biotechnol.* 2007, *128*, 776-787. https://doi.org/10.1016/j.jbiotec.2006.12.025

Kristiansen, B.; Charley, R. Continuous process for production of citric acid. *Scientific and Engineering Principles*, Proceedings of the sixth international fermentation symposium, London, Canada, July 20-25, 1980. pp. 221-227.

Kuhn, H.; Friederich, U.; Fiechter, A. Defined minimal medium for a thermophilic *Bacillus* sp. developed by a chemostat pulse and shift technique. *Eur. J. Appl. Microbiol.* 1979, *6*, 341-349. https://doi.org/10.1007/BF00499164

Kumar, K.; Venkatraman, V.; Bruheim, P. Adaptation of central metabolite pools to variations in growth rate and cultivation conditions in *Saccharomyces cerevisiae. Microb. Cell Fact.* 2021, *20*, 64. https://doi.org/10.1186/s12934-021-01557-8

La Roche, J.; Boyd, P.W.; McKay, R.M.L.; Geider, R.J. Flavodoxin as an *in situ* marker for iron stress in phytoplankton. *Nature* 1996, *382*, 802–804. https://doi.org/10.1038/382802a0.

Lameiras, F.; Heijnen, J.J.; van Gulik, W. M. Development of tools for quantitative intracellular metabolomics of *Aspergillus niger* chemostat cultures. *Metabolomics* 2015, *11*, 1253-1264. https://doi.org/10.1007/s11306-015-0781-z

Lang, W.K.; Glassey, K.; Archibald, A.R. Influence of phosphate supply on teichoic acid and teichuronic acid content of *Bacillus subtilis* cell walls. *J. Bacteriol.* 1982, *151*, 367-375. https://doi.org/10.1128/jb.151.1.367-375.1982

Lee, S.Y.; Chang, H.N. Production of poly(3-hydroxybutyric acid) by recombinant *Escherichia coli* strains: genetic and fermentation studies. *Can. J. Microbiol*. 1995, *41*, 207-215. https://doi.org/10.1139/m95-189

Li, S., Jendresen, C.B., Nielsen, A.T. Increasing production yield of tyrosine and mevalonate through inhibition of biomass formation. *Proc. Biochem.* 2016, *51*, 1992-2000. https://doi.org/10.1016/j.procbio.2016.09.007

Li, S.H.-J.; Li, Z.; Park, J. O.; King, C.G.; Rabinowitz, J.D.; Wingreen, N.S.; Gitai, Z. *Escherichia coli* translation strategies differ across carbon, nitrogen and phosphorous limitation conditions. *Nat. Microbiol*. 2018, *3*, 939-947. https://doi.org/10.1038/s41564-018-0199-2

Linton, J.D.; Austin, R.M.; Haugh, D.E. The kinetics and physiology of stipitatic acid and gluconate production by carbon sufficient cultures of *Penicillium stipitatum* growing in continuous culture. *Biotechnol. Bioeng.* 1984, *26*, 1455-1464. https://doi.org/10.1002/bit.260261210

Lis, A.V.; Schneider, K.; Weber, J.; Keasling, J.D.; Jensen, M.K.; Klein, T. Exploring small-scale chemostats to scale up microbial processes: 3-hydroxypropionic acid production in *S. cerevisiae. Microb. Cell Fact.* 2019, *18*:50. https://doi.org/10.1186/s12934-019-1101-5

Liu, Y.; Esen, O.; Pronk, J.T.; van Gulik, W.M. Uncoupling growth and succinic acid production in an industrial *Saccharomyces cerevisiae* strain. *Biotechnol. Bioeng.* 2020, *118*, 1557-1567. https://doi.org/10.1002/bit.27672

Löser, C.; Urit, T.; Förster, S.; Stujert, A.; Bley, T. Formation of ethyl acetate *Kluyveromyces marxianus* on whey during aerobic batch and chemostat cultivation at iron limitation.

Appl. Microbiol. Biotechnol. 2012, *96*, 685-696. https://doi.org/10.1007/s00253-012-4205-y

Löser, C.; Urit, T.; Stukert, A.; Bley, T. Formation of ethyl acetate from whey by *Kluyveromyces marxianus* on a pilot scale. *J. Biotechnol.* 2013, *163*, 17-23. https://doi.org/10.1016/j.jbiotec.2012.10.009

MacLeod, R.A.; Snell, E.E. Some mineral requirements of the lactic acid bacteria. *J. Biol. Chem.* 1947, *170*, 351-365.

Maharjan, R.P.; Ferenci, T.A. shifting mutational landscape in 6 nutritional states: Stress-induced mutagenesis as a series of distinct stress input-mutation output relationships. *PLoS Biol.* 2017, 15, e2001477. https://doi.org/10.1371/journal.pbio.2001477

Martin, J.E.; Imlay, J.A. The alternative aerobic ribonucleotide reductase of *Escherichia coli*, NrdEF, is a manganese-dependent enzyme that enables cell replication during periods of iron starvation. *Mol. Microbiol.*, 2011, *80*, 319-334. https://doi.org/10.1111/j.1365-2958.2011.07593.x

Marzan, L.W.; Shimizu, K. Metabolic regulation of *Escherichia coli* and its *phoB* and *phoR* genes knockout mutants under phosphate and nitrogen limitations as well as at acidic condition. *Microb. Cell Fact.* 2011, *10*, 39. https://doi.org/10.1186/1475-2859-10-39

Massé, E., Gottesman, S. A small RNA regulates the expression of genes involved in iron metabolism in *Escherichia coli*. *Proc. Natl. Acad. Sci. USA* 2002, *99*, 4620-4625. https://doi.org/10.1073/pnas.032066599

Masuda, A.; Toya, Y.; Shimizu, H. Metabolic impact of nutrient starvation in mevalonate-producing *Escherichia coli*. *Bioresource Technol.* 2017, *245*, 1634-1640. https://doi.org/10.1016/j.biortech.2017.04.110

Mateles, R. I., Battat, E. (1974). Continuous culture used for media optimization. *Appl. Microbiol.* 1974, *28*, 901-905. https://doi.org/10.1128/am.28.6.901-905.1974

Maxon, W.D. Continuous fermentation. *Ind. Eng. Chem.* 1960, *1*, 64-65. https://doi.org/10.1021/ie50601a045

Maxon, W.D. Continuous fermentation; a discussion of its principles and applications. *Appl. Microbiol.* 1955, *3*, 110–120. https://doi.org/10.1128/am.3.2.110-122.1955

Mazel, D.; Marlière, P. Adaptive eradication of methionine and cysteine from cyanobacterial light-harvesting proteins. *Nature* 1989, *341*, 245-248. https://doi.org/10.1038/341245a0

McHugh, J.P.; Rodríguez-Quiñones, F.; Abdul-Tehrani, H.; Svistunenko D.A.; Poole, R.K.; Cooper, C.E.; Andrews, S.C. Global iron-dependent gene regulation in *Escherichia coli*: a new mechanism for iron homeostasis. *J. Biol. Chem*. 2003, *278*, 29478-29486. https://doi.org/10.1074/jbc.M303381200

McIntyre, J.J.; Bull, A.T.; Bunch, A.W. Vancomycin production in batch and continuous culture. *Biotechnol. Bioeng.* 1996, *49*, 412-420. https://doi.org/10.1002/(SICI)1097-0290(19960220)49:4<412::AID-BIT8>3.0.CO;2-S

Meers, J.L.; Tempest, D.W. The influence of extracellular products on the behavior of mixed microbial populations in magnesium-limited chemostat cultures. *J. Gen. Microbiol.* 1968, *52*, 309-317. https://doi.org/10.1099/00221287-52-2-309

Melis, A., Zhang, L., Forestier, M., Ghirardi, M. L., Seibert, M. (2000) Sustained photobiological hydrogen gas production upon reversible inactivation of oxygen evolution in the green alga *Chlamydomonas reinhardtii*. *Plant Physiol.* 122, 127-135.

Merchant, S.S., Helmann, J.D. Elemental economy: microbial strategies for optimizing growth in the face of nutrient limitation. *Adv Microb. Physiol.* 2012, *60*, 91-210. https://doi.org/10.1016/B978-0-12-398264-3.00002-4

Minihane, B.J.; Brown, D.E. (1986). Fed-batch culture technology. *Biotechnol. Adv.* 1986, *4*, 207-218. https://doi.org/10.1016/0734-9750(86)90309-5

Monod, J. Recherches sur la croissance des cultures bactériennes, Paris, France: Hermann et Cie. 1942.

Monod, J. The growth of bacterial cultures. *Annu. Rev. Microbiol.* 1949, *8*, 371-374.

Morita, T.; Fukuoka, T.; Imura, T.; Kitamoto, D. Accumulation of cellobiose lipids under nitrogen-limiting conditions by two ustilaginomycetous yeasts. *Pseudozyma aphidis* and *Pseudozyma hubeiensis*. *FEMS Yeast Res.* 2013, *13*, 44-49. https://doi.org/10.1111/1567-1364.12005.

Mukherjee, M.; Sarkar, P.; Goswami, G.; Das, D. Regulation of butanol biosynthesis in *Clostridium acetobutylicum* ATCC 824 under the influence of zinc supplementation and magnesium starvation. *Enzyme Microb. Technol.* 2019, *129*, 109352. https://doi.org/10.1016/j.enzmictec.2019.05.009

Muro-Pastor, M.I.; Reyes, J.C.; Florencio, F.J. Cyanobacteria perceive nitrogen status by sensing intracellular 2-oxoglutarate levels. *J. Biol. Chem.* 2001, *276*, 38320-38328. https://doi.org/10.1074/jbc.M105297200

Muro-Pastor, M.I.; Reyes, J.C.; Florencio, F.J. Ammonium assimilation in cyanobacteria. *Photosynth. Res.* 2005, *83*, 135-150. https://doi.org/10.1007/s11120-004-2082-7

Nayak, M.; Suh, W.I.; Chang, Y.K.; Lee. B. (2019) Exploration of two-stage cultivation strategies using nitrogen starvation to maximize the lipid productivity in *Chlorella* sp. HS2. *Biores. Technol.* 2019, *276*, 110-118. https://doi.org/10.1016/j.biortech.2018.12.111

Neijssel, O.M., Tempest, D.W. The role of energy-spilling reactions in the growth of *Klebsiella aerogenes* NCTC 418 in aerobic chemostat culture. *Arch. Microbiol*. 1976, *110*, 305–311. https://doi.org/10.1007/BF00446843

Neijssel, O.M.; Tempest, D.W. The regulation of carbohydrate metabolism in *Klebsiella aerogenes* NCTC 418 organisms, growing in chemostat culture. *Arch. Microbiol*. 1975, *106*, 251-258. https://doi.org/10.1007/BF00446531

Nguyen, N.-P.-T.; Raynaud, C.; Meynial-Salles, I.; Soucaille, P. Reviving the Weizmann process for commercial n-butanol production. *Nat. Commun.* 2018, *9*, 3682. https://doi.org/10.1038/s41467-018-05661-z

Nikaido H. Molecular basis of bacterial outer membrane permeability revisited. *Microbiol. Mol. Biol. Rev.* 2003, *67*, 593-656. https://doi.org/10.1128/MMBR.67.4.593-656.2003

Niyas, A.M.M.; Eiteman, M.A. Phosphatases and phosphate affect the formation of glucose from pentoses in *Escherichia coli*. *Eng. Life Sci.* 2017, *17*, 579-584. https://doi.org/10.1002/elsc.201600177

Novick, A.; Szilard, L. Experiments with the chemostat on spontaneous mutations on bacteria. *Proc. Natl. Acad. Sci*. 1950, *36*, 708-719. https://doi.org/10.1073/pnas.36.12.708

Osanai, T.; Imamura, S.; Asayama, M.; Shirai, M.; Suzuki, I.; Murata, N.; Tanaka, K. Nitrogen induction of sugar catabolic gene expression in *Synechocystis* sp. PCC 6803. *DNA Res.* 2006, *13*, 185-195. https://doi.org/10.1093/dnares/dsl010

Otten, A., Brocker, M.; Bott, M. Metabolic engineering of *Corynebacterium glutamicum* for the production of itaconate. *Metabol. Eng.* 2015, *30*, 156-165. https://doi.org/10.1016/j.ymben.2015.06.003

Owens, J.D.; Legan, J.D. Determination of the Monod substrate saturation constant for microbial growth. *FEMS Microbiol Rev.* 1987, *46*, 419-432. https://doi.org/10.1111/j.1574-6968.1987.tb02478.x

Paalme, T.; Kahru, A.; Elken, R.; Vanatalu, K.; Tiisma, K.; Vilu, R. (1995) The computer-controlled continuous culture of *Escherichia coli* with a smooth change in dilution rate (A-stat). *J. Microbiol. Meth.* 1995, *24*, 145-153. https://doi.org/10.1016/0167-7012(95)00064-X

Pardee, A.B. Purification and properties of a sulfate-binding protein from *Salmonella typhimurium*. *J. Biol. Chem.* 1966, *241*, 5886-5892. https://doi.org/10.1016/S0021-9258(18)96353-2

Parente, A.F.A.; Bailão, A.M.; Borges, C.L.; Parente, J.A.; Magalhães, A.D.; Ricart, C.A.O.; Soares, C.M.A. Proteomic Analysis Reveals That Iron Availability Alters the Metabolic Status of the Pathogenic Fungus *Paracoccidioides brasiliensis*. *PLoS one* 2011, *6*, e22810. https://doi.org/10.1371/journal.pone.0022810

Park, N.H.; Rogers, P.L. L-phenylalanine production in continuous culture using a hyperproducing mutant of *Escherichia coli* K-12. *Chem. Eng. Commun*. 1986, *45*, 185–196. https://doi.org/10.1080/00986448608911382

Peebo, K., Neubauer, P. Application of continuous culture methods to recombinant protein production in microorganisms. *Microorganisms*, 2018, *6*, 56. https://doi.org/10.3390/microorganisms6030056

Pereira, D.S.; Donald, L.J.; Hosfield, D.J.; Duckworth, H.W. Active site mutants of *Escherichia coli* citrate synthase. *J. Biol. Chem.* 1994, 269, 412-417. https://doi.org/10.1016/S0021-9258(17)42366-0

Perez-Zabaleta, M.; Guevara-Martínez, M.; Gustavsson, M.; Quillahuamán, J.; Larsson, G., van Maris, A.J.A. Comparison of engineered *Escherichia coli* AF1000 and BL21 strains for *(R)*-3-hydroxybutyrate production in fed-batch cultivation. *Appl. Microbiol. Biotechnol.* 2019, *103*, 5627–5639. https://doi.org/10.1007/s00253-019-09876-y

Peterson, C.N.; Mandel, M.J.; Silhavy, T.J. *Escherichia coli* starvation diets: Essential nutrients weigh in distinctly. *J. Bacteriol*. 2005, *187*, 7549-7553. https://doi.org/10.1128/JB.187.22.7549-7553.2005

Philpott, C.C.; Protchenko, O. Response to iron deprivation in *Saccharomyces cerevisiae*. *Eukary. Cell* 2008, *7*, 20-27. https://doi.org/10.1128/EC.00354-07

Pirt, S.J. Fed-batch culture of microbes. *Ann. N.Y. Acad. Sci.* 1979, *326*, 119-125. https://doi.org/10.1111/j.1749-6632.1979.tb14156.x

Pirt, S.J. The theory of fed batch culture with reference to the penicillin fermentation. *J. Appl. Chem. Biotechnol.* 1974, *24*, 415-424. https://doi.org/10.1002/jctb.2720240706

Powell, E.O. Criteria for the growth of contaminants and mutants in continuous culture. *J. Gen. Microbiol*. 1958, *18*, 259-268. https://doi.org/10.1099/00221287-18-1-259

Rakicka, M.; Rukowicz, B.; Rywińska, A.; Lazar, Z.; Rymowicz, W. Technology of efficient continuous erythritol production from glycerol. *J. Clean Prod.* 2016, *139*, 905-913. https://doi.org/10.1016/j.jclepro.2016.08.126

Rakicka, M.; Rywińska, A.; Lazar, Z.; Rymowicz, W. Two-stage continuous culture – Technology boosting erythritol production. *J. Clean Prod.* 2017, *168*, 420-427. https://doi.org/10.1016/j.jclepro.2017.09.060

Reiling, H.E.; Laurila, H.; Fiechter, A. Mass culture of *Escherichia coli*: Medium development for low and high density cultivation of *Escherichia coli* B/r in minimal and complex media. *J. Biotechnol.* 1985, *2*, 191-206. https://doi.org/10.1016/0168-1656(85)90038-0

Reitzer, L. Nitrogen assimilation and global regulation in *Escherichia coli*. *Annu. Rev. Microbiol.* 2003, *57*, 155-176.

Reitzer, L.J. Ammonia assimilation and the biosynthesis of glutamine, glutamate, aspartate, asparagine, L-alanine, and D-alanine. In: *Escherichia coli* and *Salmonella*: Cellular and Molecular Biology. Neidhardt, F. C., Curtiss, III, R., Ingraham, J. L., Lin, E. C. C., Low, K. B., Magasanik, B., (eds). Washington, D.C., American Society for Microbiology Press, 1996, pp. 391-407.

Rhodes, P.M. The production of oxytetracycline in chemostat culture. *Biotechnol. Bioeng.* 1984, *26*, 382-385. https://doi.org/10.1002/bit.260260415

Richter, H.; Martin, M.E.; Angenent, L.T. A two-stage continuous fermentation system for conversion of syngas into ethanol A two-stage continuous fermentation system for conversion of syngas into ethanol. *Energies* 2013, *6*, 3987-4000. https://doi.org/10.3390/en6083987

Riesenberg, D.; Schulz, V.; Knorre, W.A.; Pohl, H.-D.; Korz, D.; Sanders, E.A.; Roß, A.; Deckwer, W.-D. High cell density cultivation of *Escherichia coli* at controlled specific growth rate. *J. Biotechnol*. 1991, *20*, 17-28. https://doi.org/10.1016/0168-1656(91)90032-Q

Robinson, A., Tempest, D.W. Phenotypic variability of the envelope proteins of *Klebsiella aerogenes*. *J. Gen. Microbiol.* 1973, *78*, 361-370. https://doi.org/10.1099/00221287-78-2-361

Roseiro, J.C.; Gírio, F.M.; Kará, A.; Amaral Collaço, M.T. (1993). Kinetic and metabolic effects of nitrogen, magnesium and sulphur restriction in *Xanthomonas campestris* batch cultures. *J. Appl. Bacteriol*. 75, 381-386. https://doi.org/10.1111/j.1365-2672.1993.tb02791.x

Rosenzweig, R.F., Sharp, R.R., Treves, D.S., Adams, J. Microbial evolution in a simple unstructured environment: genetic differentiation in *Escherichia coli*. *Genetics* 1994, *137*, 903-917. https://doi.org/10.1093/genetics/137.4.903

Rutgers, M.; Teixeira De Mattos, M.J.; Postma, P.W.; Van Dam, K. Establishment of the steady state in glucose-limited chemostat cultures of *Klebsiella pneumoniae*. *J. Gen. Microbiol.* 1987, *133*, 445-451. https://doi.org/10.1099/00221287-133-2-445

Ryan, P.R.; Delhaize, E.; Jones, D.L. Function and mechanism of organic anion exudation from plant roots. *Annu. Rev. Plant Physiol. Plant Mol. Biol.* 2001, *52*, 527-560.

Ryu, H.W.; Hahn, S.K.; Chang, Y.K.; Chang, H.N. Production of poly(3-hydroxybutyrate) by high cell density fed-batch culture of *Alcaligenes eutrophus* with phosphate limitation. *Biotechnol. Bioeng.* 1997, *55*, 28-32. https://doi.org/10.1002/(SICI)1097-0290(19970705)55:1<28::AID-BIT4>3.0.CO;2-Z

Rywińska, A.; Juszczyk, P.; Wojtatowicz, M.; Rymowicz, W. Chemostat study of citric acid production from glycerol by *Yarrowia lipolytica*. *J. Biotechnol.* 2011, *152*, 54-57. https://doi.org/10.1016/j.jbiotec.2011.01.007

Sauer, U.; Lasko, D.R.; Fiaux, J.; Hochuli, M.; Glaser, R.; Szyperski, T.; Wüthrich, K.; Bailey, J.E. Metabolic flux ratio analysis of genetic and environmental modulations of *Escherichia coli* central carbon metabolism. *J. Bacteriol*. 1999, *181*, 6679-6688. https://doi.org/10.1128/JB.181.21.6679-6688.1999

Schmideder, A.; Weuster-Botz, D. High-performance recombinant protein production with *Escherichia coli* in continuously operated cascades of stirred-tank reactors. *J. Industr. Microbiol. Biotechnol.* 2017, *44*, 1021-1029. https://doi.org/10.1007/s10295-017-1927-y

Schönheit, P.; Brandis, A.; Thauer, R.K. Ferredoxin degradation in growing *Clostridium pasteurianum* during periods of iron deprivation. *Arch. Microbiol*. 1979, *120*, 73–76. https://doi.org/10.1007/BF00413277

Schreiber, F.; Littmann, S.; Lavik, G.; Escrig, S.; Meibom, A.; Kuypers, M.M.M.; Ackermann, M. Phenotypic heterogeneity driven by nutrient limitation promotes growth in fluctuating environments. *Nat. Microbiol.* 2016, *1*, 16055. https://doi.org/10.1038/nmicrobiol.2016.55

Schrettl, M.; Bignell, E.; Kragl, C.; Joechl, C.; Rogers, T.; Arst, Jr., H.N.; Haynes, K.; Haas, H. Siderophore biosynthesis but not reductive iron assimilation is essential for *Aspergillus fumigatus* virulence. *J. Exp. Med.* 2004, *200*, 1213–1219. https://doi.org/10.1084/jem.20041242

Schuhmacher, T.; Loffler, M.; Hurler, T.; Takors, R. Phosphate limited fed-batch processes: impact on carbon usage and energy metabolism in *Escherichia coli*. *J. Biotechnol.* 2014, *190*, 96-104. https://doi.org/10.1016/j.jbiotec.2014.04.025

Schulze, U., Lidén, G., Villadsen, J. Dynamics of ammonia uptake in nitrogen limited anaerobic cultures of *Saccharomyces cerevisiae. J. Biotechnol.* 1996, *46,* 33-42. https://doi.org/10.1016/0168-1656(95)00176-X

Senn, H.; Lendenmann, U.; Snozzi, M.; Hamer, G.; Egli, T. The growth of *Escherichia coli* in glucose-limited chemostat cultures: a re-examination of the kinetics. *Biochim. Biophys. Acta* 1994, *1201*, 424-436. https://doi.org/10.1016/0304-4165(94)90072-8

Shang, L.; Jiang, M.; Chang, H.N. Poly(3-hydroxybutyrate) synthesis in fed-batch culture of *Ralstonia eutropha* with phosphate limitation under different glucose concentrations. *Biotechnol. Lett.* 2003, *25,* 1415-1419. https://doi.org/10.1023/A:1025047410699

Shehata, T.E.; Marr, A.G. Effect of nutrient concentration on the growth of *Escherichia coli*. *J. Bacteriol.* 1971, *107*, 210-216. https://doi.org/10.1128/jb.107.1.210-216.1971

Sheldon, J.R.; Heinrichs, D.E. Recent developments in understanding the iron acquisition strategies of gram positive pathogens. *FEMS Microbiol. Rev.* 2015, *39*, 592-630. https://doi.org/10.1093/femsre/fuv009

Shen, X.-F.; Liu, J.-J.; Chauhan, A.S.; Hu, H.; Ma, L.-L.; Lam, P.K.S.; Zeng, R.J. Combining nitrogen starvation with sufficient phosphorus supply for enhanced biodiesel productivity of *Chlorella vulgaris* fed on acetate. *Algal Res.* 2016, *17,* 261-267. https://doi.org/10.1016/j.algal.2016.05.018

Singh, A.K.; Mallick, N. Advances in cyanobacterial polyhydroxyalkanoates production. *FEMS Microbiol. Lett.* 2017, *264*, fnx189. https://doi.org/10.1093/femsle/fnx189

Smit, G.; Straver, M.H.; Lugtenberg, B.J.; Kijne, J.W. Flocculence of *Saccharomyces cerevisiae* cells is induced by nutrient limitation, with cell surface hydrophobicity as a major

determinant. *Appl. Environ. Microbiol.* 1992, *58*, 3709-3714. https://doi.org/10.1128/aem.58.11.3709-3714.1992

Stojiljkovic, I.; Cobeljic, M.; Hantke, K. *Escherichia coli* K-12 ferrous ion uptake mutants are impaired in their ability to colonize the mouse intestine. *FEMS Microbiol. Lett.* 1993, *108*, 111-115. https://doi.org/10.1111/j.1574-6968.1993.tb06082.x

Stouthamer, A.H.; Bettenhaussen, C.W. Determination of the efficiency of oxidative phosphorylation in continuous cultures of *Aerobacter aerogenes*. *Arch. Microbiol*. 1975, *102*, 187–192. https://doi.org/10.1007/BF00428367

Sun, L.; Ren, L.; Zhuang, X.; Ji, X.; Yan, J.; Huang, H. Differential effects of nutrient limitations on biochemical constituents and docosahexaenoic acid production of *Schizochytrium sp*. *Bioresource Technol.* 2014, *159*, 199-206. https://doi.org/10.1016/j.biortech.2014.02.106

Sun, Z.; Ramsay, J.A.; Guay, M.; Ramsay, B.A. Automated feeding strategies for high-cell-density fed-batch cultivation of *Pseudomonas putida* KT2440. *Appl. Microbiol. Biotechnol.* 2006, *71*, 423-431. https://doi.org/10.1007/s00253-005-0191-7

Szul, M.J., Dearth, S.P. Carbon fate and flux in *Prochlorococcus* under nitrogen limitation. *mSyst.* 2019, *4*, e00254-18. https://doi.org/10.1128/mSystems.00254-18

Tavares, J.M.; Duarte, L.C.; Amaral-Collaço, M.T.; Gírio, F.M. Phosphate limitation stress induces xylitol overproduction by *Debaryomyces hansenii*. *FEMS Microbiol. Lett.* 1999, *171*, 115-120. https://doi.org/10.1111/j.1574-6968.1999.tb13420.x

Tempest, D.W.; Dicks, J.W.; Ellwood, D.C. Influence of growth condition on the concentration of potassium in *Bacillus subtilis* var. *niger* and its possible relationship to cellular ribonucleic acid, teichoic acid and teichuronic acid. *Biochem. J.* 1968, *106*, 237-243. https://doi.org/10.1042/bj1060237

Tempest, D.W.; Dicks, J.W.; Meers, J.L. Magnesium-limited growth of *Bacillus subtilis* in pure and mixed cultures, in a chemostat. *J. Gen. Microbiol.* 1967, *49*, 139-147. https://doi.org/10.1099/00221287-49-1-139

Tempest, D.W.; Hunter, J.R.; Sykes, J. Magnesium-limited growth of *Aerobacter aerogenes* in a chemostat. *J. Gen. Microbiol*. 1965, *39*, 355-366. https://doi.org/10.1099/00221287-39-3-355

Tissières, A.; Watson, J.D. Ribonucleoprotein particles from *Escherichia coli. Nature* 1958, *182*, 778-780. https://doi.org/10.1038/182778b0

Tokuyama, K.; Toya, Y.; Matsuda, F.; Cress, B.F.; Koffas, M.A.G.; Shimizu, H. Magnesium starvation improves production of malonyl-CoA-derived metabolites in *Escherichia coli. Metabol. Eng.* 2019, *52*, 215-223. https://doi.org/10.1016/j.ymben.2018.12.002

Trilli, A.; Michelini, V.; Mantovani, V.; Pirt, S.J. Estimation of productivities in repeated fed-batch cephalosporin fermentation. *J. Appl. Chem. Biotechnol.* 1977, *27*, 219-224. https://doi.org/10.1002/jctb.5020270132

van Bodegom, P. Microbial Maintenance: A critical review on its quantification. *Microb. Ecol.* 2007, *53*, 513-523. https://doi.org/10.1007/s00248-006-9049-5

van Maris, A.J.A.; Geertman, J.-M.A.; Vermeulen, A.; Groothuizen, M.K.; Winkler, A.A.; Piper, M.D.W.; van Dijken, J.P.; Pronk, J.T. Directed evolution of pyruvate decarboxylase-negative *Saccharomyces cerevisiae*, yielding a C2-independent, glucose-tolerant, and pyruvate-hyperproducing yeast. *Appl. Environ. Microbiol.* 2004, *70*, 159-166. https://doi.org/10.1128/AEM.70.1.159-166.2004

Varrone, C.; Skiadasa, I.V.; Gavala, H.N. Effect of hydraulic retention time on the modelling and optimization of joint 1,3 PDO and BuA production from 2G glycerol in a chemostat process. Chem. Eng. J. 2018, *347*, 525-534. https://doi.org/10.1016/j.cej.2018.04.071

Vázquez-Lima, F.; Silva, P.; Barreiro, A.; Martínez-Moreno, R.; Morales, P.; Quirós, M.; González, R.; Albiol, J.; Ferrer, P. Use of chemostat cultures mimicking different phases of wine fermentations as a tool for quantitative physiological analysis. *Microb. Cell Fact.* 2014, *13*, 85. https://doi.org/10.1186/1475-2859-13-85

Volgusheva, A.; Styring, S.; Mamedov, F. Increased photosystem II stability promotes H2 production in sulfur-deprived *Chlamydomonas reinhardtii. Proc. Natl. Acad. Sci. USA* 2013, *110*, 7223-7228. https://doi.org/10.1073/pnas.1220645110

von Wobeser, E.A. Genome-wide expression analysis of environmental stress in the cyanobacterium *Synechocystis* PCC 6803. *Ph.D. thesis, Institute for Biodiversity and Ecosystem Dynamics, University of Amsterdam, p. 68.* 2010.

Vrabl, P.; Schinagl, C.W.; Artmann, D.J.; Krüger, A.; Ganzera, M.; Pötsch, A.; Burgstaller, W. The dynamics of plasma membrane, metabolism and respiration (PM-M-R) in *Penicillium ochrochloron* CBS 123824 in response to different nutrient limitations – a multi-level approach to study organic acid excretion in filamentous fungi. *Front. Microbiol.* 2017, *8*, 2475. https://doi.org/10.3389/fmicb.2017.02475

Wadhwa, M.; Srinivasan, S.; Bachhawat, A.K.; Venkatesh, K.V. Role of phosphate limitation and pyruvate decarboxylase in rewiring of the metabolic network for increasing flux towards isoprenoid pathway in a TATA binding protein mutant of *Saccharomyces cerevisiae*. *Microb. Cell Fact.* 2018, *17*, 152. https://doi.org/10.1186/s12934-018-1000-1

Walker, G. M.; Maynard, A. I. Magnesium-limited growth of *Saccharomyces cerevisiae*. *Enzyme Microb. Technol.* 1996, *18*, 455-459. https://doi.org/10.1016/0141-0229(95)00130-1

Wang, F.; Lee, S.Y. Poly(3-hydroxybutyrate) production with high productivity and high polymer content by a fed-batch culture of *Alcaligenes latus* under nitrogen limitation. *Appl. Environ. Microbiol.* 1997, *63*, 3703-3706. https://doi.org/10.1128/aem.63.9.3703-3706.1997

Wang, Y.; Xu, H.; Yang, J.; Zhou, Y.; Wang, X.; Dou, S.; Li, L.; Liu, G.; Yang, M. Effect of sulfur limitation strategies on glucose-based carbohydrate production from *Chlorella sorokiniana*. *Renewable Energy* 2022, *200*, 449-456. https://doi.org/10.1016/j.renene.2022.09.106

Warsi, O.M.; Andersson, D.I.; Dykhuizen, D.E. Different adaptive strategies in *E. coli* populations evolving under macronutrient limitation and metal ion limitation. *BMC Evol. Biol.* 2018, *18*, 72. https://doi.org/10.1186/s12862-018-1191-4

Weikert, C.; Sauer, U.; Bailey, J.E. Use of a glycerol-limited, long-term chemostat for isolation of *Escherichia coli* mutants with improved physiological properties. *Microbiology* 1997, *143*, 1567-1574. https://doi.org/10.1099/00221287-143-5-1567

Wendel, B.M.; Pi, H.; Krüger, L.; Herzberg, C.; Stülke, J.; Helmann, J.D.; A central role for magnesium homeostasis during adaptation to osmotic stress. mBIO 2022, *13*, e00092-22 https://doi.org/10.1128/mbio.00092-22

Werner-Washburne, M.; Braun, E.L., Crawford, M. E., Peck, V.M. Stationary phase in *Saccharomyces cerevisiae. Mol. Microbiol.* 1996, *19*, 1159-1166. https://doi.org/10.1111/j.1365-2958.1996.tb02461.x

Wick, L., M., Weilenmann, H., Egli, T. The apparent clock-like evolution of *Escherichia coli* in glucose-limited chemostats is reproducible at large but not at small population sizes and can be explained with Monod kinetics. *Microbiology* 2002, *148*, 2889-2902. https://doi.org/10.1099/00221287-148-9-2889

Willrodt, C.; Hoschek, A.; Bühler, B.; Schmid, A.; Julsing, M.K. Decoupling production from growth by magnesium sulphate limitation boosts de novo limonene production. *Biotechnol Bioeng*, 2016, *113*, 1305-1314. https://doi.org/10.1002/bit.25883

Wouters, J.T.M.; Buysman, P.J. Production of some exocellular enzymes by *Bacillus licheniformis* 749/C in chemostat cultures. *FEMS Microbiol. Lett.* 1977, *1*, 109-112. https://doi.org/10.1111/j.1574-6968.1977.tb00592.x

Wu, S.; Zhao, X.; Shen, H.; Wang, Q.; Zhao, Z.K. Microbial lipid production by *Rhodosporidium toruloides* under sulfate-limited conditions. *Bioresource Technol.* 2011, *102*:1803-1807. https://doi.org/10.1016/j.biortech.2010.09.033

Yamanè, T.; Shimizu, S. Fed-batch techniques in microbial processes. In: Bioprocess Parameter Control. Advances in Biochemical Engineering/Biotechnology, vol 30. Springer, Berlin, Heidelberg. 1984. Pp. 147-194. https://doi.org/10.1007/BFb0006382

Yano, T.; Kurokawa, M.; Nishizawa Y. Optimum substrate feed rate in fed-batch culture with the DO-stat method. *J. Fermentation Bioeng.* 1991, *71*, 345-349. https://doi.org/10.1016/0922-338X(91)90348-K

Yee, L.; Blanch, H.W. Defined media optimization for growth of recombinant *Escherichia coli* X90. *Biotechnol. Bioeng.* 1993, *41*, 221-230. https://doi.org/10.1002/bit.260410208

Yoo, M.; Croux, C.; Meynial-Salles, I.; Soucaille, P. Metabolic flexibility of a butyrate pathway mutant of *Clostridium acetobutylicum. Metabol. Eng.* 2017, *40*, 138-147.

Yoo, S.-H.; Keppel, C.; Spalding, M.; Jane, J.-L. Effects of growth condition on the structure of glycogen produced in cyanobacterium *Synechocystis* sp. PCC6803. *Intl. J. Biol. Mol.* 2007, *40*, 498-504. https://doi.org/10.1016/j.ijbiomac.2006.11.009

Yoshida, F.; Yamane, T.; Nakamoto, K.-I. Fed-batch hydrocarbon fermentation with colloidal emulsion feed. *Biotechnol. Bioeng.* 1973, *15*, 257-270. https://doi.org/10.1002/bit.260150204

Youngquist, J. T.; Korosh, T.C.; Pfleger, B.F. Functional genomics analysis of free fatty acid production under continuous phosphate limiting conditions. *J. Ind Microbiol Biotechnol* 2017, *44*, 759-772.

Youngquist, J.T.; Rose, J.P; Pfleger, B.F. Free fatty acid production in *Escherichia coli* under phosphate limited conditions. *Appl. Microbiol. Biotechnol*. 2013, *97*, 5149-5159

Zhang, J.-H.; Zeng, X.; Chen, X.-S.; Mao, Z.-G. Metabolic analyses of the improved ε-poly-L-lysine productivity using a glucose-glycerol mixed carbon source in chemostat cultures. *Bioproc Biosyst Eng.* 2018, *41*, 1143-1151. https://doi.org/10.1007/s00449-018-1943-y

Zhang, L.; Happe, T.; Melis, A. Biochemical and morphological characterization of sulfur-deprived and H_2-producing *Chlamydomonas reinhardtii* (green alga). *Planta* 2002, *214*, 552-561. ttps://doi.org/10.1007/s004250100660

Zhang, Y.; Xiong, H.; Chen, Z.; Fu, Y.; Xu, Q.; Chen, N. Effect of fed-batch and chemostat cultivation processes of *C. glutamicum* CP for L-leucine production. *Bioeng.* 2021, *12*, 426-439. https://doi.org/10.1080/21655979.2021.1874693

Zheng, Z.-M.; Xu, Y.-Z.; Wang, T.-P.; Dong, C.-Q.; Yang, Y.-P.; Liu, D.-H. Ammonium and phosphate limitation in 1,3-propanediol production by *Klebsiella pneumoniae*. *Biotechnol. Lett.* 2010, *32*, 289-294. https://doi.org/10.1007/s10529-009-0150-y

Zhu, Y.; Eiteman, M.A.; Altman, R.; Altman, E. High glycolytic flux improves pyruvate production by a metabolically engineered *Escherichia coli* strain. *Appl. Environ. Microbiol.* 2008, *74*, 6649-6655. https://doi.org/10.1128/AEM.01610-08

Zinebi, S.; Raval, G.; Petitdemange, H. Effect of oxygenation and sulfate concentrations on pyruvate and lactate formation in *Klebsiella oxytoca* ZS growing in chemostat culture. *Current Microbiol.* 1994, *29*, 79-85. https://doi.org/10.1007/BF01575752

Zinn, M., Witholt, B., Egli, T. Dual nutrient limited growth: models, experimental observations and applications. *J. Biotechnol.* 204, *113*, 263-279. https://doi.org/10.1016/j.jbiotec.2004.03.030

Ziv, N.; Brandt, N.J.; Gresham, D. The Use of Chemostats in Microbial Systems Biology. *J Vis. Exp*. 2013, *80*, e50168. https://doi.org/10.3791/50168

Table 2.1- Reported yield coefficients for elements using various microorganisms. Where necessary, reported data have been converted so that the yield coefficient is defined as the mass of cells on a dry basis generated per mass of that element consumed (g cells/g element). Each element is available in the medium as a salt or other metabolizable species.

Element	$Y_{X/element}$ (g/g)	Microorganism	Growth Conditions	Operational Condition	Reference
Nitrogen (N)	6	*Bacillus caldotenax*	Pulse Shift; Glucose, methionine, biotin (65°C)	Chemostat: $D = 1.2\ h^{-1}$	Kuhn et al., 1979
	7.2	*Bacillus subtilis*	P-limited	Chemostat: $D = 0.1\ h^{-1}$	Dauner et al., 2001
	7.3			$D = 0.4\ h^{-1}$	
	8.1	*Bacillus subtilis*	N-limited	Chemostat: $D = 0.1\ h^{-1}$	Dauner et al., 2001
	7.7			$D = 0.4\ h^{-1}$	
	5	*Escherichia coli* B/r	Pulse Shift	Chemostat: $D = 0.45\ h^{-1}$	Reiling et al., 1985
	7.9 ± 0.3	*Escherichia coli*	C-limited; Elemental analysis of cells	Chemostat: $D = 0.1\ h^{-1}$	Folsom and Carlson, 2015
	8.0 ± 0.4			$D = 0.2\ h^{-1}$	
	7.8 ± 0.2			$D = 0.3\ h^{-1}$	
	7.8 ± 0.1			$D = 0.4\ h^{-1}$	
	7.5 ± 0.1	*Escherichia coli*	Fe-limited; Elemental analysis of cells	Chemostat: $D = 0.1\ h^{-1}$	Folsom and Carlson, 2015
	7.5 ± 0.1			$D = 0.2\ h^{-1}$	
	7.7 ± 0.0			$D = 0.3\ h^{-1}$	
	7.5 ± 0.0			$D = 0.4\ h^{-1}$	

	9.7 ± 0.3 9.9 ± 0.3 8.8 ± 0.1 8.9 ± 0.2	*Escherichia coli*	N-limited; Elemental analysis of cells	Chemostat: D = 0.1 h^{-1} D = 0.2 h^{-1} D = 0.3 h^{-1} D = 0.4 h^{-1}	Folsom and Carlson, 2015
	10	*Escherichia coli* arginine auxotroph containing plasmid	N-limited; Medium contained arginine and ampicillin	Chemostat: D = 0.4 h^{-1}	Yee and Blanch, 1992
	8.35 8.22 8.26	*Escherichia coli* C Δ*ldhA* Δ*poxB* Δ*ppsA*	N-limited Elemental analysis of medium	Chemostat: D = 0.155 h^{-1} D = 0.208 h^{-1} D = 0.283 h^{-1}	Moxley and Eiteman, 2021
	7.9	*Escherichia coli* W, B, and K-12	Not growth limited; Elemental analysis of cells	Exponential Growth at 20°C or 30°C	Bauer and Ziv, 1976
	11.5	*Penicillium stipitatum*	N-limited; Medium prepared	Chemostat: D = 0.11 h^{-1}	Linton et al., 1984
	9.1	*Pseudomonas* C	Pulse Shift; Methanol	Chemostat: D = 0.32 h^{-1}	Mateles and Battat, 1974
	8.0	*Pseudomonas fluorescens*	Not growth limited; Elemental analysis of cells	Exponential Growth at 30°C	Bauer and Ziv, 1976
	7.0	*Pseudomonas putida*	Not growth limited	Fed-batch	Sun et al., 2006
Phosphorus (P)	28	*Bacillus caldotenax*	Pulse Shift; Glucose, methionine, biotin (65°C)	Chemostat: D = 1.2 h^{-1}	Kuhn et al., 1979

	Bacillus subtilis	K-limited;	Chemostat:	Tempest et al.,
53		Elemental analysis of cells	D = 0.05 h^{-1}	1968
59			D = 0.10 h^{-1}	
31			D = 0.20 h^{-1}	
29			D = 0.40 h^{-1}	
	Bacillus subtilis	N-limited	Chemostat:	Dauner et al.,
42			D = 0.1 h^{-1}	2001
38			D = 0.4 h^{-1}	
	Bacillus subtilis	P-limited;	Chemostat:	Tempest et al.,
77		Elemental analysis of cells	D = 0.10 h^{-1}	1968
59			D = 0.20 h^{-1}	
43			D = 0.40 h^{-1}	
	Bacillus subtilis	P-limited	Chemostat:	Dauner et al.,
96			D = 0.1 h^{-1}	2001
65			D = 0.4 h^{-1}	
	Escherichia coli B/r	Pulse Shift	Chemostat:	Reiling et al.,
36			D = 0.45 h^{-1}	1985
	Escherichia coli	P-limited;	Chemostat:	Yee and Blanch,
34	arginine auxotroph containing plasmid	Medium contained arginine and ampicillin	D = 0.4 h^{-1}	1993
34.7	*Escherichia coli* W	Not growth limited;	Exponential Growth	Bauer and Ziv,
49.8	*Escherichia coli* B	Elemental analysis of cells	at 20°C or 30°C	1976
41.7	*Escherichia coli* K-12			
	Pseudomonas C	Pulse Shift; Methanol	Chemostat:	Mateles and
28			D = 0.32 h^{-1}	Battat, 1974
43	*Pseudomonas fluorescens*	Not growth limited; Elemental analysis of cells	Exponential Growth at 30°C	Bauer and Ziv, 1976

	42.0	*Pseudomonas putida*	Not growth limited	Fed-Batch	Sun et al., 2006
Sulfur (S)	278	*Escherichia coli* B/r	Pulse Shift	Chemostat: $D = 0.45\ h^{-1}$	Reiling et al., 1985
	163	*Escherichia coli* arginine auxotroph containing plasmid	S-limited; Medium contained arginine and ampicillin	Chemostat: $D = 0.4\ h^{-1}$	Yee and Blanch, 1992
	244	*Pseudomonas putida*	Low S medium allowed to become exhausted	Batch; 80 minutes after S starvation	Beil et al., 1996
Magnesium (Mg)	571	*Bacillus caldotenax*	Pulse Shift; Glucose, methionine, biotin (65°C)	Chemostat: $D = 1.2\ h^{-1}$	Kuhn et al., 1979
	770	*Bacillus subtilis*	K-limited; Elemental analysis of cells	Chemostat: $D = 0.05\ h^{-1}$	Tempest et al., 1968
	670			$D = 0.10\ h^{-1}$	
	530			$D = 0.20\ h^{-1}$	
	450			$D = 0.40\ h^{-1}$	
	714	*Bacillus subtilis*	Mg-limited; Elemental analysis of cells	Chemostat: $D = 0.10\ h^{-1}$	Tempest et al., 1967
	567			$D = 0.21\ h^{-1}$	
	444			$D = 0.405\ h^{-1}$	
	397			$D = 0.57\ h^{-1}$	
	830	*Bacillus subtilis*	P-limited	Chemostat: $D = 0.10\ h^{-1}$	Tempest et al., 1968
	670			$D = 0.20\ h^{-1}$	
	500			$D = 0.40\ h^{-1}$	
	588	*Escherichia coli* B/r	Pulse Shift	Chemostat: $D = 0.45\ h^{-1}$	Reiling et al., 1985

	278	*Escherichia coli* arginine auxotroph containing plasmid	Mg-limited; Medium contained arginine and ampicillin	Chemostat: $D = 0.4\ h^{-1}$	Yee and Blanch, 1992
		Klebsiella aerogenes	Mg-limited;	Chemostat:	Tempest et al.,
	832		Medium composition	$D = 0.10\ h^{-1}$	1965
	588			$D = 0.20\ h^{-1}$	
	460			$D = 0.41\ h^{-1}$	
	432			$D = 0.43\ h^{-1}$	
	378			$D = 0.60\ h^{-1}$	
	347			$D = 0.82\ h^{-1}$	
	236	*Pseudomonas putida*	Pulse shift	Fed-Batch	Sun et al., 2006
	128	*Pseudomonas* C	Pulse Shift; Methanol	Chemostat: $D = 0.32\ h^{-1}$	Mateles and Battat, 1974
Iron (Fe)	7,700	*Escherichia coli* B/r	Pulse-shift	Chemostat $D = 0.45\ h^{-1}$	Reiling et al., 1985
	5,600	*Escherichia coli*	Low iron content medium; Elemental analysis of cells	Batch	Abdul-Tehrani et al., 1999
		Escherichia coli	Iron limited;	Chemostat:	Folsom et al.,
	130,000		Elemental analysis of cells	$D = 0.10\ h^{-1}$	2014
	150,000			$D = 0.20\ h^{-1}$	
	120,000			$D = 0.30\ h^{-1}$	
	100,000			$D = 0.40\ h^{-1}$	
	43,000	*Kluyveromyces marxianus*	Iron limited;	Chemostat: $D = 0.15\ h^{-1}$	Löser et al., 2012
	1,700	*Pseudomonas* C	Pulse Shift; Methanol	Chemostat: $D = 0.32\ h^{-1}$	Mateles and Battat, 1974

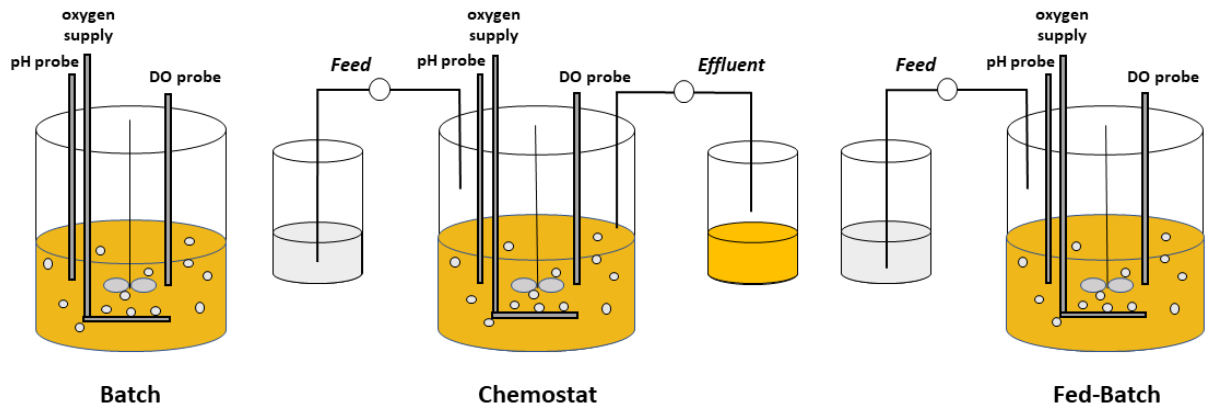

Figure 2.1- The three general modes of fermentation operation: batch, continuous, and fed-batch processes.

CHAPTER 3

PHENOTYPIC CHARACTERIZATION OF PHOSPHOFRUCTOKINASE VARIANTS IN *ESCHERICHIA COLI*

[1]Rajpurohit, H. and Eiteman, M.A. To be submitted to *Applied and Environmental Microbiology*

3.1 ABSTRACT

Phosphofructokinase 1 (PfkA) modulates the ATP-dependent phosphorylation of fructose-6-phosphate, and is a key, controlling enzyme in glycolysis for *Escherichia coli* and other organisms. In this study, 22 chromosomally expressed PfkA variants were constructed in *E. coli* C and with the wild-type strain and the Δ*pfkA* strain compared for growth rate using glucose as the sole carbon source. The majority of variants (14 of 22) attained a growth rate less than 20% of the growth rate of the wild-type strain, and thus similar to the knockout strain (0.12 h^{-1}). Three variants (R171S, F76Y and R77A), representing a range of growth phenotypes, and strains expressing the wild-type PfkA and the Δ*pfkA* deletion strain were additionally examined for key intracellular metabolites and gene expression under nitrogen-limited steady-state conditions. These five strains could be distinguished by two groupings: strains with relatively high growth rate under batch conditions (wild-type and R77A variant) showed the greatest glucose consumption rate and formed acetate, whereas strains with low growth rate (F76Y, R77A and Δ*pfkA*) exhibited low glucose consumption and did not accumulate acetate. As PfkA mutation severity increased, the intracellular concentrations of acetyl-CoA, fructose-1,6-bisphosphate and the sum of dihydroxyacetate and glyceraldehyde-3-phosphate decreased. Mutation severity had a limited effect on expression of *maeB* and *icd* genes, but generally correlated with reduced expression of *zwf* and *pta* genes.

Importance

Phosphofructokinase 1 is a key enzyme controlling glycolytic flux in many organisms. This study provides a metabolic engineering tool to modify central metabolism. Targeted substitutions in PfkA provide a means to modulate the physiological behavior of cells between the wild-type and knockout extremes.

3.2 INTRODUCTION

The flux distribution of central carbon metabolism between the Embden-Meyerhof-Parnas Pathway (EMP), the Entner-Doudoroff Pathway (EDP), and/or the Pentose Phosphate Pathway (PPP) plays an important role in cellular physiology and metabolism (Holms, 1986). For example, wild-type *Escherichia coli* growing on glucose at its maximum growth rate diverts about 78% of glucose-6-phosphate (glucose-6P) towards the EMP, about 22% to the PPP and essentially no carbon into the EDP (Holms, 1986). Because entry into the oxidative PPP generates 2 mol NADPH/mol glucose-6P in *E. coli* whereas the EMP pathway generates no NADPH, the flux distribution between the EMP and the PPP impacts NADPH availability for biosynthetic reactions (Siedler et al., 2011).

Glycolytic flux and the partition of carbon between the EMP and PPP pathways are relevant to microbial processes synthesizing many important biochemicals including 3-hydroxypropionic acid, lycopene, bacitracin, isobutanol. These biochemicals require NADPH as an electron donor for their synthesis and are often limited by NADPH availability (Reynolds et al., 2017, Alper et al., 2005; Zhu et al., 2019; Shi et al., 2013). In wild-type *E. coli*, NADPH is primarily generated by three routes: 1) endogenous transhydrogenase activity, 2) from glucose-6P by sequential glucose-6P 1-dehydrogenase and 6-phosphogluconate dehydrogenase at entrance to the PPP, and 3) isocitrate dehydrogenase in the TCA cycle (Sauer et al., 2004; Reynolds et al., 2017). Among these routes, the oxidative PPP typically dominates NADPH generation in *E. coli* during growth on glucose (Matsuoka and Kurata, 2020).

One strategy to alter the flux distribution between the EMP and the PPP pathways is to increase or decrease the expression of key enzymes at the branchpoint. For example, overexpression of glucose-6P dehydrogenase (coded by *zwf* gene), 6-phosphogluconolactonase

(*pgl*) or 6-phosphogluconate dehydrogenase (*gnd*) in *E. coli* increases the generation of NADPH-dependent products (Lim et al., 2002; Lin et al., 2014; Perez-Zabaleta et al., 2016). Fortunately, overexpression of these genes does not significantly affect glucose uptake rate or specific growth rate in *E. coli* under batch conditions with glucose as the sole carbon source (Nicolas et al., 2007). In contrast, a deletion in the *pgi* gene (phosphoglucose isomerase, Pgi) eliminates the EMP pathway conversion of glucose-6P to fructose-6P, decreases the growth rate by 73% (Sauer et al., 2004) and leads to the upregulation of the EDP, a pathway which generates 1 mol NADPH/mol glucose (Hua et al., 2003). Similarly, a Δ*pfkA* strain (phosphofructokinase 1, PfkA), which maintains 20-30% residual activity as a result of the isoenzyme coded by the *pfkB* gene (Siedler et al., 2011, Siedler et al., 2012), directs 62% of glucose-6P towards the PPP (Hollinshead et al., 2016). However, a *pfkA* knockout reduces the availability of phosphoenolpyruvate (PEP), reduces growth rate by more than 70%, and slows the glucose uptake rate by 64-75% (Siedler et al., 2012). Growth of Δ*pfkA* strains on glucose is accompanied by the partial cyclization of carbon through the PPP: flux is observed from fructose-6P back to glucose-6P via the reversible Pgi (Siedler et al., 2012).

Deletions of either glycolytic genes *pgi* or *pfkA* do divert carbon towards PPP and increase NADPH formation, but constitute an all-or-nothing approach which severely decreases cell growth rate and provides limited ability to modulate flux. Finer modulation of partitioning between the EMP and PPP could potentially serve as a means to control NADPH formation and glycolytic activity. Because the reaction catalyzed by Pgi is reversible, PfkA is a preferred target for affecting the partitioning between the EMP and PPP pathways (Figure 3.1). Modulating PfkA expression in the context of myo-inositol formation has previously been examined using a degradation tag (Brockman and Prather, 2015). Another approach is to alter the intrinsic activity

of PfkA via site-directed mutagenesis to make targeted amino acid substitutions which decrease but do not eliminate the affinity of the substrate(s) (increasing apparent K_M) or the catalytic activity (decreasing k_{CAT}). This strategy has been examined previously as a means to reduce flux into the TCA cycle (Tovilla-Coutiño et al., 2020) and at the pyruvate node (Moxley and Eiteman, 2021).

Phosphofructokinase 1 (EC 2.7.1.11) is an allosteric enzyme that catalyzes the phosphorylation of fructose-6P by ATP to fructose-1,6-bisphosphate (fructose-$16P_2$) in the presence of magnesium (Shirakihara and Evans, 1988). This tetrameric enzyme shows cooperative kinetics with fructose-6P, hyperbolic kinetics with ATP, allosteric activation by ADP and GDP, and inhibition by PEP (Berger et al., 1992). Because deletion of *pfkA* alone reduces the growth rate on glucose significantly (Siedler et al., 2011), growth rate should be a convenient estimate of the severity of PfkA amino acid substitutions on activity. Intracellular fructose-$16P_2$ regulates the transcription factor Cra independent of the glycolytic carbon source, which in turn regulates expression of lower glycolytic enzymes and controls glycolytic flux (Kochanowski et al., 2012, Lehning et al., 2017). Thus, intracellular fructose-$16P_2$ has been used as an indicator of glycolytic activity in living cells (Koberstein et al., 2022).

The goal of this study is to create variants of PfkA which reduce the glycolytic flux. We hypothesize that PfkA variants of *E. coli* having reduced activity would alter their metabolism in response to this perturbation, as determined by glucose uptake, the expression of genes and the concentration of intracellular metabolites such as fructose-$16P_2$.

3.3 MATERIAL AND METHODS

Strains and genetic modifications

Strains used in this study are shown in Table 3.2. The *pfkA* gene knockout in *E. coli* C (ATCC 8739) was constructed by previous methods (Datsenko and Wanner, 2000). Knockouts were selected on Lysogeny Broth (LB) plates supplemented with 40 mg/L kanamycin (LB-Kan). Forward primers external to the target gene and reverse primers within the kanamycin resistance cassette were used to confirm proper chromosomal integration (Table 3.3). The kan^R marker was removed by expression of FLP recombinase from pCP20 (Datsenko and Wanner, 2000). Gene knockouts and removal of the markers were verified by colony PCR using GoTaq® DNA polymerase (Promega, Madison, WI, USA).

A homologous recombination method was used to integrate point-mutated *pfkA* variants in MEC1013. pKSI-1 plasmids containing a point mutation in *pfkA* was used as donor DNA for chromosomal integration (Yang et al., 2014). Plasmids listed in Table 3.4 were constructed using NEBuilder HiFi Assembly (New England Biolabs, Ipswich, MA, USA) or *Escherichia coli* DH5α-mediated assembly (Kostylev et al., 2015). The point-mutated *pfkA* variant, kanamycin cassette and more than 500 bp of flanking homology region were amplified from the respective plasmid and used to transform electrocompetent MEC1013 expressing the lambda red system from pKD46 (Datsenko and Wanner, 2000), and positive transformants were selected on LB-Kan. Integration was confirmed by colony PCR with GoTaq® DNA polymerase, and point-mutated *pfkA* genes were amplified from the chromosome, gel purified, and sequenced (ACGT, Inc., Wheeling, IL, USA).

Plasmid construction

Phusion High-Fidelity Polymerase (New England Biolabs, Ipswich, MA, USA) or PrimeStar Max High-Fidelity Polymerase (Takara Bio, Mountain View, CA, USA) was used to amplify DNA for cloning and genome integration. Assembled plasmids with NEbuilder® Hifi assembly were chemically transformed into *E. coli* DH5α cells and were selected on LB plates containing approriate antibiotics. Quick-DNA Miniprep and Zyppy Plasmid Miniprep Kits were used to purify genomic and plasmid DNA (Zymo Research, Irvine, CA, USA). Zymoclean Gel DNA Recovery Kits were used to purify PCR fragments (Zymo Research, Irvine, CA, USA). Restriction enzymes were purchased from New England Biolabs. Plasmids were confirmed by restriction digest and sequencing (ACGT, Inc., Wheeling, IL, USA). To construct pHR1, a kanamycin cassette was amplified from pKD4 (Datsenko and Wanner, 2000), *pfkA* gene with 500 bp of flanking DNA in upstream region and 78 bp downstream from ATCC 8739, 516 bp downstream of *pfkA* gene from ATCC 8739 were cloned into pKSI vector backbone. All plasmids harboring a single point-mutated *pfkA* gene were generated from pHR1 using mutagenic primers that incorporated mutations into homologous regions using PCR-based site mutagenesis (Table 3.3).

Residues targeted for modification were selected by visual inspection of the PfkA atomic structure (1PFK, Shirakihara and Evans, 1989) using software for molecular visualization (Pymol Molecular Graphics System, Schrödinger, Inc., New York, NY). Factors such as structure, charge, and polarity of amino acids and codon usage frequency of *E. coli* were considered to construct the *pfkA* variants.

Media and Growth Conditions

E. coli strains were routinely maintained and cultured in Lysogeny Broth (LB). A defined medium contained (final concentrations, per L): 5.0 g glucose, 3.504 g NH_4Cl, 1.44 g KH_2PO_4, 2.51 g K_2HPO_4, 2.0 g K_2SO_4, 0.02 g $Na_2(EDTA)\cdot 2H_2O$, 0.45 g $MgSO_4\cdot 7H_2O$, 0.02 g thiamine HCl, 0.25 mg $ZnSO_4\cdot 7H_2O$, 0.125 mg $CuCl_2\cdot 2H_2O$, 1.25 mg $MnSO_4\cdot H_2O$, 0.875 mg $CoCl_2\cdot 6H_2O$, 0.06 mg H_3BO_3, 0.25 mg $Na_2MoO_4\cdot 2H_2O$, 5.5 mg $FeSO_4\cdot 7H_2O$, and 50 mg citric acid. Thiamine was filtered sterilized, while other medium components were autoclaved in compatible mixtures, combined and then adjusted to a pH of 7.2 with 30% (w/v) KOH. A nitrogen-limited medium was identical except for containing 20.0 g/L glucose and 1.0 g/L NH_4Cl. When necessary for plasmid maintenance, 100 µg/mL ampicillin or 40 µg/mL kanamycin was included in the medium.

Shake flask cultures

Each strain was first grown in 3 mL LB medium to an OD of 2, and then 100 µL used to inoculate 3 mL defined medium. After growth this culture was used to inoculate three 250 mL baffled flasks containing 50 mL defined medium to an initial optical density (OD) of 0.02. Flasks were incubated at 37°C at an agitation of 250 rpm. Approximately 6-8 periodic samples were used to calculate growth rate.

Continuous process

Nitrogen-limited steady-state processes were conducted as chemostats. Each strain was initially cultured in LB and then inoculated into a 125 mL baffled shake flask containing 20 mL NLim medium. When the shake flask culture reached an OD of 2, the 20 mL contents were used to inoculate a 1 L bioreactor (Bioflo 310, New Brunswick Scientific Co., New Brunswick, NJ, USA) containing 750 mL NLim medium. After batch growth, the chemostat was initiated at a

nominal dilution rate of 0.1 h^{-1}. The process operated at 37°C using 400 rpm agitation. Air and/or oxygen-supplemented air was sparged at 0.75 L/min to maintain a dissolved oxygen concentration above 40% of saturation. Additional 30% w/v KOH was used to fine control the pH to 7.0, and antifoam 204 (Sigma) was used as necessary. To ensure a steady-state, measurements were initiated at least 5 residence times after the chemostat commenced, and multiple samples collected were separated by at least one residence time.

RT-qPCR

During each chemostat culture after achieving a steady-state, samples for total RNA were collected (10^9 cells), centrifuged (16,000×g, 2 min), and the cell pellet was suspended in 1×RNA protect (New England Biolabs, Ipswich, MA, USA), and stored at -80°C until RNA extraction. Monarch Total RNA Miniprep Kit (New England Biolabs, Ipswich, MA, USA) was used to prepare total RNA from frozen samples. RNA was used as a template for PCR to confirm absence of genomic DNA. One-step quantitative reverse transcriptase PCR (RT-qPCR) was performed using Luna Universal One-Step RT-qPCR Kit (New England Biolabs, Ipswich, MA, USA) on a StepOne Plus instrument (Applied Biosystems, Foster City, CA). Gene-specific primers were designed to create amplicons of 150-200 bp of target genes by using Primer 3 software. Primer pairs for *pfkA, zwf, icd, maeB,* and *pta* and the housekeeping gene *rpoD* were confirmed to have similar efficiencies in the range of 2-6 ng. Triplicate 20 µL reactions containing the same amount of total RNA for each sample were analyzed. No-template and no-RT controls were included. The $2^{-\Delta\Delta C_T}$ method was used to calculate fold change in expression from C_T values generated by the StepOne Plus software (Livak and Schmittgen, 2001).

Quenching and extraction

During each chemostat culture, a sample was directly withdrawn to a sample tube containing 60% (v/v) methanol and 70 mM HEPES (2-[4-(2-hydroxyethyl)-1-piperazine-1-yl]ethanesulfonic acid, pH-7.4) buffer quenching solution at -80°C (Hoque et al., 2005; Faijes et al., 2007). Sample tubes containing quenching solution were weighed before and after the sampling. Quenched samples were centrifuged (10,000×g for 5 min at -5°C), and the cell pellet processed for extraction of metabolites (Schaefer et al., 1999, Hoque et al., 2005).

A perchloric acid extraction procedure was used to extract fructose-16P_2, dihydroxyacetone-P (DHAP), glyceraldehyde-3P (GAP), ATP, ADP, AMP, and acetyl-CoA (Schaefer et al., 1999, de Koning and de Dam, 1992, Hoque et al., 2005). After centrifugation approximately 25% volume of 35% (v/v) perchloric acid (-20°C) was added, the cell pellet was resuspended and stored at -80°C in aliqouts. After one freeze-thaw cycle, proteins and cell fragments were removed by centrifugation (10,000×g for 30 min at -5°C), the supernatant neutralized with 5M K_2CO_3, and then centrifuged again (10,000×g for 10 min at -5°C). The supernatant was stored at -80°C in 900 μL aliquots until further analysis. Throughout the procedure the temperature was maintained below 0°C (Schaefer et al., 1999; Hoque et al., 2005).

An acid/base quenching procedure was used to extract NAD(P)H (Lilius et al., 1979). A sample was directly withdrawn into twice the volume of 0.3 N HCl (to extract NADP) or 0.3 N KOH (to extract NADPH). Both acid- and base-extracted samples were incubated at 60°C for 7 min to extract respective redox metabolties then cooled to 0°C in an ice bath. Extracts were stored at 4°C prior to use (Lowry et al., 1961). Immediately before analysis, acid extracts were adjusted with 0.3 N KOH to pH 6.5 and base extracts with 0.3 N HCl to pH 7.5, incubated for 10 min at 0°C to precipitate proteins, and centrifuged (10,000×g for 15 min) (Beri et al., 2016).

Intracellular metabolites analyses

Enzymatic analyses of cell extracts based on NAD(P)H formation were performed at 37°C and using 0.2 M triethanolamine buffer (pH 7.6) (Hoque et al., 2005). Assays for intracellular metabolites were adapted from previous studies (Lilius et al., 1979, de Koning and de Dam, 1992, Schaefer et al., 1999, Hoque et al., 2005, Beri et al., 2016).

Intracellular ATP was measured in the presence of 5 mM $MgCl_2$ and 0.4 mM NADP by sequentially adding glucose-6P dehydrogenase (0.17 U/mL) and phosphoglucose isomerase (0.7 U/mL) (Lang and Michal, 1974). After the absorbance stabilized, 5 mM fructose and hexokinase (2.8 U/mL) were added to calculate ATP (Trautschold et al., 1985).

Intracellular fructose-$16P_2$, DHAP, and glyceraldehyde-3P (GAP) were assayed with 0.15 mM NADH in 1.5 M triethanolamine (pH 8.5) by sequential addition of glycerol-3P dehydrogenase (0.15 U/ mL), triosephosphate isomerase (2.5 U/mL), and aldolase (1 U/ mL) (Michal and Beutler, 1974).

Intracellular ADP was measured in 125 mM KCl, 10 mM $MgSO_4$, 2.8 mM PEP, and 0.27 mM NADH by the sequential addition of lactate dehydrogenase (2.4 U/mL) and pyruvate kinase (2.0 U/mL). Intracellular AMP was assayed in the sample by addition of myokinase (1.4 U/mL) and 0.10 mM ATP (Jaworek and Welsch, 1985).

Intracellular acetyl-CoA was measured in the presence of 0.2 mM tris-HCl, 1.5 mM NAD and 5 mM malate by sequential addition of malate dehydrogenase (0.9 U/mL) and citrate synthase (0.075 U/mL) (Decker, 1985).

Intracellular NADP and NADPH were quantified using a cycling assay (Lilius et al., 1979, Beri et al., 2016). NADPH and $NADP^+$ were assayed in the presence of 1.12 M bicine buffer, 0.55 mM thiazolyl blue tetrazolium bromide, 2.45 mM phenazine ethosulfate, 10 mM

glucose-6P, and 5 U/mL glucose-6P dehydrogenase (Beri et al., 2016). The slope of the absorbance change was compared with standards prepared through the same extraction and assay procedures.

Analytical methods

A spectrophotometer (UV-650 spectrophotometer, Beckman Instruments, San Jose, CA, USA) was used for the measurement of all intracellular metabolites and for the optical density at 600 nm (OD) to monitor cell growth. For dry cell weight measurement of the chemostat culture, three 20.0 mL samples were centrifuged (3300 × g, 10 min, 4°C), the pellets washed/centrifuged three times with 20 mL DI water, and then dried at 60°C for 24 h.

Samples were routinely frozen at -20°C for glucose and organic acid analysis, and thawed samples were centrifuged (8000×g for 5 min), and filtered (0.45 µm nylon, Acrodisc, Pall Corporation, Port Washington, NY). High performance liquid chromatography (HPLC) using 4 mN H_2SO_4 at 60°C and 0.6 mL/min with a Coregel 64-H ion-exclusion column (Transgenomic Ltd., Glasgow, United Kingdom), and refractive index detector was used to quantify glucose and organic acids (Eiteman and Chastain, 1997). Student's t-test was used to compare data statistically, with 95% confidence interval the basis for significance.

To confirm the absence of ammonium in the effluent for N-limited chemostats, triplicate samples (5 mL) were stored at -20°C, thawed on ice, centrifuged (16,000 × g, 5 min), and then analyzed using the hydroxybenzyl alcohol method (Ammonia-CHEMets, CHEMetrics LLC, Midland, VA, USA).

3.4 RESULTS

Construction of PfkA variants

We sought to reduce the catalytic activity of phosphofructokinase (PfkA) and thereby alter microbial physiology generally, and the distribution of fluxes between the EMP pathway and the PPP specifically during growth of *E. coli* on glucose as the sole carbon source. In order to test the effect of modified PfkA, different point mutations in the *pfkA* gene, corresponding to targeted amino acid substitutions, were introduced into the chromosome. Certain amino acids substitutions, such as those within the active site, would be expected to eliminate catalytic activity. For example, D127 facilitates the nucleophilic attack of the 1-hydroxyl on fructose-6P on the γ-phosphate of ATP (Berger and Evans, 1992), and substitution D127E, D127Y (Berger and Evans, 1992), and D127S (Hellinga and Evans, 1987) lead to more than 99% decrease in activity. Because of the strong reduction in activity anticipated by these modifications, D127 was not targeted for site directed mutagenesis. The goal instead is to modulate activity to affect growth and metabolism. We targeted amino acid residues that are 1) in the mobile loops (G10 to P14, P123 to I137, M169 to L176) stabilizing the catalytic phosphoryl group transfer near the active site, or 2) associated with the pocket that stabilizes fructose-6P and ATP.

D103 is an important residue to position Mg^{2+} and stabilize the transition state (Shirakihara and Evans, 1988) and was targeted for mutagenesis. We also selected R171, which is spatially adjacent to the active site, and substitutions here are known to affect k_{CAT} and K_M without eliminating activity (Hellinga and Evans, 1987; Shirakihara and Evans, 1988; Zheng and Kemp, 1994). Residue I126 was also targeted because a substitution here affects both K_M and k_{CAT} (Zheng and Kemp, 1992), and can induce the R252 residue to flop into the binding cleft (Zheng and Kemp, 1992). Another small mobile loop (G11;G12;D13;P14) appears to be

involved in catalysis. Specifically, G11 stabilizes the phosphoryl transfer from ATP to fructose-6P, as the amide group of G11 forms a hydrogen bond with phosphate group of ATP during the transition stage (Shirakihara and Evans, 1988). Given the proximity of G10 and G11 to the active site, these residues were targeted for mutagenesis.

The α-helix (G248 to G254) is believed to stabilize fructose-6P, and H249 interacts with the phosphate of fructose-6P (Shirakihara and Evans, 1988). R72 also stabilizes the transition state by interacting with the phosphate of fructose-6P (Zheng and Kemp, 1992). Both H249 and R72 were targeted for amino acid substitution.

Residues Y41, F76, R77, R82, and R111 are within 9Å of the N-3 of the adenosine ring of ATP at the active site (Wang and Kemp, 1999). Modification of these residues was previously studied for selectivity of other nucleotide triphosphates, and substitutions at Y41 and F76 with similar bulky groups cause moderate changes kinetic parameters (Wang and Kemp, 1999). Similarly, R77 supports the hydrophobic pocket and stabilizes the ATP through an arginine crown formed with R88 and R111 (Wang and Kemp, 1999). We selected Y41, F76, and R77 for substitutions.

In summary, 10 residues (G10, G11, Y41, R72, F76, R77, D103, I126, R171, H249) were selected to generate 22 PfkA variants (single-point mutations) which were chromosomally integrated into *E. coli*. These PfkA variants were examined for their impact on microbial physiology (specific growth rate) and metabolic activity (transcription and metabolites).

Substitutions in PfkA affect cell growth rate

E. coli Δ*pfkA* has previously been observed to have an 80% lower growth rate (0.11 h^{-1}) on glucose as the sole carbon source compared to the wild-type strain (Siedler et al., 2012), and therefore the maximum specific growth rate (μ_{max}) is believed to be a direct indicator of

glycolytic flux (Paalme et al., 1997). We measured the specific growth rate of wild-type *E. coli* on glucose to be 0.94 ± 0.13 h^{-1} and the Δ*pfkA* strain to be 0.12 ± 0.01 h^{-1} (Figure 3.2). Many examined amino acid substitutions resulted in a specific growth rate only slightly greater than the knockout strain: R72K/S/V (0.15-0.17 h^{-1}), D103A/E/V (0.17-0.19 h^{-1}), I126A/E/K/S (0.13-0.14 h^{-1}), G10A (0.13 h^{-1}), and G11A (0.15 h^{-1}). Growth rate of strains with a substitution at H249 depended on the amino acid: substitution of a bulky residue (H249F) resulted in a strain having more than 2× the growth rate (0.38 h^{-1}) as one having an H249 substitution with a smaller residue (H249D, 0.14 h^{-1} and H249A, 0.18 h^{-1}). Similarly, the growth rate of variants with a R171 substitution was influenced by the size and polarity/charge: R171K (0.46 h^{-1}) resulted in 20% greater growth rate than a small hydrophobic substitution (R171A, 0.38 h^{-1}) and 80% greater than a small polar substitution (R171S, 0.26 h^{-1}). Four variants with substitutions in the hydrophobic pocket which stabilizes ATP (Y41F, F76Y, R77A, and R77K) showed intermediate growth rates (0.33-0.57 h^{-1}). We consider the reduced growth rate compared to the wild-type strain to be an indicator of the "mutation severity", and selected strains with a range of growth rates to investigate the effect of mutation severity on cell physiology.

Steady-state process

Cells growing in shake flasks experience dynamic conditions of pH and oxygenation, and each strain has a different specific growth rate. In order to examine variants having a range of mutation severity during growth under the identical conditions, we compared the wild-type strain, three *pfkA* variants and Δ*pfkA* under steady-state conditions in a controlled bioreactor. We selected nitrogen (N)-limited conditions in a chemostat and a dilution rate of 0.1 h^{-1}, just below the maximum specific growth rate of the Δ*pfkA* strain, to compare five strains showing a range of maximum specific growth rates and mutation severity: MEC1012 (Δ*pfkA*, 0.12 h^{-1}), MEC1230

(PfkA[R171S], 0.26 h^{-1}), MEC1300 (PfkA[F76Y], 0.33 h^{-1}), MEC1302 (PfkA[R77A], 0.57 h^{-1}) and MEC1356 (wild-type PfkA, 0.94 h^{-1}).

N-limited, aerobic conditions were confirmed by a) the dissolved-oxygen (DO) concentration maintained above 40% saturation, b) the absence of anaerobic products such as formate, succinate, and lactate, d) presence of glucose in the effluent, and e) absence of nitrogen in the effluent.

Physiology and respiration.

PfkA variants biomass yield on glucose ($Y_{X/Glu}$) at same dilution rate 0.1 h^{-1} under nitrogen limitation was related to the mutation severity (Table 3.1). The biomass yield on glucose of 0.26-0.31 g/g was the greatest for the three strains with greatest mutation severity: PfkA[F76Y], PfkA[R171S] and the Δ*pfkA* strain. MEC1356 expressing the wild-type *pfkA* and PfkA[R77A] showed identical yields at 0.19 g/g ($p>0.05$). Similarly, the glucose consumption rates (q_{Glu}) could be divided into two groups: the three strains with greatest mutation severity showed low glucose consumption rates (1.7-2.1 mmol g^{-1} h^{-1}), whereas the two strains with low mutation severity exhibited about 50% greater glucose consumption rates (2.9 - 3.0 mmol g^{-1} h^{-1}). The three strains with greatest mutation severity furthermore generated very little acetate under glucose-excess and N-limited steady-state conditions. PfkA[R77A] generated the most acetate, followed by the wild-type *pfkA* strain. No trend was observed for oxygen consumption rate nor carbon dioxide evolution rate. The respiratory quotients for PfkA variants and the Δ*pfkA* strain were close to 1 (Table 3.1).

Intracellular metabolites

The overall aim of this study was to alter metabolism by tuning PfkA activity by the use of targeted amino acid substitutions on this enzyme. Because a PfkA modification cannot be

measured directly via a biochemical product such as pyruvate or acetate (Moxley and Eiteman, 2021, Tovilla-Coutiño et al., 2020), we measured glycolytic metabolites and adenylate charge by rapid quenching of samples (Figure 3.3).

Acetyl-CoA pool is associated with increased acetate formation during N-limited cultures compared to glucose limited cultures (Hua et al., 2003). For the five strains examined under N-limited conditions at a dilution rate of 0.1 h^{-1}, we observed a decrease in acetyl-CoA with increased mutation severity: PfkA[R77A] and the wild-type PfkA, the strains with the highest specific growth rate in batch culture, resulted in 0.53-0.55 nmol acetyl CoA/mg, compared to 0.21-0.27 nmol acetyl CoA/mg for the two slowest growing PfkA[R171A] and Δ*pfkA* strains (Figure 3.3). The intermediate strain, PfkA[F76Y], showed an intermediate pool of acetyl CoA at 0.43 nmol/mg.

Fructose-16P_2 is the direct product of phosphofructokinase (Shirakihara and Evans, 1988), and unsurprisingly, the fructose-16P_2 concentration was also correlated to the mutation severity. The wild-type PfkA strain showed 2.1 nmol fructose-16P_2/mg under N-limited steady-state conditions. In order of increasing mutation severity, PfkA[R77A] showed 0.91 nnmol fructose-16P_2/mg, while PfkA[F76Y] and PfkA[R171S] had steady-state concentrations of 0.54-0.56 nmol fructose-16P_2/mg. The Δ*pfkA* strain showed a steady-state concentration of 0.17 nmol fructose-16P_2/mg.

The metabolites dihydroxyacetone-P (DHAP) and glyceraldehyde-3P (GAP) are interconvertible products of fructose-16P_2, and the sum of their concentrations (DHAP+GAP) was also related to mutation severity (Figure 3.3). Specifically, DHAP + GAP levels were lowest in the Δ*pfkA* strain (0.2 nmol/mg), intermediate in the variants (1.0-1.9 nmol/mg), and the greatest in the wild-type strain (2.3 nmol/mg) (Figure 3.3).

The adenine nucleotides, adenosine triphosphate (ATP), adenosine diphosphate (ADP), and adenosine monophosphate (AMP) stoichiometrically couple energy producing and energy consuming metabolic reactions. The Adenylate Energy Charge (AEC) defined as [(ATP) + 1/2 (ADP)]/[(ATP)+(ADP)+(AMP)] is directly correlated to the metabolically available energy stored in the adenylate system (Chapman et al., 1971, Swedes et al., 1975). Under the N-limited conditions, all strains exhibited an AEC of 0.52 – 0.63 (Figure 3.3). We also measured NADPH/NADP in the five strains. The NADPH/NADP ratio was significantly greater ($p<0.05$) in each variant (25 – 100 %) compared to the wild-type ratio of NADPH/NADP (Figure 3.3).

qRT-PCR

Transcription patterns for the genes *pfkA*, *zwf*, *icd*, *maeB*, and *pta* relative to the housekeeping gene *rpoD* were analyzed for three variant strains (PfkA[F76Y], PfkA[R77A], PfkA[R171S]), the Δ*pfkA* strain (MEC1012), and the wild-type strain (MEC1356) growing under N-limited conditions at 0.1 h^{-1}. The *pfkA* gene was selected to analyze transcripts of PfkA variants compared to the wild-type and deletion strains. Other genes were selected for their importance for entry into the pentose phosphate pathway (*zwf*), NADPH formation (*maeB*, *icd*), and phosphorylation of acetyl-CoA (*pta*).

Transcript levels of *pfkA* gene in MEC1012 (Δ*pfkA*) was similar to the no template control confirming no PfkA expression in the knockout strain. The two variants with greater mutation severity, PfkA[R171S] and PfkA[F76Y] showed a significant 2.1- to 2.8-fold increase in the PfkA transcript ($p<0.05$) while the variant with the lowest mutation severity, PfkA[R77A], showed a PfkA transcript indistinguishable from wild-type expression (Figure 3.4).

MEC1012 (Δ*pfkA*) showed a 1.7-fold increase in the *zwf* transcript compared to the wild type strain. In contrast, each of the three PfkA variants showed 70-90% less transcript compared to the wild-type strain (Figure 3.4).

The transcript for the *maeB* gene expressing the NADP-dependent malic enzyme did not show a trend among the five strains. While PfkA[R171S] showed slightly lower transcript, PfkA[F76Y] and PfkA[R77A] showed slightly greater transcript than the wild-type gene ($p<0.05$) (Figure 3.4). Similarly, the transcript levels for the *icd* gene coding the TCA cycle enzyme isocitrate dehydrogenase did not show a trend among the variants and Δ*pfkA* strain, and the transcripts for the Δ*pfkA* strain and PfkA[F76Y] were not significantly different than the *icd* transcript in the wild-type strain. Only PfkA[R77A] and PfkA[R171S] showed signficantly lower *icd* transcript (30-60%) than the wild-type strain ($p<0.05$).

Phosphotransacetylase (Pta) coded by *pta* gene is the first step in the pathway to form acetate in *E. coli*. A consistent trend was observed for the transcript of the *pta* gene: the greater the mutation severity, the lower the relative *pta* transcript. The Δ*pfkA*, PfkA[R171S], and PfkA[F76Y] strains each showed an expression level 96-98% lower than the wild-type *pta*, while PfkA[R77A] showed a 66% lower *pta* transcript relative to the wild-type strain (Figure 3.4).

3.5 DISCUSSION

PfkA plays a key role in glycolysis

Phosphorylation of fructose-6P mediated by phosphofructokinase 1 (PfkA) is the rate controlling reaction in glycolysis in diverse organisms (Passanneau and Lowry, 1964, Blangy et al., 1968), and with its unique allosteric properties and regulation, PfkA has been extensively studied (Atkinson and Walton, 1965; Blangy et al., 1968; Passonneau and Lowry, 1964; Robinson and Fraenkel, 1978; Kotlarz and Buc, 1977). In *E. coli* two isoenzymes mediate the

conversion: PfkA accounts for about 90% of the activity and non-allosteric PfkB plays a minor role (Robinson and Fraenkel, 1978; Kotlarz and Buc, 1977; Babul, 1978). PfkA is allosterically inhibited by phosphoenolpyruvate (PEP), shows cooperativity with fructose-6P and hyberbolic kinetics with ATP (Blangy et al., 1968). Monophosphonucleosides (AMP), fructose-6P, diphosphonucleosides (ADP, GDP) are the activators of PfkA (Atkinson and Walton, 1965). ADP also inhibits the enzyme by binding at the ATP site and affects the cooperativity of enzyme to fructose-6P (Blangy et al., 1968). Deletion of PfkA was reported to cause a 90% reduction in growth rate of *E. coli* on glucose under aerobic conditions (Robinson and Fraenkel, 1978, Brockman et al., 2015), consistent with our observations using ATCC 8739 which showed an 87% decrease in maximum specific growth rate (Figure 3.2).

Various strategies have been examined to upregulate or downregulate PfkA expression. Overexpressing PfkA in *E. coli* led to a 2× increase in lactate formation due to activation of the methylglyoxal pathway, though glycolytic intermediates such as pyruvate and PEP did not increase (Emmerling et al., 1999). The activity of Pfk1 in *Aspergillus niger* was improved by truncating the C-terminal residues that contain sites for allosteric inactivation by citrate. Alone, this strategy required phosphorylation of the enzyme (Mlakar and Legiša, 2006), while an additional T89E PfkA substitution removed the requirement for phosphorylation of the truncated protein (Capuder et al., 2009). Post-translational control of PfkA enzyme using the SsrA tag, which promotes degradation of PfkA via SspB induction, has been used to incur a controlled reduction in PfkA activity and glycolytic flux (Brockman et al., 2015).

In the current work a modest set of single-substitution PfkA *E. coli* variants was created having altered activity. Because the Entner-Duodoroff and pentose phosphate pathways do not compensate for growth on glucose in absence of PfkA (Hollinshead et al., 2015), and because of

the tight control PfkA has on glycolytic flux, we hypothesized that the severity of the mutation and its effect on activity would be directly correlated with maximum specific maximum growth rate using glucose as the sole carbon source.

PfkA variants display a range of growth rate phenotypes

We targeted a variety of amino acid residues associated with the active site or the mobile loops. For example, we selected highly conserved residues G10, G11, and I126 in the mobile loops which are not directly involved in catalytic activity (Wu et al., 1991; Ronimus and Morgan, 2001; Shirakihara and Evans, 1988; Kemp and Gunasekera, 2002). In eukaryotic PfkA, alanine occupies the residue corresponding with *E. coli* G11 (Wu et al., 1991), and thus a G10A or G11A substitution could be anticipated to have minor effects on the enzyme and cell growth. I126 stabilizes R252, a residue which orients the guanidinium group with fructose-6P but which is not involved in catalysis (Zheng and Kemp, 1992). The substitution I126A leads to a 600× increase in K_M for fructose-6P while k_{CAT} is reduced by only 50% (Zheng and Kemp, 1992). Remarkably, G10A, G11A, or I126A/E/S/K substitutions each resulted in growth rates only slightly greater than the Δ*pfkA* strain (MEC1012), over 85% lower than the strain (MEC1356) expressing the wild-type enzyme (Figure 3.2), demonstrating the importance of the mobile loops to activity, and suggesting that the mobile loops might not provide ideal targets for a mild modulation of PfkA activity.

Amino acid substitutions at other conserved sites D103 (associated with magnesium ion binding) and R72 (bridge between ATP and fructose-6P) also severely restricted the growth rate regardless of the specific substitution (Figure 3.2). The D103A substitution has previously been measured to lower the k_{CAT} by 95% with no change in K_M (Berger and Evans, 1992), and in the current study the D103A showed 80% lower growth rate than the wild-type strain (Figure 3.2).

A substitution of aspartate with identically charged glutamate (D103E) or with a hydrophobic side-chain (D103V) also resulted in variants having growth rates similar to the Δ*pfkA* strain. Similarly, we altered the R72 residue which stabilizes phosphoryl group transfer and interacts with the 1-phosphoryl group of the reaction product fructose-1$6P_2$ was selected. The R72S substitution decreases k_{cat} by 95%, increases the fructose-6P K_M by 3× and reduces the Hill constant by 50% (Berger and Evans, 1990). However, all three R72 variants, even the similarly charged R72K substitution, showed a severe decrease in growth rate, 81-84% lower than the wild-type strain. Alteration of certain residues close to the active site results in strains which behave like a Δ*pfkA* knockout.

In contrast, other highly conserved residues, such as R171 and H249, appear to be more amenable to substitutions which modulate the enzyme mildly and thus might lead to a broader range of growth rate phenotypes. Previous studies have shown the R171S substitution causes a negligible change in K_M and a nearly 75% decrease in k_{CAT} compared to wild-type (Hellinga and Evans, 1987). Because of this comparatively modest change in kinetic parameters, R171 was selected to test the effect of size (R171A) and polarity of amino acid (R171K/S). Figure 3.5 shows PYMOL representations of these R171 substitutions and the resulting interactions. In the native enzyme, positively charged arginine interacts with the negatively charged 1-phosphate on fructose-1$6P_2$ (Shirakihara and Evans, 1988) (Figure 3.5a), and this interaction is largely maintained in R171K (Figure 3.5b) but lost in R171S or R171A (Figure 3.5cd). Consistent with the change in this interaction, the R171K variant showed 51% lower growth rate than the wild-type, while R171A was 61% lower, and R171S 73% lower, than the wild-type strain. The R171 residue therefore would be a preferred single site to generate a broad range of growth rate phenotypes (compared to D103, G10, G11, R72). The H249 residue in *E. coli* PfkA binds with

fructose-6P via hydrogen bond between a side-chain nitrogen with negatively charged 6-*o*-phosphoryl group of fructose-6P (Shirakihara and Evans, 1988). Previously, a H298A substitution in human Pfk-M that is sequentially similar to *E. coli* PfkA H249 increased the fructose-6P K_M by a factor of 5 with a negligible change in k_{cat} (Ferreras et al., 2009), and therefore H249 was selected as a target for modification. Although the H249A substitution decreased growth rate by 81% compared to the wild-type, a substitution with a bulkier phenylalanine (H249F) decreased growth rate by only 60% (Figure 3.2). Substituting the basic histidine with the negatively charged aspartate (H249D) resulted in a strain having a growth rate close to the Δ*pfkA* knockout.

Another conserved residue R77 was selected for its role in the formation of an arginine crown (with R82 and R111) which interacts with the N-1 or N-6 of the adenine group on ATP (Wang and Kemp, 1999) and is a located at the end of the hydrophobic pocket for ATP. The R77A substitution causes a 2.5× increase in the K_M for ATP and 30% reduction in k_{CAT} compared to the wild-type (Wang and Kemp, 1999). In the native enzyme, the arginine provides a structural element to the pocket and interacts with adenine (Figure 3.6a), and this interaction is maintained in R77K (Figure 3.6b) but lost in R77A (Figure 3.6). Moreover, substitution of alanine for arginine (R77A) leaves a gap. Surprisingly, the anticipated difference between these interactions was not reflected in the growth rate, as both R77A and R77K showed similar growth rate, only 40% lower than the wild-type; indeed, the R77A and R77K attained the highest growth rate among all the variants examined (Figure 3.2). Substitutions at R77 with negatively charged amino acids (R77E and R77D) were not examined, and since that increase the K_M for ATP by 10-20×, they would be anticipated to lower growth rates significantly (Wang and Kemp, 1999).

Substitutions in PfkA affect glycolytic intermediates and glycolytic flux

Modifications of phosphofructokinase (PfkA) affect glycolytic flux and intracellular concentrations of glycolytic metabolites. Although intracellular metabolite concentration is not always correlated to pathway flux (Hackett et al., 2016), environmental or genetic changes on metabolism can be assessed by key flux signaling metabolites (Litsios et al., 2018). In mice models, increased glycolytic flux correlates with elevated levels of several intermediates including fructose-16P_2, DHAP and GAP (Passanneau and Lowry, 1964). Fructose-16P_2 is widely recognized as an important flux signaling metabolite whose intracellular concentration is linearly correlated with the glycolytic flux in numerous microbial species including *Bacillus subtilis* (Chubukov et al., 2013), *E. coli* (Kochanowski et al., 2013), and *Saccharomyces cerevisiae* (Przybylski et al., 1985). In *E. coli*, fructose-16P_2 interacts with the transcription factor Cra as part of a flux-sensing system reporting the glycolytic flux (Kochanowski et al., 2013), and its inhibition of Cra (Ramseier et al., 1993) regulates central metabolic genes including *crr* (glucose PTS system), *icd* (isocitrate dehydrogenase), *aceA* (isocitrate lyase), *gapA* (glyceraldehyde-3P dehydrogenase) and *ppsA* (PEP synthase) (Ramseier, 1996, Shimada et al., 2005; Shimada et al., 2011). Because fructose-16P_2 is the product of PfkA, increasing the mutation severity of this enzyme would be expected to curtail the fructose-16P_2 pool. Like previous studies using glucose-limited conditions (Kochanowski et al., 2013), the current study using N-limited conditions generally demonstrated a correlation between intracellular fructose-16P_2 (Figure 3.4) and glucose uptake rate (Table 3.1). For example, under steady-state conditions the Δ*pfkA* knockout maintained about 90% lower fructose-16P_2 and 30% lower glucose uptake rate than the wild-type strain (MEC1365), while PfkA variants consistently showed intermediate levels of fructose-16P_2 (Figure 3.3). Most other studies modify glycolytic flux by altering the

dilution rate under glucose-limited conditions (Nanchen et al., 2006; Hua et al., 2004; Kochanowski et al., 2013, Vemuri et al., 2006). However, altering dilution rate in carbon-limited processes changes the steady-state concentration of the carbon source (de Vries, et al., 1970; Harder & Dijkhuizen, 1983), and impacts the expression of a wide range of genes in carbon metabolism and regulation (Vemuri et al., 2006). Thus, the challenge of distinguishing between glucose uptake-related and growth rate-related phenomena strictly speaking remains. In this study, glycolytic flux was altered by modifying the PfkA enzyme while holding the dilution rate at a fixed low rate of 0.10 h^{-1}. Our results using PfkA variants therefore further demonstrate the central relationship between fructose-16P_2 and glycolytic flux. Perturbation of metabolism by the construction of variants at PfkA and other key enzymatic conversions offers a new complimentary strategy for studying metabolism at differing glycolytic fluxes, but at the same dilution rate. Complete metabolic flux analysis using labeled substrates would provide important details for the consequences of altering activity of PfkA (Hua et al., 2003).

The lower glycolytic reaction products of fructose-16P_2 are also associated with glycolytic flux (Kochanowski et al., 2013). In particular, the concentrations of both fructose-16P_2 and the sum DHAP + GAP increase with the dilution rate under glucose-limited conditions from 0.1 h^{-1} to 0.4 h^{-1} (Schaub and Reuss, 2008). The reversible products of aldolase, DHAP and GAP, are themselves interchangeable by triosephosphate isomerase (Figure 3.1). Analogous to fructose-16P_2, we observed a direct correlation at a single dilution rate between the severity of the PfkA modification and intracellular DHAP + GAP (Figure 3.3). For example, the strain expressing wild-type PfkA maintained 11.3× greater DHAP + GAP than the Δ*pfkA* strain, while variants R77A, F76Y, and R171S exhibited 5.0-9.3 times the level of the Δ*pfkA* strain (Figure 3.3). Previous research has reported that a glucose pulse during glucose-limited conditions alters

the concentration of glycolytic metabolites (Schaefer et al., 1999; Hoque et al., 2005; Schaub and Reuss, 2008). In this study, reduced triose and fructose-16P_2 levels occurred despite the presence of glucose at the same growth rate during N-limited growth.

Substitutions in PfkA affect acetate formation

Substitutions in PfkA surprisingly resulted in transcriptional changes in the *pta* gene coding phosphoacetyltransferase and in acetate formation at steady-state under N-limited conditions. Wild-type *E. coli* is widely known to accumulate acetate when grown under carbon-excess conditions, including under nitrogen limitation (Hua et al., 2003, Hua et al., 2004; Folsom and Carlson, 2015) and iron limitation (Baez et al., 2022; Folsom and Carlson, 2015). Acetate accumulation also occurs during carbon-limited steady-state growth at high glucose uptake rate in *E. coli* (Vemuri et al., 2006, Valgepea et al., 2011, Kayser et al., 2005). However, *pta* expression is not strongly influenced by dilution rate under carbon-limited conditions in *E. coli* (Vemuri et al., 2006) and *Corynebacterium glutamicum* (Graf et al., 2020). Acetate accumulation at high glycolytic flux instead has been proposed to be influenced by repression of *acs* coding for acetyl-CoA synthetase (Valgepea et al., 2010). In the current study, acetate accumulation was related to mutation severity: acetate was observed in the two strains with the highest maximum specific growth rate (R77A and wild-type PfkA), but essentially no acetate was observed in the three strains with lowest maximum specific growth rate (Δ*pfkA*, R171S and F76Y). Furthermore, acetate formation (Table 3.1) correlated with higher intracellular acetyl-CoA (Figure 3.3) and greater transcription of *pta* gene coding for phosphotransacetylase (Figure 3.4). In previous studies, a Δ*pgi* strain similarly exhibited 30% less acetyl-CoA than a wild-type strain under glucose-limited conditions (Hoque et al., 2011), and metabolic flux analysis showed 64% lower acetate formation in a Δ*pgi* strain than in wild-type *E. coli* under N-limited conditions

(Hua et al., 2003). As noted above from glucose-limited studies, acetate formation occurs under high glycolytic flux, and one effect of increased mutation severity of PfkA is a reduction in glycolytic flux (Table 3.1). Thus, the diminished formation of acetate in strains with the greatest mutation severity could merely be a consequence of lower glycolytic flux. Since acetate formation at high glycolytic flux has not been attributed to *pta* expression, the relationship between metabolism in PfkA variants and *pta* is less clear. The reduced expression of *pta* in Δ*pfkA* (and variant strains) and low acetyl-CoA concentration reported here could explain the poor performance of the Δ*pfkA* strain in the biochemical production of mevalonate, a product of acetyl-CoA (Satowa et al., 2020; Wang et al., 2022). Interestingly, fructose-16P_2 has been demonstrated to be involved in *pta* activation in *B. subtilis* (Presecan-Siedel et al., 1999).

Adenylate charge indicates metabolic state. Adenine nucleotides are an indicator of cellular metabolic energy (Swedes et al., 1975), and the stored energy in adenine nucleotide pools is quantified by the adenylate energy charge (AEC, Chapman et al., 1971). Cells growing under unrestricted batch conditions with excess nutrients show an AEC above 0.8 (Chapman et al., 1971, Swedes et. al., 1975). Several studies of *E. coli* under glucose-limited steady-state growth report AEC of 0.72-0.85 (Kahru et al., 1987; Hoque et al., 2011), while a Δ*pgi* strain maintained 50% lower ATP leading to an AEC of 0.78 (Hoque et al., 2011). In one shake flask study, a low nitrogen medium showed a similar AEC (0.9) which decreased (0.6) as nitrogen was depleted, and decreased further as culture viability diminished (Chapman et al., 1971). N-limited cultures of *Azotobacter beijerinckii* at 0.1 h^{-1} maintained an AEC of 0.72 (Marriott et al., 1981), identical to *E. coli* as the culture exhausts nitrogen (Dietzler et al., 1974). During a phosphate-limited constant-feed fed-batch *E. coli* cultures, the AEC decreased from 0.8 to 0.5 over 10 h, suggesting consumption of low energy reserves (Schuhmacher et al., 2014). Phosphate limitation also leads

to growth uncoupling due to increased energy demand and elevates the glucose uptake rate (Schuhmacher et al., 2014, Rajpurohit and Eiteman, 2022). In this work, N-limited conditions the AEC was 0.52-0.64 in all strains (Figure 3.3), and the substitution did not affect this value. However, the R77A variant showed an ATP/ADP ratio of 3.3, compared to ATP/ADP values of 1-2 for all other strains (data not shown), similar to the 2.0 ratio observed in N-limited growth of *A. beijerinckii* (Marriott et al., 1981). This observation is noteworthy because the R77A variant showed the greatest steady-state acetate formation, nearly twice that of the wild-type (Table 3.3), and was the only variant studied under steady-state conditions in which the substitution was associated with the ATP binding pocket (Figure 3.6a). Additional research will be needed to clarify the relationship between PfkA, acetate formation and ATP.

ACKNOWLEDGMENTS

The authors thank Sarah Lee and W. Chris Moxley for technical support for this project. We also thank Dr. Ellen Niedle and Chantel Duscent-Maitland for facilitating the qRT-PCR work. The authors acknowledge financial support of the U.S. National Science Foundation (CBET-1802533) and the U.S. Department of Agriculture, National Institute of Food and Agriculture (2017-06510).

3.6 REFERENCES

Alper H, Miyakou K, Stephanopolous G. 2005. Construction of lycopene-overproducing *E. coli* strains by combining systematic and combinatorial gene knockout targets. Nat Biotechnol 23:612-616.

Atkinson DE, Walton GM. 1965. Kinetics of regulatory enzymes. J Biol Chem 240: 757-763.

Babul J. 1978. Phosphofructokinases from *Escherichia coli*. J Biol Chem 253:4350-4355.

Baez A, Sharma AK, Bryukhanov A, Anderson ED, Rudack L, Olivares-Nernandez R, Tuan D, Shiloach J. 2022. Iron availability enhances the cellular energetics of aerobic *Escherichia coli* cultures while upregulating anaerobic respiratory chains. New Biotechnol 71:11-20.

Berger SA, Evans PR. 1990. Active-site mutants altering the cooperativity of *E. coli* phosphofructokinase. Nature 343:575-576.

Berger SA, Evans PR. 1992. Site-directed mutagenesis identifies catalytic residue in the active site of *Escherichia coli* phosphofructokinase. Biochem 31:9237-9242.

Beri D, Olson DG, Holwerda EK, Lynd LR. 2016. Nicotinamide cofactor ratios in engineered strains of *Clostridium thermocellum* and *Thermoanaerobacterium saccharolyticum*. FEMS Microbiol Lett 363:fnw091.

Blangy D, Buc H, Monod J. 1968 Kinetics of the allosteric interactions of phosphofructokinase from *Escherichia coli*. J Mol Biol 31:13-35.

Brockman IM, Prather KLJ. 2015. Dynamic knockdown of *E. coli* central metabolism for redirecting fluxes of primary metabolites. Metabol. Eng. 28:104-113.

Capuder M, Šolar T, Benčina M, Legiša M. 2009. Highly active, citrate inhibition resistant form of *Aspergillus niger* 6-phosphofructo-1-kinase encoded by a modified *pfkA* gene. J Biotechnol 144:51-57.

Chapman AG, Fall L, Atkinson DE. 1971. Adenylate energy charge in *Escherichia coli* during growth and starvation. J Bacteriol 108:1072-1086.

Chubukov V, Uhr M, Le Char L, Kleijen RJ, Jules M, Link H, Aymerich S, Stelling J, Sauer U. 2013. Trasncriptional regulation is insufficient to explain substrate-induced flux changes in *Bacillus subtilis*. Mol Syst Biology 9:709.

Datsenko KA, Wanner BL. 2000. One-step inactivation of chromosomal genes in *Escherichia coli* K-12 using PCR products. Proc Natl Acad Sci USA 97:6640-6645.

de Koning W, van Dam K. 1992. A method for the determination of changes of glycolytic metabolites in yeast on a subsecond time scale using extraction at neutral pH. Anal Biochem 204: 118-123.

de Vries W, Kapteijn WMC, van der Beek EG, Stouthamer AH. 1970. Molar growth yields and fermentation balances of *Lactobacillus casei* L3 in batch cultures and in continuous cultures. J Gen Microbiol 63:333-345.

Decker K. 1974. Acetyl Coenzyme A: UV-method. In: Methods of enzymatic analysis. Volume 4, 2rd edition, pp. 1988-1993. Editor Hans-UIrich Bergmeyer. Publisher-Verlag Chemie Weinheim Academic Press.

Dietzler DN, Lais CJ, Leckie MP. 1974. Simultaneous increases of the adenylate energy charge and the rate of glycogen synthesis in nitrogen-starved *Escherichia coli* W4597(K). Archives Biochem Biophys 160:14-25.

Eiteman MA, Chastain MJ. 1997. Optimization of the ion-exchange analysis of organic acids from fermentation. Analytica Chimica Acta: 338:69-75.

Emmerling M, Bailey JE, Sauer U. 1999. Glucose catabolism of *Escherichia coli* strains with increased activity and altered regulation of key glycolytic enzymes. Metab Eng 1:117-127.

Faijes M, Mars AE, Smid EJ. 2007. Comparison of quenching and extraction methodologies for metabolome analysis of *Lactobacillus plantarum*. Microbial Cell Fact 6:27.

Ferreras C, Hernández ED, Martínez-Costa OH, Aragón JJ. 2009. Subunit interactions and composition of the fructose 6-phosphate catalytic site and the fructose 2,6-bisphosphate allosteric site of mammalian phosphofructokinase. J Biol Chem 284:9124-9131.

Folsom JP, Carlson RP. 2015. Physiological, bioimass elemental composition and proteomic analyses of *Eschericha coli* ammonium-limited chemostat growth, and comparison with iron- and glucose-limited chemostat growth. Microbiology 161:1659-1670.

Graf M, Haas T, Teleki A, Feith A, Cerff M, Wiechert W, Nöh K, Busche T, Kalinowski J, Takors R. 2020. Revisiting the growth modulon *Corynebacterium glutamicum* under glucose limited chemostat conditions. Front Bioeng Biotechnol 8:584614.

Hackett S. R. Zanotelli V. R. T., Xu, W., Goya, J., Park, J. O., Perlman, D. H., Gibney, P.A. Botstein, D., Stoery J.D., Rabinowitz. 2016. Systems-level analysis of mechanisms regiulating yeast metabolic flux. Science, 354:aaf2786-1.

Harder, W., Dijkhuizen, L. 1983. Physiological responses to nutrient limitation. *Ann. Rev. Microbiol.* 37:1-23.

Hellinga HW, Evans PR. 1987. Mutations in the active site of *Escherichia coli* phosphofructokinase. Nature 327:437-439.

Hollinshead WD, Rodriguez S, Martin HG, Wang G, Baidoo EE, Sale KL, Keasling JD, Mukhopadhyay A, Tang YJ. 2016. Examining *Escherichia coli* glycolytic pathways, catabolite repression, and metabolite channeling using *Δpfk* mutants. Biotechnol Biofuels 9:212.

Holms WH. 1986. The central metabolic pathways of *Escherichia coli*: relationship between flux and control at a branch point, efficiency of conversion to biomass and excretion of acetate. Current topics in Cellular Regulation 28:69-105.

Hoque MA, Ushiyama H, Tomita M, Shimizu K. 2005. Dynamic responses of the intracellular metabolite concentrations of the wild type and *pyk*A mutant *Escherichia coli* against pulse addition of glucose or NH_3 under those limiting continuous cultures. Biochem Eng J 26:38-49.

Hoque MA, Fard AT, Rahman M, Alattas O, Akazawa K, Merican AM. 2011. Comparison of dynamic responses of cellular metabolites in *Escherichia coli* to pulse addition of substrates. Biologia 66:954-966.

Hua Q, Yang C, Baba T, Mori H, Shimizu K. 2003. Responses of the central metabolism in *Escherichia coli* to phosphoglucose isomerase and glucose-6-phosphate dehydrogenase knockouts. J Bacteriology 185:7053-7067.

Hua Q, Yang C, Oshima T, Mori H, Shimizu K. 2004. Analysis of gene expression in *Escherichia coli* in response to changes of growth-limiting nutrient in chemostat cultures. Appl Environ Microbiol 70:2354-2366.

Jaworek D, Welsch J. 1985. Adenosine 5'-diphosphate and adenosine 5'-monophosphate: UV-method, Chapter 3.10.1- In: Methods of enzymatic analysis, 3rd ed, Volume 7, Ed: Hans-UIrich Bergmeyer. Verlag Chemie Weinheim Academic Press. pp. 365-370.

Kahru A, Paalme T, Vilu R. 1987. Effect of temperature on the ATP pool and adenylate energy charge in *Escherichia coli*. FEMS Microbiol Lett 41:305-308.

Kayser A, Weber J, Hecht V, Rinas U. 2005. Metabolic flux analysis of *Escherichia coli* in glucose-limited continuous cultures. I. Growth-rate-dependent metabolic efficiency at steady state. Microbiol 151:693-706.

Kemp RG, Gunasekera D. 2002. Evolution of the allosteric ligand sites of mammalian phosphofructo-1-kinase. Biochem 41:9426-9430.

Koberstein JN, Stewart ML, Smith CB, Tarasov AI, Ashcroft FM, Stork PJS, Goodman RH. 2022. Monitoring glycolytic dynamics in single cells using a fluorescent biosensor for fructose 1,6-bisphosphate. Proc Natl Acad Sci USA 119:e2204407119.

Kochanowski K, Volkmer B, Gerosa L, Haverkorn van Rijsewijk BR, Schmidt A, Heinemann M. 2013. Functining of a metabolic flux sensor in *Escherichia coli*. Proc Natl Acad Sci USA 110:1130-1135.

Kostylev M, Otwell AE, Richardson RE, Suzuki Y. 2015. Cloning should be simple: *Escherichia coli* DH5alpha- mediated assembly of multiple DNA fragments with short end homologies. PLoS One 10:e0137466

Kotlarz D, Buc H. 1977. Two *Escherichia coli* fructose-6-phosphate kinases. Preparative purification, oligomeric structure and immunological studies. Biochimica et Biophysica Acta 484:35-48.

Lang G, Michal G. 1974. Methods for determination of metabolites (Carbohydrate metabolites: D-glucose-6-phosphate and D-fructose-6-phosphate). Methods of Enzymatic Analysis Volume 3, 2nd Edition,. H.-U. Bergmeyer, ed., Verlag Chemie Weinheim Academic Press. pp. 1238-1242.

Lehning CE, Siedler S, Ellabaan MMH, Sommer MOA. 2017. Assessing glycolytic flux alterations resulting from genetic perturbations in *E. coli* using a biosensor. Metabolic Eng 42:194-202.

Lilius E-M, Multanen V-M, Toivenen V. 1979. Quantitative extraction and estimation of intracellular nicotinamide nucleotide of *Escherichia coli*. Anal Biochem 99:22-27.

Lim S-J, Jung Y-M, Shin H-D, Lee Y-H. 2002. Ampification of the NADPH-related genes *zwf* and *gnd* for the oddball biosynthesis of PHB in an *E. coli* transformant harboring a cloned *phbCAB* operon. J Biosci Bioeng 93:543-549.

Lin Z, Xu Z, Li Y, Wang Z, Chen T, Zhao X. 2014. Metabolic engineering of *Escherichia coli* for the production of riboflavin. Microbial Cell Fact 13:104.

Litsios A, Ortega ÁD, Wit EC, Heinemann M. 2018. Metabolic-flux dependent regulation of microbial physiology. Current Opinion Microbiol 42:71-78.

Livak KJ, Schmittgen TD. 2001. Analysis of relative gene expression data using real-time quantitative PCR and the 2-ΔΔCT method. Methods 25:402-408.

Lowry OH, Passonneau JV, Rock MK. 1961. The stability of pyridine nucleotides. J. Biol Chem 236:2756-2759.

Marriott ID, Dawes EA, Rowley BI. 1981. Effect of growth rate and nutrient limitation on the adenine nucleotide content, energy charge and enzymes of adenylate metabolism in *Azotobacter beijerinckii*. J Gen Microbiol 125:375-382.

Matsuoka Y, Kurata H. 2020. Computer-aided rational design of efficient NADPH production system by *Escherichia coli pgi* mutant using a mixture of glucose and xylose. Front Bioeng Biotechnol 8:227.

Michal G, Beutler H-O. 1974. D-fructose-1,6-diphosphate, dihydroxyacetone phosphate and D-glyceraldehyde-3-6-phosphate, In: Methods of Enzymatic Analysis, H.U. Bergmeyer, ed., Volume 3, Verlag Chemie Weinheim Academic Press. pp. 1315-1319.

Mlakar T, Legiša M. 2006. Citrate inhibition-resistant form of 6-phosphofructo-1-kinase from *Aspergillus niger*. Appl Environ Microbiol 72:4515-4521.

Moxley WC, Eiteman MA. 2021. Pyruvate production by *Escherichia coli* by use of pyruvate dehydrogenase variants. Appl Environ Microbiol 87:e00487-21.

Nanchen A, Schicker A, Sauer U. 2006. Nonlinear dependency of intracellular fluxes on growth rate in miniaturized continuous cultures of *Escherichia coli.* Appl Environ Microbiol 72:1164-1172.

Nicolas C, Kiefer P, Letisse F, Krömer J, Massou S, Soucaille P, Wittmann C, Lindley ND, Portais JC. 2007. Response of the central metabolism of *Escherichia coli* to modified expression of the gene encoding the glucose-6-phosphate dehydrogenase. FEBS Lett 581:3771-7.

Paalme T, Elken R, Kahru A, Vanatulu K, Vilu R. 1997. The growth rate control in *Escherichia coli* at near to maximum growth rates: the A-stat approach. Ant van Leeuwen 71:217-230.

Passonneau JV, Lowry OH. 1964. The role of phosphofructokinase in metabolic regulation. Adv Enzyme Regulation 2:265-274.

Perez-Zabaleta M, Sjöberg G, Guevara-Martínez M, Jarmander J, Gustavsson M, Quillaguamán J, Larsson G. 2016. Increasing the production of (R)-3-hydroxybutyrate in recombinant *Escherichia coli* by improved cofactor supply. Microb Cell Fact 15:91.

Presecan-Siedel E, Galinier A, Longin R, Deutscher J, Danchin A, Glaser P, Martin-Verstraete I. 1999. Catabolite regulation of the *pta* as a part of carbon flow pathways in *Bacillus subtilis*. J Bacteriol 181:6889-6897.

Przybylski F, Otto A, Nissler K, Schellenberger W, Hofmann E. 1985. Effects of fructose 1,6-bisphosphate on the activation of yeast phosphofructokinase by fructose 2,6-bisphosphate and AMP. Biochimica et Biophysica Acta 831:350-352.

Rajpurohit R, Eiteman MA. 2022. Nutrient-limited operational strategies for the microbial production of biochemicals. Microorganisms 10:2226.

Ramseier TM, Nègre D, Cortay J-C, Scarabel M, Cozzone AJ, Saier Jr MH. 1993. *In vitro* binding of the pleiotrophic transcriptional regulatory protein, FruR, to the *fru*, *pps*, *ace*, *pts* and *icd* operons of *Escherichia coli* and *Salmonella typhimurium*. J Mol Biol 234:28-44.

Ramseier TM. 1996. Cra and the control of carbon flux via metabolic pathways. Res Microbiol 147:6-7.

Reynolds TS, Courtney CM, Erickson, KE, Wolfe LM, Chatterjee A, Nagpal P, Gill RT. 2017. ROS mediated selection for increased NADPH availability in *Escherichia coli*. Biotechnol Bioeng, 114:2685-2689

Robinson JP, Fraenkel DG. 1978. Allosteric and non-allosteric *E. coli* phosphofructokinases: effects on growth. Biochem Biophys Res Comm 81:858-863.

Ronimus RS, Morgan HW. 2001. The biochemical properties and phylogenies of phosphofructokinases from extremophiles. Extremophiles 5:357-373.

Satowa D, Fujiwara R, Uchio S, Nakano M, Otomo C., Hirata Y, Matsumoto T, Noda S, Tanaka T, Kondo A. 2020. Metabolic engineering of *E. coli* for improving mevalonate production

to promote NADPH regeneration and enhance acetyl-CoA supply. Biotechnol Bioeng 117:2153-2164.

Sauer U, Canonaco F, Heri S, Perrenoud A, Fischer E. 2004. The soluble and membrane-bound transhydrogenases UdhA and PntAB have divergent functions in NADPH metabolism of *Escherichia coli.* J Biol Chem 279:6613-6619.

Schaefer U, Boos W, Weuster-Botz D. 1999. Automated sampling device for monitoring intracellular metabolite dynamics. Analytical Biochem 207:88-96.

Schaub J, Reuss M. 2008. *In vivo* dynamics of glycolysis in *Escherichia coli* shows need for growth-rate dependent metabolme analysis. Biotechnol Prog 24:1402-1407.

Schuhmacher T, Löffler M, Hurler T, Takors R. 2014. Phosphate limited fed-batch processes: impact on carbon usage and energy metabolism in *Escherichia coli*. J Biotechnol 190:96-104.

Shi A, Zhu X, Lu J, Zhang X, Ma Y. 2013. Activating transhydrogenase and NAD kinase in combination for improving isobutanol production. Metabolic Eng 16:1-10

Shimada T, Yamamoto K, Ishihama A. 2011. Novel members of the Cra regulon involved in carbon metabolism in *Escherichia coli*. J Bacteriol 193:649-659.

Shimada T, Fujita N, Maeda M, Ishihama A. 2005. Systematic search for the Cra-binding promoters using genomic SELEX system. Genes to cells 10:907-918.

Shirakihara Y, Evans PR. 1988. Crystal structure of the complex of phosphofructokinase from *Escherichia coli* with its reaction products. J Mol Biol 204:973-994.

Siedler S, Bringer S, Bott M. 2011. Increased NADPH availability in *Escherichia coli*: improvement of the product per glucose ratio in reductive whole-cell biotransformation. Appl Microbiol Biotechnol 92:929-937.

Siedler S, Bringer S, Blank LM, Bott M. 2012. Engineering yield and rate of reductive biotransformation in *Escherichia coli* by partial cyclization of the pentose phosphate pathway and PTS-independent glucose transport. Appl Microbiol Biotechnol 93:1459-1467.

Swedes JS, Sedo RJ, Atkinson DE. 1975. Relation of growth and protein synthesis to the adenylate energy charge in an adenine-requiring mutant of *Escherichia coli*. J Biol Chem 250:6930-6938.

Tovilla-Coutiño DB, Momany C, Eiteman MA. 2020. Engineered citrate synthase alters acetate accumulation in *Escherichia coli*. Metabol. Eng. 61:171-180.

Trautschold I , Lamprecht W, Schweitzer G. 1985. UV-method with hexokinase and glucose-6P dehydrogenase. In: Methods of enzymatic analysis, H.U. Bergmeyer, ed., Volume 7, VCH publishers, Weinheim. pp. 342-350.

Valgepea K, Adamberg K, Nahku R, Lahtvee P-J, Arike L, Vilu R. 2010. Systems biology approach reveals that overflow metabolism of acetate in *Escherichia coli* is triggered by carbon catabolite repression of acetyl-CoA synthetase.. BMC Syst Biol 4:166.

Valgepea K, Adamberg K, Vilu R. 2011. Decrease of energy spilling in *Escherichia coli* continuous cultures with rising specific growth rate and carbon wasting. BMC Syst Biol 5:106.

Vemuri, G. N., Altman, E., Sandgurdekar, D. P., Khodursky, A. B., Eiteman, M. A., 2006. Overflow metabolism in *Escherichia coli* during steady-state growth: transcriptional regulation and effect of the redox ratio. Appl Environ Microbiol. 72:3653-3661.

Wang X, Kemp RG. 1999. Identification of residues of *Escherichia coli* phosphofructokinase that contribute to nucleotide binding and specificity. Biochem 38:4313-4318.

Wang Y, Zhou S, Li R, Liu Q, Shao X, Zhu L, Kang M-K, Wei G, Kim S-W, Wang C. 2022. Reassessing acetyl-CoA supply and NADPH availability for mevalonate biosynthesis from glycerol in *Escherichia coli*. Biotechnol Bioeng 119:2868-2877.

Wu L-F, Reizer A, Reizer J, Cai B, Tomich JM, Saier JR MH. 1991. Nucleotide sequence of the *Rhodobacter capsulatus fruK* gene, which encodes fructose-1-phosphate kinase: evidence for a kinase superfamily including both phosphofructokinases of *Escherichia coli*. J Bacteriol 173:3117-3127.

Yang J, Sun B, Huang H, Jiang Y, Diao L, Chen B, Xu C, Wang X, Liu J, Jiang W. 2014. High-efficiency scarless genetic modification in *Escherichia coli* by using lambda red recombination and I-SceI cleavage. Appl Environ Microbiol 80:3826-3834.

Zheng R-L, Kemp RG. 1992. The mechanism of ATP inhibition of wild type and mutant phosphofructo-1-kinase from *Escherichia coli*. J Biol Chem 267:23640-23645.

Zheng R-L, Kemp RG. 1994. Identification of interactions that stabilize the transition state in *Escherichia coli* phosphofructo-1-kinase. J Biol Chem 269:18475-18479.

Zhu S, Cai D, Liu Z, Zhang B, Li J, Chen S, Ma X. 2019. Enhancement of bacitracin production by NADPH generation via overexpressing glucose-6-phosphate dehydrogenase Zwf in *Bacillus licheniformis.* Appl Biochem Biotechnol 187:1502-1514.

Table 3.1- Physiology and respiration parameters of nitrogen-limited chemostat cultures of the *E. coli* wild-type PfkA C strain, the PfkA knockout strain, and the PfkA variants. All strains were grown at 0.1 h^{-1} using glucose as the sole carbon source.

Strain	$Y_{X/S}$	$q_{glucose}$ (mmol/gh)	q_{O2} (mmol/gh)	q_{CO2} (mmol/gh)	$q_{acetate}$ (mmol/gh)	C balance (%)	RQ
Δ*pfkA*	0.261 ± 0.044	2.0 ± 0.3	6.0 ± 0.1	5.9 ± 0.6	0 ± 0	82%	0.98 ± 0.18
$PfkA^{[R171S]}$	0.270 ± 0.019	2.1 ± 0.2	7.1 ± 0.2	7.0 ± 0.8	0.06 ± 0.00	90%	0.99 ± 0.01
$PfkA^{[F76Y]}$	0.311 ± 0.010	1.7 ± 0.1	6.3 ± 0.3	5.2 ± 0.1	0.00 ± 0.01	89%	0.82 ± 0.05
$PfkA^{[R77A]}$	0.186 ± 0.003	3.0 ± 0.0	7.2 ± 0.2	7.5 ± 0.5	0.80 ± 0.01	77%	1.04 ± 0.01
PfkA	0.192 ± 0.026	2.9 ± 0.4	9.0 ± 0.1	7.4 ± 0.9	0.47 ± 0.05	73%	0.82 ± 0.20

Table 3.2- Strains used in this study.

Strain	Relevant characteristics	Reference
ATCC 8739	*Escherichia coli* C	Wild-type
MEC1012	ATCC 8739 *pfkA*::Kan	This study
MEC1013	ATCC 8739 *pfkA*::(FRT)	This study
MEC1227	MEC1013 *pfkA*::*pfkA*$^{[D103A]}$-Kan	This study
MEC1228	MEC1013 *pfkA*::*pfkA*$^{[D103V]}$-Kan	This study
MEC1229	MEC1013 *pfkA*::*pfkA*$^{[D103E]}$-Kan	This study
MEC1230	MEC1013 *pfkA*::*pfkA*$^{[R171S]}$-Kan	This study
MEC1231	MEC1013 *pfkA*::*pfkA*$^{[R171A]}$-Kan	This study
MEC1233	MEC1013 *pfkA*::*pfkA*$^{[H249A]}$-Kan	This study
MEC1234	MEC1013 *pfkA*::*pfkA*$^{[H249F]}$-Kan	This study
MEC1235	MEC1013 *pfkA*::*pfkA*$^{[H249D]}$-Kan	This study
MEC1236	MEC1013 *pfkA*::*pfkA*$^{[I126S]}$-Kan	This study
MEC1237	MEC1013 *pfkA*::*pfkA*$^{[I126A]}$-Kan	This study
MEC1238	MEC1013 *pfkA*::*pfkA*$^{[I126E]}$-Kan	This study
MEC1239	MEC1013 *pfkA*::*pfkA*$^{[G10A]}$-Kan	This study
MEC1240	MEC1013 *pfkA*::*pfkA*$^{[I126K]}$-Kan	This study
MEC1241	MEC1013 *pfkA*::*pfkA*$^{[G11A]}$-Kan	This study
MEC1242	MEC1013 *pfkA*::*pfkA*$^{[R72S]}$-Kan	This study
MEC1243	MEC1013 *pfkA*::*pfkA*$^{[R72V]}$-Kan	This study
MEC1244	MEC1013 *pfkA*::*pfkA*$^{[R72K]}$-Kan	This study
MEC1284	MEC1013 *pfkA*::*pfkA*$^{[R171K]}$-Kan	This study
MEC1299	MEC1013 *pfkA*::*pfkA*$^{[Y41F]}$-Kan	This study
MEC1300	MEC1013 *pfkA*::*pfkA*$^{[F76Y]}$-Kan	This study
MEC1301	MEC1013 *pfkA*::*pfkA*$^{[R77K]}$-Kan	This study
MEC1302	MEC1013 *pfkA*::*pfkA*$^{[R77A]}$-Kan	This study
MEC1356	MEC1013 *pfkA*::*pfkA*-Kan	This study

Table 3.3- Plasmids used in this study.

Name	Relevant characteristics	Description	Source
pKD4	Amp^R, Kan^R; R6K ori	Source of Kan^R cassette	Datsenko and Wanner, 2000
pKD46	Amp^R; pSC101 ori (ts); *araBAD* promoter for λ Red genes	λ Red helper plasmid	Datsenko and Wanner, 2000
pCP20	Amp^R, Cam^R; pSC101 ori (ts)	Expression of FLP recombinase	Datsenko and Wanner, 2000
pKSI-I	Amp^R; pUC ori	pBluescript II KS(-) backbone with I-SceI site–MCS–I-SceI site cassette	Yang et al., 2014
pHR1	Amp^R; pUC ori	pKSI-I + *pfkA* + Kan^R	This study
pHR01.1	Amp^R; pUC ori	pKSI-1 + *pfkA*[D103E]	This study
pHR01.2	Amp^R; pUC ori	pKSI-I + *pfkA*[D103V]	This study
pHR01.3	Amp^R; pUC ori	pKSI-I + *pfkA*[D103A]	This study
pHR02.1	Amp^R; pUC ori	pKSI-I + *pfkA*[R171S]	This study
pHR02.2	Amp^R; pUC ori	pKSI-I + *pfkA*[R171A]	This study
pHR02.3	Amp^R; pUC ori	pKSI-I + *pfkA*[R171K]	This study
pHR03.1	Amp^R; pUC ori	pKSI-I + *pfkA*[H249A]	This study
pHR03.2	Amp^R; pUC ori	pKSI-I + *pfkA*[H249F]	This study
pHR03.3	Amp^R; pUC ori	pKSI-I + *pfkA*[H249D]	This study
pHR04.1	Amp^R; pUC ori	pKSI-I + *pfkA*[I126S]	This study
pHR04.2	Amp^R; pUC ori	pKSI-I + *pfkA*[I126A]	This study
pHR04.3	Amp^R; pUC ori	pKSI-I + *pfkA*[I126A]	This study
pHR04.4	Amp^R; pUC ori	pKSI-I + *pfkA*[I126K]	This study
pHR05.1	Amp^R; pUC ori	pKSI-I + *pfkA*[G10A]	This study
pHR06.1	Amp^R; pUC ori	pKSI-I + *pfkA*[G11A]	This study
pHR07.1	Amp^R; pUC ori	pKSI-I + *pfkA*[R72S]	This study
pHR07.2	Amp^R; pUC ori	pKSI-I + *pfkA*[R72V]	This study
pHR07.3	Amp^R; pUC ori	pKSI-I + *pfkA*[R72K]	This study
pHR08.1	Amp^R; pUC ori	pKSI-I + *pfkA*[Y41F]	This study
pHR09.1	Amp^R; pUC ori	pKSI-I + *pfkA*[F76Y]	This study
pHR10.1	Amp^R; pUC ori	pKSI-I + *pfkA*[R77K]	This study
pHR10.2	Amp^R; pUC ori	pKSI-I + *pfkA*[R77A]	This study

Table 3.4- Primers used in this study

Name	Description	Sequence 5'-3'
MEP144	pfkA_F	TACGCATGGGATATGAGGCGGTACAG
MEP145	pfkA_R	GTGACTGACGAATCACCACGTTATCACC
MEP520	pfkA-plasmid_F	GCCTGGTAGGGATAACAGGGTAATTGCG
MEP521	pfkA-plasmid_R	CGCAATTACCCTGTTATCCCTACCAGGC
MEP522	Kan confirmation_R	CTGCCATCACGAGATTTCGATTCC
MEP645	KD4-pfkA_F	CTTCCGGCAACAGATTTTATTTTGCATTCCAAAGTTCAGAGGTAGTCATGGTGTAG GCTGGAGCTGCTTC
MEP646	KD4-pfkA_R	CTAAAGGAATCTGCCTTTTTCCGAAATCATTAATACAGTTTTTTCGCGCACATATG AATATCCTCCTTAG
MEP895	5'_DS_pfkA	TAGAACTAGTGGATCCCCCGGGCAATTGCGTCCACGTCAT
MEP897	5'_UPS_pfkA	CTTGATATCGAATTCCTGCATACGCATGGGATATGAGGCG
MEP898	3'_UPS_pfkA	TGGACCATGGCTAATTCCCATGATAAGCGAAGCGCATCAG
MEP900	3'_Kan	CTGATGCGCTTCGCTTATCATGGGAATTAGCCATGGTCCA
MEP901	5'_Kan	TTGCAGAATTCATGTAGGCCGTGTAGGCTGGAGCTGCTTC
MEP902	5'_KSI	ATGACGTGGACGCAATTGCCCGGGGGATCCACTAGTTCTA
MEP903	3'_KSI	CGCCTCATATCCCATGCGTATGCAGGAATTCGATATCAAG
MEP905	3'_DS_pfkA	GAAGCAGCTCCAGCCTACACGGCCTACATGAATTCTGCAA
MEP906	5'-pfkA1.1	GGTTATCGGCGGTGAAGGTTCCTACATG
MEP907	3'-pfkA1.1	CCATGTAGGAACCTTCACCGCCGATAACCAC
MEP908	5'-pfkA1.2	GGTTATCGGCGGTGTGGGTTCCTACATG
MEP909	3'-pfkA1.2	CCATGTAGGAACCCACACCGCCGATAAC
MEP910	5'-pfkA1.3	GGTTATCGGCGGTGCGGGTTCCTACATG
MEP911	3'-pfkA1.3	CATGTAGGAACCCGCACCGCCGATAACCAC
MEP912	5'-pfkA2.1	GGAAGTGATGGGCAGCTATTGTGGCGATC
MEP913	3'-pfkA2.1	CAGATCGCCACAATAGCTGCCCATCACTTCC
MEP914	5'-pfkA2.2	GGAAGTGATGGGCGCGTATTGTGGCGATC
MEP915	3'-pfkA2.2	CAGATCGCCACAATACGCGCCCATCACTTCC

MEP917	3’-pfkA2.3	CAGATCGCCACAATATTTGCCCATCACTTCCA
MEP918	5’-pfkA_integration	GATGAGGAACGGCAAGAAATTATTGATATCGTGACTTCCT
MEP919	3’-pfkA_integration	CTGAATGCCTTGTTGTACTGTTCGTACAATTCGCGCGTTG
MEP930	5'-pfkA3.1	CGCAACTGTGCTGGGCGCGATCCAGCGCGGTGGTTC
MEP931	3'-pfkA3.1	GAACCACCGCGCTGGATCGCGCCCAGCACAGTTGCG
MEP932	5'-pfkA3.2	CGCAACTGTGCTGGGCTTCATCCAGCGCGGTGGTTC
MEP933	3'-pfkA3.2	GAACCACCGCGCTGGATGAAGCCCAGCACAGTTGCG
MEP934	5'-pfkA3.3	CGCAACTGTGCTGGGCGATATCCAGCGCGGTGGTTC
MEP935	3'-pfkA3.3	GAACCACCGCGCTGGATATCGCCCAGCACAGTTGCG
MEP936	5'-pfkA4.1	CGGTCTGCCGGGCACTAGCGACAACGACATCAAAGG
MEP937	3'-pfkA4.1	CCTTTGATGTCGTTGTCGCTAGTGCCCGGCAGACCG
MEP938	5'-pfkA4.2	CGGTCTGCCGGGCACTGCGGACAACGACATCAAAGG
MEP939	3'-pfkA4.2	CCTTTGATGTCGTTGTCCGCAGTGCCCGGCAGACCG
MEP940	5'-pfkA4.3	CGGTCTGCCGGGCACTGAAGACAACGACATCAAAGG
MEP941	3'-pfkA4.3	CCTTTGATGTCGTTGTCTTCAGTGCCCGGCAGACCG
MEP942	5'-pfkA4.4	CGGTCTGCCGGGCACTAAAGACAACGACATCAAAGG
MEP943	3'-pfkA4.4	CCTTTGATGTCGTTGTCTTTAGTGCCCGGCAGACCG
MEP944	5'-pfkA5.1	GGTGTGTTGACAAGCGCGGGTGATGCGCCAGGCATG
MEP945	3'-pfkA5.1	CATGCCTGGCGCATCACCCGCGCTTGTCAACACACC
MEP946	5'-pfkA6.1	GTGTTGACAAGCGGTGCGGATGCGCCAGGCATGAACG
MEP947	3'-pfkA6.1	CGTTCATGCCTGGCGCATCCGCACCGCTTGTCAACAC
MEP948	5'-pfkA7.1	GTTCCTCGGTTCTGCGAGCTTCCCGGAATTCCGCGAC
MEP949	3'-pfkA7.1	GTCGCGGAATTCCGGGAAGCTCGCAGAACCGAGGAAC
MEP950	5'-pfkA7.2	GTTCCTCGGTTCTGCGGTGTTCCCGGAATTCCGCGAC
MEP951	3'-pfkA7.2	GTCGCGGAATTCCGGGAACACCGCAGAACCGAGGAAC
MEP952	5'-pfkA7.3	GTTCCTCGGTTCTGCGAAATTCCCGGAATTCCGCGAC
MEP953	3'-pfkA7.3	GTCGCGGAATTCCGGGAATTTCGCAGAACCGAGGAAC
MEP970	5’-sequencing pKSI-Kan	GGCCTGACCTGAATCAATTC

MEP995	5’-pfkA2.3	CGTGGTGGAAGTGATGGGCAAATATTGTGGCGATCT
MEP996	5’-sequencing pKSI-pfkA	CTTCCCGTGCATCGGTCTGCCG
MEP998	5’-pfkA8.1	GTAATGGGCATTTATGACGGCTTCCTGGGTCTGTATGA
MEP999	3’-pfkA8.1	GGTCTTCATACAGACCCAGGAAGCCGTCATAAATGCC
MEP1000	5’-pfkA9.1	CTGCGCGTTTCCCGGAATACCGCGACGAGAAC
MEP1001	3’-pfkA9.1	GGATGTTCTCGTCGCGGTATTCCGGGAAACGC
MEP1002	5’-pfkA10.1	GCGCGTTTCCCGGAATTAAAGGACGAGAACATCCG
MEP1003	3’-pfkA10.1	GGCGCGGATGTTCTCGTCTTTGAATTCCGGGAAAC
MEP1004	5’-pfkA10.2	GCGCGTTTCCCGGAATTCGCGGACGAGAACATC
MEP1005	3’-pfkA10.2	CGCGGATGTTCTCGTCCGCGAATTCCGGGAAAC
MEP855	C_rpoD-RT-Fwd	TGATGCTGGCTGAAAACACC
MEP856	C_rpoD-RT-Rev	AGTTCAACGGTGCCCATTTC
MEP1035	C_pfkA-RT-Fwd	GAAAGAAACCGGTCGTGAAA
MEP1036	C_pfkA-RT-Rev	TGTCGTGGTGAACCAACTGT
MEP1037	C_zwf-RT-Fwd	TGGCCTTGACCACAAACATA
MEP1038	C_zwf-RT-Rev	CAGGCTTCTTCCACTTCGTC
MEP1039	C_sthA-RT-Fwd	CCATCGGGAAACAAAAGAGA
MEP1040	C_sthA-RT-Rev	GCCATCGTCGGGTAGTTAAA
MEP1047	C_icd-RT-Fwd	ATATGCCGGTCAGGACAAAG
MEP1048	C_icd-RT-Rev	CTTAGCGCCTTCCATCAGAC
MEP1049	C_maeB-RT-Fwd	CGCGCAGTTTCTGTTCAATA
MEP1050	C_maeB-RT-Rev	GCAAGGGCGTTCTGTTTAAG
MEP1056	C_pta-RT-Fwd	TAATCCGGCAGAGATCAACC
MEP1057	C_pta-RT-Rev	TTTGCGGTAGTGTGAACAGC

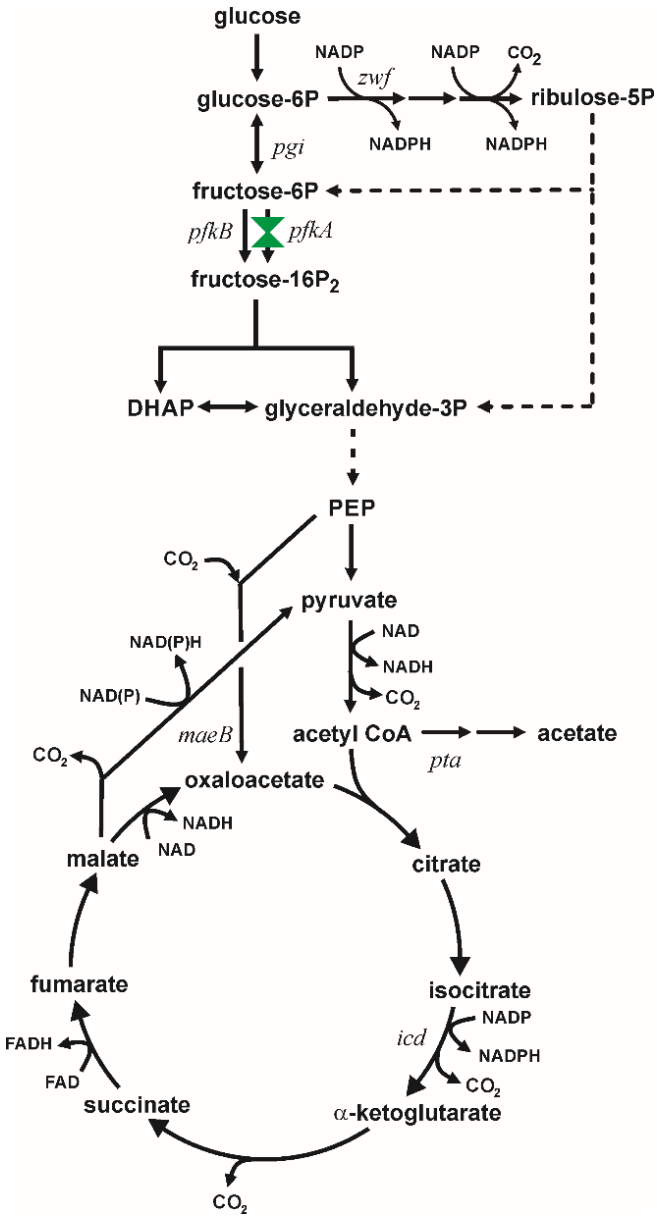

Figure 3.1- Metabolism of glucose in *Escherchia coli* showing carbon flux partition at glucose-6P between the EMP pathway and the Pentose Phosphate Pathway. This study focuses on modulating metabolism by constructing variants in PfkA coded by the *pfkA* gene.

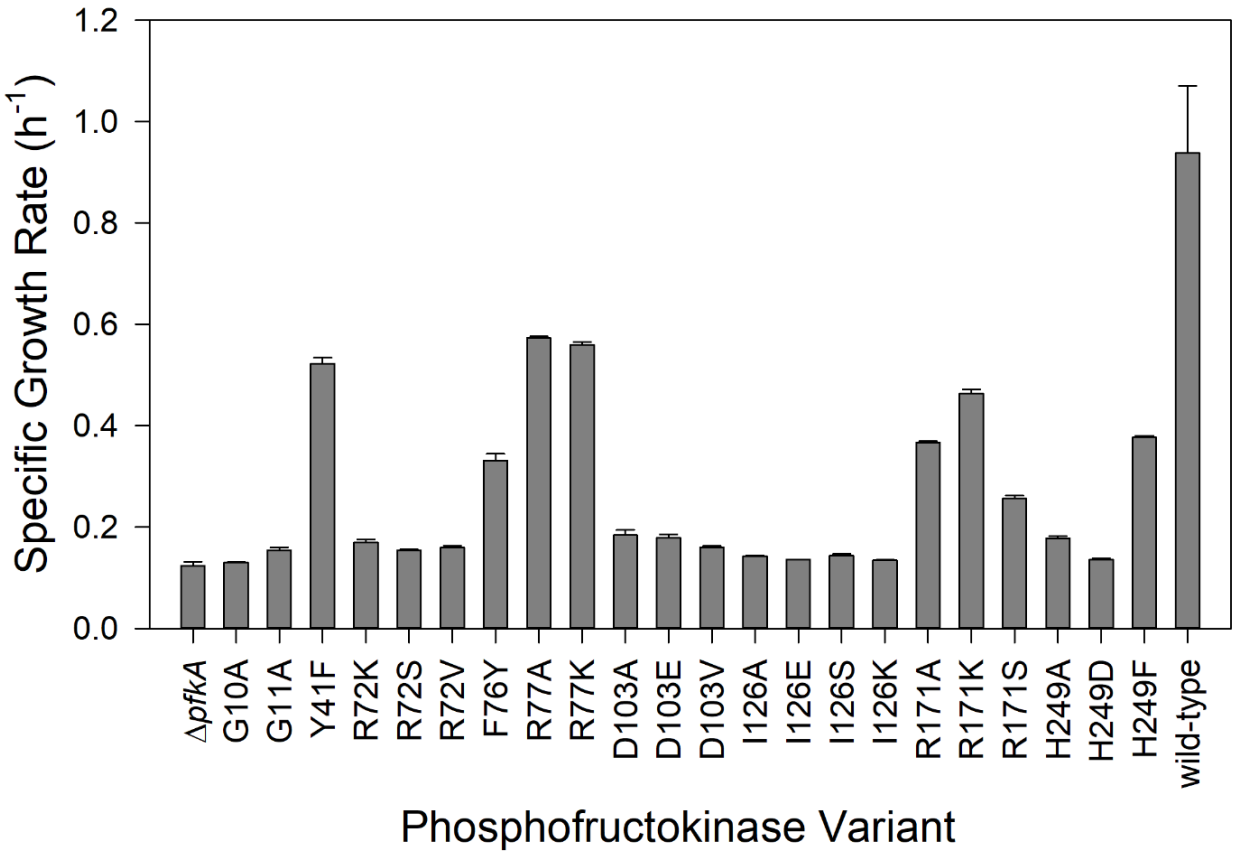

Figure 3.2- Specific growth rates of *E. coli* PfkA variants using glucose as the sole carbon source. The Δ*pfkA* strain, and strains expressing wild-type PfkA and 22 single amino acid substitutions were examined (error bars indicate standard deviation of triplicate experiments).

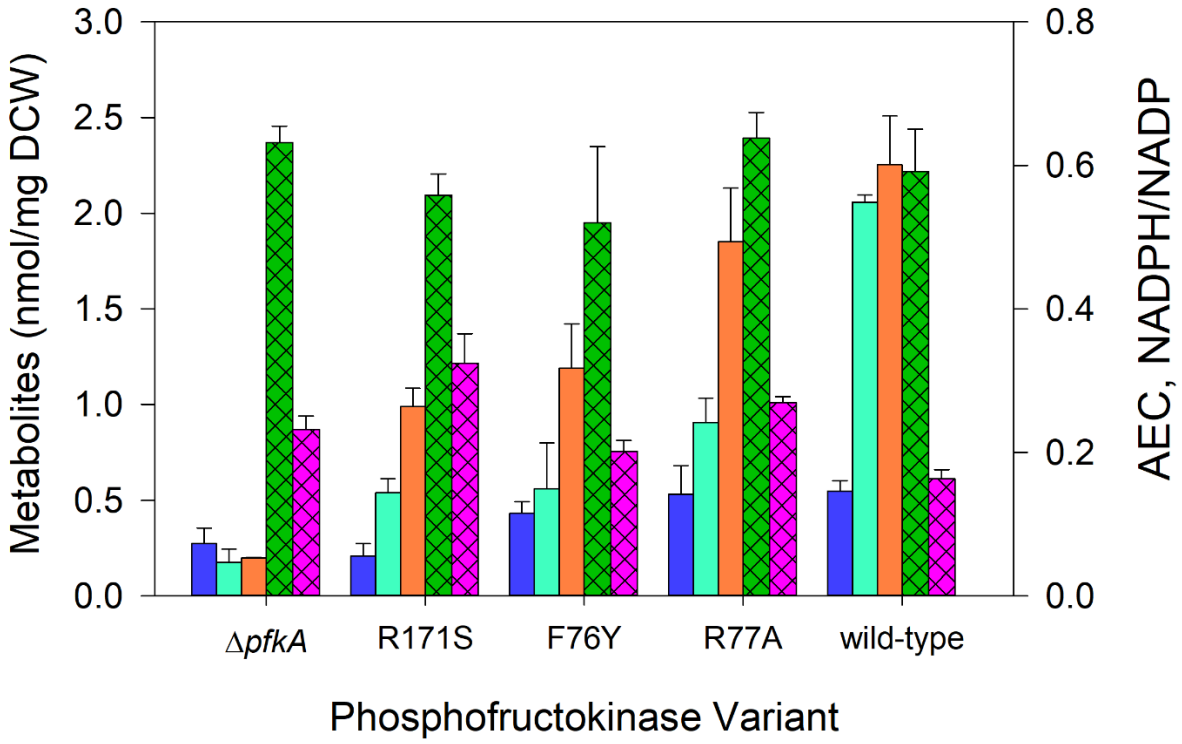

Figure 3.3- Intracellular acetyl-CoA, fructose-16P_2, GAP+ DHAP concentrations (nmol mg^{-1}), NADPH/NADP ratio and adenylate charge during nitrogen-limited chemostats at a dilution rate of 0.1 h^{-1} using glucose as the sole carbon source: Acetyl-CoA (■), fructose-16P_2 (■), GAP+DHAP (■), adenylate charge (AEC, hatched ■), and NADPH/NADP ratio (hatched ■).). *E. coli* expressing wild-type PfkA, three variant strains, and a Δ*pfkA* strains are arranged in ascending order of their maximum specific growth rate.

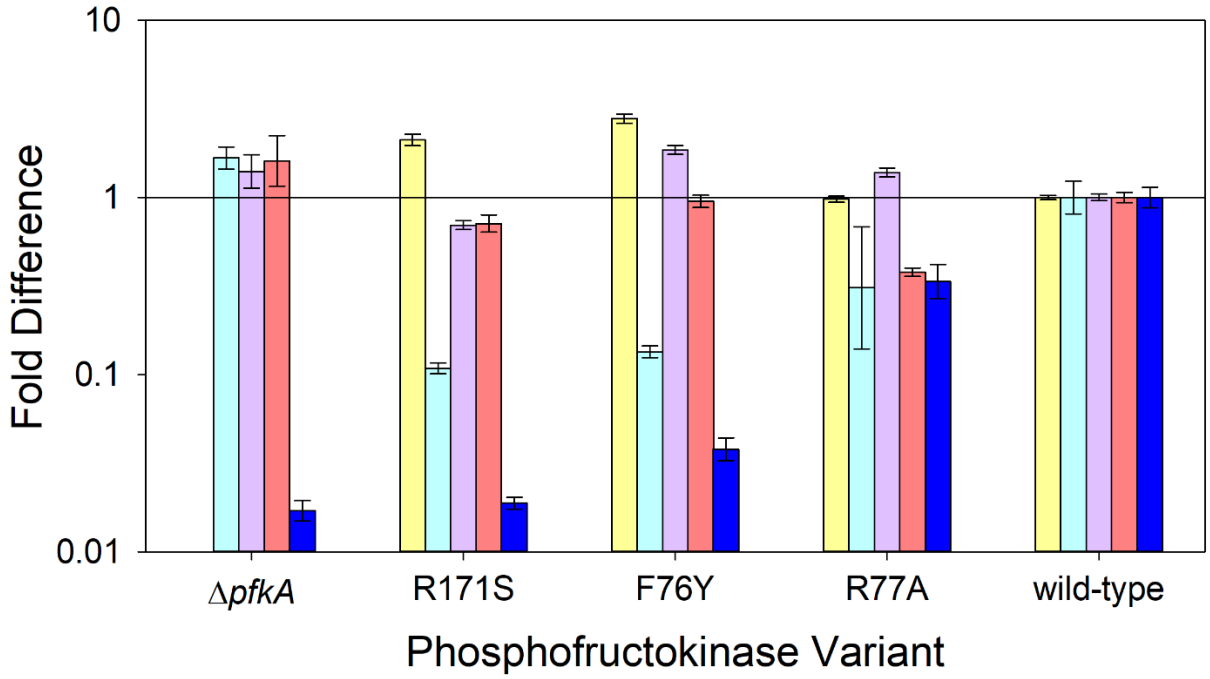

Figure 3.4- Relative expression of selected genes compared to the wild-type strain during nitrogen-limited chemostats at a dilution rate of 0.1 h^{-1} using glucose as the sole carbon source: *pfkA* (), *zwf* ()), *maeB* (), *icd* (), and *pta* (). *E. coli* expressing wild-type PfkA, three variant strains, and a Δ*pfkA* strains are arranged in ascending order of their maximum specific growth rate.

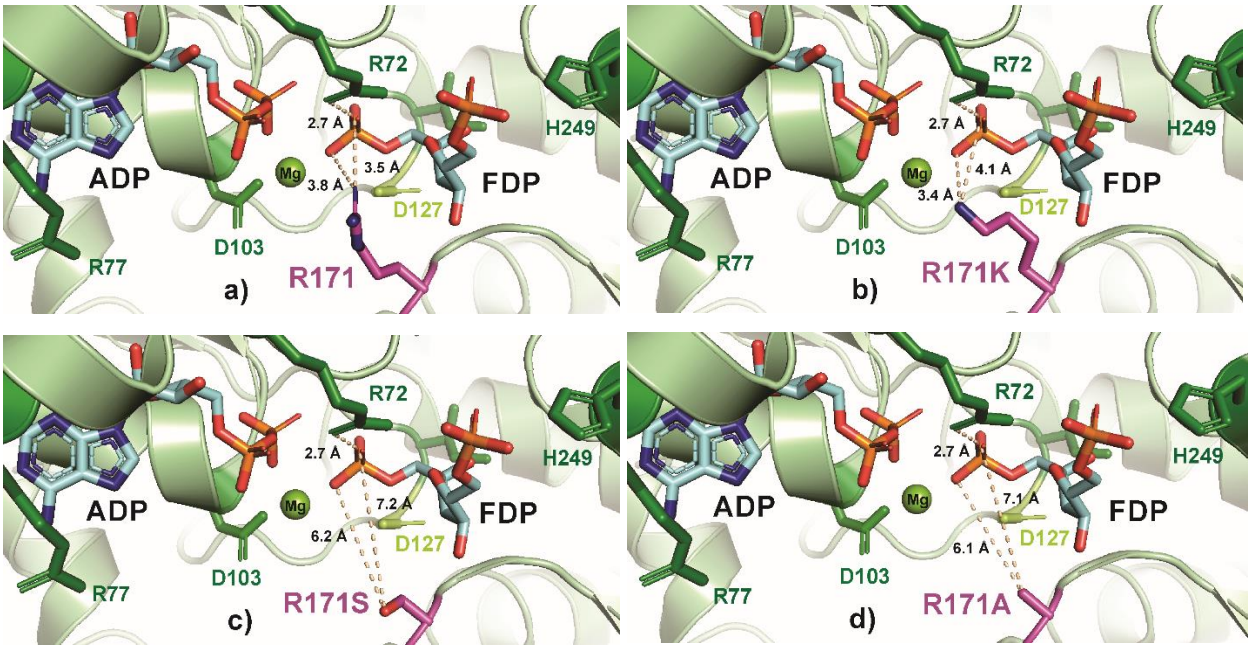

Figure 3.5- PyMOL cartoon-stick representation of PfkA with focus on residue R171 (a) and substitutions R171K (b), R171S (c) and R171A (d), and the interactions between this residue and the product fructose-16P_2 (FDP). Direct interactions between the 171 residue and the substrate are shown in wheat-colored dash lines. The PfkA structure contains the products ADP and fructose-16P_2.

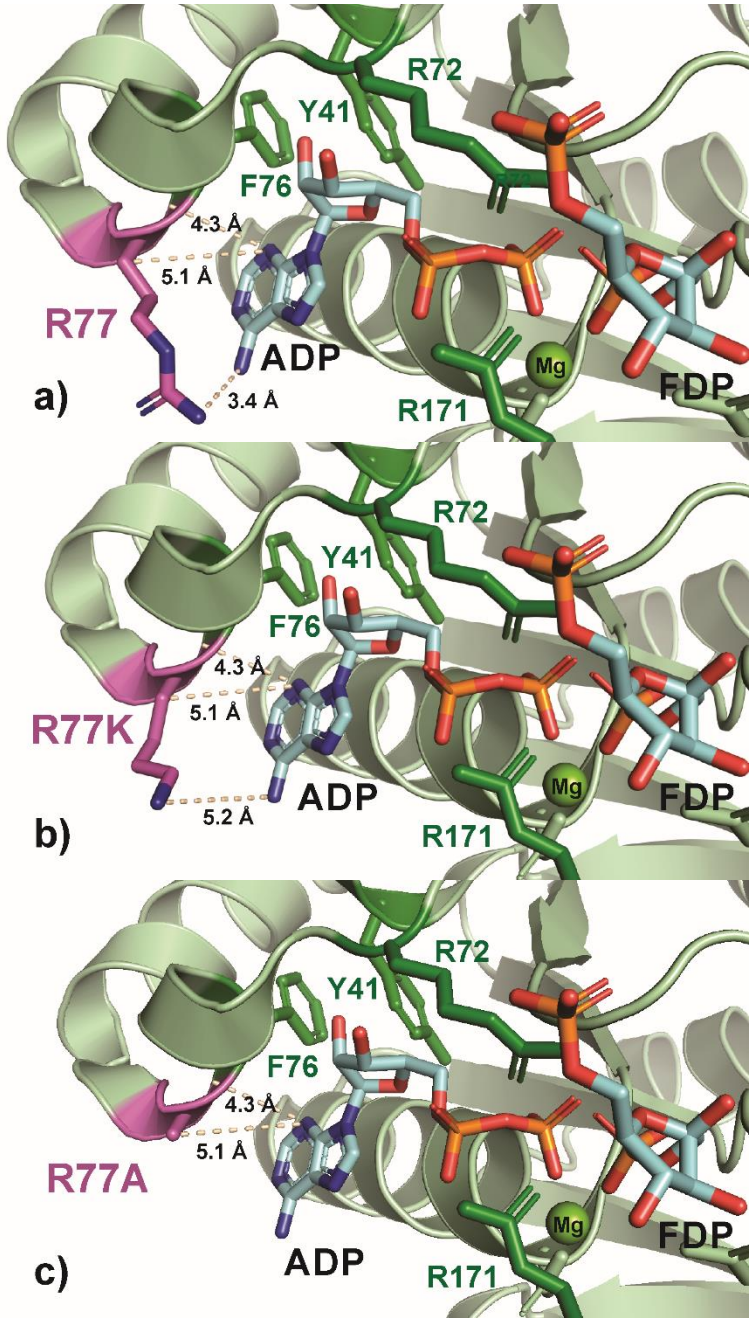

Figure 3.6- PyMOL cartoon-stick representation of PfkA with focus on residue R77 (a) and substitutions R77K (b) and R77A (c), and the interactions between this residue and the product ADP. Direct interactions between the 77 residue and the substrate are shown in wheat-colored dash lines. The PfkA structure contains the products ADP and fructose-16P_2.

CHAPTER 4

3-HYDROXYBUTYRATE PRODUCTION BY *ESCHERICHIA COLI* CITRATE SYNTHASE VARIANTS

[1]Rajpurohit H., Eiteman MA. To be submitted to *Microbial Cell Factories*

4.1 ABSTRACT

Background: The microbial chiral product (R)-3-hydroxybutyrate (3-HB) is a precursor to several industrial (e.g., biopolymer, butanol) and medical compounds (e.g., antibiotics, skin grafting polymer). Acetyl-CoA is a key precursor for 3-HB, and several native pathways compete with 3-HB production. Besides acetate formation pathway, a principal competing pathway for acetyl-CoA is mediated by citrate synthase enzyme (coded by *gltA*) which directs 63% of carbon flux from acetyl-CoA towards TCA cycle. Eliminating citrate synthase activity by deletion of *gltA* gene leads to a growth defect in the organism in glucose supplemented defined medium and requires addition of glutamate. Previously, altering the citrate synthase activity through structure-guided protein engineering by construction of GltA variants showed a significant improvement in products such as citramalate and acetate.

Results: The effect of five GltA variants on 3-HB production catalyzed through overexpression of thiolases (*phaA*) and NADPH-dependent acetoacetyl-CoA reductase (*phaB*) from *Cupriavidus necator* was analyzed. Four variants showed nearly 5-fold greater 3-HB yield compared to the wild-type. Deletion of acetate forming genes (*poxB, pta-ackA*) and GltA variants led to 10-fold greater pyruvate accumulation in these four variants than wild-type. Overexpression of native thioesterases TesB and YciA eliminated pyruvate formation while diverted acetyl-CoA towards acetate formation. To increase CoA pools, CoaA (*E. coli* pantothenate kinase) was overexpressed which decreased pyruvate formation by 50% but did not improve 3-HB yield. Controlled batch studies demonstrated that GltA[A267T] variant produced the greatest 3-HB titer of 4.88 g/L and yield of 0.17 g/g glucose in defined medium compared to wild-type (0.69 g/L; 0.03 g/g glucose) and other variants. In phosphate starved repetitive batch, *E. coli ldhA poxB pta-ackA gltA*:*gltA*$^{[A267T]}$ produced 15.9 g/L 3-HB (effective concentration 21.3 g/L with dilution) with

0.16 g/g glucose yield and acetate as a byproduct with 3.4 g/L titer. Pyruvate accumulated during each batch and was assimilated towards biomass and 3-HB formation.

Conclusions: Results obtained in this study demonstrates that GltA variants offer a means to increase intracellular acetyl-CoA pools for the generation of acetyl-CoA derived products. Enhancing substrate affinity of the introduced pathway genes like thiolase towards acetyl-CoA will further increase the flux towards 3-HB formation and also reduce pyruvate and acetate accumulation.

4.2 INTRODUCTION

(R)-3-hydroxybutyric acid (3-HB) is a chiral building block for the production of fine chemicals in the chemical, food, and pharmaceutical industry (Gao et al., 2002, Kawata et al., 2014), and an advantage of the microbial route for 3-HB synthesis is the ease of generating the pure enantiomer (Biernacki et al., 2017). Microbial synthesis of 3-HB has been accomplished in both bacteria and yeast (Gao et al., 2002, Beirnacki et al., 2017).

As a model organism, *Escherichia coli* has been widely studied for the generation of 3-HB by overexpressing heterologous pathways. One pathway to 3-HB involves the enzymes acetyl-CoA C-acetyltransferase or β-ketothiolase ([EC 2.3.1.9], coded by the *phaA* gene) and acetoacetyl-CoA reductase ([EC 1.1.1.36], *phaB*) (Figure 4.1). Using genes from *Cupriavidus necator* resulted in about 0.4 g/L 3-HB in shake flask culture (Gao et al., 2002). Inclusion of *ptb* (phospho-transbutyrylase) and *buk* (butyrate kinase) from *Clostridium acetobutylicum*, allowing formation of ATP through the intermediate of 3-hydroxybutyryl-phosphate, led to 5 g/L 3-HB in a glucose-supplemented complex medium in shake flask culture and 12 g/L 3-HB with 8.5 g/L acetate in a fed-batch process (Gao et al., 2002). Addition of acetate in *E. coli* expressing the genes *phaA*, *phaB*, and *pct* (encoding propionyl-CoA transferase) attained titers of 5.2 g/L and a

productivity of 0.22 g/L·h in test tube cultures (Matsumoto et al., 2012). In another study, overexpression of *phaA, phaB,* and *tesB* (coding a thioesterase) led to 3.6 g/L 3-HB in 48 h with a 0.41 g/g yield in glucose-supplemented complex medium (Tseng et al., 2009), while fed-batch culture of this strain accumulated 12.2 g/L 3-HB at 0.5 g/L·h (Liu et al., 2007). In comparison, under microaerobic conditions, a native producer *Halomonas* sp. generated 15.2 g/L 3-HB (Kawata et al., 2012). A nitrate fed-batch process using *Halomonas* sp. in which the stored poly(3-hydroxybutryate) was degraded to 3-HB led to 40.3 g/L at 0.48 g/L·h in shake flask studies under microaerobic conditions (Kawata et al., 2014).

Acetyl-CoA is a key precursor for 3-HB, and several native pathways which metabolize acetyl-CoA compete with the 3-HB pathway. Most strategies for 3-HB production also generate acetate as a by-product (Gao et al., 2002, Jarmander et al., 2015). Deletion or repression of *pta-ackA* or *poxB* genes are common approaches to reduce acetate formation, and this strategy has previously also been applied to several other acetyl-CoA-derived products such as citramalate (Wu and Eiteman, 2016), butyric acid (Wang et al., 2019), *n*-butanol (Kim et al., 2017), and 3-HB (Perez-Zabaleta et al., 2019). However, the primary metabolic competition for acetyl-CoA availability is the enzyme citrate synthase (*gltA* gene), through which 63% of the acetyl-CoA flows during steady-state, glucose-limited culture (Zhao et al., 2004). Although outright deletion of citrate synthase increases the yield of acetyl-CoA-derived products from glucose, including citramalate (Wu and Eiteman, 2016) and mevalonate (Satowa et al., 2020), this deletion prevents growth on glucose as the sole carbon source, necessitating a medium supplement such as glutamate (Gilvarg and Davis,1956). Alternatively, approaches have been proposed to reduce rather than eliminate citrate synthase flux. For example, decreasing the *gltA* promoter strength increased intracellular oxaloacetate and acetyl-CoA concentrations led to improved lysine

production in *Corynebacterium glutamicum* (van Ooyen et al., 2012). Reducing the activity of citrate synthase directly using targeted amino acid substitutions lowered k_{CAT} and increased K_M, resulting in the diversion of carbon from the TCA cycle to the model compound acetate (Tovilla-Coutiño et al., 2020), as well as to citramalate (Wu et al., 2020).

Nutrient limitation can also have a profound effect on the formation of 3-HB. During an N-limited fed-batch cultivation on mixed sugars, *E. coli* overexpressing the *t3* (β-ketothiolase) and *rx* (acetoacetyl-CoA reductase) genes from *Halomonas boliviensis* generated 1.8 g/L 3-HB and 2.7 g/L acetate (Jarmander et al., 2015). An N-limited exponential-linear feed process with *E. coli* expressing *t3* and *rx* genes led to 4.1 g/L 3-HB and 7 g/L acetate, while a P-limited exponential-linear process yielded 6.8 g/L 3-HB and 9 g/L acetate (Guevara-Martínez et al., 2015). A combination of repeated batch followed by N-starved process with *E. coli* additionally overexpressing the *zwf* gene intended to increase flux through the NADPH-generating pentose phosphate pathway led to 12.7 g/L 3-HB in *E. coli* AF1000 strain (Perez-Zabaleta et al., 2016) and 16.3 g/L in *E. coli* BL21 strain (Perez-Zabaleta et al., 2019). More recently, overexpression of another thioesterase (*yciA* gene) along with the *zwf*, *t3*, and *rx* genes in a repeated batch followed by N-starved process generated 14.3 g/L 3-HB in *E. coli* AF1000 strain (Guevera-Martinèz et al., 2019).

The goal of this study was to use citrate synthase variants for the formation of acetyl-CoA-derived 3-HB. We hypothesized that creating a metabolic restriction at the intermediate acetyl-CoA could divert more acetyl-CoA towards 3-HB (Figure 4.1). We also examined the effect of the overexpression of two commonly used thioesterases, TesB and YciA, pantothenate kinase (CoaA) and applying phosphate starved conditions for 3-HB production.

4.3 MATERIALS AND METHODS

Strains and genetic modifications

Strains used in this study are shown in Table 4.1, and plasmids used are shown in Table 4.2. Gene knockout strains were constructed using lambda-red recombination (Datsenko and Wanner, 2001) with primers having 50 bp homology (Table 4.3). Knockouts were selected on Lysogeny Broth (LB) plates supplemented with kanamycin and confirmed using forward primers external to the target gene and reverse primers within the kanamycin resistance (Table 4.3). The kan^R marker was removed by expression of FLP recombinase from pCP20 (Datsenko and Wanner, 2001), and confirmed by external primers to the gene target (Table 4.3).

A homologous recombination method was used to integrate point-mutated *gltA* variants in MEC1381. pKSI-gltA(W) plasmid (pHR-gltA) containing a point mutation in *gltA* was used as donor DNA for chromosomal integration. The point-mutated *gltA* variant, kanamycin cassette and 500 bp of flanking homology region were amplified from the respective plasmid and used to transform electrocompetent MEC1381 expressing the lambda red system from pKD46 (Datsenko and Wanner, 2001). Transformants were grown on LB plates supplemented with kanamycin (Wu et al., 2020). The kan^R marker was removed, confirmed by PCR using external primers to the gene target (Table 4.3). Point-mutated *gltA* genes were amplified from the chromosome, gel purified, and sequenced to confirm correct mutations (ACGT, Inc., Wheeling, IL, USA).

Plasmid construction

Plasmids were constructed using NEBuilder HiFi Assembly (New England Biolabs, Ipswich, MA, USA) or *Escherichia coli* DH5α-mediated assembly (Moxley and Eiteman, 2021). Phusion High-Fidelity Polymerase (New England Biolabs, Ipswich, MA, USA) or PrimeStar Max High-Fidelity Polymerase (Takara Bio, Mountain View, CA, USA) was used to amplify

DNA for cloning and genome integration. Quick-DNA Miniprep and Zyppy Plasmid Miniprep Kits were used to purify genomic and plasmid DNA (Zymo Research, Irvine, CA, USA). DNA Clean and Concentrator and Zymoclean Gel DNA Recovery Kits were used to purify PCR fragments (Zymo Research, Irvine, CA, USA). Plasmids were confirmed by restriction digest (New England Biolabs, Ipswich, MA, USA) and sequencing (ACGT, Inc., Wheeling, IL, USA).

To construct pHR-gltA for sited-directed mutagenesis, a kanamycin cassette was amplified from pKD4 (Datsenko and Wanner, 2001), the *gltA* gene from *E. coli* W with 570 bp of flanking DNA upstream and 584 bp downstream were cloned into the pKSI vector (Yang et al., 2014) using NEbuilder® Hifi assembly. The assembled plasmid was transformed into *E. coli* DH5α cells using chemical transformation. Point mutations were introduced to the plasmid using method described previously (Wu et al., 2020).

The genes *phaA* and *phaB* from *Cupriavidus necator* were codon optimized (Invitrogen, Thermo Fisher Scientific, Waltham, MA, USA) and cloned into the pTrc99A plasmid (Amann et al., 1988) to form plasmid pHR-AB. Each gene was constructed in an operon containing the trc promoter and the rrnB T1 terminator. The plasmid size was determined by restriction digest, and the sequence was confirmed by DNA sequencing method. The low copy plasmid pACYC184 (Chang and Cohen, 1978; Rose, 1988) containing the native thioesterase *yciA* (pHR-*yciA*), thioesterase *tesB* (pHR-*tesB*), or pantothenate kinase *coaA* (pHR-*coaA*) used Anderson promoter J23107 (http://parts.igem.org/Promoters/Catalog/Anderson; strength = 0.34), ribosome binding site RBS_B0034 (http://parts.igem.org/Part:BBa_B0034), and terminators identical to the native *E. coli* W genes. Each gene was cloned into the multiple cloning site of the vector using NEbuilder® Hifi assembly (NEB, Ipswich, MA, USA), chemically transformed into *E. coli*

DH5α cells, and colonies isolated on plates with appropriate antibiotic. Each plasmid was confirmed by restriction digest and sequencing.

The plasmid pHR-AB was electroporated in all the *gltA* variant strains, the Δ*gltA* strain MEC1381, and the strain with the wild-type *gltA* gene (MEC1365). The pHR-*yciA*, pHR-*tesB,* or pHR-*coaA* plasmid was transformed into strains containing pHR-AB plasmid by electroporation.

Media and Growth Conditions

The strains were routinely cultured and maintained in Lysogeny Broth. For production of 3-HB, a defined medium to which glucose was added contained (per L): 8.0 g NH_4Cl, 1.2 g KH_2PO_4, 1.0 K_2HPO_4, 2.0 g K_2SO_4, 0.6 g $MgSO_4 \cdot 7H_2O$, 0.02 g thiamine HCl, 0.25 mg $ZnSO_4 \cdot 7H_2O$, 0.125 mg $CuCl_2 \cdot 2H_2O$, 1.25 mg $MnSO_4 \cdot H_2O$, 0.875 mg $CoCl_2 \cdot 6H_2O$, 0.06 mg H_3BO_3, 0.25 mg $Na_2MoO_4 \cdot 2H_2O$, 5.5 mg $FeSO_4 \cdot 7H_2O$, 50 mg citric acid, and 5.23 g (25 mM) or 31.35 g (150 mM) 3-[*N*-morpholino]propanesulfonic acid (MOPS) as indicated. Thiamine and trace metals solutions were filter sterilized, while other medium components were autoclaved in compatible mixtures and combined. Calcium pantothenate (final concentration 1 mM) was filter sterilized when used, as were antibiotics as required for plasmid maintenance or strain selection: ampicillin (150 µg/mL), kanamycin (40 µg/mL), and chloramphenicol (30 µg/mL).

Shake Flask Cultures

All shake flask studies were initiated by transferring a single colony from an LB plate to 3 mL LB liquid culture.

For growth rate studies of strains lacking plasmids, after 6-10 h of growth the LB culture was used to inoculate 3 mL defined medium containing 5 g/L glucose to an initial optical density (OD) of 0.05. When the OD reached 2-4, this culture was used to inoculate triplicate 250 mL baffled shake flasks containing 50 mL of defined medium with 5 g/L glucose in 150 mM MOPS

to an initial OD of 0.02. Growth rate was determined by measuring the OD of 6-8 samples of each culture during an exponential growth (Wu et al., 2020).

For studies on 3-HB production using strains containing one or two plasmids, after 6-10 h of growth the LB culture was used to inoculate 3 mL defined medium containing 5 g/L glucose to an initial OD of 0.05. When the OD reached 2-4, 200 µL of this culture was used to inoculate triplicate 250 mL baffled shake flasks containing 20 mL of defined medium with 8 g/L glucose in 150 mM MOPS. Cultures of MEC1381 (the Δ*gltA* strain) were additionally supplemented with 1 g/L glutamate (Wu and Eiteman, 2016). After growth to an OD of 0.4-0.6, cultures were induced with 200 µM IPTG (Isopropyl β-D-1-thiogalactopyranoside) (Wu and Eiteman, 2017), and after 6 h, samples were collected for the measurement of extracellular products. All shake flasks cultures were grown at 30°C on a rotary shaker at 250 rpm.

Batch and repeated batch processes

A single colony from an LB plate was used to inoculate 3 mL LB. After 6 h of growth, this culture was used to inoculate a 500 mL shake flask containing 50 mL of defined medium with 30 g/L glucose in 150 mM MOPS to an initial OD of 0.02. When the shake flask culture reached an OD of 1.5-2, the entire 50 mL contents were used to inoculate a 2.5 L bioreactor (Bioflo 2000, New Brunswick Scientific Co., New Brunswick, NJ, USA) containing 1.2 L defined medium with 30 g/L glucose in 25 mM MOPS. Cultures were induced with 50 µM IPTG at an OD of 0.6-0.8 (Mühlmann et al., 2017). Duplicate batch processes at 30°C and 400 rpm were performed.

A repeated batch study was conducted with identical initial composition except 40 g/L glucose, 0.9 g/L $MgSO_4 \cdot 7H_2O$ and 10 g/L NH_4Cl. The process was induced at an OD of ~ 1 with 50 µM IPTG. At OD of ~18, 5 mM betaine was added as an osmoprotect (Zu et al., 2008). After

depletion of glucose and pyruvate, a solution of 52 mL containing 39 g glucose and 50 mg ampicillin was introduced into the fermenter.

In all bioreactor processes the dissolved oxygen was maintained above 40% of saturation by sparging air with oxygen as necessary at 1.25 L/min, with agitation at 400 rpm (batch) or 500 rpm (repeated batch). The pH was controlled using either 30% KOH (w/v) or 20% H_2SO_4 (w/v). Antifoam 204 (Sigma) was used as necessary (Moxley et al., 2023).

Analytical methods

The optical density at 600 nm (OD) (UV-650 spectrophotometer, Beckman Instruments, San Jose, CA, USA) was used to monitor cell growth. Samples were routinely frozen at -20°C analysis, and thawed samples were centrifuged (13000 × g for 5 min) and filtered (0.45 µm nylon filter, 13 mm, Agilent Technologies, CA, USA). High performance liquid chromatography using 4 mN H_2SO_4 at 60°C and 0.6 mL/min with a Coregel 64-H ion-exclusion column (Transgenomic Ltd., Glasgow, United Kingdom), and refractive index detector was used to quantify glucose and organic acids (Eiteman and Chastain, 1997). Student's t-test was used to compare data statistically, with 95% confidence interval the basis for significance.

4.4 RESULTS

Growth Rates of GltA Variant Strains

This study compared a strain expressing a wild-type citrate synthase, five citrate synthase variants identified previously to decrease citrate synthase activity in *E. coli*, with substitutions K167A, A267T, M372S, V361A and F383M (Stokell et al., 2003, Wu et al., 2020, Tovilla-Coutiño et al., 2020), and a citrate synthase knockout strain. *E. coli* MEC1365 containing *ldhA*, *poxB*, and *pta-ackA* deletions was selected as the background strain for comparison to mitigate carbon loss due to acetate production (Wu and Eiteman, 2017). MEC1365 attained a growth rate

of 0.580 ± 0.008 h^{-1} with the production of pyruvate (0.016 ± 0.002 g/g) and acetate (0.004 ± 0.007 g/g). Compared to the wild-type GltA strain, the GltA variant strains showed similar, lower growth rates (0.434 – 0.503 h^{-1}) and greater pyruvate (0.000 – 0.148 g/g) and acetate (0.016-0.024 g/g) yields (Figure 4.2). Though acetate yields were not significantly different among GltA variants, the A267T variant accumulated nearly double the pyruvate as the other variants. The growth rate of MEC1381 (Δ*gltA*) was not examined because this strain is unable to grow on glucose as the sole carbon source.

Production of 3-HB by GltA Variant Strains

Plasmid pHR-AB expressing *phaA* encoding β-ketothiolase and *phaB* encoding acetoacetyl-CoA reductase (Figure 4.1) was transformed into all *E. coli* strains to evaluate 3-HB production in shake flask culture. The conversion of 3-hydroxybutyryl-CoA to 3-hydroxybutyrate was assumed to be mediated by native thioesterases. Shake flasks were conducted at 30°C using glucose as the sole carbon source, except cultures of MEC1381 (Δ*gltA*) which was supplemented with glutamate (Figure 4.3). MEC1365 (wild-type GltA) generated the lowest 3-HB (0.02 ± 0.00 g/g) and pyruvate (0.01 g/g ± 0.00 g/g) yields. Four GltA variant strains generated significantly greater 3-HB (0.10 ± 0.00 g/g) than the wild-type, although no significant difference was observed between the four variants (K167A, A267T, V361A, F383M). These four GltA variant strains also accumulated more pyruvate (>0.18 g/g) than MEC1365. MEC1567 (GltA[M372S]) produced 0.04 ± 0.01 g/g 3-HB and did not accumulate pyruvate and acetate (Figure 4.3). The Δ*gltA* knockout strain produced the greatest 3-HB (0.12 ± 0.01 g/g) and pyruvate (0.24 ± 0.02 g/g).

Production of 3-HB by GltA Variant Strains Expressing Thioesterases

Accumulation of pyruvate in GltA variants expressing *phaA*/*phaB* suggested a bottleneck between pyruvate and acetyl-CoA, a step mediated in *E. coli* by the pyruvate dehydrogenase complex under aerobic conditions. One potential cause of pyruvate accumulation could be a limited conversion of 3-hydroxybutyryl-CoA to 3-HB by native thioesterases. In addition to potentially reducing flux through the reversible steps of this introduced pathway, a bottleneck in this conversion could limit the availability of CoASH which acts as a substrate for pyruvate dehydrogenase. To test whether pyruvate accumulation could be attributed to insufficient conversion to 3-HB, native acyl-CoA hydrolases (EC 3.1.2.20) coded by the *tesB* gene (Tseng et al., 2009) or the *yciA* gene (Guevera-Martinèz et al., 2019) were each individually overexpressed in a low copy number plasmid under a constitutive promoter J231007 and introduced into strains containing the pHR-AB plasmid.

TesB is a native promiscuous thioesterase in *E. coli* that mediates the irreversible one-step hydrolysis of short-chain acyl-CoAs (Naggert et al., 1991). In shake flask experiments, overexpressed TesB in MEC1365 expressing the wild-type citrate synthase resulted in a 2.5× increase in 3-HB yield (0.05 ± 0.00 g/g) and a 2.0× increase in acetate yield (0.04 ± 0.00 g/g). In GltA variant strains and the Δ*gltA* knockout strain, overexpression of TesB significantly decreased pyruvate accumulation but consistently increased acetate formation about 5-fold (Figure 4.4). The Δ*gltA* knockout strain MEC1381 showed the greatest 3-HB yield (0.19 ± 0.00 g/g), 1.6× greater than the yield observed in absence of TesB overexpression. The GltA[K167A] variant attained the greatest 3-HB yield (0.16 ± 0.00 g/g) among the variants, about 1.6× greater than observed in the same strain without overexpression of TesB. The GltA[M372S] variant

showed a similar 3-HB yield (0.05 ± 0.00 g/g) as the wild-type citrate synthase strain MEC1365 (Figure 4.4).

YciA is one of the seven "hot dog" fold thioesterases in *E. coli*, containing a conserved fold of a five-stranded anti-paralled β-sheet wrapped around an elongated α-helix (Zhuang et al., 2008). Similar to TesB, YciA is a promiscuous thioesterase with substrates ranging from short to long-chain acyl-CoAs since hot dog fold structures lack defined non-solvated binding pockets and a conserved catalytic residue leading to multiple catalytic residues (Caswell et al., 2021). When YciA was overexpressed in variant strains which also contained the pHR-AB plasmid, the formation of both pyruvate and 3-HB was significantly diminished (Figure 4.5). For example, the GltA[A267T] variant expressing pHR-AB generated 0.10 g/g 3-HB and 0.20 g/g pyruvate in the absence of YciA (Figure 4.3), but only 0.03 g/g 3-HB and 0.006 g/g pyruvate with YciA overexpression. Instead, overexpression of YciA resulted in 7-18× greater acetate formation: for example, the GltA[A267T] variant expressing pHR-AB generated 0.02 g acetate/g glucose (Figure 4.3), but this variant additionally expressing pHR-*yciA* generated 0.18 g acetate/g glucose (Figure 4.5). The greatest acetate yield was generated by the Δ*gltA* knockout strain MEC1381 (0.35 ± 0.00 g/g).

The overexpression of either thioesterase, TesB or YciA, did significantly diminish pyruvate accumulation in 3-HB generating *E. coli* GltA variants. However, in both cases thioesterase overexpression simultaneously increased the formation of acetate. In the case of TesB, decreased pyruvate was balanced by increased 3-HB and acetate, whereas in the case of YciA, acetate formation increased at the expense of pyruvate and 3-HB. These results suggest that buildup of acetyl-CoA was indeed a factor in pyruvate synthesis in GltA variants.

Production of 3-HB by GltA Variants Strains Expressing Pantothanate Kinase

Considering the central role of the conversion of pyruvate to acetyl-CoA in the formation of 3-HB in GltA variants, we next examined the effect of overexpressing pantothenate kinase with medium supplementation of pantothenate (vitamin B_5) on 3-HB formation. Pantothenate kinase (CoaA or PanK) mediates the ATP-dependent conversion of pantothenate to 4P-pantothenate as the first step in the CoASH biosynthetic pathway. The enzyme is inhibited by intracellular CoASH and its thioesters (Vallari et al., 1987). Overexpression of CoaA did result in significantly lower pyruvate accumulation in all strains examined (Figure 4.6). For example, the GltA[A267T] variant with overexpressed CoA generated 0.121 ± 0.003 g/g pyruvate, 40% less than the same variant with only native CoaA expression. This decreased formation of pyruvate was not however accompanied by a concomitant increase in 3-HB or acetate formation.

Batch processes

Shake flask studies were conducted to screen for the best GltA variants, though such cultures have several disadvantages including absence of pH control necessitating a high buffer concentration, inability to use high glucose concentration, and lack of oxygen mass transfer to support high cell density. We therefore selected MEC1365 (wild-type GltA), and the variants GltA[A267T], GltA[M372S] and GltA[K167A] for batch studies with 30 g/L glucose as the sole carbon source. Each strain was transformed the plasmid pHR-AB expressing the *phaA* and *phaB* genes coding for enzymes 3-HB pathway (Figure 4.1). MEC1365 generated 0.71 g/L 3-HB with the productivity of 0.054 g/L·h and also accumulated 0.47 g/L pyruvate (Figure 4.7a). The GltA[A267T] variant produced 4.9 g/L 3-HB with a productivity of 0.14 g/L·h and yield of 0.17 g/g (Figure 4.7b). This variant also accumulated about 8.8 g/L pyruvate, which was at the time of glucose depletion (22 h) itself metabolized for additional biomass and 3-HB formation.

GltA[M372S] generated 1.0 g/L 3-HB at the rate of 0.08 g/L·h and yield of 0.041 g/g (Figure 4.7c). The GltA[K167A] variant MEC1411 generated 4.6 g/L 3-HB with a yield of 0.16 g/g (Figure 4.7d). Similar to GltA[A267T], 6.0 g/L pyruvate accumulated and was quickly metabolized at the time of glucose depletion. In all four strains acetate accumulated to less than 0.4 g/L.

Because TesB modestly improved 3-HB yield in shake flask culture, we repeated the batch processes using the wild-type GltA strain MEC1365 and the GltA[K167A] variant MEC1411, both expressing *phaA*, *phaB*, and *tesB* on two plasmids. Although no pyruvate was generated in either case, MEC1365 generated 1.5 g/L 3-HB and 1.7 g/L acetate, while GltA[K167A] generated 4.3 g/L 3-HB and 3.2 g/L acetate (data not shown). Unlike the consumption of pyruvate observed after glucose was depleted in strains not overexpressing TesB, in this case acetate was not converted into 3-HB after glucose depletion.

Repeated Batch processes

MEC1394 (GltA[K167A])/pHR-AB generated the greatest 3-HB titer and yield in the batch process (Figure 4.7b), and therefore was selected for a high cell density fermentation. Because pyruvate accumulated and itself was consumed after glucose was depleted (Figure 4.7b), a repeated batch process whereby glucose was added three times approximately after both glucose and pyruvate were consumed. GltA[K167A] produced 15.9 g/L 3-HB (effective concentration of 21.3 g/L without dilution) with an overall yield of 0.16 g/g glucose and 0.23 g/L·h productivity (Figure 4.8). The glucose consumption rate decreased with each glucose addition: 5.9 g/L·h, 3.9 g/L·h, and 1.6 g/L·h during the final period. Acetate was continuously generated and reached 3.4 g/L final concentration.

4.5 DISCUSSION

The goal of this study was to assess targeted substitutions in citrate synthase (GltA) and their affect on the generation of an acetyl-CoA derived product, (R)-3-hydroxybutyric acid (3-HB). Citrate synthase is a key enzyme in central metabolism at the entry of acetyl-CoA into the TCA cycle which serves as a metabolic control site between central carbon metabolism and biomass synthesis (Weitzman 1966a; Danson and Weitzman, 1973). Type II citrate synthases form hexamers which are allosterically regulated by NADH under aerobic conditions (Weitzman 1966b; Weitzman and Dunmore, 1969; Duckworth and Tong, 1976). The *E. coli* enzyme has been extensively studied in the context of structure and function, typically using site-directed mutagenesis to understand important residues for activity and allosteric inhibition by NADH (Handford et al., 1987; Donald et al., 1991; Pereira et al., 1994; Stokell et al., 2003; Maurus et al., 2003). For example, the F383 residue is highly conserved in Type II enzymes and forms an "unusual edge-on interaction" with the acetyl group of acetyl-CoA (Weigand and Remington 1986; Pereira et al., 1994). The F383A substitution leaves a large cavity which destabilizes the active site, reducing k_{CAT} by 97% (Pereira et al., 1994), while the less severe F383M substitution decreases k_{CAT} by 93% (Wu et al., 2020). Similarly, the K167A substitution weakens allosteric binding for NADH and discourages hexamer formation (Stokell et al., 2003). The K167A variant increases K_M for acetyl-CoA by 2× and K_M for NADH by 2.6× but does not change the K_M for oxaloacetate and the catalytic activity (Stokell et al., 2003). In absence of acetyl-CoA, residues 267-297 possess high thermal factors indicating mobility, and in the presence of acetyl-CoA this mobile loop undergoes considerable conformational changes (Ayed and Duckworth, 1999). Substitutions in this mobile loop can affect both catalytic activity and acetyl-CoA affinity (Ayed and Duckworth, 1999; Nguyen et al., 2001; Tovilla-Coutiño et al., 2020). For example, the

A267T substitution increases apparent K_M for acetyl-CoA by 2.3× and decreases k_{CAT} from 34 to 2.1 s^{-1} (Tovilla-Coutiño et al., 2020). In this work we selected several citrate synthase substitutions characterized in previous studies (Stokell et al., 2003; Tovilla-Coutiño et al., 2020; Wu et al., 2020) to modulate the activity of the enzyme to affect *E. coli* physiology and to alter the availability of acetyl-CoA for the production of 3-HB: A267T (located in the mobile loop proximal to the active residue H264), F383M (involved in stabilization of acetyl-CoA binding), K167A (affecting NADH and acetyl-CoA binding), V361A, and M372S (located in the α-helix adjacent to catalytic residue D362). Importantly, the residues F383, K167, A267, and V361 are highly conserved in Type II citrate synthase (Eikmanns et al., 1994; Nguyen et al., 2001). Therefore, these substitutions likely would have similar effects on other prokaryotes expressing a Type II enzyme and which are of interest for the production of any acetyl-CoA-derived biochemical product.

Altering citrate synthase affects growth rate and by-product formation

Citrate synthase variants having substitutions close to the active site (F383M, A267T, V361A) or involved in NADH (K167A) or acetyl-CoA binding (F383M, A267T, K167A) affect cell physiology, and this study with a different strain was consistent with previous work (Wu et al., 2020; Tovilla-Coutiño et al., 2020). The maximum specific growth rates of all variants were 13-25% lower than MEC1365 expressing the wild-type citrate synthase (Figure 4.2). The GltA[M372S] variant showed the highest growth rate among the variants (only 13% lower than MEC1365). Though V361 and M372 are located on the same α-helix and neither is involved in catalytic activity or substrate binding, the GltA[V361A] variant showed a 21% lower specific growth rate than MEC1365, probably because of the proximity of V361 to the catalytic residue residue D362 (Nguyen et al., 2001). Nevertheless, our results provide further evidence in

support of the conclusion that any restriction of flux through citrate synthase with the aim of improving acetyl-CoA availability for the production of biochemicals will also lead to a strain having a lower growth rate on glucose as the sole carbon source.

Because of the *poxB pta-ackA* deletions in all examined strains, cells would be expected not to accumulate acetate, and indeed less than 0.005 g/g acetate was observed in MEC1365 (Figure 4.2). However, all variants except GltA[M372S] surprisingly showed elevated acetate (Figure 4.2). For example, the GltA[A267T] variant produced 0.15 g/g pyruvate and 0.022 g/g acetate. Although the route for acetate formation is uncertain given the absence of phosphotransacetylase and pyruvate oxidase, clearly the introduction of modifications in citrate synthase creates a metabolic bottleneck at acetyl-CoA which leads to accumulation of both pyruvate and acetate.

Altering citrate synthase affects 3-HB production

Citrate synthase has long been recognized as a key conduit controlling entry into the TCA cycle, and genetic tools have sought to modify citrate synthase expression/activity to increase or decrease the carbon flow to the TCA cycle. For example, placing expression under an inducible promoter (Walsh and Koshland, 1985), engineering a less active promoter (van Ooyen et al., 2012), using mRNA based lysine riboswitches (Zhou and Zheng, 2015), artificial micro RNA inhibition (Tillbrook et al., 2014) and CRISPRi-based inhibition (Heo et al., 2016) have been used in several organisms in the context of improving formation of acetyl-CoA-derived products such as butanol and polyhydroxybutyrate or oxaloacetate-derived products such as lysine. These strategies can be limited by lack of scalability and need for medium supplementation. An outright deletion of GltA does improve formation of acetyl-CoA-derived products (e.g., Figure 4.3), but also requires supplementation with glutamate or another TCA cycle intermediate

(Gilvarg and Davis, 1956; Satowa et al., 2020; Wu and Eiteman, 2016). The chromosomal GltA variants used in the current study are stable and can be grown without medium supplementation.

In shake flask culture, four of the five citrate synthase variants showed >5-fold increase in 3-HB yield from glucose compared to MEC1365 expressing the wild-type enzyme, while GltA[M372S], which also attained the highest growth rate of the variants, showed a 2.2-fold increase in 3-HB generation (Figure 4.3). In controlled batch culture, the GltA[A267T] variant formed 3-HB at a yield of 0.17 ± 0.01 g/g from glucose as the sole carbon source (Figure 4.7b), equivalent to the yield reported when both *zwf* and *yciA* were overexpressed (Guevera-Martínez et al., 2019). The use of GltA variants offers a complimentary strategy to increase yield of acetyl-CoA-derived products during unrestricted growth without overexpressing any other gene.

The 3-HB production appears to be inversely proportional to growth rate (Figure 4.2; Figure 4.3) and correlates with the severity of citrate synthase substitutions studied previously for growth and acetate production (Tovilla-Coutiño et al., 2020). The GltA[K167A] variant in *Klebsiella pneumoniae* increased 1,3-propanediol yield from glycerol by only 10% though biomass and acetate yields, and growth rate, were not significantly affected (Lee et al., 2019). Interestingly, the stated goal in that work was to *increase* the activity of citrate synthase using the K167A substitution by reducing the NADH binding during a microaerobic process. In contrast in our work, GltA[K167A] decreased growth rate by 20% but increased 3-HB yield by a factor of 5 under fully aerobic conditions. These results with *E. coli* suggest that diminished NADH-binding in GltA[K167A] which might increase citrate synthase flux under aerobic conditions is much less than the effect of reduced acetyl-CoA binding (Stokell et al., 2003). Though different microbes are being compared, the evidence suggests GltA[K167A] could enhance citrate synthase flux under anaerobic conditions but reduce citrate synthase flux under

aerobic conditions, and thus examining product formation using the K167A substitution under various levels of oxygenation would be of great interest. Note that the 1,3-propanediol pathway is biochemically separated from citrate synthase, while the 3-HB pathway commences with two moles of acetyl-CoA. Finally, since the K167A substitution affects hexamer formation (Stokell et al., 2003), this substitution may also play a role in the ability of citrate synthase to participate in multienzyme complexes which channel substrates, which might also differ under aerobic and anaerobic conditions (Bulutoglu et al., 2016).

Pyruvate accumulation suggests a metabolic bottleneck

We encountered significant pyruvate accumulation in most GltA variants during the cell growth rate studies (i.e., without the 3-HB pathway), as well as in the context of 3-HB production. Numerous studies focused on products from acetyl-CoA have also reported pyruvate accumulation. For example, deletion of *pta-ackA* genes with the goal of ethanol production led to a 30-fold increase in pyruvate accumulation compared to the strain without these knockouts (Seol et al., 2014), while pyruvate also accumulated as a consequence of the *pta* knockout during tryptophan (Liu et al., 2016) and valine (Park et al., 2010) production and *pta* and *poxB* knockouts in 3-HB production (Perez-Zabaleta et al., 2019). Although maintaining the presence of the *pta-ackA* genes largely prevents pyruvate accumulation during the formation of an acetyl-CoA-derived product, acetate then accumulates with no benefit to the desired product (Sekar et al., 2016, Perez-Zabaleta et al., 2019). Accumulation of pyruvate by the deletion of the *pta* gene has been attributed to intracellular CoASH imbalance (Ohtake et al., 2017). In the current study, though modest pyruvate was observed in MEC1365 (with wild-type GltA), pyruvate formation reached 0.20 g/g in variants and 0.23 g/g for the Δ*gltA* strain (Figure 4.3), suggesting a bottleneck for the variants which could be due to a variety of factors related to citrate synthase.

One hypothesis explored was that, because CoASH regeneration via citrate synthase is diminished in variants, the hydrolysis of 3-hydroxybutyryl-CoA to CoASH limited CoASH availability for the conversion of pyruvate to acetyl-CoA via the pyruvate dehydrogenase complex.

To improve the hydrolysis of 3-hydroxybutyryl-CoA we compared overexpression of two native *E. coli* thioesterases, TesB and YciA. These thioesterases have been used in a wide range of studies, including the formation of adipic acid (Kallscheuer et al., 2017), butyrate (Wang et al., 2019) and 3-hydroxyvalerate (Miscevic et al., 2020). Generally understood to have broad specificity to C_5 – C_{14} acyl-CoAs (McMahon and Prather, 2014) and 3-hydroxyacyl-CoA esters (Zheng et al., 2004), the presence of TesB previously improved 3-HB formation without acetate accumulation (Liu et al., 2007). In the current study in shake flasks, overexpression of TesB did increase 3-HB yield slightly and essentially eliminate pyruvate formation, however, acetate accumulation increased dramatically (Figures 4.3, 4.4). For example, overexpression of TesB in the GltA[K167A] variant with the 3-HB pathway led to a 58% increase in 3-HB formation but a 5.8-fold increase in acetate compared to GltA[K167A] expressing TesB at the native activity. Inexplicitly, in the controlled bioreactor the improvement in 3-HB yield observed in the shake flasks disappeared while acetate accumulation was even greater. Specifically, under unrestricted growth in the bioreactor using a medium with a greater concentration of glucose, overexpression of TesB in GltA[K167A] led to slight decrease in 3-HB (4.3 g/L versus 4.6 g/L without TesB), but led to greater acetate formation (3.2 g/L versus 0.3 g/L without TesB). Thus, overexpression of TesB did eliminate a bottleneck of pyruvate formation in variants caused by curtailing citrate synthase activity, but TesB merely shifted the product to acetate. Clearly, a careful tuning between the hydrolysis of acetyl-CoA and 3-hydroxybutyryl-CoA is necessary.

The thioesterase YciA was also examined in shake flask cultures with all the variants. YciA possess lower affinity (2.45× K_M) and catalytic activity (90% lower) towards acetyl-CoA compared to higher chain carbon acyl groups like butyryl-CoA (Zhuang et al., 2008). Moreover, previous research showed no increased acetate formation during 3-HB with overexpressed YciA (Guevera-Martinez et al., 2019). Surprisingly, in the current study overexpression of YciA led a 20-fold increase in acetate formation at the expense of 3-HB formation (Figure 4.5). Thus, we found YciA behaved much like TesB in eliminating the bottleneck of pyruvate accumulation, but performed worse in the sense of shifting the acetyl-CoA derived product from 3-HB to acetate. We interpret these results to be the consequence of a significant increase in acetyl-CoA pool in citrate synthase variants. A much greater intracellular acetyl-CoA concentration could result in this thioester being the predominate reaction substrate, regardless of the kinetics of these thioesterases (i.e., acetyl-CoA compared to 3-hydroxybutyryl-CoA). Thus, the results with both TesB and YciA suggest value in using a thioesterase with either lower expression or low affinity for acetyl-CoA.

Pantothenate kinase overexpression decreases pyruvate accumulation but does not improve 3-HB production

Although overexpression of either thioesterase did eliminate pyruvate formation, little improvement was observed in 3-HB formation. Another approach to reduce pyruvate accumulation is to increase the total CoASH pool. The approach of reducing citrate synthase activity would be expected to promote accumulation of acetyl-CoA (Wu et al., 2020), which is a potent inhibitor of pyruvate dehydrogenase (Schwartz et al., 1968), leading to pyruvate accumulation. One way to improve CoASH availability directly is by the overexpression of pantothenate kinase (CoaA), which is the rate limiting step in CoASH biosynthesis (Jackowski

and Rock, 1981). Previous research has confirmed that the total CoASH/acetyl-CoA concentration is increased by overexpression of this enzyme (Vadali et al., 2004a). Moreover, overexpression of pantothenate kinase has been studied before to improve acetyl-CoA derived products including isoamyl acetate (Vadali et al., 2004b), succinate (Lin et al., 2004), and fatty acids (Satoh et al., 2020). When we overexpressed CoaA on a low copy number plasmid with pantothenate supplementation, pyruvate accumulation indeed did diminish in all the GltA variants by about 40-75% compared to the same variants with only native expression of CoaA, although both 3-HB and acetate formation were not significantly changed (Figures 4.3 and 4.6). The pantothenate kinase from *E. coli* is tightly controlled by CoAs and acyl-CoAs (Vallari et al., 1987; Ogata and Chohna, 2015), and therefore the enzyme could be suppressed in variants in which the acetyl-CoA pool is expected to be elevated. Nevertheless, the absence of pyruvate accumulation demonstrates that overexpressed CoaA did relieve the bottleneck between pyruvate and acetyl-CoA, and demonstrates that the accumulation of pyruvate is a consequence of insufficient CoASH and/or accumulation of acetyl-CoA. The observation that 3-HB formation did not benefit from CoaA overexpression, despite the reduction of pyruvate, suggests that the activity of β-ketolase remains insufficient to direct the increased availability of acetyl-CoA into the pathway. Other classes of pantothenate kinase may also be worth pursuing: Type II found in *Staphylococcus aureus* and Type III found in *Helicobater pylori* and *Pseudomonas aeruginosa* are not regulated by free CoAs and acyl-CoA (Brand and Strauss, 2005, Hong et al., 2006). Overexpression of CoaA from *P. putida* and the heterologous pathway for polyhydroxyalkanoate production in *E. coli* improved the polymer content 50% (Kudo et al., 2023).

Competition between citrate synthase and 3-HB pathway

During heterologous production of biochemical, controlling the competition for the essential precursor between central carbon enzyme and the introduced pathway is critical to improve the biochemical production. Compared to the secondary or intermediate pathways, catalytic efficiency of primary central metabolism pathway such as glycolysis is generally high (Bar-Even et al., 2011). Therefore, when a heterologous pathway is introduced, the first enzyme in that pathway will compete directly for precursors with the efficient host enzyme. In this case, acetyl-CoA is the precursor for the introduced 3-HB pathway and native citrate synthase. Under aerobic conditions, acetyl-CoA pools are reported to be 20-600 µM in *E. coli* cells (Takamura and Nomura, 1988). Wild-type GltA has a $K_{M(acetyl\text{-}CoA)}$ of 120-151 µM and a k_{CAT} of 34-81 s^{-1} (Duckworth et al., 2013; Quandt et al., 2015; Tovilla-Coutiño et al., 2020). The first step of 3-HB production pathway is catalyzed by overexpression of PhaA from *C. necator,* for which kinetic parameters with respect of acetyl-CoA are not available, though the kinetic parameters for the enzyme from Gram-negative *Zoogloea ramigera* are $K_{M(acetyl\text{-}CoA)}$ of 390 µM and a k_{CAT} of 2.1 s^{-1} (Nishimura et al., 1978; Anderson et al., 1990). To estimate competition between the two enzymes by taking average kinetic values for GltA of K_M equal to 135 µM and k_{CAT} = 50 s^{-1}, a maximum stated acetyl-CoA concentration of 600 µM, and applying Michaelis-Menten kinetics, the wild-type GltA will operate at 82% of its maximum rate (41 s^{-1}) while PhaA at will operate at 61% of its maximum (about 1.3 s^{-1}). Naturally this analysis is simplistic since the actual activity is impacted by numerous factors such as the presence of cofactors and complicated by regulatory networks. Nevertheless, the overexpression of PhaA would tend to decrease the concentration of acetyl-CoA, and at 200 µM, the wild-type GltA will operate at 60% (30 s^{-1}) while PhaA will operate at 34% (0.1 s^{-1}). The ratio of activity between the two

competing enzymes (rate of GltA/rate of PhaA) has therefore increase from 32 at 600 µM to 42 at 200 µM acetyl-CoA concentration. This estimation shows that increasing the overexpression of PhaA can the counterproductive effect of decreasing the effectiveness of the PhaA protein relative to the native GltA. One approach which is the focus of this work to rebalance the competition between the native enzyme and the competing heterologous pathway is to change the kinetic parameters of the native enzyme. For example, the GltA[A267T] variant possesses kinetic parameters very similar to PhaA: a $K_{M(acetyl\text{-}CoA)}$ of 351 µM and a k_{CAT} of 2.1 s^{-1} (Tovilla-Coutiño et al., 2020). At 600 µM acetyl-CoA, the ratio of activity between GltA and PhaA is 1.54, while at 200 µM acetyl-CoA, the ratio of activity between GltA and PhaA is essentially unchanged at 1.58. Not only does altering kinetic parameters of native enzymes offer the prospect of allowing a heterologous pathway more effectively to compete kinetically with native pathways, but careful design of the modification on the native enzyme can create a system which is less sensitive to changes in intracellular concentrations which may occur with changes in nutrients or in operational mode.

Redox imbalance and nutrient limitation strategies

To increase the productivity and titer for 3-HB, strategies such as repeated batch, N-starvation/depleted/limited, and P-starvation/depleted/limited have been reported (Gao et al., 2002; Guevera-Martínez et al., 2015; Jarmander et al., 2015; Perez-Zabaleta et al., 2016; Guevera-Martínez et al., 2019). Compared to N-limitation, P-limited strategies provided greater 3-HB yield and productivity which was attributed to higher metabolic activity under P-limitation due to internal phosphate storage (Guevera-Martínez et al., 2015). Previous research using phosphate-limited *B. subtilis* glucose cultures at 0.1 h^{-1} demonstrated increased carbon flux towards the pentose phosphate pathway and transhydrogenase flux toward NADH compared to

C-limited growth (Dauner et al., 2001). Because PhaB catalyzing acetoacetyl-CoA to hydroxybutyryl-CoA requires NADPH and is speculated to be a rate-limiting step for 3-HB production (Abe and Doi, 2003), a phosphate depleted process was selected for the repeated batch using GltA[A267T]. In this study, this phosphate- starved repeated batch strategy produced a 15.9 g/L 3-HB (effective concentration of 21.4 g/L considering dilution effect of acid/base addition and glucose feed) with a yield of 0.16 g/g glucose (Figure 4.8) without overexpressing additional genes such as *zwf* and *yciA/tesB/coaA* or supplementing glutamate. Low concentrations of phosphate in the beginning of the batch was used to allow the cultures to be phosphate depleted after OD reached 30 (end of first repeated batch). Despite deleting genes responsible for acetate formation, the 3.4 g/L acetate titer was observed that can be attributed to the the promiscuous native thioesterase activity

GltA variants in combination of process engineering offer an effective strategy to generate acetyl-CoA derived products by modulating carbon flow between TCA cycle for biomass production and an introduced pathway for the product formation. Modifying kinetic parameters of enzymes involved in the introduced pathway is another strategy to increase acetyl-CoA derived products. In case of 3-HB production, increasing K_M for acetyl-CoA or/and k_{CAT} of PhaA via protein engineering can divert greater acetyl-CoA towards 3-HB production. Pyruvate accumulation can be reduced by modifying PDH to eliminate inhibition due to the increased acetyl-CoA or/and NADH formation. In addition to protein engineering, chromosomal integration of 3-HB pathway under constitutitve promoter will further improve the process by eliminating the need of antibiotic/inducer addition and reducing the metabolic burden to maintain the plasmid.

ACKNOWLEDGMENTS

The authors thank Ajay S. Arya, Sarah Lee and W. Chris Moxley for technical support for this project. We also thank Reese Lofgren for assisting with initial stage of work and Gabriel Eschedor for allowing to use HPLC instrument. The authors acknowledge financial support of the U.S. National Science Foundation (CBET-1802533) and the U.S. Department of Agriculture, National Institute of Food and Agriculture (2017-06510).

4.6 REFERENCES

Amann, E., Ochs, B., Abel, K-J. (1988). Tightly regulated *tac* promoter vectors useful for the expression of unfused and fused proteins in *Escherichia coli*. *Gene*, 69, 301-315.

Anderson, V.E., Bahnson, B.J., Wlassics, I.D., Walsh, C.T. (1990). The reaction of acetyldithio-CoA, a readily enolized analog of acetyl-CoA with thiolase from *Zoogloea ramigera*. *J Biol Chem*, 265(11), 6255-6261.

Ayed, A., Duckworth, H.W. (1999). A stable intermediate in the equilibrium unfolding of *Escherichia coli*. *Protein Sci*, 8, 1116-1126.

Bar-Even, A., Noor, E., Savir, Y., Liebermeister, W., Davildi, D., Tawfik, D.S., Mili, R. (2011). The moderately efficient enzyme: evolutionary and physiochemical trends shaping enzyme parameters. *Biochem*, 50, 4402-4410.

Brand L.A., Strauss, E. (2005). Characterization of a new pantothenate kinase isoform from *Helicobacter pyroli*. *J Biol Chem*, 280, 20185-20188.

Biernacki, M., Riechan, J., Hähnel, U., Roick, T. Baronian, K., Bode, R., Kunze, G. (2017). Production of (R)-3-hydroxybutyric acid by *Arxhula adeninivorans*. *AMB Express*, 7:4

Bulutoglu, B., Garcia, K. E., Wu, F., Minteer, S. D., Banta, S. (2016). Direct evidence for metabolon formation and substrate channeling in recombinant TCA cycle enzymes. *ACS Chem Biol* 11, 2847-253.

Caswell, B.T., de Carvalho, C.C., Nguyen, H., Roy, M., Nguyen, T., Cantu, D.C. (2021). Thioesterase enzyme families: Functions, structures, and mechanisms. *Protein Science*, 31, 652-676.

Chang, A. C., Cohen, S. N. (1978). Construction and characterization of amplifiable multicopy DNA cloning vehicles derived from the P15A cryptic miniplasmid. *J Bacteriol* 134, 1141-1156.

Danson, M.J., Weitzman, P.D.J. (1973). Functional groups in the activity and regulation of *Escherichia coli*. *Biochem J,* 135, 513-524.

Datsenko, K. A., Wanner, B. L. (2000). One-step inactivation of chromosomal genes in *Escherichia coli* K-12 using PCR products. *Proc Nat Acad Sci USA* 97(12), 6640–6645.

Donald, L. J., Crane, B. R., Anderson, D. H., Duckworth, H. W. (1991). The role of cysteine 206 in allosteric inhibition of *Escherichia coli* citrate synthase. *J. Biol. Chem.* 266, 20709-20713.

Duckworth, H.W., Tong, E.K. (1976). The binding of reduced nicotinamide adenine dinucleotide to citrate synthase of *Escherichia coli* K12. *Biochem*, 15(1), 108-114.

Duckworth, H.W., Nguyen, N. T., Gao, Y., Donald, L. J., Maurus, R., Ayed, A., Bruneau, B., Brayer, G. D. (2013). Enzyme-substate complexes of allosteric citate synthase: evidence for a novel intermdiats in substrate binding. *Biochim. Biophys. Acta* 1834, 2546-2554

Eikmanns, B.J., Thum-Schmitz, N., Eggeling, L., Lüdtke, K-U, Sahm, H. (1994). Nucleotide sequence, expression and transcriptional analysis of the *Corynebacterium glutamicum gltA* gene encoding citrate synthase. *Microbiol*, 140, 1817-1828.

Eiteman, M. A., Chastain, M. J. (1997). Optimization of the ion-exchange analysis of organic acids from fermentation. *Anal Chim Acta,* 338, 69-75.

Gao, H-J, Wu, Q., Chen, G-Q (2002). Enhanced production of ᴅ-(-)-3-hydroxybutyric acid by recombinant *Escherichia coli*. *FEMS Microbiol Lett* 213, 59-65.

Gilvarg, C., Davis, B.D. (1956). The role of the tricarboxylic acid cycle in acetate oxidation in *Escherichia coli*. *J biol Chem*, 222, 307-319.

Guevara-Martínez, M., Sjöberg Gällnö, K., Sjöberg, G., Jarmander, J., Perez-Zabaleta, M., Quillaguamán, J., Larsson, G. (2015). Regulating the production of (R)-3-hydroxybutyrate in *Escherichia coli* by N or P limitation. *Front Microbiol* 6, 844.

Guevara-Martínez, M., Perez-Zabaleta, M., Gustavsson, M., Quillaguamán, J., Larsson, G. (2019). The role of the acyl-CoA thioesterase "YciA" in the production of (R)-3-hydroxybutyrate in *Escherichia coli*. *Appl Microbiol Biotechnol*, 103, 3693-3704.

Handford, P.A., Ner, S.S., Bloxhanm, D.P., Wilton, D.C. (1987). Site-directed mutagenesis of citrate synthase; the role of the active-site aspartate in the binding of acetyl-CoA but not oxaloacetate. *Biochimica et Biophysica Acta*, 953, 232-240.

Heo, M.-J., Jung, H.-M., Um, J., Lee, S.-W., Oh, M.-K. (2016). Controlling citrate synthase expression by CRISPR/Cas9 genome editing for n-butanol production in *Escherichia coli*. *ACS Synth Biol* 6, 182-189.

Hong, B.S., Yun, M.K., Zhang, Y-M, Chohnan, S., Rock, C.O., White, S.W., Jackowski, S., Park, H-W, Leonardi, R. (2006). Prokaryotic Type II and Type III pantothenate kinases: the same monomer fold creates dimer with distinct catalytic properties. *Structure* 14, 1251-1261.

Jackowski, S., Rock, C.O. (1981). Regulation of Coenzyme A biosynthesis. *J Bacteriol* 148, 926-932.

Jarmander, J., Belotserkovsky, J., Sjöberg, G., Guevara-Martínez. M., Perez-Zabaleta, M., Quillaguamán, J., Larsson, G. (2015). Cultivation strategies for production of (R)-3-

hydroxybutyric acid from simultaneous consumption of glucose, xylose and arabinose by *Escherichia coli*. *Microb Cell Fact* 14, 51.

Kallscheuer, N., Gätgens, J., Lübcke, M., Pietruszka, J., Bott, M., Polen, T. (2017). Improved production of adipate with *Escherichia coli* by reversal of b-oxidation. *Appl Microbio. Biotechnol* 101, 2371-2382.

Kawata, Y., Kawasaki, K., Shigeri, Y. (2012). Efficient secreted production of (R)-3-hydroxybutyric acid from living *Halomonas* sp. KM-1 under successive aerobic and microaerobic conditions. *Appl Microbiol Biotechnol*, 96, 913-920.

Kawata, Y., Ando, H., Matsushita, I., Tsubota, J. (2014). Efficient secretion of (R)-3-hydroxybutyric acid from *Halomonas* sp. KM-1 by nitrate fed-batch cultivation with glucose under microaerobic conditions. *Bioresource Technol*, 156, 400-403.

Kim, S.-K., Seong, W., Han, S.-H., Lee, D.-H., Lee, S.-G. (2017). CRISPR interference guided multiplex repression of endogenous competing pathway genes for redirecting metabolic flux in *Escherichia coli*. *Microb Cell Fact* 16:188.

Kudo, H., Ono, S., Abe, K., Matsuda, M., Hasunuma, T., Nishizawa, T., Asayama, M., Nishihara, H., Chohnan, S. (2023). Enhanced supply of acetyl-CoA by exogenous pantothenate kinase promotes synthesis of poly(3-hydroxybutyrate). *Microbial Cell Factories*, 22:75.

Lee, J.H., Jung, H-M, Jung, M-Y, Oh, M-K. (2019). Effects of *gltA* and *arcA* mutations on biomass and 1,3-propanediol production in *Klebsiella pneumoniae*. *Biotechnol Bioprocess Eng*, 24, 95-102.

Lin, H., Vadali, R.V., Bennett, G.N., San, K.-Y. (2004). Increasing the acetyl-CoA pool in the presence of overexpressed phosphoenolpyruvate carboxylase or pyruvate carboxylase enhances succinate production in *Escherichia coli*. *Biotechnol Progress*, 20, 1599-1604.

Liu, Q., Ouyang, S.-P., Chung, A., Wu, Q., Chen, G.-Q. (2007). Microbial production of *R*-3-hydroxybutyric acid by recombinant *E. coli* harboring genes of *phbA*, *phbB* and *tesB*. *Appl Microbiol Biotechnol*, 76, 811-818.

Liu, L., Duan, X., Wu, J. (2016). L-tryptophan production in *Escherichia coli* improved by weakening the Pta-AckA pathway. *PloS One*, 11(6), e0158200.

Maurus, R., Nguyen, N. T., Stokell, D. J., Ayed, A., Hultin, P. G., Duckworth, H.W., Brayer, G. D. (2003). Insights into the evolution of allosteric properties. The NADH binding site of hexameric type II citrate synthases. *Biochemistry* 42, 5555-5565.

Matsumoto, K., Okei, T., Honma, I., Ooi, T., Aoki, H., Taguchi, S. (2013). Efficient (R)-3-hydroxybutyrate production using acetyl CoA regenerating pathway catalyzed by coenzyme A transferase. *Appl Microbiol Biotechnol*, 97, 205-210.

McMahon, M. D., Prather, K. L. (2014). Functional screening and in vitro analysis reveal thioesterases with enhanced substrate specificity profiles that improve short-chain fatty acid production in *Escherichia coli*. *Appl Environ Microbiol*, 80, 1042-1050.

Miscevic, D., Srirangan, K., Kefale, T., Kilpatrick, S., Chung, D. A., Moo-Young, M., Chou, C. P. (2020). Heterologous production of 3-hydroxyvalerate in engineered *Escherichia coli*. *Metabol. Eng.* 61, 141-151.

Moxley, W.C., Eiteman, M.A. (2021). Pyruvate production by *Escherichia coli* by use of pyruvate dehydrogenase variants. *Appl Environ Microbiol*, 8(13), e00487-21.

Mühlmann, M., Forsten, E., Noack, S., Büchs, J. (2017). Optimizing recombinant protein expression via automated induction profiling in microtiter plates at different temperatures. *Microb Cell Fact*, 16:220

Naggert, J., Narasimhan, M.L., DeVeaux, L., Cho, H., Randhawa, Z.L., Cronan, J.E., Green, B.N., Smith, S. (1991). Cloning, sequencing, and characterization of *Escherichia coli* Thioesterase II*. *J Biol Chem* 266(17), 11044-11050.

Nishimura, T., Saito, T., Tomita, K. (1978). Purification and properties of β-ketothiolase from *Zoogloea ramigera*. *Arch Microbiol*, 116, 21-27.

Nguyen, N.T., Maurus, R., Stokell, D.J., Ayed, A., Duckworth, H.W., Brayer, G.D. (2001). Comparitive analysis of folding and substrate binding sites between regulated hexameric type II citrate synthases and unregulated dimeric type I enzymes. *Biochem*, 40, 13177-13187.

Ogata, Y., Chohnan, S. (2015). Prokaryotic type III pantothenate kinase enhances coenzyme A biosynthesis in *Escherichia coli*. *J Gen Appl Microbiol*, 61, 266-269.

Ohtake, T., Pontrelli, S., Laviña, Liao, J., Putri, S.P., Fukusaki, E. (2017). Metabolomics-driven approach to solving a CoA imbalance for improved 1-butanol production in *Escherichia coli*. *Metabol Eng*, 41, 135-143.

Park, J. H., Kim, T. Y., Lee, K. H., Lee, S. Y. (2011). Fed-Batch culture of *Escherichia coli* for L-valine production based on in silico flux response analysis. *Biotechnol Bioeng* 108, 934-946.

Pereira, D.S., Donald, L.J., Hosfield, D.J., Duckworth, H.W. (1994). Active site mutants of *Escherichia coli* citrate synthase. *J Biol Chem*, 269, 412-417.

Perez-Zabaleta, M., Guevara-Martínez. M., Gustavsson. M., Quillaguamán. J., Larsson, G., van Maris, A.J.A. (2019). Comparison of engineered *Escherichia coli* AF1000 and BL21 strains for (R)-3-hydroxybutyrate production in fed-batch cultivation. *Appl Microbiol Biotechnol* 103(14), 5627-5639.

Perez-Zabaleta, M., Sjöberg, G., Guevara-Martínez, M., Jarmander, J., Gustavsson, M., Quillaguamán, J., Larsson, G. (2016). Increasing the production of (R)-3-hydroxybutyrate in recombinant *Escherichia coli* by improved cofactor supply. *Microb Cell Fact* 15, 91.

Quandt, E.M., Gollighar, J., Blount, Z.D., Ellington, A. D., Georgiou, G., Barrick, J.E., (2015). Fine-tuning citrate synthase flux potentinates and refines metabolic innovation in the Lenski evolution experiment. *eLife,* 4, e09696.

Rose, R. E. (1988). The nucleotide sequence of pACYC184. *Nucleic Acids Res* 16, 355.

Satoh, S., Ozaki, M., Matsumoto, S., Nabatame, T., Kaku, M., Shudo, T., Asayama, M., Chohnan, S. (2020). Enhancement of fatty acid biosynthesis by exogenous acetyl-CoA carboxylase and pantothenate kinase in *Escherichia coli*, *Biotechnol. Lett.* 42, 2595-2605.

Satowa, D., Fujiwara, R., Uchio, S., Nakano, M., Otomo, C. Hirata, Y., Matsumoto, T., Noda, S., Tanaka, T., Kondo, A. (2020). Metabolic engineering of *E. coli* for improving mevalonate production to promote NADPH regeneration and enhance acetyl-CoA supply. *Biotechnol Bioeng* 117, 2153-2164.

Schwartz, E.R., Old, L. O., Reed, L.J. (1968). Regulatory properties of pyruvate dehydrogenase from *Escherichia coli*. *Biochem. Biophys. Res. Commun.* 31, 495-500.

Sekar, B.S., Seol, E., Raj, S.M., Park, S. (2016). Co-production of hydrogen and ethanol by *pfkA*-deficient *Escherichia coli* with activated pentose-hosphate pathway: reduction of pyruvated accumulation. *Biotechnol Biofuels* 9:95.

Seol, E., Ainala, S. K., Sekar, B. S., Park, S. (2014). Metabolic engineering of *Escherichia coli* strains for co-production of hydrogen and ethanol from glucose. *Intl J Hydro Energy* 39, 19323-19330.

Seol, E., Sekar, B.S., Raj, S.M., Park, S. (2016). Co-production of hydrogen and ethanol from glucose by modification of glycolytic pathways in *Escherichia coli*- from Embden-Meyerhof-Parnas pathway to pentose phosphate pathway. *Biotechnol J.*, 11, 249-256

Stokell, D. J., Donald, L. J., Maurus, R., Nguyen, N. T., Sadler, G., Choudhary, K., Hultin, P. G., Brayer, G. D., Duckworth, H. W. (2003). Probing the roles of key residues in the unique regulatory NADH binding site of type II citrate synthase of *Escherichia coli*. *J Biol Chem* 278, 35435–35443.

Takamura, Y., Nomura, G. (1988). Changes in the intracellular concentration of acetyl-CoA and malonyl-CoA in relation to the carbon and energy metabolism of *Escherichia coli* K12. *J Gen Microbiol*, 134, 2249-2253.

Tillbrook, K., Poirier, Y., Gebbie, L., Schenk, P.M., McQualter, R.B., Brumbley, S.M. (2014). Reduced peroximal citrate synthase activity increases substrate availability for polyhydroxyalkanoate biosynthesis in plant peroxisomes. *Plant Biotechnol J*, 12, 1044-1052.

Tovilla-Coutiño, D. B., Momany, C., Eiteman, M. A. (2020). Engineered citrate synthase alters acetate accumulation in *Escherichia coli*. *Metabolic Eng* 61, 171-180.

Tseng, H. C., Martin, C. H., Nielsen, D. R., & Prather, K. L. (2009). Metabolic engineering of *Escherichia coli* for enhanced production of (R)- and (S)-3-hydroxybutyrate. *Appl Environ Microbiol 75*(10), 3137-3145.

Vadali, R.V., Bennett, G.N., San, K.-Y. (2004a). Cofactor engineering of CoA/acetyl-CoA and its effect on meta boli flux redistribution in *Escherichia coli*, *Metabol. Eng.* 6, 133-139.

Vadali, R.V., Bennett, G.N., San, K.-Y. (2004b). Applicability of CoA/acetyl-CoA manipulation system to enhance isoamyl acetate production in *Escherichia coli*. *Metabol Eng*, 6, 294-299.

Vallari, D.S., Jackowski, S., Rock, C.O. (1987). Regulation of pantothenate kinase by Coenzyme A and its thioesters. *J Biol Chem*, 262, 2468-2471.

van Ooyen, J., Noack, S., Bott, M., Reth, A., Eggeling, L. (2012). Improved ʟ-lysine production with *Corynebacterium glutamicum* and systemic insight into citrate synthase flux and activity. *Biotechnol Bioeng* 109, 2070–2081.

Walsh, K., Koshland Jr, D.E., (1985). Characterization of rate-controlling steps *in vivo* by use of an adjustable expression vector. *Proc Natl Acad Sci USA*, 82, 3577-3581.

Wang, L., Chauliac, D., Moritz, B.E., Zhang, G., Ingram, L.O., Shanmugam, K.T. (2019). Metabolic engineering of *Escherichia coli* for the production of butyric acid at high titer and productivity. *Biotechnol Biofuels*, 12:62.

Weigand, G., Remington, S.J. (1986). Citrate synthase: structure, control, and mechanism. *Ann Rev Biophys Biophys Chem*, 15, 97-117.

Weitzman, P.D.J. (1966a). Regulation of citrate synthase activity in *Escherichia coli*. *Biochmi Biophys Acta*, 128, 211-213.

Weitzman, P.D.J. (1966b). Reduced nicotinamide-adenine dinucleotide as an allosteric effector of citrate-synthase activity in *Escherichia coli*. *Biochem J*, 101, 44c-45c.

Weitzman, P.D.J., Dunmore, P. (1969). Regulation of citrate synthase activity by α-ketoglutarate. Metabolic and taxonomic significance. *FEBS Lett*, 3(4), 265-267.

Wu, X., Eiteman, M. A. (2016). Production of citramalate by metabolically engineered *Escherichia coli*. *Biotechnol. Bioeng.* 113, 2670-2675.

Wu, X., Eiteman, M. A. (2017). Synthesis of citramalic acid from glycerol by metabolically engineered *Escherichia coli*. *J Ind Microbol Biotechnol* 44, 1483-1490.

Wu, X., Tovilla-Coutiño, D. B., Eiteman, M. A. (2020). Engineered citrate synthase improves citramalic acid generation in *Escherichia coli*. *Biotechnol Bioeng* 117(9), 2781–2790.

Yang, J., Sun, B., Huang, H., Jiang, Y., Diao, L., Chen, B., Xu, C., Wang, X., Liu, J., Jiang, W. 2014. High-efficiency scarless genetic modification in *Escherichia coli* by using lambda red recombination and I-SceI cleavage. Appl Environ Microbiol 80:3826-3834.

Zhao, J., Baba, T., Mori, H., Shimizu, K. (2004). Effect of *zwf* gene knockout on the metabolism of *Escherichia coli* grown on glucose or acetate. *Metabolic Eng* 6, 164-174.

Zheng, Z., Gong, Q., Liu, T., Deng, Y., Chen, H.-C., Chen, G.-Q. (2004). Thioesterase II of *Escherichia coli* plays an important role in 3-hydroxydecanoic acid production. *Appl. Environ. Microbiol.* 70, 3807-3813.

Zhou, L-B, Zeng, A-P. (2015). Exploring lysine riboswitch for metabolix flux control and improvement of L-Lysine synthesis in *Corynebacterium glutamicum*. *ACS Synth Biol*, 4, 729-734.

Zhu, Y., Eiteman, M.A., Altman, R., Altman, E. (2008). High glycolytic flux improves pyruvate production by a metabolically engineered *Escherichia coli* strain. *Appl Environ Microbiol*, 74(21), 6649-6655.

Zhuang, Z., Song, F., Zhao, H., Li, L., Cao, J., Eisenstein, E., Herzberg, O., Dunaway-Mariano, D. (2008). Divergence of function in the hot dog fold enzyme superfamily: the bacterial thioesterase YciA. *Biochem*, 47, 2789-2796.

Table 4.1- Strains used in this study.

Strain	Relevant characteristics	Reference
ATCC 9637	*Escherichia coli* W	Wild-type
MEC1316	ATCC 9637 Δ*poxB* Δ*ldhA*	Moxley et al., 2023
MEC1353	ATCC 9637 Δ*gltA*	This study
MEC1365	MEC1316 Δ*poxB* Δ*ldhA* Δ*pta-ackA*	This study
MEC1381	MEC1365 Δ*gltA*	This study
MEC1394	MEC1381 Δ*gltA*::*gltA*$^{[A267T]}$	This study
MEC1410	MEC1381 Δ*gltA*::*gltA*$^{[F383M]}$	This study
MEC1411	MEC1381 Δ*gltA*::*gltA*$^{[K167A]}$	This study
MEC1482	MEC1381 Δ*gltA*::*gltA*$^{[V361A]}$	This study
MEC1567	MEC1381 Δ*gltA*::*gltA*$^{[M372S]}$	This study

Table 4.2- Plasmids used in this study.

Name	Relevant characteristics	Description	Source
pKD4	Amp^R, Kan^R; R6K ori	Source of Kan^R cassette	Datsenko and Wanner, 2000
pKD46	Amp^R; pSC101 ori (ts); *araBAD* promoter for λ-Red genes	λ-Red helper plasmid	Datsenko and Wanner, 2000
pCP20	Amp^R, Cam^R; pSC101 ori (ts)	Expression of FLP recombinase	Datsenko and Wanner, 2000
pTrc99A	Amp^R; pBR322 ori	IPTG inducible expression, trc promoter	Amann et al., 1988
pACYC184	Cam^R, Tet^R; p15A ori	Low copy number plasmid	ATCC Product-37033™
pKSI-I	Amp^R; pUC ori	pBluescript II KS(-) backbone with I-SceI site–MCS–I-SceI site cassette	Yang et al., 2014
pHR-gltA	Amp^R; pUC ori	pKSI-I + *gltA* + Kan^R	This study
pHR-AB	Amp^R; pUC ori	pTrc99A::trc-*phaA*-rrnB1, trc-*phaB*-rrnB1	This study
pHR-tesB	Amp^R; pUC ori	pACYC184::J23107- RBS_B0034-*tesB*-*tesB* terminator	This study

Table 4.3- Primers used in this study

Name	Description	Sequence 5'-3'
MEP310	Up-gltA-F	TCATGCAAAACACTGCTTCCAGATG
MEP328	gltA-F	ACTACGGGCACAGAGGTTAACTTTC
MEP330	Seq-F	CTTTCCGCCTGATGGGCTTCG
MEP417	M13R	CAGGAAACAGCTATGAC
MEP477	pKSI-HA-gltA-R	CTTGATATCGAATTCCTGCAGTCATGCAAAACACTGCTTC
MEP505	pksUps_HACS	TGCTTTTGTATCAGCCATTTAAGGTCTCCTTAGCGCC
MEP508	CSend_HAKan	GGACCATGGCTAATTCCCATTAACGCTTGATATCGCT
MEP509	Kan_HApksDwn	ACAACTTAGCAATCAACCAGTGTAGGCTGGAGCTGCTTC
MEP510	Kan_HACSend	AGCGATATCAAGCGTTAATGGGAATTAGCCATGGTCC
MEP520	gltA_PBaseF	GCCTGGTAGGGATAACAGGGTAATTGCG
MEC521	gltA_PBaseR	CGCAATTACCCTGTTATCCCTACCAGGC
MEP522	Kan_Verf	CTGCCATCACGAGATTTCGATTCC
MEP525	V361A_F	GATGATACCAGAGTAGAAATCCGCGTTCGGGTACAGTTTC
MEP526	V361A_R	GAAACTGTACCCGAACGCGGATTTCTACTCTGGTATCATC
MEP529	M372S_F	CATGGAAGACGGAATACCGCTCGCTTTCAGGATGATAC
MEP530	M372S_R	GTATCATCCTGAAAGCGAGCGGTATTCCGTCTTCCATG
MEP539	A267T_F	CCGCTTCGTTGGTACCACCGTGCGCAG
MEP540	A267T_R	CTGCGCACGGTGGTACCAACGAAGCGG
MEP632	F383M_F	GGTACGTGCCATTGCCATAATGACGGTGAACAT
MEP633	F383M_R	ATGTTCACCGTCATTATGGCAATGGCACGTACC
MEP659	gltA_K168A_F	GTTCCGCCTGCTGTCGGCGATGCCGACCATGGCCGC
MEP660	gltA_K168A_R	GCGGCCATGGTCGGCATCGCCGACAGCAGGCGGAAC
MEP698	phaA_fwd	GCTCGGTACCCGGGGATGACCGATGTTGTTATTGTTAG
MEP699	phaA_rev	TCGACTCTAGAGGATTTATTTACGTTCAACTGCCAG
MEP700	pTrc99A_fwd	GTTGAACGTAAATAAATCCTCTAGAGTCGACCTGCAG
MEP701	pTrc99A_rev	AACAACATCGGTCATCCCCGGGTACCGAGCTCG

MEP714	phaB_fwd	GCTCGGTACCCGGGGATGACCCAGCGTATTGCATATG
MEP715	phaB_rev	TCGACTCTAGAGGATTTAACCCATATGCAGACCAC
MEP716	pTrc99A_fwd	CTGCATATGGGTTAAATCCTCTAGAGTCGACCTGCAG
MEP717	pTrc99A_rev	AATACGCTGGGTCATCCCCGGGTACCGAGCTCG
MEP735	phaA_5'	ATGACCGATGTTGTTATTGTTAGCGC
MEP736	phaA_3'	TTATTTACGTTCAACTGCCAGGGC
MEP737	phaB_5'	ATGACCCAGCGTATTGCATATGTTAC
MEP738	phaB_3'	TTAACCCATATGCAGACCACCAT
MEP739	ptrc99A_phaA_fwd	GGCGGGCAGGACGCCCGCCCGCCATAAACTGCC
MEP740	ptrc99A_phaA_rev	CGCAAAAAACATTATAATCCGCTCCCGGCGGAT
MEP741	phaB_fwd	CGCCGGGAGCGGATTATAATGTTTTTTGCGCCGACATCATAACGGTTCTGGC
MEP742	phaB_rev	AGTTTATGGCGGGCGGGCGTCCTGCCCGCCACC
MEP827	MEP329_F	CCAGTGCGGCCAATGTTTTTTGT
MEP828	MEP310_F	ACTGATTAATGTGGCTGGTGG
MEP829	gltA_R	CACAGTTGACTAAGCGCAGG
MEP1070	KS (gltA-W)-fwd	CCACCAGCCACATTAATCACCGGGGGATCCACTAGTTCTAG
MEP1071	DS (gltA-W)- rev	CTAGAACTAGTGGATCCCCCGGTGATTAATGTGGCTGGTGG
MEP1145	pACYC184-F	GAGTCAACGCCATGAGCGGCCTCATTTCTTATTCTGAGTT
MEP1146	pACYC184-R	CTTTCACTAGTAATAATACCTAGGGCTGAGCTAGCCGTAAAtcagtcatagtatcgtgg
MEP1147	tesB-(pACYC184)-F	CCTAGGTATTATTACTAGTGAAAGAGGAGAAATACTACatgagtcaggcgctcaaa
MEP1148	tesB-(pACYC)-R	GCCGCTCATGGCGTTGACTCGGCGAGAATGCCTATAACGC
MEP1149	yciA (pACYC184)-F	CCTAGGTATTATTACTAGTGAAAGAGGAGAAATACTACATGTCTACAACACATA ACGT
MEP1150	yciA (pACYC184)-R	GGCCGCTCATGGCGTTGACTCTAACGGCACCACCGAAATT
MEP1151	pACYC184-gene-seq F	GGTTTCCGTGTTTCGTAAAGTC
MEP1152	pACYC184-gene-seq R	GCGGACTGTTGTAACTCAGA
MEP1153	pTrc99A-phaA-seq R	GGATCACCTTTACGCTGCGG
MEP1154	pTrc99A-phaB-seq R	CCTCTTGTGCCAGTGCCATG

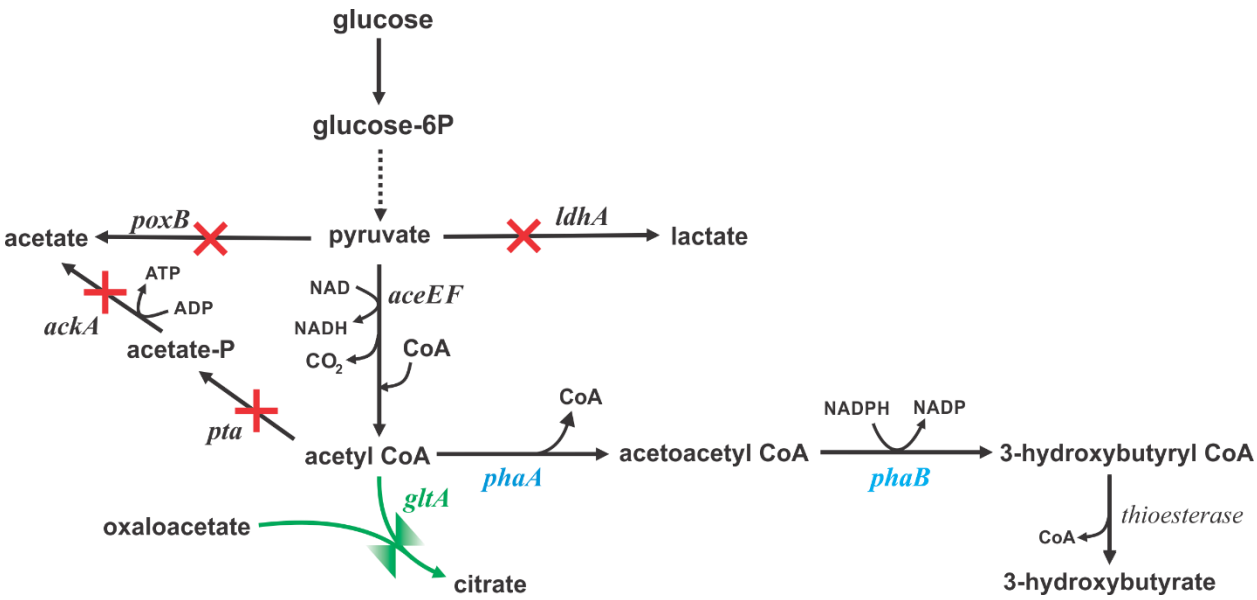

Figure 4.1- Biochemical pathway to 3-hydroxybutyrate. The strains studied each had deletions in the *poxB*, *ldhA*, *pta*, and *ackA* genes (×). Several strains additionally had chromosomal mutations in the *gltA* gene coding citrate synthase (valve, green). The *phaA* and *phaB* genes from *C. necator* (blue) were expressed on the pTrc99A plasmid.

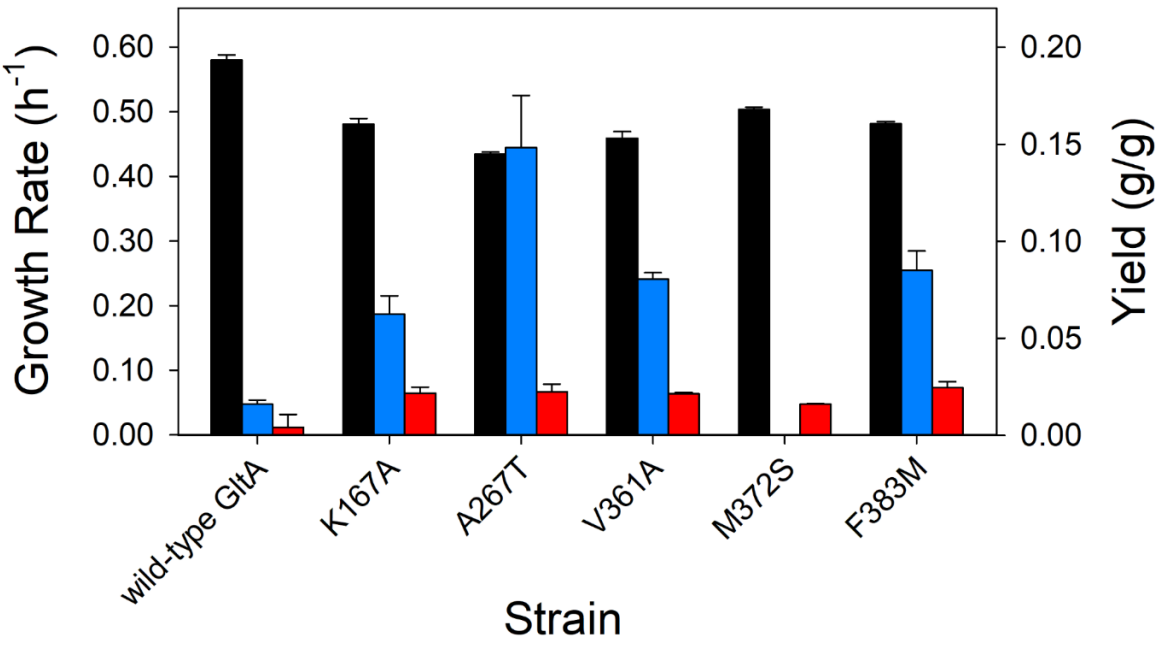

Figure 4.2- Growth rate (black) and product yield (pyruvate, blue; acetate, red) for *E. coli* citrate synthase variants. *E. coli* W strains with Δ*poxB* Δ*ldhA* Δ*pta-ackA* background were grown in triplicate in a 250 mL baffled shake flask with 50 mL defined medium containing glucose as the sole carbon source.

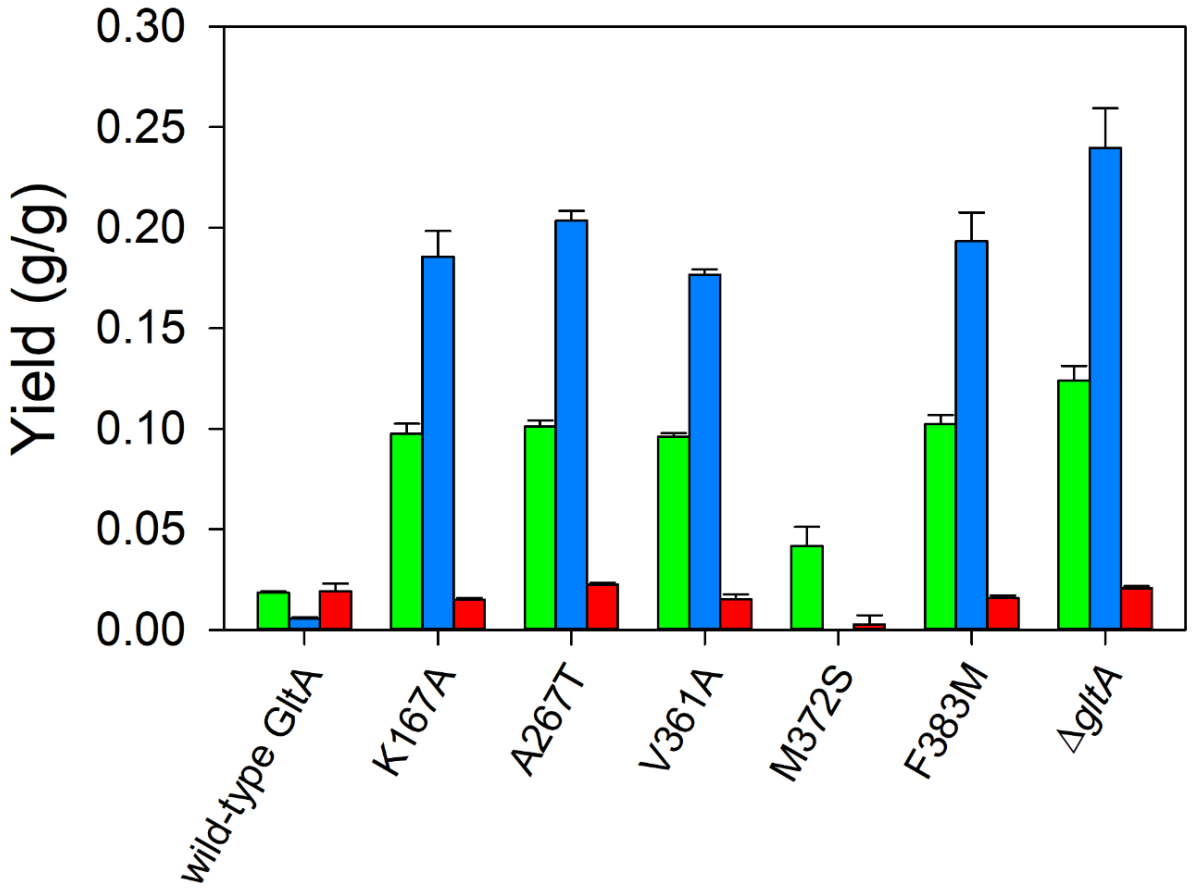

Figure 4.3- Effect of citrate synthase (GltA) substitutions on product yields using glucose as the sole carbon source in shake flask culture. Yields of 3-hydroxybutyrate (green), pyruvate (blue) and acetate (red) are shown for variants containing the plasmid pHR-AB. All strains have deletions in *poxB*, *ldhA*, *pta* and *ackA* genes.

.

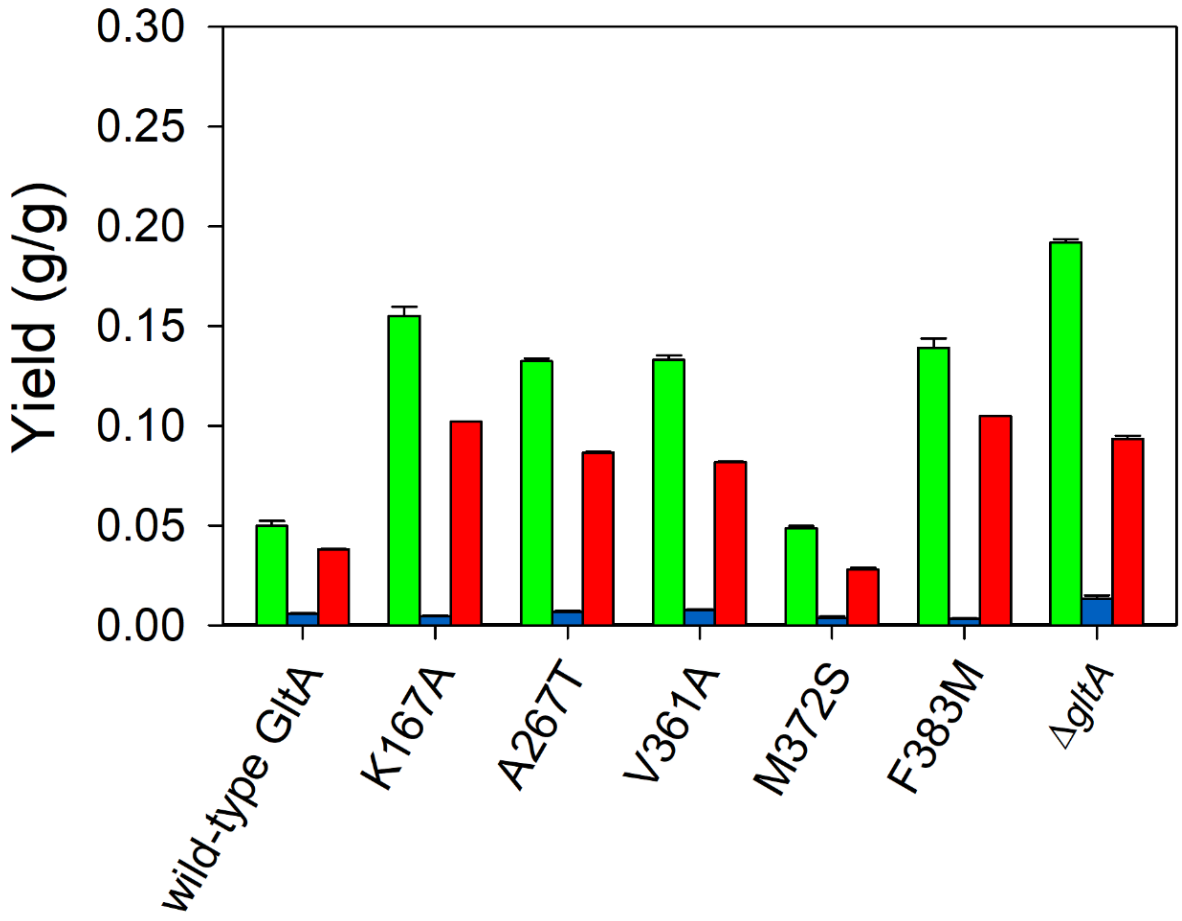

Figure 4.4- Effect of TesB expression on product yields using glucose as the sole carbon source in shake flask culture using GltA variant strains. Yields of 3-hydroxybutyrate (green), pyruvate (blue) and acetate (red) are shown for variants containing the plasmids pHR-AB and pHR-*tesB*. All strains have deletions in *poxB, ldhA*, *pta*, and *ackA* genes.

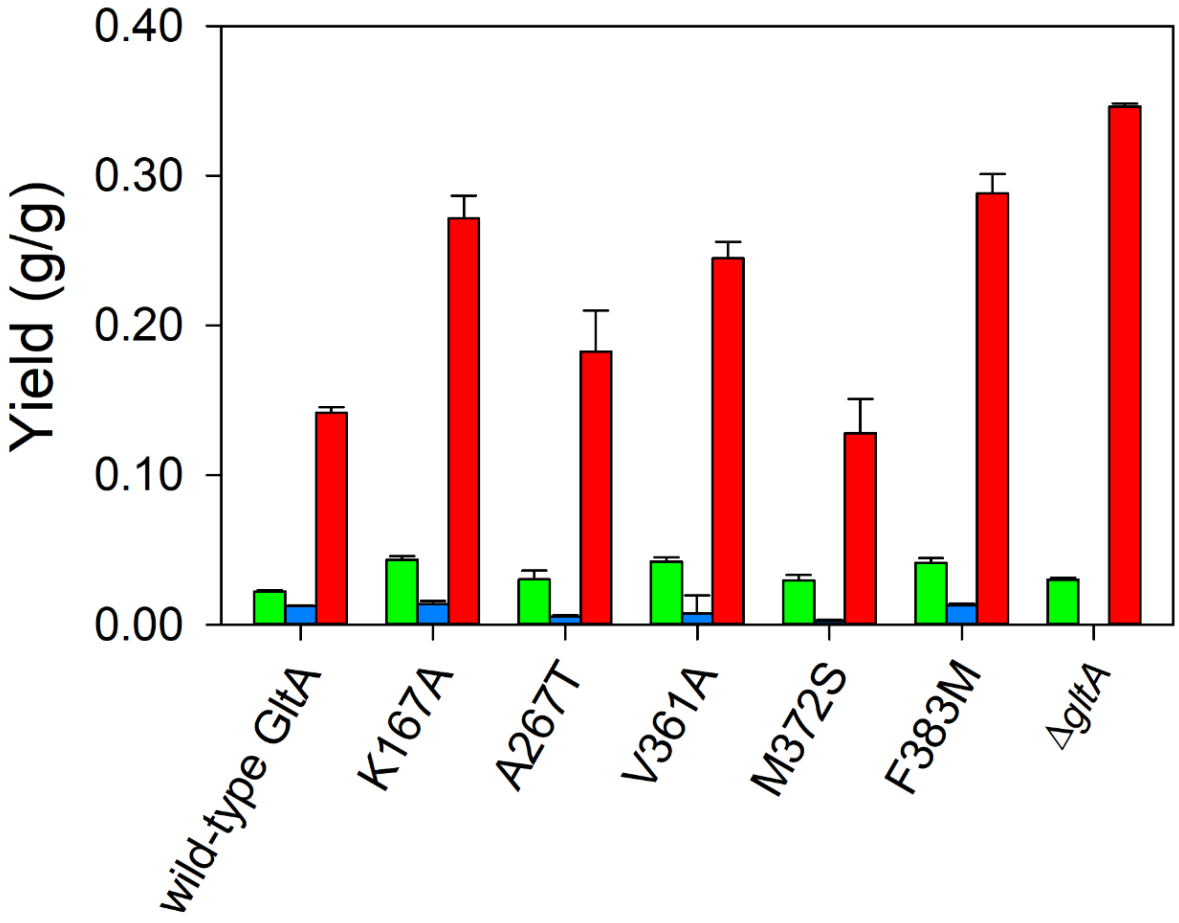

Figure 4.5- Effect of YciA expression on product yields using glucose as the sole carbon source in shake flask culture using GltA variant strains. Yields of 3-hydroxybutyrate (green), pyruvate (blue) and acetate (red) are shown for variants containing the plasmids pHR-AB and pHR-*yciA*. All strains have deletions in *poxB*, *ldhA*, *pta*, and *ackA* genes.

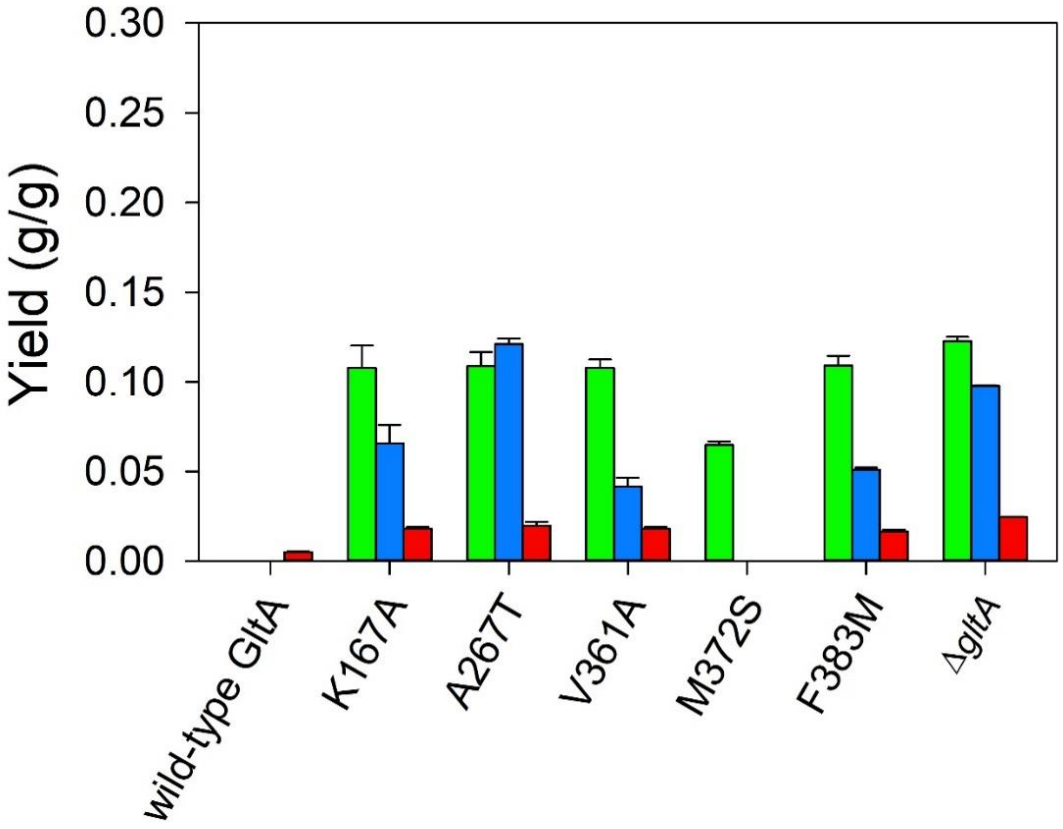

Figure 4.6- Effect of CoaA expression on product yields using glucose as the sole carbon source in shake flask culture using GltA variant strains. Yields of 3-hydroxybutyrate (green), pyruvate (blue) and acetate (red) are shown for variants containing the plasmids pHR-AB and pHR-*coaA*. All strains have deletions in *poxB*, *ldhA*, *pta*, and *ackA* genes.

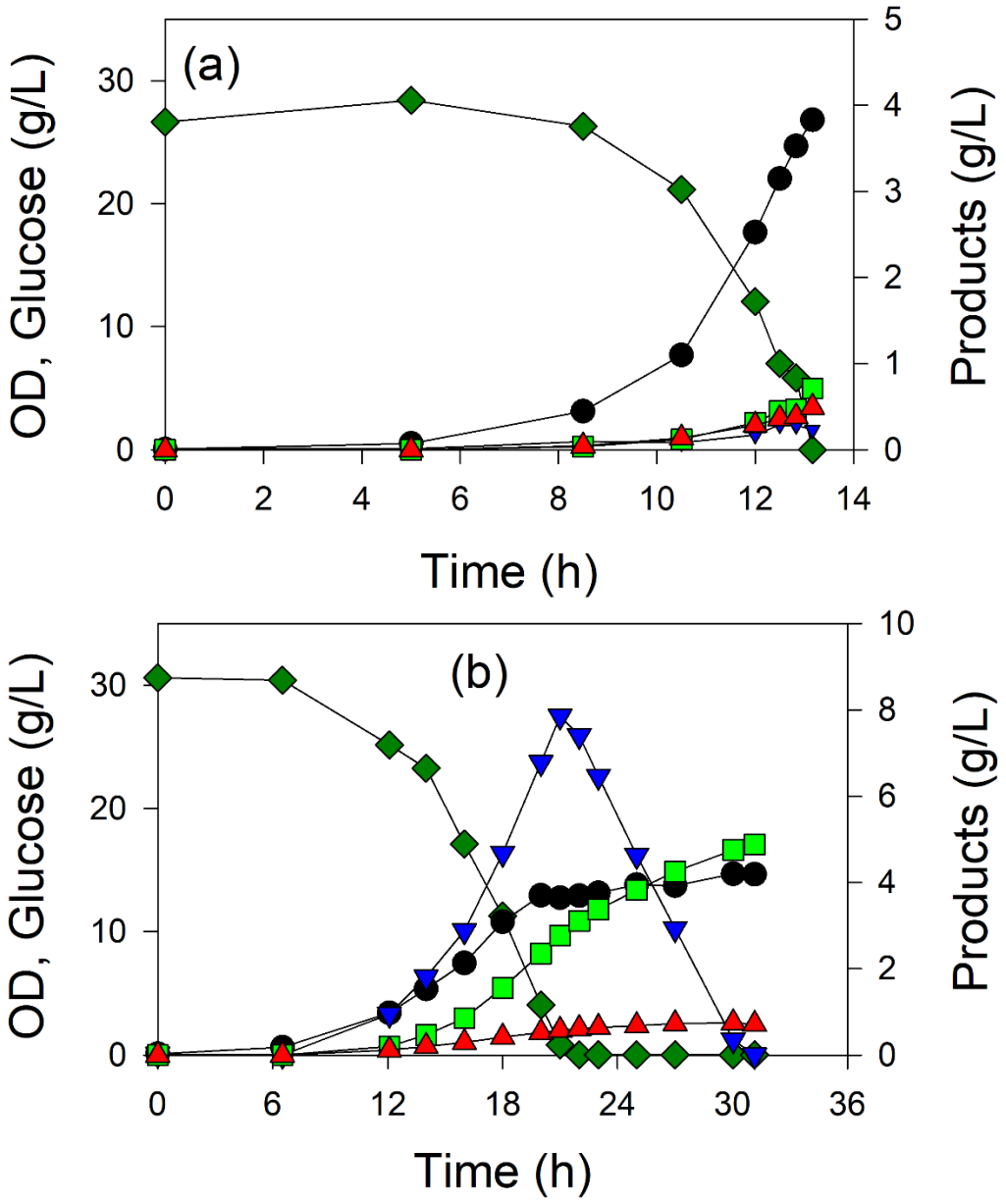
(a)
OD, Glucose (g/L)
Products (g/L)
Time (h)
0
10
20
30
0
1
2
3
4
5
0
2
4
6
8
10
12
14
(b)
OD, Glucose (g/L)
Products (g/L)
Time (h)
0
10
20
30
0
2
4
6
8
10
0
6
12
18
24
30
36

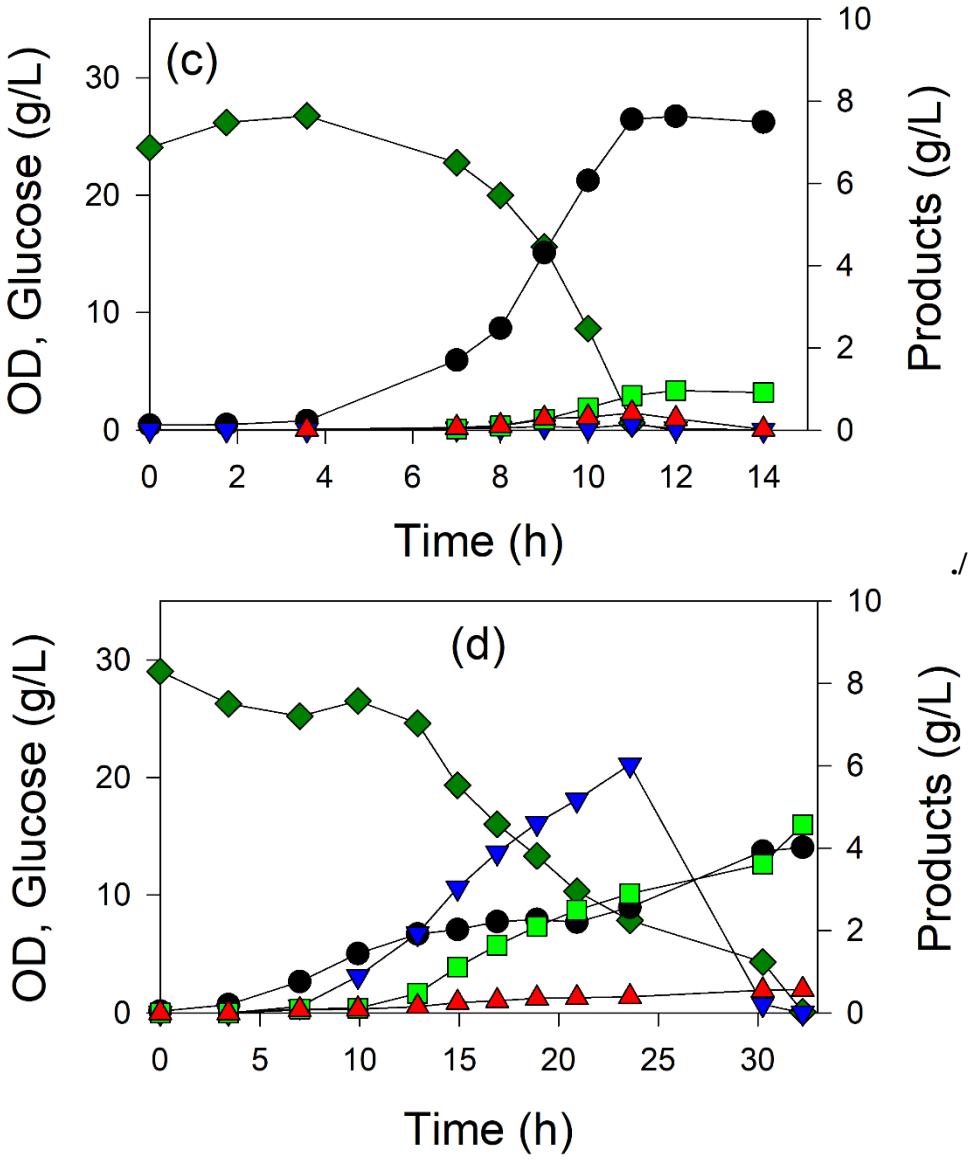

Figure 4.7- Controlled growth of W Δ*ldhA* Δ*poxB* Δ*pta-ackA* strains expressing different chromosomal gltA genes coding citrate synthase enzymes in defined medium with 30 g/L glucose and 25 mM MOPS, induced with 50 μM IPTG. Each strain expressed genes in the 3-HB pathway via plasmid pHR-AB in 1.25 L fermenter. Concentrations of glucose (◆), pyruvate (▼), OD (●), acetate (▲), 3-HB (■) were measured during the course of the 1.25 L batch processes. (a) wild-type GltA, (b) GltA[A267T], (c) GltA[M372S], (d) GltA[K167A].

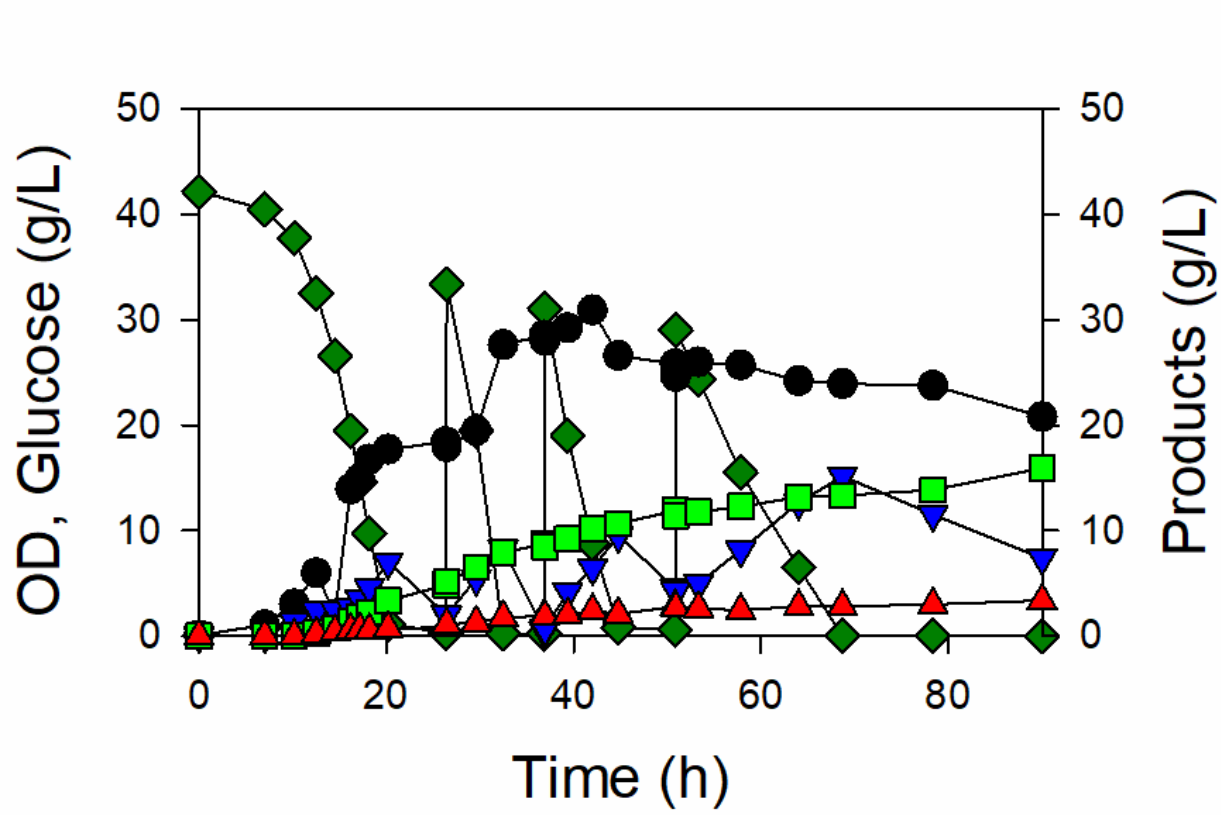

Figure 4.8- Controlled repeated batch growth MEC1394 (W Δ*ldhA* Δ*poxB* Δ*pta-ackA* Δ*gltA::gltA*$^{[A267T]}$) containing plasmid pHR-AB in a defined medium supplemented with 40 g/L glucose and 25 mM MOPS, induced with 50 μM IPTG. A 52 mL solution of 39 g glucose and 50 mg ampicillin was added in the beginning of repeated batch (three times). Concentrations of glucose (◆), pyruvate (▼), OD (●), acetate (▲), 3-HB (■) were measured during the course of the 1.25 L batch processes.

CHAPTER 5

COMBINATION OF *ESCHERICHIA COLI* CITRATE SYNTHASE AND PHOSPHOFRUCTOKINASE A VARIANTS FOR THE PRODUCTION OF MEVALONATE

[1]Rajpurohit, H. and Eiteman, M.A. To be submitted to *Biotechnology Letters*

5.1 ABSTRACT

Chromosomally expressed citrate synthase (GltA) and phosphofructokinase A (PfkA) variants containing a single amino acid substitution in either of these two enzymes were constructed in *Escherichia coli*. These strains were transformed with a plasmid expressing the *atoB* gene from *E. coli*, and the *mvaE*, and *mvaS* genes from *Lactobacillus casei*, and compared for mevalonate formation from glucose in shake flasks. The strain with wild-type GltA and PfkA formed 0.20 g/g mevalonate. PfkA variants and the Δ*pfkA* strain generated less mevalonate relative to the wild-type, while GltA variants led to greater mevalonate formation. The PfkA[R77A] GltA[A267T] variant attained 0.30 g/g mevalonate.

5.2 INTRODUCTION

The goal of metabolic engineering is to engineer microbial cell factories to create efficient systems to generate biochemicals (Han et al., 2023). Common strategies include knocking out unnecessary pathways (Tomar et al., 2003; Parimi et al., 2017), and enhancing product formation by optimizing pathway enzymes (Atsumi and Liao, 2008; Steiner and Schwan et al., 2012; Chen et al., 2018; Moxley et al., 2022; Li et al., 2023), expressing genes under strong or synthetic promoters (Deuschle et al., 1986; van Ooyen et al., 2012) and tuning transcription (Engstrom and Pfleger, 2017; Shin et al., 2022). In addition to targeting the introduced pathway, approaches also aim to increase required precursors (Bogorad et al., 2013; Wu and Eiteman, 2016; Ku et al., 2020) or redox factors (Ng et al., 2015; Han and Eiteman, 2017).

Several important metabolic junctures determine the availability of essential metabolites and energy/redox cofactors. For example, during growth on glucose, many microbes partition carbon between the pentose phosphate pathway and the Embden-Parnas-Meyerhof pathway.

This partition is determined by the relative activities of glucose-6-dehydrogenase (coded by *zwf* gene in *Escherichia coli*) leading to the pentose phosphate pathway and phosphoglucose isomerase (*pgi*) and phosphofructokinase (*pfkA*) sequentially leading to the EMP pathway. Similarly, entry into the tricarboxylic acid (TCA) cycle is controlled by citrate synthase (*gltA*). The partitioning of carbon between metabolic pathways not only influences precursor availability, but can also NADPH/NADH availability (Hua et al., 2003). Several studies have focused on controlling flux at such junctures to improve the production of biochemicals. For example, hydrogen (H_2) yield during growth on glucose was improved from 1.44 g/g to 1.88 g/g by increasing NADPH availability through overexpression of glucose 6-dehydrogenase (encoded by *zwf*) and deletion of phosphofructokinase A (encoded by *pfkA*) (Sekar et al., 2016). The formation of butanol, derived from acetyl-CoA, increased from 2.7 g/L to 6.1 g/L by the combination of a *pgi* deletion with a 32% reduction in GltA activity by replacing the native promoter (Saini et al., 2016). Increased mevalonate production was reported by using the non-oxidative bifido pathway for acetyl-CoA availability, with the overexpression of *zwf* and CRISPRi-based downregulation of the *pfkA* gene (Li et al., 2021).

Mevalonate is an important precursor for squalene, cholesterol, isoprenoids, terpenes and flavonoids via the mevalonate pathway present in both eukaryotes and some prokaryotes (Martin et al., 2003). The pathway uses three molecules of acetyl-CoA as the key metabolite to form mevalonate via reactions catalyzed by acetoacetate-CoA synthetase (encoded by *atoB*), 3-hydroxy-3-methylglutaryl-CoA (HMG-CoA) synthase (encoded by *mvaS*), and HMG-CoA reductase (encoded by *mvaE*) (Ferguson et al., 1959). Acetyl-CoA is proposed to limit mevalonate synthesis (Satowa et al., 2020), and various studies have sought to improve acetyl-CoA availability. Another approach is to reduce flux through the EMP pathway to increase

NADPH availability for HMG-CoA reductase. For example, deletion of the *gltA* and *ppc* genes individually improved mevalonate production by 1.34-1.37-fold while the Δ*gltA* Δ*ppc* strain led to 1.42× greater mevalonate (Satowa et al., 2020) in a yeast extract-supplemented tube culture. Deletion of *pfkA* with the goal of improving flux through the NADPH-generating pentose phosphate pathway actually decreased mevalonate production by 9% (Wang et al., 2022). In another study, various deletions (Δ*aceBA*, Δ*pgi*, Δ*pfkA*) with the goal of increasing NADPH availability also decreased mevalonate as much as 30% compared to a wild-type control (Satowa et al., 2020). Overexpressing phosphoketolase in a Δ*gltA* strain also did not improve mevalonate (Satowa et al., 2020). Mevalonate production was predicted to improve with overexpression of ArcA in a Δ*pgi* strain growing in the mixture of glucose and xylose (Matsuoka and Kurata, 2020). Outright deletion of genes associated with central metabolism (e.g., *pgi*, *pfkA*, *gltA*) as a means to redirect carbon metabolism away from competing metabolic pathways has not been successful in improving mevalonate formation.

An alternative to gene deletions is the reduction of expressed (*in vivo*) enzyme activity. Modulation of enzyme activity may be accomplished by altering promoter strength (van Ooyen et al., 2012). Another approach to modulate enzyme activity is by introducing targeted amino acid substitutions in an expressed enzyme which alters the enzyme's kinetic parameters, thereby limiting but not eliminating flux through the competing pathway. Protein engineering has long been used to alter the intrinsic kinetic parameters of an enzyme (Fersht et al., 1984), although the technique is typically used to *improve* activity or some other characteristic. In the case of reducing enzyme *in vivo* activity, such a strategy has been applied to construct variants which increase the formation of acetate (Tovilla-Coutiño et al., 2020), citramalate (Wu et al., 2020), pyruvate (Moxley and Eiteman, 2021) and acetoin (Moxley et al., 2023).

In this work, a combination of GltA and PfkA *E. coli* variants is examined for the production of mevalonate. The hypothesis is that a GltA variant which reduces but does not eliminate the entry of acetyl-CoA into the TCA cycle will lead to greater acetyl-CoA availability for mevalonate formation. Similarly, a PfkA variant which reduces but does not eliminate glycolytic flux will lead to greater NADPH availability for HMG-CoA reductase. Thus, fine tuning PfkA and GltA enzymes should improve the availability of precursors needed for mevalonate.

5.3 MATERIAL AND METHODS

Media

Cultures were routinely grown on Lysogeny Broth (LB) during plasmid and strain construction. As needed, antibiotics were included in medium (final concentration): ampicillin (100 µg/mL), kanamycin (40 µg/mL), and chloramphenicol (30 µg/mL).

The defined basal medium to which carbon/energy sources were added contained (per L): 3.504 g NH_4Cl, 1.2 g KH_2PO_4, 1.0 K_2HPO_4, 2.0 g K_2SO_4, 0.6 g $MgSO_4 \cdot 7H_2O$, 0.25 mg $ZnSO_4 \cdot 7H_2O$, 0.125 mg $CuCl_2 \cdot 2H_2O$, 1.25 mg $MnSO_4 \cdot H_2O$, 0.875 mg $CoCl_2 \cdot 6H_2O$, 0.06 mg H_3BO_3, 0.25 mg $Na_2MoO_4 \cdot 2H_2O$, 5.5 mg $FeSO_4 \cdot 7H_2O$, 20 mg $Na_2EDTA \cdot 2H_2O$, 20 mg citric acid, 20 mg thiamine·HCl, 2 g/L casamino acids and 20.9 g 2-[4-(2-hydroxyethyl)piperazin-1-yl]ethanesulfonic acid (90 mM HEPES). Thiamine was filtered sterilized, and other medium components were autoclaved or filtered in the compatible mixtures and combined such that final pH is 7.2.

Strains and genetic modifications

Strains used in this study are shown in Table 5.1. Gene deletions in *E. coli* W were constructed by methods previously described (Datsenko and Wanner, 2000). Knockouts were

selected on plates supplemented with kanamycin. Forward primers external to the target gene and reverse primers within the kanamycin resistance cassette were used to confirm proper chromosomal integration (Table 5.3). The kan^R marker was removed by expression of FLP recombinase from pCP20 (Datsenko and Wanner, 2000). Gene knockouts and removal of the markers were verified by colony PCR.

For the construction of the variants, a lambda-red homologous recombination method was used described previously (Wu et al., 2020; Rajpurohit and Eiteman, 2023 (to be *submitted*)). Plasmids pHR-gltA(W) and pHR-pfkA(W) containing a point mutation in *gltA* and *pfkA* were used as a donor DNA to generated GltA and PfkA variants respectively. A PCR product containing a variant gene, kanamycin cassette and homology regions greater than 500 bp was amplified from the donor plasmid and integrated chromosomally using pKD46 plasmid (Wu et al., 2020). Point-mutated *gltA* and *pfkA* genes were amplified from the chromosome, gel purified, and sequenced for the confirmed mutations (ACGT, Inc., Wheeling, IL, USA).

Plasmid construction

Plasmids used in this study are listed in Table 5.2. Plasmids were constructed using NEBuilder® HiFi Assembly (New England Biolabs, Ipswich, MA, USA). PrimeSTAR® Max High-Fidelity Polymerase (Takara Bio, Mountain View, CA, USA) was used to amplify DNA for cloning and genome integration. Quick-DNA Miniprep and Zyppy™ Plasmid Miniprep Kits were used to purify genomic and plasmid DNA (Zymo Research, Irvine, CA, USA). Zymoclean™ Gel DNA Recovery Kits were used to purify PCR fragments (Zymo Research, Irvine, CA, USA). Restriction enzymes were purchased from New England Biolabs. Plasmids were confirmed by restriction digest and sequencing (ACGT, Inc., Wheeling, IL, USA). Plasmids pHR-gltA and pHR-pfkA were constructed as described previously (Wu et al., 2020).

The plasmid pMVA1 expressing mevalonate production pathway was gifted by Morton Otto Alexander Sommer (Rugbjerg et al., 2018).

Shake flask experiments

A single colony from an LB plate was used to inoculate 3 mL basal medium containing 10 g/L glucose. After 6-10 h of growth, this culture was used to inoculate three 125 mL baffled flask containing 25 mL of basal medium with 10 g/L glucose to an initial optical density at 600 nm (OD) of 0.02. All cultures were grown at 37°C on a rotary shaker at 250 rpm. After glucose depleted (24-36 h), samples were taken for extracellular metabolite concentrations.

Analytical methods

The optical density at 600 nm (OD) (UV-650 spectrophotometer, Beckman Instruments, San Jose, CA, USA) was used to monitor cell growth. Samples were routinely frozen at -20°C analysis, and thawed samples were centrifuged (13000×g for 5 min) and filtered (0.45 µm nylon filter, 13 mm, Agilent Technologies, CA, USA). High performance liquid chromatography using 4 mN H_2SO_4 at 60°C and 0.6 mL/min with a Coregel 64-H ion-exclusion column (Transgenomic Ltd., Glasgow, United Kingdom), and refractive index detector was used to measure glucose and organic acids (Eiteman and Chastain, 1997). Student's t-test was used to compare data statistically, with 95% confidence interval the basis for significance.

5.4 RESULTS AND DISCUSSION

Citrate synthase (GltA) and phosphofructokinase A (PfkA) are crucial metabolic nodes in glucose-utilizing central carbon metabolism. Modulating citrate synthase affects the acetyl-CoA distribution between biomass and product formation (Wu et al., 2020) while altering PfkA affects the glycolytic flux (Rajpurohit and Eiteman, in review). As a key intermediate in the synthesis of terpene derived products such as fragrances, flavors, and pharmaceuticals (Martin et

al., 2003), mevalonate was chosen to test the strategy of combining enzyme variants located at primary metabolic junctions. Mevalonate producing pathway requires acetyl-CoA as a precursor and NADPH as a redox cofactor (Wada et al., 2017). Previously, strategies such as overexpressing pentose phosphate pathway genes (Satowa et al., 2020; Li et al., 2021) for NADPH generation, or deletion of citrate synthase (Satowa et al., 2020) have yielded limited benefit for mevalonate production. For example, the Δ*gltA E. coli* is unable to grow on glucose as the sole carbon source (Gilvarg and Davis, 1956). Thus, the ideal activity of GltA lies between the extremes of wild-type activity and the gene deletion.

We first constructed an array of GltA and PfkA variants, and transformed the variants with the pMVA1 plasmid carrying the mevalonate pathway genes (Figure 5.1) (Rugbjerg et al., 2018). Specifically, four PfkA variants were compared with the wild-type PfkA control and the Δ*pfkA* strain (Figure 5.2). The Δ*pfkA* strain accumulated the least mevalonate at 0.04 ± 0.01 g mevalonate/g glucose, compared to the strain expressing the wild-type PkfA which attained a yield of 0.20 ± 0.01 g mevalonate/g glucose. The four PfkA variants showed intermediate mevalonate yields from 0.06 g/g to 0.14 g/g (Figure 5.2), with the yield correlating with the severity of the substitution (Rajpurohit and Eiteman, in review). These results suggest that decreasing the PfkA activity, which itself reduces glycolytic flux (Rajpurohit and Eiteman, in review), does not improve mevalonate formation through the prospect of greater NADPH availability via the pentose phosphate pathway. Indeed, previous research demonstrates that a reduction in PfkA activity lowers the intracellular acetyl-CoA concentration (Rajpurohit and Eiteman, in review), which would be detrimental to the formation of an acetyl-CoA-derived product such as mevalonate. These results are consistent with previous studies showing that a

pfkA deletion decreases mevalonate formation significantly (Satowa et al., 2020; Wang et al., 2022).

We next introduced two different single amino acid substitutions in these six PfkA variants (i.e., wild-type PfkA, four variant PfkA strains and the Δ*pfkA* strain), resulting in 12 additional strains. The substitutions in GltA enzyme examined were K167A (Stokell et al., 2003) and A267T (Tovilla-Coutiño et al., 2020). In all strains except the wild-type PfkA strain which was not studied, the GltA[K167A] and GltA[A267T] variants increased mevalonate yield compared to the strain expressing the wild-type GltA. In general, GltA[A267T] accumulated the greatest mevalonate, with PfkA[R77A] GltA[A267T] achieving a yield of 0.30 g/g, 50% greater than the wild-type GltA/PfkA ($p<0.05$). Interestingly, the Δ*pfkA* strains additionally expressing the GltA[A267T] or GltA[K167A] variant citrate synthase, both attained a yield equal to the wild-type GltA/PfkA strain, and approximately 6× greater mevalonate than the Δ*pfkA* strain with wild-type GltA. A variant GltA is able to overcome the reduction in glycolytic flux and acetyl-CoA availability caused by the *pfkA* knockout.

Acetate formation was observed in the strains with PfkA[R77A] background (0.01 to 0.02 g/g glucose) whereas other strains produced acetate yield <0.01 g/g glucose (data not shown). No pyruvate accumulation was observed in the shake flask screen.

Future controlled batch studies at the 1-liter scale with selected PfkA/GltA variants will elucidate whether these improvements in mevalonate yield can also be achieved at higher cell density.

ACKNOWLEDGMENTS

The authors acknowledge financial support of the U.S. National Science Foundation (CBET-1802533). The authors also acknowledge the generous donation of the pMVA1 plasmid from Morten O.A. Sommer at Technical University of Denmark.

5.5 REFERENCES

Atsumi S, Liao JC. 2008. Directed evolution of *Methanococcus jannaschii* citramalate synthase for biosynthesis of 1-propanol and 1-butanol by *Escherichia coli*. Appl Environ Microbiol 74(24):7802-7808.

Bogorad I, Lin TS, Liao J. Synthetic non-oxidative glycolysis enables complete carbon conservation. Nature 502:693-697.

Chen H, Liu C, Li M, Zhang H, Xian M, Liu H. 2018. Directed evolution of mevalonate kinase in *Escherichia coli* by random mutagenesis for improved lycopene. RSC Adv 8:15021.

Datsenko KA, Wanner BL. 2000. One-step inactivation of chromosomal genes in *Escherichia coli* K-12 using PCR products. Proc Natl Acad Sci USA 97:6640-6645.

Deuschle U, Kammerer W, Gentz R, Bujard H. 1986. Promoters of *Escherichia coli*: a hierarchy of *in vivo* strength indicates alternate structures. EMBO J 5(11):2987-2994.

Engstrom MD, Pfleger BF. 2017. Transcriptional control engineering and applications in synthetic biology. Synth Syst Biotechnol 2:176-191.

Farmer WR, Liao JC. 2001. Precursor balancing for metabolic engineering of lycopene production in *Escherichia coli*. Biotechnol Prog 17:57-61.

Ferguson JJ, Durr IF, Rudney H. 1959. The biosynthesis of mevalonic acid. Proc Natl Acad Sci USA 45(4):499-504.

Fersht AR, Shi J-P, Wilkinson AJ, Blow DM, Carter P, Waye MMY, Winter GP. 1984. Analysis of enzyme structure and activity by protein engineering. Angew Chem Int Ed Engl 23:467-473.

Gilvarg C, Davis BD. 1956. The role of the tricarboxylic acid cycle in acetate oxidation in *Escherichia coli*. J biol Chem 222:307-319.

Han Q, Eiteman MA. 2017. Coupling xylitol dehydrogenase with NADH oxidase improves L-xylulose production in *Escherichia coli* culture. Enzyme Microb Technol 106:106-113.

Han T, Nazarbekov A, Zou X, Lee SY. 2023. Recent advances in systems metabolic engineering. Curr Opin Biotechnol 84:103004.

Holms WH. 1986. The central metabolic pathways of *Escherichia coli*: relationship between flux and control at a branch point, efficiency of conversion to biomass and excretion of acetate. Curr Top Cell Regulation 28:69-105.

Hua Q, Yang C, Baba T, Mori H, Shimizu K. 2003. Response of the central metabolism in *Escherichia coli* to phosphoglucose isomerase and glucose-6-phosphate dehydrogenase knockouts. J Bacteriol 185: 7053-7067.

Ku JT, Chen AY, Lan EI. 2020. Metabolic engineering design strategies for increasing acetyl-CoA flux. Metabolites 10:166.

Li Y, Xian H, Xu Y, Zhu Y, Sun Z, Wang Q, Qi Q. 2021. Fine tuning the glycolytic flux ratio of EP-bifido pathway for mevalonate production by enhancing glucose-6-phosphate dehydrogenase (Zwf) and CRISPRi suppressing 6-phosphofructo kinase (PfkA) in *Escherichia coli*. Microb Cell Fact 20:32.

Li Z, Gao C, Ye C, Guo L, Liu J, Chen X, Song W, Wu J, Liu L. 2023. Systems engineering of *Escherichia coli* for high-level shikimate production. Metab Eng 75:1-11.

Maleki N, Safari M, Eiteman MA. 2018. Conversion of glucose-xylose mixtures to pyruvate using a consortium of metabolically engineered *Escherichia coli*. Eng Life Sci 18:40-47.

Martin VJJ, Pitera D, Withers ST, Newman JD, Keasling JD. 2003. Engineering a mevalonate pathway in *Escherichia coli* for production of terpenoids. Nat Biotechnol 21(7):796-802.

Matsuoka Y, Kurata H. 2020. Computer-aided rational design of efficient NADPH production system by *Escherichia coli pgi* mutant using a mixture of glucose and xylose. Front Bioeng Biotechnol 8:227.

Moxley WC, Eiteman MA. 2021. Pyruvate production by *Escherichia coli* by use of pyruvate dehydrogenase variants. Appl Environ Microbiol 87:e00487-21.

Ng CY, Farasat I, Maranas CD, Salis HM. 2015. Rational design of a synthetic Entner-Doudoroff pathway for improved and controllable NADPH regeneration. Metab Eng 29:86-96.

Parimi NS, Durie IA, Wu X, Niyas AMM, Eiteman MA. 2017. Eliminating acetate formation improves citramalate production by metabolically engineered *Escherichia coli*. Microb Cell Fact 16:114.

Rugbjerg P, Myling-Petersen N, Porse A, Sarup-Lytzen K, Sommer MOA. 2018. Diverse genetic error modes constrain large-scale bio-based production. Nat Commun 9:787.

Saini M, Li S-Y, Wang ZW, Chiang C-J, Chao Y-P. 2016. Systematic engineering of the central metabolism in *Escherichia coli* for effective production of *n*-butanol. Biotechnol Biofuels 9:69.

Satowa D, Fujiwara R, Uchio S, Nakano M, Otomo C, Hirata Y, Matsumoto T, Noda S, Tanaka T, Kondo A. 2020. Metabolic engineering of *E. coli* for improving mevalonate production to promote NADPH regeneration and enhance acetyl-CoA supply. Biotechnol Bioeng 117:2153-2164.

Shin J, South EJ, Dunlop MJ. 2022. Transcriptional tuning of mevalonate pathway enzymes to identify the impact on limonene production in *Escherichia coli*. ACS Omega 7:18331-18338.

Steiner K, Schwab H. 2012. Recent advances in rational approaches for enzyme engineering. Comput Struct Biotechnol J 2(3):e201209010.

Stokell DJ, Donald LJ, Maurus R, Nguyen NT, Sadler G, Choudhary K, Hultin PG, Brayer GD, Duckworth HW. 2003. Probing the roles of key residues in the unique regulatory NADH binding site of type II citrate synthase of *Escherichia coli*. J Biol Chem 278:35435–35443.

Sundar Sekar B, Seol E, Raj SM, Park S. 2016. Co-production of hydrogen and ethanol by *pfkA*-deficient *Escherichia coli* with activated pentose-phosphate pathway: reduction of pyruvate accumulation. Biotechnol Biofuels 9:95.

Tomar A, Eiteman MA, Altman E. 2003. The effect of acetate pathway mutations on the production of pyruvate in *Escherichia coli*. Appl Microbiol Biotechnol 62:76-82.

Tovilla-Coutiño DB, Momany C, Eiteman MA. 2020. Engineered citrate synthase alters acetate accumulation in *Escherichia coli*. Metab Eng 61:171-180.

van Ooyen J, Noack S, Bott M, Reth A, Eggeling L. 2012. Improved L-lysine production with *Corynebacterium glutamicum* and systemic insight into citrate synthase flux and activity. Biotechnol Bioeng 109(9):2070-2081.

Wada K, Toya Y, Banno S, Yoshikawa K, Matsuda F, Shimizu H. 2017. ^{13}C-metabolic flux analysis for mevalonate-producing strain of *Escherichia coli*. J Biosci Bioeng 123(2):177-182.

Wang S, Jin X, Jiang W, Wang Q, Qi Q, Liang Q. 2022. The expression modulation of the key enzyme Acc for highly efficient 3-hydroxypropionic acid production. Front Microbiol 13:902848.

Wu X, Tovilla-Coutiño DB, Eiteman MA. 2020. Engineered citrate synthase improves citramalic acid generation in *Escherichia coli*. Biotechnol Bioeng 117(9):2781–2790.

Table 5.1- Strains used in this study.

Strain	Relevant characteristics	Reference
ATCC 9637	*Escherichia coli* W	Wild-type
MEC1377	ATCC 9637 Δ*pfkA*	This study
MEC1603	MEC1377 Δ*gltA*::*gltA*$^{[K167A]}$	This study
MEC1605	MEC1377 Δ*gltA*::*gltA*$^{[A267T]}$	This study
MEC1606	MEC1377 Δ*pfkA*::*pfkA*$^{[R77A]}$-Kan	This study
MEC1607	MEC1603 Δ*pfkA*::*pfkA*$^{[R77A]}$-Kan	This study
MEC1608	MEC1605 Δ*pfkA*::*pfkA*$^{[R77A]}$-Kan	This study
MEC1609	MEC1377 Δ*pfkA*::*pfkA*$^{[R171K]}$-Kan	This study
MEC1610	MEC1603 Δ*pfkA*::*pfkA*$^{[R171K]}$-Kan	This study
MEC1611	MEC1605 Δ*pfkA*::*pfkA*$^{[R171K]}$-Kan	This study
MEC1612	MEC1377 Δ*pfkA*::*pfkA*$^{[R171S]}$-Kan	This study
MEC1613	MEC1603 Δ*pfkA*::*pfkA*$^{[R171S]}$-Kan	This study
MEC1614	MEC1605 Δ*pfkA*::*pfkA*$^{[R171S]}$-Kan	This study
MEC1615	MEC1377 Δ*pfkA*::*pfkA*$^{[H249F]}$-Kan	This study
MEC1616	MEC1603 Δ*pfkA*::*pfkA*$^{[H249F]}$-Kan	This study
MEC1617	MEC1605 Δ*pfkA*::*pfkA*$^{[H249F]}$-Kan	This study

Table 5.2- Plasmids used in this study**.**

Name	Relevant characteristics	Description	Source
pKD4	Amp^R, Kan^R; R6K ori	Source of Kan^R cassette	Datsenko and Wanner, 2000
pKD46	Amp^R; pSC101 ori (ts); *araBAD* promoter for λ-Red genes	λ-Red helper plasmid	Datsenko and Wanner, 2000
pCP20	Amp^R, Cam^R; pSC101 ori (ts)	Expression of FLP recombinase	Datsenko and Wanner, 2000
pMVA1	Cam^R; p15 ori	Expressing *atoB*, *mvaS*, and *mvaE*	Rugbjerg et al., 2018
pHR-pfkA	Amp^R; pUC ori	pKSI-I + *pfkA* + Kan^R	This study
pHR-gltA	Amp^R; pUC ori	pKSI-I + *gltA* + Kan^R	This study

Table 5.3- Primers used in this study.

Name	Description	Sequence 5'-3'
MEP144	pfkA_F	TACGCATGGGATATGAGGCGGTACAG
MEP145	pfkA_R	GTGACTGACGAATCACCACGTTATCACC
MEP328	gltA-F	ACTACGGGCACAGAGGTTAACTTTC
MEP829	gltA_R	CACAGTTGACTAAGCGCAGG
MEP520	pKSI-plasmid_F	GCCTGGTAGGGATAACAGGGTAATTGCG
MEP521	pKSI-plasmid_R	CGCAATTACCCTGTTATCCCTACCAGGC
MEP522	Kan confirmation _R	CTGCCATCACGAGATTTCGATTCC
MEP645	KD4-pfkA_F	CTTCCGGCAACAGATTTTATTTTGCATTCCAAAGTTCAGAGGTAGTCATGGTGTAGGCTGGAGCTGCTTC
MEP646	KD4-pfkA_R	CTAAAGGAATCTGCCTTTTTCCGAAATCATTAATACAGTTTTTTCGCGCACATATGAATATCCTCCTTAG
MEP895	5'_DS_pfkA	TAGAACTAGTGGATCCCCCGGGCAATTGCGTCCACGTCAT
MEP897	5'_UPS_pfkA	CTTGATATCGAATTCCTGCATACGCATGGGATATGAGGCG
MEP898	3'_UPS_pfkA	TGGACCATGGCTAATTCCCATGATAAGCGAAGCGCATCAG
MEP900	3'_Kan	CTGATGCGCTTCGCTTATCATGGGAATTAGCCATGGTCCA
MEP901	5'_Kan	TTGCAGAATTCATGTAGGCCGTGTAGGCTGGAGCTGCTTC
MEP1072	5'_KSI	CCTATGACGTGGACGCGATTGCCCGGGGGATCCACTAGTT
MEP903	3'_KSI	CGCCTCATATCCCATGCGTATGCAGGAATTCGATATCAAG
MEP1073	3'_DS_pfkA	TAGAACTAGTGGATCCCCCGGGCAATCGCGTCCACGTCAT

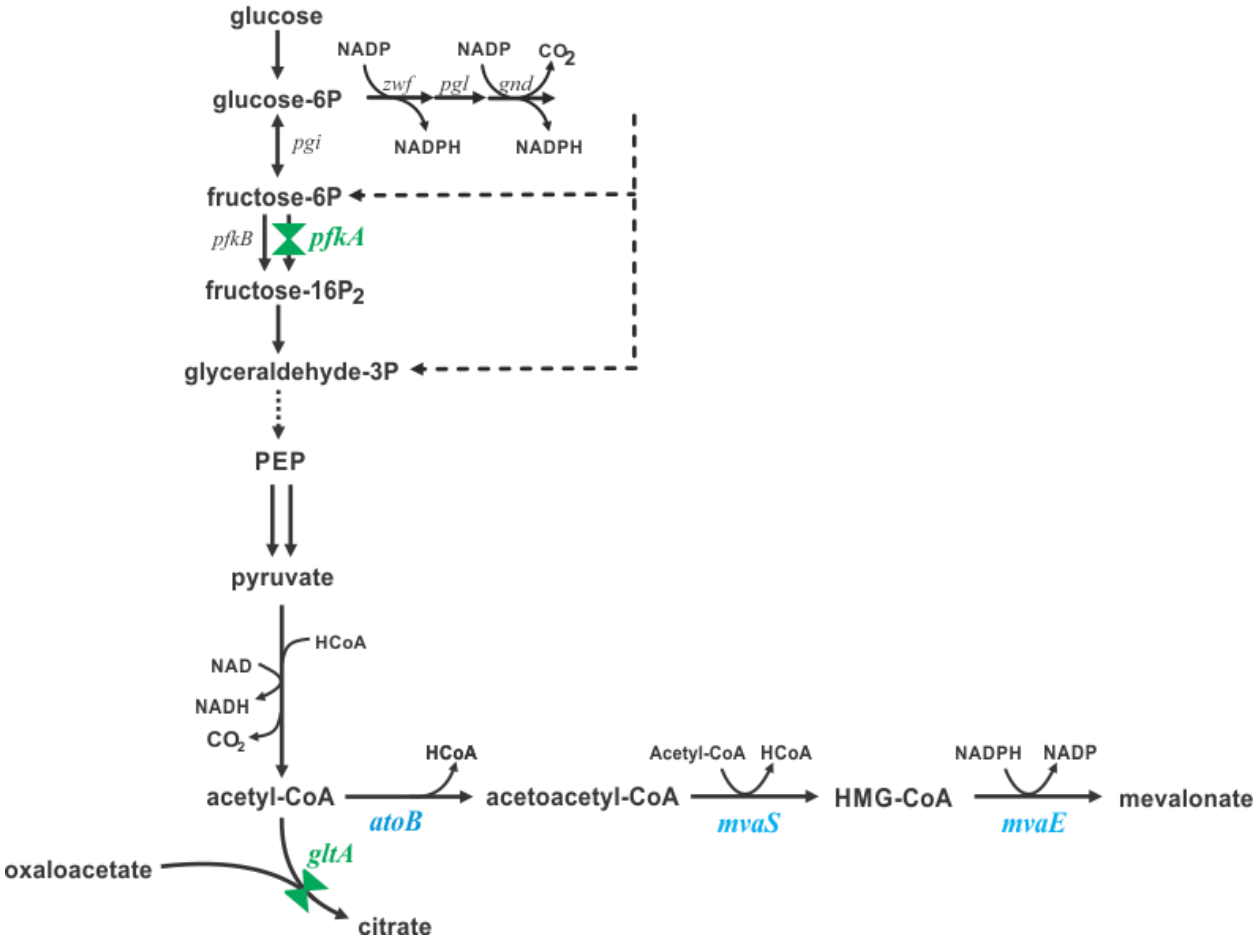

Figure 5.1- Biochemical pathway to mevalonate. Several strains additionally had chromosomal mutations in the *gltA* gene coding citrate synthase (green) and phosphofructokinase (green). The plasmid pMVA1 expressed genes *atoB* from *E. coli*, *mvaS*, and *mvaE* from *Lactobacillus casei*.

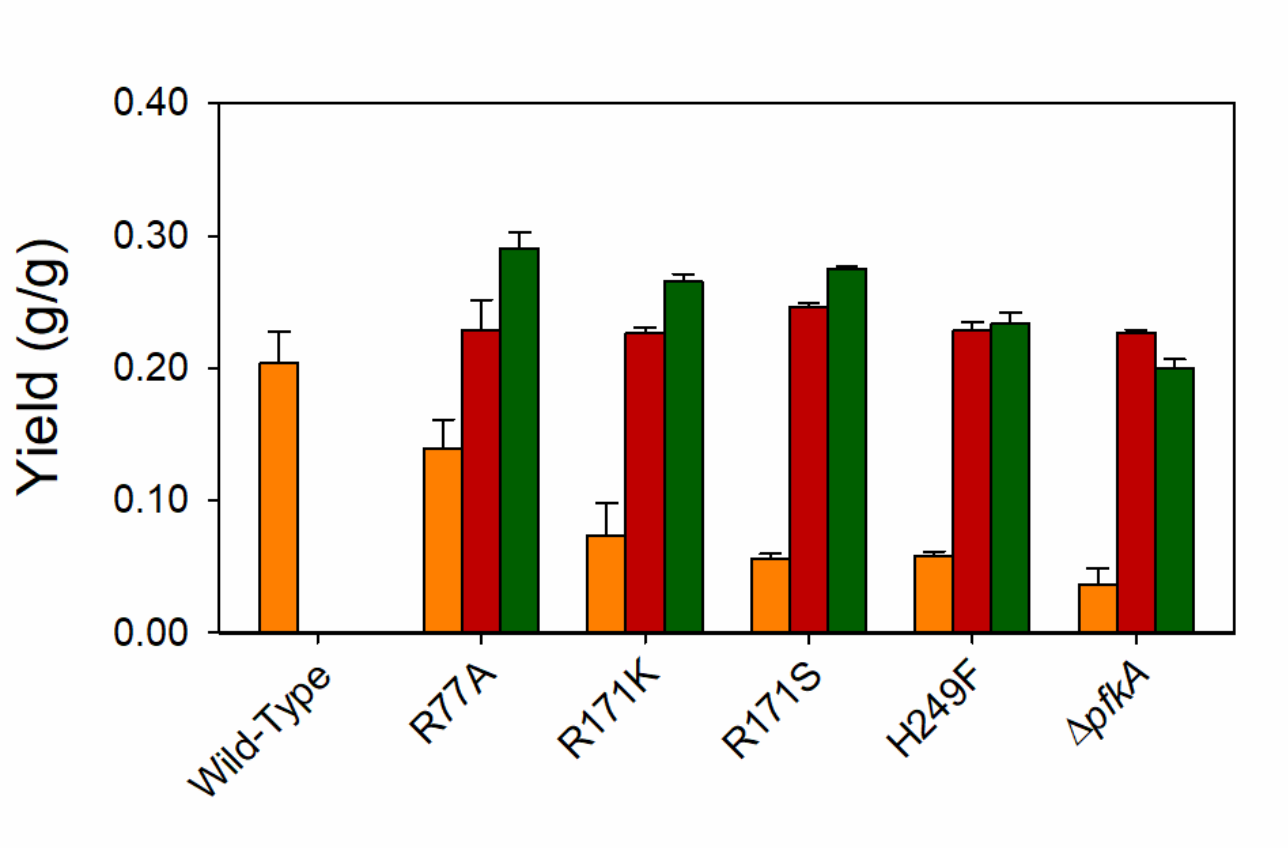

Figure 5.2- Comparison of phosphofructokinase (PfkA) substitutions (■) on mevalonate yields using glucose with 2 g/L casamino acids in shake flask culture. Chromosomally integrated alleles of $GltA^{[K167A]}$ (■) and $GltA^{[A267T]}$ (■) were also compared with PfkA variants.

CHAPTER 6

CONCLUSIONS AND FUTURE DIRECTIONS

6.1 CONCLUSIONS

The aim of this work was to modulate the key metabolic nodes in the glycolysis to redirect the carbon flow. First metabolic node targeted was phosphofructokinase A, that irreversibly phosphorylates fructose-6P and is allosterically regulated in *E. coli*. The metabolic substrate for PfkA, fructose-6P, is a building block for various chemicals such as erythritol, mannose, and psicose (Taylor et al., 2023). By decreasing activity of PfkA using site-directed mutagenesis, carbon flow can be redirected towards pentose phosphate pathway for NADPH derived products (Siedler et al., 2011), fructose-6P derived products (Taylor et al., 2023) or glucose-6P derived products (Brockman and Prather, 2015). A second metabolic node studied was citrate synthase which mediates the entry of acetyl-CoA and oxaloacetate to TCA cycle. Previously, citrate synthase was modified to produce citramalate that requires equimolar ratio of pyruvate and acetyl-CoA (Wu et al., 2020). Modifying citrate synthase to have lower catalytic activity has potential applications towards acetyl-CoA derived products (Perez Zabaleta et al., 2019; Satowa et al., 2020) as well as oxaloacetate derived products (van Ooyen et al., 2012).

Chapter 3 demonstrates that PfkA variants offer a means to control the glycolytic flux and its metabolites. Unlike pyruvate dehydrogenase variants (Moxley and Eiteman, 2021), seemingly mild amino acid substitutions in PfkA like G10A and G11A located near active site

surprisingly led to a growth rate similar to the PfkA knockout strain. Most of the variants with substitutions near the active site also showed similar growth phenotypes as PfkA knockout strain when growing on glucose as the sole carbon source. This phenomenon demonstrates that PfkA is highly regulated enzyme and is very sensitive to the modifications near active site. Based on initial shake flask studies, three PfkA variants (F76A, R77A, and R171S) with a range of growth rates were selected for nitrogen-limited, glucose-excess chemostat studies and were compared with wild-type PfkA and *pfkA* deleted strain. The steady state N-limited cultures showed a direct correlation between glycolytic intermediates fructose-1,6P_2, glyceraldehyde-3P, dihydroxyacetone, and acetyl-CoA and severity of PfkA variants. Interestingly, *pta* transcript levels in PfkA variants were also dependent on the severity of amino acid substitutions and acetate production is an indication of this effect. This library of single amino acid substituted PfkA variants is a way to control glycolytic flux at the same growth rate using glucose-excess steady state conditions.

Chapter 4 examined citrate synthase variants for the production of acetyl-CoA derived (R)-3-hydroxybutyrate (3-HB), synthesized by three enzymes. Citrate synthase variants were constructed based on previous research (Stokell et al., 2003; Wu et al., 2020; Tovilla-Coutiño et al., 2020) to redirect acetyl-CoA flow from TCA cycle towards 3-HB. Variants were compared with wild-type GltA and the *gltA* knockout strain in shake flask studies. Four of the five citrate synthase variants showed 5-fold greater 3-HB yield on glucose than the wild-type, and 80% of the yield observed with the *gltA* knockout growing with a glutamate supplement. More than 30-fold pyruvate accumulated in these four GltA variants compared to the wild-type, which was reduced using overexpression of thioesterases that redirected acetyl-CoA towards acetate formation but did not increase 3-HB production. Among variants studied in 1.25 L batch reactor,

allele *gltA*$^{[A267T]}$ performed the best for 3-HB production with maximum titer of 4.9 g/L and yield of 0.17 g/g glucose. This strain in a prolonged repeated batch study generated 16 g/L of 3-HB with a yield of 0.16 g/g glucose.

In Chapter 5, a combination of both citrate synthase variants (acetyl-CoA precursor) and phosphofructokinase variants (NADPH redox factor) was tested for mevalonate production. Previous reports discussed that mevalonate-based isoprenoid pathway is limited by acetyl-CoA and NADPH supply. Results showed that the mevalonate production is not limited by NADPH supply as decreasing the glycolytic flux using PfkA variants also decreases the glycolytic intermediate acetyl-CoA supply used for mevalonate synthesis. The combination of PfkA (R77A) and GltA variants (A267T) improved the mevalonate yield on glucose by 50% compared to the wild-type. This study shows that by using an appropriate combination of PfkA and GltA variants, yield of products requiring NADPH and acetyl-CoA can be enhanced.

6.2 FUTURE DIRECTIONS

Use of PfkA variants established a proof of concept for controlling glycolytic flux at PfkA metabolic node. The targeted approach to construct variants applied in this research was based on existing structural knowledge and therefore led to a limited library. Alternatively, the variant library can be expanded by random mutagenesis, which would likely generate more variants with growth rates closer to the wild-type. Various NADPH-detecting biosensors (Ng et al., 2015) could be used for screening a large library in microtiter plates. Also, PfkA variants studied in this research could be examined in other organisms as many microbes share PfkA sequence similarity.

The use of citrate synthase variants would tend to increase acetyl-CoA pools. The work with 3-HB demonstrated that a consequence of blocking metabolism at citrate synthase can be

pyruvate accumulation, which is not unexpected because acetyl-CoA inhibits pyruvate dehydrogenase. Use of promiscuous native thioesterases produced acetate. These results demonstrate the need for engineering the pathway enzymes, for example, by increasing their affinity towards the specific substrate. For example, increasing the affinity of PhaA (thiolase) for acetyl-CoA could increase acetyl-CoA conversion to acetoacetyl-CoA. Targeting acetoacetyl-CoA binding sites in PhaA could decrease the reversibility of the reaction. Futhermore, engineered pathway genes should be chromosomally integrated in the host genome to avoid additional metabolic burden for plasmid maintenance (Wang et al., 2016).

In this work, *E. coli* was used as a model organism to target glycolytic metabolic nodes. Since many organisms have similar PfkA and GltA enzymes, this work should be translated to other non-model organisms. For example, targeting citrate synthase of *Streptomyces* could increase the acetyl-CoA derived antibiotics under aerobic conditions (Viollier et al., 2001). Also, citrate synthase in plants could be targeted to control TCA cycle (Tillbrook et al., 2014) to produce flavanones, isoprenoids, and polyhydroxyalkanoates.

Finally, since *E. coli* W utilizes various carbon sources, in particular sucrose (sugar beets), as well as glucose and xylose (lignocellulosic biomass), these are ideal strains to study the conversion of renewable resources at larger scale.

6.3 REFERENCES

Brockman IM, Prather KLJ. 2015. Dynamic knockdown of *E. coli* central metabolism for redirecting fluxes of primary metabolites. Metabol. Eng. 28:104-113.

Ng CY, Farasat I, Maranas CD, Salis HM. 2015. Rational design of a synthetic Entner-Doudoroff pathway for improved and controllable NADPH regeneration. Metab Eng 29:86-96.

Perez-Zabaleta M, Guevara-Martínez M, Gustavsson M, Quillaguamán J, Larsson G, van Maris AJA. 2019. Comparison of engineered *Escherichia coli* AF1000 and BL21 strains for (R)-3-hydroxybutyrate production in fed-batch cultivation. Appl Microbiol Biotechnol 103(14):5627-5639.

Satowa D, Fujiwara R, Uchio S, Nakano M, Otomo C, Hirata Y, Matsumoto T, Noda S., Tanaka T, Kondo A. 2020. Metabolic engineering of *E. coli* for improving mevalonate production to promote NADPH regeneration and enhance acetyl-CoA supply. Biotechnol Bioeng 117, 2153-2164.

Siedler S, Bringer S, Bott M. 2011. Increased NADPH availability in *Escherichia coli*: improvement of the product per glucose ratio in reductive whole-cell biotransformation. Appl Microbiol Biotechnol 92:929-937.

Stokell DJ, Donald LJ, Maurus R, Nguyen NT, Sadler G, Choudhary K, Hultin PG, Brayer GD, Duckworth HW. 2003. Probing the roles of key residues in the unique regulatory NADH binding site of type II citrate synthase of *Escherichia coli*. J Biol Chem 278:35435–35443.

Taylor JE, Palur DSK, Zhang A, Gonzales JN, Arredondo A, Coulther TA, Lechner AB, Rodriguez EP, Fiehn O, Didzbalis J, Siegel JB, Atsumi S. 2023. Awakening the natural capability of psicose production in *Escherichia coli*. NPJ Sci Food *7*(1):54.

Tillbrook K, Poirier Y, Gebbie L, Schenk PM, McQualter RB, Brumbley SM. 2014. Reduced peroximal citrate synthase activity increases substrate availability for polyhydroxyalkanoate biosynthesis in plant peroxisomes. Plant Biotechnol J 12:1044-1052.

Tovilla-Coutiño DB, Momany C, Eiteman MA. 2020. Engineered citrate synthase alters acetate accumulation in *Escherichia coli*. Metabolic Eng 61:171-180.

van Ooyen, J., Noack, S., Bott, M., Reth, A., Eggeling, L. (2012). Improved L-lysine production with Corynebacterium glutamicum and systemic insight into citrate synthase flux and activity. *Biotechnol Bioeng* 109, 2070–2081.

Viollier PH, Minas W, Dale GE, Folcher M, Thompson CJ. 2001. Role of acid metabolism in *Streptomyces coelicolor* morphological differentiation and antibiotic resistance. J Bacteriol 183(10):3184-3192.

Wang J, Niyompanich S, Tai Y-S, Wang J, Bai W, Mahida P, Gao T, Zhang K. 2016. Engineering of a highly efficient *Escherichia coli* strain for mevalonate fermentation through chromosomal integration. Appl Environ Microbiol 82:7176-7184.